Stabilisation d'émulsions d'arômes par la gomme d'Acacia Caractérisation et compréhension physico-chimique des interactions eau-gomme-arôme

Camille Faucon

THÈSE POUR OBTENIR LE GRADE DE DOCTEUR DE L'INSTITUT AGRO MONTPELLIER ET DE L'UNIVERSITE DE MONTPELLIER

En Biochimie et Physicochimie alimentaire

École doctorale GAIA
Agroressources, Procédés, Aliments, Bioproduits

Unité de recherche IATE
Ingénierie des Agropolymères et des Technologies Emergentes

Stabilisation d'émulsions d'arômes par la gomme d'Acacia : Caractérisation et compréhension physico-chimique des interactions eau-gomme-arôme

Présentée par Camille FAUCON

Le 21 novembre 2022

Sous la direction de Christian SANCHEZ
et Pascale CHALIER

Devant le jury composé de

Thomas CROGUENNEC, Professeur, Institut Agro Rennes Angers	Rapporteur
Ali ASSIFAOUI, Maître de conférence, Université de Bourgogne	Rapporteur
Isabelle SOUCHON, Directrice de recherche, INRAE	Présidente du jury
Denis RENARD, Directeur de recherche, INRAE	Examinateur
Isabelle JAOUEN, Directrice R&D, Alland&Robert	Invitée
Christian SANCHEZ, Professeur, Université de Montpellier	Directeur de thèse
Pascale CHALIER, Maître de conférence, Université de Montpellier	Co-directrice de thèse

UNIVERSITÉ DE MONTPELLIER

L'INSTITUT agro Montpellier

Stabilization of Aroma Emulsions by Acacia gum-water system: Characterization and Physicochemical Understanding of water/gum/aroma Interactions

Camille FAUCON

Ph.D. Thesis

Supervisors: Christian SANCHEZ (PR) and Pascale CHALIER (CR)

November, 2022

« La pierre n'a point d'espoir d'être autre chose qu'une pierre.

Mais, de collaborer, elle s'assemble et devient temple. »

- Antoine de Saint-Exupéry

Remerciements

Cette thèse est l'aboutissement de trois années de formation professionnelle et de cheminement personnel, mais c'est avant tout une grande expérience humaine. Je tiens à remercier dans les lignes qui suivent, toutes les personnes qui ont contribué de près ou de loin à la concrétisation de ces travaux.

Je souhaite tout d'abord remercier l'entreprise Alland & Robert qui a permis de financer cette thèse autour d'une collaboration avec l'équipe I2M de l'UMR IATE. Merci d'avoir mis à disposition toutes les conditions idéales pour réaliser ce projet. J'ai été ravie de travailler dans cet environnement enrichissant autour du biopolymère qu'est la gomme d'Acacia. J'ai également apprécié les échanges lors des réunions de travail.

Je voudrais remercier mon directeur de thèse, Christian Sanchez, pour m'avoir guidée du commencement jusqu'à l'achèvement de cette thèse. Merci pour ses conseils avisés, ses encouragements et le temps qu'il m'a accordé tout au long de ces trois années. Notre collaboration était fondée sur la confiance mutuelle, l'enthousiasme partagé et la liberté de travail. Je souhaite lui exprimer toute ma gratitude pour le soutien et la bienveillance qu'il m'a témoignés, pour la formation scientifique qu'il m'a prodiguée ainsi que pour son implication qui a mené à l'originalité de ce travail. Toutes les qualités scientifiques et humaines de Christian m'ont permis de vivre au quotidien cette thèse comme un accomplissement professionnel et personnel. J'ai apprécié également les instants où la science laissait place à des moments de réflexion et d'échange sur la vie, et sur la complexité des relations humaines qui la constituent.

Je remercie Pascale Chalier, ma co-directrice de thèse, qui m'a donné l'opportunité de réaliser ma thèse au sein de l'équipe I2M. Merci pour ses conseils, sa gentillesse et son écoute. Ses recommandations ont régulièrement permis d'apporter de la précision et de l'amélioration à ce travail.

J'adresse également mes remerciements à l'ensemble de l'équipe I2M, pour leur collaboration et conseils lors des réunions d'équipe. Un remerciement supplémentaire pour Céline Charbonnel qui m'a formée sur les différents équipements du laboratoire.

J'exprime mes remerciements à l'ensemble des membres du jury pour avoir accepté d'évaluer ces travaux de thèse : Monsieur Thomas Croguennec et Monsieur Ali Assifaoui en tant que rapporteurs, Monsieur Denis Renard en tant qu'examinateur, Madame Isabelle Souchon en tant que présidente du jury et Madame Isabelle Jaouen en tant que membre invité. Je les remercie également pour nos discussions et leurs commentaires le jour de ma soutenance.

Je souhaiterais remercier aussi les membres de mon comité de suivi de thèse, Monsieur Stéphane Pezennec et Monsieur Éric Dubreucq pour leurs commentaires et suggestions, faisant avancer mon projet de thèse. Merci également à Monsieur Éric Rondet, mon référent, pour son implication.

Merci à Nathan Thoulouze que j'ai eu la chance d'encadrer lors de son stage. Merci pour son sérieux, son application et sa contribution à ce travail.

Je souhaiterais également remercier chaleureusement tous les membres de l'UMR IATE que j'ai côtoyés durant ces trois années de thèse. A mes collègues du labo, certains sont déjà docteurs et d'autres sur le point de le devenir. Marouane Kabbej, Allison Vercasson, Emma Pignères, Estelle Doisneau, Héloïse Bazart, Paul Derkenne, Coline Perdrier, Aynura Rzayeva, Pauline Pinel, Camille Costes. Merci pour leur solidarité, leur aide, leur soutien et leur bonne humeur. Avec eux j'ai eu l'occasion de passer de très bons moments à Montpellier. Une mention particulière pour Amandine Antoine-Michard, Chloë Bonnenfant et Isabelle Dedieu avec qui j'ai partagé chaque minute de ma thèse et bien plus encore. Sans oublier Lucille Gey, qui avant de partir pour un tour du monde a également contribué à l'égaiement de ces trois années. Je leur souhaite tout le meilleur pour la suite.

Pour finir, je voudrais aussi remercier ma famille et mes proches pour leurs encouragements et leur soutien. Merci d'avoir été là le jour J, merci aussi à ceux qui m'ont suivie en ligne. Je n'oublierai jamais ce moment. Un merci particulier à Jordan, pour son soutien inconditionnel au quotidien ainsi que toutes ses attentions quelques soient les circonstances.

Toutes ces rencontres ont et continuent de me faire grandir. Elles ont été le fruit de moments riches qui resteront longtemps marqués.

Table of contents

General Introduction 1

References 9

Chapter I: State of the art 13

1. Acacia gums composition and chemical structure 15

2. Thermodynamic properties of liquids (water and organic solvents) 19

2.1. Intermolecular interactions in liquids 19

2.2. Isothermal and adiabatic compressibilities 19

2.3. Volume fluctuations 20

2.4. Gibbs free energy of cavity creation 22

2.3. Particularities of aroma compound thermodynamic properties 23

3. Tensiometry 25

3.1. Concept of interfacial tension 25

3.2. Methods of measurements of the interfacial tension 26

3.2.1. Oil-water interfacial tension 26

3.2.2. Dilational rheology 27

4. Liquid – liquid interfaces: water in interaction with hydrophobic surfaces 28

4.1. The water interfacial depletion zone 28

4.2. On the role of water in interfacial physics 28

4.2.1. Interest of volumetric properties 28

4.2.2. The dynamic two-phase structure of water 28

4.2.3. A 3D-approach of protein adsorption to hydrophobic interfaces 29

5. Generalities on Acacia gum interfacial properties 30

5.1. GA interfacial rheological behavior and similarities with proteins, polymers and microgels 30

5.2. Oil hydrophobicity effect on interfacial properties 31

6. Emulsion homogenization and stability 32

6.1. Emulsification process 32

6.2. Destabilization mechanisms 33

6.3. Oil hydrophobicity effect 34

7. References 34

Chapter II: Thermodynamic properties of liquids 43

On the relationship between volume fluctuations in liquids and the Gibbs free energy of cavity formation 45

Abstract 45

1. Introduction 45

2. Methods of calculations 48

2.1. The isothermal compressibility 48

2.2. The Gibbs free energy of cavity formation 49

2.3. The average density fluctuations in number f_V and in volume f_V^* 50

3. Results and discussion 50
3.1. The Gibbs free energy of cavity formation and the average density fluctuations in volume of organic compounds and water 50
3.2. The correlation between the Gibbs free energy of cavity formation and the average density fluctuations in volume 57
3.3. Critical evaluation of the SPT model 60
4. Conclusions 63
5. Acknowledgements 63
6. References 63

Chapter III: Acacia gum interfacial properties at aroma – water interfaces 67
Natural hyperbranched biopolymer at liquid interfaces differing in oil-water interaction energy 69
Abstract 69
1. Introduction 70
2. Materials and methods 72
2.1. Materials 72
2.2. Methods 73
3. Results 75
3.1 Effect of oil hydrophobicity on thermodynamic properties of interfacial water and interface viscoelastic properties 75
3.2. Effect of water interactions on AGPs interfacial adsorption 80
3.2.1. Initial oil-GA-water interactions 80
3.2.2. AGP-water interactions contributing to the differences between A. senegal and A. seyal 83
3.2.3. The influence of oil-water van der Waals and hydrogen bond interaction energy on interfacial pressure and rheology 86
4. Discussion 89
5. Conclusions 97
6. Supplemental info 98
6.1. Viscous modulus of n-hexadecane and 1-octanol 98
6.2. Elastic modulus decrease during phase 3 98
6.3. The surface concentration of AGPs 101
6.4. Hydration isotherms determination 103
7. Acknowledgements 103
8. Complementary studies 104
8.1. Determination of gum surface concentration using a protein model 104
8.2. Alternative hypothesis for the decrease of E' during phase 3 105
9. References 105

Chapter IV: Stability of Acacia gum oil-in-water emulsions 115
Effect of the oil hydrophobicity on the stability and structure of Acacia *senegal* gum oil-in-water emulsion 117
Abstract 117

1. Introduction 117
2. Materials and methods 119
2.1. Materials 119
2.2 Methods 120
2.2.1. Emulsification process 120
2.2.3. Mean volumetric droplet diameter D4,3 of emulsion 120
2.2.3. Emulsion structure and stability measurements 121
3. Results and discussion 121
3.1. Oil hydrophobicity and droplet size distribution of Acacia gum-based emulsions 121
3.2. Impact of hydrodynamic-mechanical fragmentation mechanisms on droplet size 124
3.2.1. High shear mixer 124
3.2.2. High pressure microfluidizer 126
3.3. Effect of oil hydrophobicity on the emulsion stability 128
3.3.1. Creaming of droplets 132
3.3.2. Growth of oil droplets 134
4. Conclusions 138
5. Complementary Information and Study 138
5.1. Principle of laser diffraction to measure particle size 138
5.2. Principle of light scattering measurement 140
5.3. Effect of the gum type (A. senegal vs A. seyal) on the emulsion stability 141
6. Acknowledgements 145
7. References 145

Chapter V: Effect of multi-component oil phase on the interfacial properties and stability of Acacia *senegal* gum oil-in-water emulsions 151
Effect of a mixture of two oils of different hydrophobicity on the interfacial properties of Acacia *senegal* gum at oil – water interfaces 153
Abstract 153
1. Introduction 154
2. Materials and methods 155
2.1. Materials 155
2.2. Methods 156
2.2.1. Preparation of the oil phase 156
2.2.2. Interfacial tension and dilational viscoelastic measurements 157
2.2.3. GC-MS analysis 157
3. Results 158
3.1. Oil – water interfacial tension 158
3.2. Dilational surface rheology 160
4. Discussion 162
5. Conclusions 166
6. Acknowledgements 166

7. Supplemental Information 166
7.1. Estimation of the Hamaker constant of oil-water binary systems 166
8. Complementary studies 168
8.1. Oil – water interfacial tension of d-limonene:carvone mixtures 168
8.2. Oil – water interfacial tension of MCT:1-octanol and MCT:orange oil mixtures 169
8.3. Influence of mixture of two aroma compounds of different hydrophobicity on the formation and aging of Acacia senegal oil-in-water emulsions 170
8.3.1. Emulsification process 170
8.3.2. Measurements of emulsion structure and stability 170
8.3.3. Volumetric droplet diameter of emulsions and aging 171
9. References 176

General Conclusion 181
Perspectives 189
References 191

Valorisation des travaux de recherche 195

Annexes 197
A. Résumé de la thèse en français 197
B. Rheological profiles of water-gum-aroma interphases 211
C. Rheological profiles of water-gum-aroma mixture interphases 212
D. Turbiscan profiles of emulsions stabilized by A. *senegal* 213
E. Turbiscan profiles of emulsions stabilized by A. *seyal* 221
F. Droplet size distribution of aroma mixture emulsions 225

List of Abbreviations in the Text

A. *senegal*	Acacia *senegal*
A. *seyal*	Acacia *seyal*
AGP	Arabinogalactan protein
BS	Backscattering
GA	Acacia gum
HIC	Hydrophobic Interaction Chromatography
HIC-F1	Fraction 1 obtained by HIC
HIC-F2	Fraction 2 obtained by HIC
HIC-F3	Fraction 3 obtained by HIC
OR	Ostwald ripening
O/W	Oil-in-water emulsion
O/W/O	Oil-in-water-in-oil emulsion
SPT	Scaled Particle Theory
T	Transmittance
TI	Turbulent inertial
TSI	Turbiscan stability index
TSS	Three stage sorption
TV	Turbulent viscous
W/O	Water-in-oil emulsion
W/O/W	Water-in-oil-in-water emulsion

List of Abbreviations used in Equations

a_p	Intermolecular interaction parameter
a_w^s	Interfacial thermodynamic activity of water
A	Interfacial area
A_{H}	Hamaker constant
c	Light velocity
C	TSS energy constant
Ca_{TV}	Capillary number for TV fragmentation
CED, E_{coh}	Cohesive energy density
CI	Creaming index
$C_{p,m}$	Isobaric heat capacity
C_S	Dispersed phase solubility
d	Drop diameter
D	Diffusion coefficient
D'	Distance between the sphere and the flat surface
D_o	Outer rotor diameter
$D_{4,3}$	Volumetric droplet diameter of emulsion
E^*	Interfacial viscoelastic modulus
E'	Interfacial elastic modulus
E''	Interfacial viscous modulus
f_V	Average density fluctuations in number
f_V^*	Average density fluctuations in volume
F_1	Energy-number fluctuations
g	Gravitational acceleration
g, Qs	Optical parameters given by the Mie theory
G	Local velocity gradient
ΔG_c	Gibbs free energy of cavity formation
ΔG_{int}	Gibbs free energy of solute-solvent interactions
ΔG_{sol}	Gibbs free energy of solvation
h	TSS isotherm constant
$h(r)$	Total correlation function (r being the distance between the centers of a pair of interacting molecules)
$\hbar$	Reduced Planck constant
H_S	Serum layer
H^s	Heat of formation of water surface
H_T	Total height of emulsion
k	TSS characteristic constant
k_B	Boltzman constant
ℓ	Photon mean free path
ℓ^*	Transport photon mean free path
M	Molar mass
n	Number of total observations
n_D	Refractive index
N	Rotor speed
N_{Av}	Avogadro number
Oi	Observed value

P	Pressure	T	Temperature
ΔP	Laplace pressure	tan δ	Loss tangent
Pi	Predicted value	v	Gravitation separation rate
P_i	Internal pressure	V	Volume
r	Effective hard sphere radius	V_m	Liquid molar volume
r_c	Cavity radius	V_M	Liquid molar volume normalized per molecule
r_i	Turbiscan measurement cell internal radius	v_s	Sound velocity
r_m	Radius of the oil molecule	V_{vdw}	Van der Waals volume
r_s	Solvent radius	$w(D')$	Van der Waals interaction energies for a distance D'
r_{sp}	Radius of the sphere		
R	Ideal gas constant	We	Weber number
R_d	Radius of the spherical drop	We_{TI}	Weber number for TI fragmentation
Re_{dr}	Reynolds number where the characteristic length equals drop diameter	$X(\%)$	Water content
		Xm	Monolayer moisture content
RMSE	Residual Root Mean Square Error	$1 + N_{11}$	Fluctuations of the number of molecules

List of Greek symbols

α_p	Isobaric thermal expansion coefficient	Δ_m	Local excess energy fluctuations
αN	Number of grafts in the polymer chain	ε	Dielectric constant
β_s	Adiabatic compressibility	ε_d	Local turbulent dissipation rate in the homogenization chamber
β_T	Isothermal compressibility		
γ	Interfacial tension	η	Viscosity
γ_{ow}	Oil-water interfacial tension	K_T	Isothermal bulk modulus
Γ	Surface concentration	Π	Interfacial pressure
Γ_w	Moles of water per unit area of the interfacial phase	ρ	Density
		τ_{OR}	Ostwald ripening characteristic time
${}^{S}\delta, {}^{S}\Delta$	(Volume-independent) mean-square amplitude in entropy fluctuations	Φ	Phase angle
		ϕ	Volume fraction of the dispersed phase
${}^{V}\delta, {}^{V}\Delta$	(Volume-independent) mean-square amplitude in volume fluctuations	ϕ_{pd}	Volume packing density
		ω	Oscillation frequency
${}^{SV}\delta$	(Volume-independent) mean-square amplitude in volume-entropy fluctuations	ω_e	Resonance frequency
		ω_0	Molar area of the solvent
		ω_p	Average molar area of the adsorbed protein
$\langle(\delta V)^2\rangle$	Mean square fluctuations in volume		
$\langle\delta V\delta(E+PV)\rangle$	Fluctuation correlation in volume and entropy	ω_T	Thermal Matsubara frequency
		Ω	Droplet growth rate
$\langle(\delta(E\ PV))^2\rangle$	Mean square fluctuations in entropy		

General Introduction

General Introduction

Emulsions consist of a mixture of two immiscible liquids, one being fragmented into small droplets (the dispersed phase) in the other one (the continuous phase) [1]–[3]. Several types of emulsion may be distinguished: oil droplets dispersed in an aqueous phase is called an oil-in-water (O/W) emulsion whereas water droplets dispersed in an oil phase is called a water-in-oil (W/O) emulsion. In addition to these two conventional types, multiple emulsions as "water-in-oil-in-water" (W/O/W) or "oil-in-water-in-oil" (O/W/O) can also be found [2]. Emulsions are thermodynamically unstable systems that tend to phase separation. The mechanisms leading to instability include both reversible and irreversible phenomena such as gravitational separation (creaming/sedimentation), flocculation, coalescence, Ostwald ripening, and phase inversion (see Fig. 1) [1], [2].

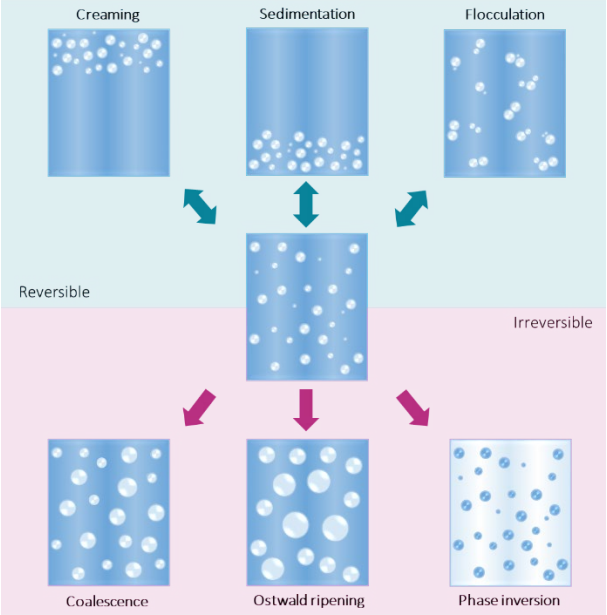

Fig. 1. Schematic representation of the main mechanisms involved in emulsion destabilization.

The stability of an emulsion refers to the ability to resist changes in its physicochemical properties over time [2]. It is primarily influenced by the processing conditions and the chemical composition of the two phases. However, emulsions being kinetically stable for a reasonable period of time (a few days, weeks, months, or years) can be formed by including substances known as emulsifiers [2]. This will result in the decrease of the interfacial tension between the two phases and consequently, the delay of the mechanisms described in Fig. 1. Emulsifiers can be as examples low weight surfactants, biomolecules, polymers, proteins, polysaccharides, ionic

molecules, solid nanoparticles or a combination of surfactants and particles [4]–[13]. They are generally amphiphilic components that concentrate at the oil-water interfaces, modifying their properties.

Acacia gum (GA, E414) is an example of such amphiphilic molecules. GA is defined by the FAO/WHO as "a dried exudation obtained from the stems and branches of Acacia *senegal* (L) Willdenow or Acacia *seyal* (leguminosae family)" [14]. Also called gum arabic, it consists of an edible gummy exudate rich in soluble fibers of low viscosity [15]. Its production originates from a protective mechanism in response to an environmental stress, such as extreme weather conditions or insects and molds invasion [15]. In addition, it improves the healing of wounds. GA is mainly harvested in arid regions of the sub-saharian belt, from Senegal to East Africa, and also beyond to Pakistan and India [16]. Nowadays the collected exudate follows a purification process consisting in the elimination of insoluble materials by physical methods, pasteurization, and spray drying [17]. This results in the gum turning into a whitish powder easily handled as illustrated in Fig. 2.b.

a.  [1] **b.** 

Fig. 2. Natural exudate of Acacia gum before **(a)** and after **(b)** harvest and purification.

GA is the oldest known natural gum whose uses can be traced back to Ancient Egyptians time for paint, ink and cosmetic purposes [15]. Medicinal uses were also attributed since GA was found in the preparation of some curative recipes [15]. Introduced in Europe in the middle age, GA applications experienced a real take-off in the modern times. Its physicochemical properties such as high water-solubility, emulsification and stabilization ability, thickening and surface adsorption capacities, enable to find a large spectrum of industrial applications [15]. In the pharmaceutical industry GA can be used for the production of syrups, coating and encapsulation of active compounds. In cosmetic industry, GA can be found in masks, creams,

[1]picture from https://www.allandetrobert.com/

lotions and powder products due to its adhesive and emulsifying properties. Painting, printing and textile further constitute other examples of non-food applications. Regarding the food industry, GA is employed in the production of non-alcoholic beverages, confectionery, bakery products, brewing, flavor and colorant encapsulation and for wine stabilization. Acacia gum is becoming a highly strategic product with a huge growth of the demand, by 25% over the last ten years [18]. Actually, the demand for Acacia gum ingredients is superior to the industrial processing capacity. In the near future, this strong tendency might further increase as consumers and environmental concerns lead to the need of developing "all natural" and sometimes only plant-based products. Consequently, many food companies are examining the possibility of replacing synthetic ingredients with natural ones [2]. One challenge then consists in expanding applications based on new knowledge on Acacia gum composition, structure and techno-functional properties. To this end, the DIVA collaborational research program was created in 2012 between the Alland & Robert Company - Natural and organic gums (Port Mort, France), a worldwide supplier of Acacia gum, and UMR IATE 1208 (Montpellier), a research unit dedicated to the engineering of agro-polymers and emerging technologies.

As mentioned earlier, GA can be used in beverage applications, more specifically through the stabilization of flavoring preparation-in-water emulsions [15], [19]. Their industrial application is often predefined and according to the selected formulation, emulsions can face instability more or less rapidly with coalescence, creaming or Ostwald ripening occurring. In this context, this Ph.D. project aims to **gain knowledge on the mechanisms involved in GA-stabilized emulsions of aroma compounds** (that constitute flavoring preparations employed in food industry) in order first to better apprehend the origin of surface properties of gums, then possibly to extend the field of application of GA to a wider range of aroma compounds.

Aromas are chemical substances having flavoring properties, *i.e.* imparting the odor and/or taste to food or modifies odor and/or taste of food (Regulation (EC) No 1334/2008) [20]. Flavoring preparation is a mixture of flavoring components. As examples, over 300 aroma compounds have been identified in strawberry [21], and over 800 in coffee [22]. Moreover, flavoring preparations can also contain other ingredients such as antioxidants or weighting agents. Aroma compounds are low molecular weight molecules with the common properties of being volatile in the gaseous atmosphere and being odorous under normal conditions of pressure and temperature [23]. They are foremost hydrophobic organic compounds varying in chemical classes, e.g. terpenoids, hydrocarbures, esters, ketones, alcohols, phenols, pyrazines, aldehydes, acids, sulfurs and so long. Consequently, they offer a wide variety of physicochemical and

thermodynamic properties, e.g. viscosity, solubility, diffusivity, hydrophobicity, vapor pressure, compressibility. Aromas are in liquid state at room temperature and constitute the oily dispersed phase of O/W emulsions of this Ph.D. interest. The abbreviation oil-water interface will be used throughout the manuscript to refer to the aroma-water interface.

O/W emulsions stability has been widely studied through the characteristics and the physicochemical properties of the continuous phase, e.g. the nature and the concentration of the emulsifier [18], [24]–[28], the pH of the solvent [29], [30] and the concentration of salts [29], [30]. In addition, the concentration [31], [32] and rheological behavior of the oil that constitutes the dispersed phase are also important characteristics impacting emulsions stability. The process of emulsification plays as well a significant role as it may influence the characteristic times of the emulsifier adsorption and its coverage degree of oil-water interfaces [1]. All these characteristics are known to impact the initial morphology of the emulsions, *i.e.* the droplet average size and the size distribution and ergo, the stability [1], [32].

Consequences on emulsion stability of the dispersed phase composition were much less explored but the importance of the nature of the oil on the emulsion stabilization has been highlighted [28], [30], [33]. For instance, the oil solubility and hydrophobicity have been found to affect the instability mechanisms through coalescence and Oswald ripening. Using the notion of hydrophobicity necessarily implies interactions with water. However, although water is the major element and the most dynamic one that constitutes the continuous phase, its role upon interfacial structuring mechanisms and emulsions stability curiously seemed to have been mainly omitted. Furthermore, volumetric properties, that are thermodynamic properties, correlated hydrophobicity with surface properties of proteins [34], [35] raising the interest to closer examine the water interactions with GA and aromas. Therefore, **the main objective of the thesis is to study the influence of water and more specifically of the interactions with water OH bonds by varying the oil (aroma compound) hydrophobicity on the mechanism of GA interface formation and emulsion stability.** The study was performed using the two commercially available Acacia gum varieties, namely A. *senegal* and A. *seyal*.

As discussed in a recent review, the interfacial properties in liquid-liquid systems are known to be associated to the aging of emulsions [1]. The adsorption properties of the emulsifier lead to the lowering of the interfacial tension and also act against coalescence and Ostwald ripening [1], [36]. Coalescence is defined as the merging of two droplets into a single one, related to the thinning and rupture of the interfacial layer between them. It may occur when moving droplets get in contact or as consequence of their flocculation [1], [2]. Ostwald ripening phenomena

consists in the partial dissolution of the dispersed phase induced by the capillary pressure, resulting in a mass transfer from small to big droplets. Though mainly driven by the solubility of the disperse liquid and strongly dependent on the size of the droplets, this phenomenon is also affected by the presence of surfactants and on the rheological properties of the interfacial layers. Therefore, to understand how GA stabilizes emulsions we must as well consider the mechanisms involved in the process of GA adsorption at oil-water interface at the microscopic scale. Thus, the scientific approach of the thesis divided as follow.

The first specific objective was to study the thermodynamic properties, in particular the volumetric properties of liquids with the aim of understanding the fundamental differences between water and hydrophobic compounds in terms of volume fluctuations and interaction energy.

The second specific objective was to study the impact of the oil hydrophobicity on the thermodynamic mechanisms of the Acacia gum layer formation at the oil-water interface. Thus, interfacial properties of Acacia gum were examined using interfacial tension measurements and dilational rheological analyses.

The third specific objective was to study the impact of the oil hydrophobicity on the droplet formation during homogenization and on the stability of emulsion. Hence, droplet size distribution analyses and monitoring of destabilization phenomena were achieved.

Aroma compounds being generally employed as mixtures of different aromas or other flavoring ingredients, the impact of a mixture of two aroma compounds of different hydrophobicity, on the interfacial and emulsifying properties of Acacia gum was examined **in addition to these three major objectives**. The idea being to observe if conclusions drawn in the previous studies, also applied. To this end, interfacial tension measurements, dilational rheology analyses, emulsion drop size analyses and monitoring of aging emulsions were performed using a blend of oils.

This manuscript is organized in six sections.

- **The General Introduction** summarizes the context, the aim and the scientific approach of the thesis.
- **Chapter I** presents an overview of the biochemical, physicochemical and structural properties of Acacia gums. It also provides a state of the art on liquids and biopolymers thermodynamics and on the influence of oil hydrophobicity on both interfacial and emulsifying properties.

- **Chapter II** reports a study on the thermodynamic properties of liquids (organic molecules and water) using the Scaled Particle Theory and the volume fluctuations (article published in the Journal of Molecular Liquids).
- **Chapter III** presents a study on the formation and structuration of the GA adsorbed layer at the oil-water interface and proposes an adsorption mechanism based on the importance of the solvent (water) (article ongoing publication in Journal of Colloid and Interface Science).
- **Chapter IV** presents a study of the effect of the oil hydrophobicity on the droplet size obtained after emulsification and on the aging of emulsions (article in preparation).
- **Chapter V** presents a study of the effect of the blending of two oils of different hydrophobicity on the GA interfacial and emulsifying properties (article in preparation).
- **The General Conclusion** summarizes the main results and the perspectives of the thesis.

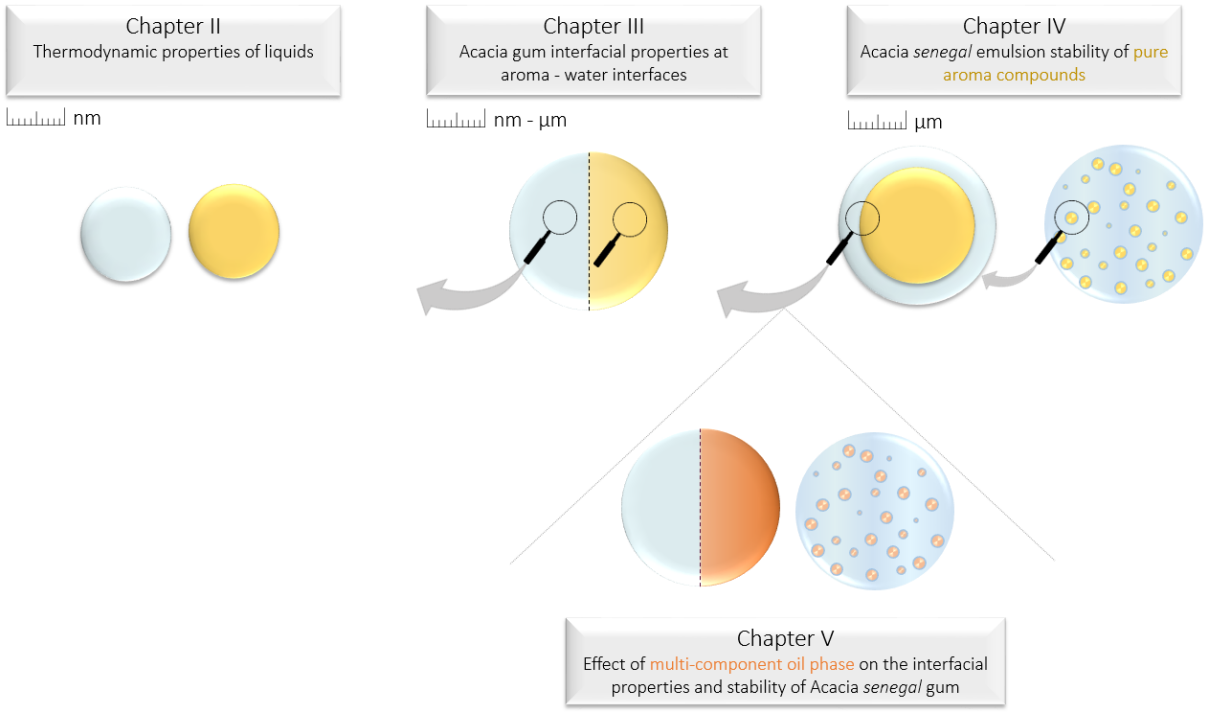

Fig. 3. General approach of the thesis project.

References

[1] F. Ravera, K. Dziza, E. Santini, L. Cristofolini, and L. Liggieri, "Emulsification and emulsion stability: The role of the interfacial properties," *Adv. Colloid Interface Sci.*, vol. 288, p. 102344, 2021, doi: 10.1016/j.cis.2020.102344.

[2] D. J. McCLements, *Food Emulsions Principles, Practices, and Techniques*. 2010.

[3] L. L. Schramm, *Emulsions, Foams and Suspensions*, Wiley-VCH. 2005.

[4] L. Bai, S. Huan, Z. Li, and D. J. McClements, "Comparison of emulsifying properties of food-grade polysaccharides in oil-in-water emulsions: Gum arabic, beet pectin, and corn fiber gum," *Food Hydrocoll.*, vol. 66, pp. 144–153, 2017, doi: 10.1016/j.foodhyd.2016.12.019.

[5] L. Leclercq and V. Nardello-Rataj, "Pickering emulsions based on cyclodextrins: A smart solution for antifungal azole derivatives topical delivery," *Eur. J. Pharm. Sci.*, vol. 82, pp. 126–137, 2016, doi: 10.1016/j.ejps.2015.11.017.

[6] Q. Jin, X. Li, Z. Cai, F. Zhang, M. P. Yadav, and H. Zhang, "A comparison of corn fiber gum, hydrophobically modified starch, gum arabic and soybean soluble polysaccharide: Interfacial dynamics, viscoelastic response at oil/water interfaces and emulsion stabilization mechanisms," *Food Hydrocoll.*, vol. 70, pp. 329–344, 2017, doi: 10.1016/j.foodhyd.2017.03.005.

[7] L. Dai, C. Sun, Y. Wei, L. Mao, and Y. Gao, "Characterization of Pickering emulsion gels stabilized by zein/gum arabic complex colloidal nanoparticles," *Food Hydrocoll.*, vol. 74, pp. 239–248, 2018, doi: 10.1016/j.foodhyd.2017.07.040.

[8] E. Bouyer, G. Mekhloufi, N. Huang, V. Rosilio, and F. Agnely, "β-Lactoglobulin, gum arabic, and xanthan gum for emulsifying sweet almond oil: Formulation and stabilization mechanisms of pharmaceutical emulsions," *Colloids Surfaces A Physicochem. Eng. Asp.*, vol. 433, pp. 77–87, 2013, doi: 10.1016/j.colsurfa.2013.04.065.

[9] É. Kiss and R. Borbás, "Protein adsorption at liquid/liquid interface with low interfacial tension," *Colloids Surfaces B Biointerfaces*, vol. 31, no. 1–4, pp. 169–176, 2003, doi: 10.1016/S0927-7765(03)00136-X.

[10] E. Dickinson, "Stabilising emulsion-based colloidal structures with mixed food ingredients," *J. Sci. Food Agric.*, vol. 93, no. 4, pp. 710–721, 2013, doi: 10.1002/jsfa.6013.

[11] P. Erni, "Deformation modes of complex fluid interfaces," *Soft Matter*, vol. 7, no. 17, pp. 7586–7600, 2011, doi: 10.1039/c1sm05263b.

[12] A. Nesterenko, A. Drelich, H. Lu, D. Clausse, and I. Pezron, "Influence of a mixed particle/surfactant emulsifier system on water-in-oil emulsion stability," *Colloids Surfaces A Physicochem. Eng. Asp.*, vol. 457, no. 1, pp. 49–57, 2014, doi: 10.1016/j.colsurfa.2014.05.044.

[13] A. P. Sullivan and P. K. Kilpatrick, "The effects of inorganic solid particles on water and crude oil emulsion stability," *Ind. Eng. Chem. Res.*, vol. 41, no. 14, pp. 3389–3404, 2002, doi: 10.1021/ie010927n.

[14] FAO, "Gum arabic," 1999. https://www.fao.org/3/W6355E/w6355e0g.htm (accessed Jul. 12, 2022).

[15] C. Sanchez *et al.*, "Acacia gum: History of the future," *Food Hydrocoll.*, vol. 78, pp. 140–160, 2018, doi: 10.1016/j.foodhyd.2017.04.008.

[16] C. O. Cecil, "Gum arabic," *Saudi Aramco World*, vol. 56(2), pp. 36–39, 2005.

[17] L. Lopez-Torrez, M. Nigen, P. Williams, T. Doco, and C. Sanchez, "Acacia senegal vs. Acacia seyal gums - Part 1: Composition andstructure of hyperbranched plant exudates," *Food Hydrocoll.*, vol. 51, no. April, pp. 41–53, 2015, doi: 10.1016/j.foodhyd.2015.04.019.

[18] C. Aphibanthammakit, "Propriétés interfaciales et émulsifiantes de gommes d'Acacia senegal, Acacia seyal et de leurs fractions," 2018.

[19] D. Verbeken, S. Dierckx, and K. Dewettinck, "Exudate gums: Occurrence, production, and applications," *Appl. Microbiol. Biotechnol.*, vol. 63, no. 1, pp. 10–21, 2003, doi: 10.1007/s00253-003-1354-z.

[20] European Commission, "Regulation (EC) No 1334/2008 on flavourings," *Off. J. Eur. Union, 2008*, vol. L 354/34, no. 1334, pp. 34–50, 2008.

[21] R. Watson, C. J. Wright, T. McBurney, A. J. Taylor, and R. S. T. Linforth, "Influence of harvest date and light integral on the development of strawberry flavour compounds," *J. Exp. Bot.*, vol. 53, no. 377, pp. 2121–2129, 2002, doi: 10.1093/jxb/erf088.

[22] W. Grosch, "Flavour of coffee. A review," *Nahrung - Food*, vol. 42, no. 6, pp. 344–350, 1998, doi: 10.1002/(sici)1521-3803(199812)42:06<344::aid-food344>3.0.co;2-v.

[23] H. Richard, "Arômes alimentaires," *Flavour Sci. Technol. (Proc. 5th Weurman Flavour Res. Symp.*, no. Figure 1, pp. 1–17, 1987, [Online]. Available: %5C%5CRobsrv-05%5Creference manager%5CArticles%5C4182.pdf.

[24] R. M. A. Mansour and E. A. Hassan, "Effect of gum concentration and gum protein concentration on emulsifying properties of some Acacia gums," *Int. J. basic Appl. Chem. Sci.*, vol. 6, no. 2, pp. 23–35, 2016.

[25] P. Erni *et al.*, "Interfacial rheology of surface-active biopolymers: Acacia senegal gum versus hydrophobically modified starch," *Biomacromolecules*, vol. 8, no. 11, pp. 3458–3466, 2007, doi: 10.1021/bm700578z.

[26] E. Dickinson, B. S. Murray, G. Stainsby, and D. M. W. Anderson, "Surface activity and emulsifying behaviour of some Acacia gums," *Top. Catal.*, vol. 2, no. 6, pp. 477–490, 1988, doi: 10.1016/S0268-005X(88)80047-X.

[27] M. Elmanan, S. Al-Assaf, G. O. Phillips, and P. A. Williams, "Studies on Acacia exudate gums: Part VI. Interfacial rheology of Acacia senegal and Acacia seyal," *Food Hydrocoll.*, vol. 22, no. 4, pp. 682–689, 2008, doi: 10.1016/j.foodhyd.2007.02.008.

[28] S. J. Reiner, G. A. Reineccius, and T. L. Peppard, "A comparison of the stability of beverage cloud emulsions formulated with different gum acacia- and starch-based emulsifiers," *J. Food Sci.*, vol. 75, no. 5, 2010, doi: 10.1111/j.1750-3841.2010.01625.x.

[29] M. Atgié, O. Masbernat, and K. Roger, "Emulsions Stabilized by Gum Arabic: Composition and Packing within Interfacial Films," *Langmuir*, vol. 35, no. 4, pp. 962–972, 2019, doi: 10.1021/acs.langmuir.8b02715.

[30] R. Chanamai and D. J. McClements, "Comparison of gum arabic, modified starch, and whey protein isolate as emulsifiers: Influence of pH, CaCl2 and temperature," *J. Food Sci.*, vol. 67, no. 1, pp. 120–125, 2002, doi: 10.1111/j.1365-2621.2002.tb11370.x.

[31] V. Paramita, T. Furuta, and H. Yoshii, "High-Oil-Load Encapsulation of Medium-Chain Triglycerides and d-Limonene Mixture in Modified Starch by Spray Drying," *J. Food Sci.*, vol. 77, no. 2, pp. 38–44, 2012, doi: 10.1111/j.1750-3841.2011.02534.x.

[32] J. Zhang, T. L. Peppard, and G. A. Reineccius, "Preparation and characterization of nanoemulsions stabilized by food biopolymers using microfluidization," *Flavour Fragr. J.*, vol. 30, no. 4, pp. 288–294, 2015, doi: 10.1002/ffj.3244.

[33] E. Dickinson, V. B. Galazka, and D. M. W. Anderson, "Emulsifying behaviour of gum arabic. Part 1: Effect of the nature of the oil phase on the emulsion droplet-size distribution," *Carbohydr. Polym.*, vol. 14, no. 4, pp. 373–383, 1991, doi: 10.1016/0144-8617(91)90003-U.

[34] K. Gekko and H. Noguchi, "Compressibility of globular proteins in water at 25°C," *J. Phys. Chem.*, vol. 83, no. 21, pp. 2706–2714, 1979, doi: 10.1021/j100484a006.

[35] K. Gekko and Y. Hasegawa, "Compressibility-Structure Relationship of Globular Proteins," *Biochemistry*, vol. 25, no. 21, pp. 6563–6571, 1986, doi: 10.1021/bi00369a034.

[36] T. C. Botti, A. Hutin, E. Quintella, and M. S. Carvalho, "Effect of interfacial rheology on drop coalescence in water-oil emulsion," *Soft Matter*, vol. 18, no. 7, pp. 1423–1434, 2022, doi: 10.1039/d1sm01382c.

Chapter I: State of the art

This chapter aimed to summarize the main information about Acacia gum and the structure of its constituent AGPs, as well as the concepts discussed throughout this Ph.D. (thermodynamics of liquids and cavities, interfacial tension, thermodynamics of biopolymer-water interactions at interfaces). This chapter also provides the description of the methods used and gathers studies and conclusions upon Acacia gum and other solute (e.g. proteins, polymers, surfactants) interfacial and emulsifying properties involving the dominant role of water in determining the so called "hydrophobic effect" or "hydrophobic interactions".

Highlights

- The protein/polysaccharide duality of AGPs and related hydration give rise to the amphiphilic properties allowing the adsorption to gas–liquid, liquid–liquid, and solid–liquid interfaces.
- Acacia gum allows the reduction of the interfacial tension between the dispersed phase and the continuous phase of an emulsion, and allows the formation of an interfacial viscoelastic barrier, promoting the formation of an emulsion by producing more stable droplet.
- AGPs adsorption process is generally described in three steps: diffusion (I) from the aqueous phase onto the interface, penetration (II), aggregation/rearrangement (III) within the interfacial layer.
- Volumetric properties of biopolymers are linked to solute intrinsic molecular properties and solute-solvent interactions. They allow to estimate microscopic events from macroscopic measurements.
- Volume fluctuations at microscopic scales are a specific signature of liquid structure.

- The oil-protein-water interfacial tension and dilational rheology depend on the oil hydrophobicity.

- 3D-approach of the proteins adsorption process on hydrophobic surfaces outlines the fundamental role of water.

Chapter I: State of the art

1. Acacia gums composition and chemical structure

The two Acacia gum (GA) varieties Acacia *senegal* (A. *senegal*) and Acacia *seyal* (A. *seyal*) were studied during this Ph.D. project. The main composition of both gums consists in highly glycosylated hydroxyproline-rich arabinogalactan-proteins (AGPs). AGPs macromolecules are hyperbranched complex polysaccharides, neutral or slightly acidic, found as a mixture of calcium, magnesium, and potassium salt. They are essentially made of sugars D-galactose, L-arabinose, L-rhamnose, D-glucuronic acid, and 4-O-methyl-D-glucuronic acid. In addition, AGPs contain about 1-3% of proteins and 3-4% of minerals. These relative proportions may vary according to the specie (A. *senegal*, A. *seyal*), the origin, *i.e.* the age of the tree, the climatic conditions and soil environment, and the process performed after harvesting [1]–[6]. AGPs can also be described as heavily branched neutral and charged sugars forming polysaccharide blocks covalently bonded to a polypeptide backbone rich in hydroxyproline alternating with alanine, threonine and serine. A. *senegal* and A. *seyal* differ mainly by their sugar, protein content, amino acid profile and branching degree. A. *senegal* is characterized by a higher protein content, *i.e.* around 2-3% versus 1% for A. *seyal*, as well as a greater branching degree, 78% and 59% respectively. A. *seyal* is defined by higher arabinose and 4-O-me-glucuronic acid contents than A. *senegal* [4], [7].

The gums can also be distinguished from their structural parameters. A. *senegal* displays a lower molecular weight M_w ($6.8x10^5$ $g.mol^{-1}$) than A. *seyal* ($8.2x10^5$ $g.mol^{-1}$) but a larger polydispersity index (M_w/M_n). In addition, A. *seyal* has a smaller intrinsic viscosity than A. *senegal*, then a smaller hydrodynamic radius, respectively of 10 nm and 15 nm in a 10 mM sodium acetate buffer solution, indicating A. *seyal* is characterized by a more compact conformation structure. Thus far, more knowledge about the elementary building blocks of the main AGPs macromolecular assembly constituting A. *senegal gum* has been proposed (Fig. I.1). According to Renard and colleagues [8], the latter AGPs can be divided into 6 building blocks of type 1, and 8 building blocks of type 2 by covalent and/or non-covalent interactions. The blocks are composed of polypeptide chains with different grafts. Grafts of blocks 1 consist in 17 arabinoside oligomers and 6 polysaccharide blocks while grafts of blocks 2 consist in

87 arabinoside oligomers and 32 polysaccharide blocks. More details can be found in Renard and al. work [8].

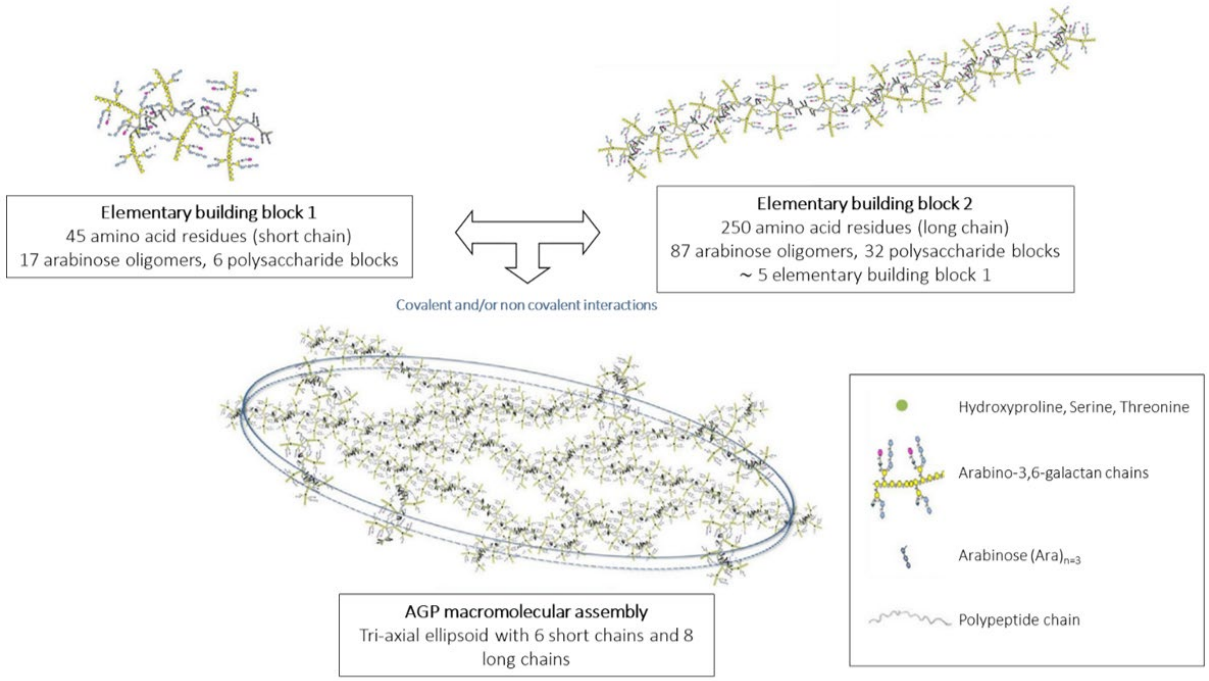

Fig. I.1. Elementary building blocks 1 and 2 used to build arabinogalactan-protein (AGP) macromolecular assembly from Acacia *senegal* gum. Building block 2 was built by a linear arrangement of five building blocks 1. The 3D-model of AGP is made of the assembly of 6 building blocks 1 and 8 building blocks 2 by covalent and/or non-covalent interactions. Adapted from Renard and al. [8].

The protein/polysaccharide duality gives rise to the amphiphilic properties allowing the adsorption of GA to gas–liquid, liquid–liquid, and solid–liquid interfaces [9]. Thus, the gum can reduce the interfacial tension between the dispersed and the continuous phases of an emulsion and form an interfacial viscoelastic barrier, promoting the formation of the emulsion with more stable droplets [10]–[14].

Hydrophobic interaction chromatography (HIC) allows to isolate three main AGP fractions of A. *senegal* according to their hydrophobicity, *i.e.* HIC-F1, HIC-F2 and HIC-F3. Studies highlighted common and distinct features between fractions [8], [15]–[19]. For instance, they display similar sugar composition, with however larger amount of charged sugars for HIC-F1 and larger amount of arabinose for HIC-F2 and HIC-F3. The polarity of molecules is inversely proportional to the protein content, with HIC-F1 < HIC-F2 < HIC-F3 and protein values of about 1%, 8-10% and 20-25%, respectively. All fractions were globally composed by three populations of AGPs, low M_w ($M_w < 7.5x10^5$ g.mol^{-1}), high M_w ($M_w > 7.5x10^5$ g.mol^{-1}) and supramolecular assemblies ($M_w > 2\text{-}3x10^6$ g.mol^{-1}). A high amount of low M_w AGP was present

in HIC-F1 while high amounts of high M_w AGP and assemblies were found in HIC-F2 and HIC-F3. Because of the presence of charged sugars and amino acids, all fractions were negatively charged with weak polyelectrolyte behavior. Due to its high molecular mass and protein-rich content, HIC-F3 is believed to contribute the most to the gum adsorption in opposition to HIC-F1 [9], [19], [20].

The biochemical compositions and structural properties of A. *senegal* (Batches n°OF110676 and n°OF152413) and A. *seyal* (Batch n°OF110724) gums used in this project are presented in Table I.1. Except for moisture and dry matter contents, values were adapted from Lopez-Torrez et al. 2016 [7].

Table I.1. Biochemical compositions and structural parameters of A. *senegal* and A. *seyal* used in the Ph.D. project. Adapted from Lopez Torrez et al. 2015 [21]. na stands for non-available.

	A. *senegal* (Batch n° OF110676)	A. *senegal* (Batch n° OF152413)	A. *seyal* (Batch n° OF110724)
Total dry matter ($mg.g^{-1}$)	899.3±0.4		888.4±4.2
Moisture (%)	10.1		11.1
Sugar ($mg.g^{-1}$)*	940.0	944.4	950.0
Arabinose (%)	30.3±2.5	30.2±0.6	47.6±0.6
Galactose (%)	35.8±1.2	40.5±1.7	36.9±1.1
Rhamnose (%)	15.5±0.4	12.4±0.4	3.0±0.3
Glucuronic acid (%)	17.4±1.2	17.8±1.7	6.7±0.4
4-O-Me-Glucuronic acid (%)	1.0±0.1	1.0±0.1	5.8±0.6
Uronic acid/neutral sugar ratio	0.23	0.23	0.14
Protein ($mg.g^{-1}$)	27.0±0.0	21.5±0.9	10.0±0.0
Mineral ($mg.g^{-1}$)	33.0±0.2	34.1±0.1	40.0±0.1
Average molar mass (M_w, $g.mol^{-1}$)	6.8×10^5	6.8×10^5	8.2×10^5
Polydispersity index (M_w/M_n)	2.0	2.0	1.5
Hydrodynamic radius R_H (nm)	15*	15*	10*
Branching degree (%)	78.2	78.0	59.2
Intrinsic viscosity ($mL.g^{-1}$)	22.8	29.8	16.5
Partial specific volume ($cm^3.g^{-1}$)	na	0.5842	na
Partial specific adiabatic compressibility ($\times10^{11}$ $cm^3.g^{-1}.Pa^{-1}$)	na	-7.1	na

*values for a 10 mM sodium acetate buffer solution [22].

2. Thermodynamic properties of liquids (water and organic solvents)

Contrary to solids where long-range order prevails, liquids with high density and far below the critical point display short-range order, extending over a few molecular diameters [23], [24]. Yet, liquids are today better described using the phonon theory of liquids, derived from the Debye theory of solids [25], [26]. Liquids and solids may then be described according to the same physical laws. In the following, we focus on the main thermodynamic properties of liquids that have been used in our work.

2.1. Intermolecular interactions in liquids

In contrast to intramolecular forces, such as the covalent bonds that hold atoms together in molecules and polyatomic ions, intermolecular forces hold molecules together in a liquid or a solid [27]. Intermolecular forces are generally much weaker than covalent bonds. For example, it requires 927 kJ to overcome the intramolecular forces and break both O–H bonds in 1 mole of water [28], but it takes only about 41 kJ to overcome the intermolecular attractions and convert 1 mole of liquid water to water vapor [29].

Intermolecular forces are electrostatic in nature, meaning they arise from the interaction between positively and negatively charged species. The three main types of intermolecular interactions are hydrogen interactions with an energy of the order of ~10-40 kJ.mol^{-1} [27], dipole-dipole, dipole-multipole and multipole-multipole interactions (known as Debye-Keesom dispersion forces), and London dispersion forces. The last two are collectively referred to van der Waals forces and are of the order of ~1-10 kJ.mol^{-1} [27], [30]. All these interactions occur simultaneously in water.

2.2. Isothermal and adiabatic compressibilities

The isothermal and adiabatic compressibilities, respectively β_T and β_S, are parameters that measure the liquid stiffness. They are indicative of volume fluctuations induced by pressure [$\beta = -\frac{1}{V}\left(\frac{\delta V}{\delta P}\right)$]. The adiabatic compressibility β_S (m^2.N^{-1}) can be determined according to the Newton-Laplace equation:

$$v_s = \sqrt{\frac{1}{\rho \beta_s}} \tag{1}$$

where v_s is the sound velocity (m.s^{-1}) and ρ is the density of liquid (kg.m^{-3}). Then, the isothermal compressibility β_T can be calculated from β_S through [31]:

$$\beta_s = \beta_T - \frac{{\alpha_p}^2 T}{\rho C_{p,m}} \tag{2}$$

where α_p is the isobaric thermal expansion coefficient (K^{-1}) and $C_{p,m}$ the isobaric heat capacity (J.K^{-1}.kg^{-1}).

The isothermal compressibility also accounts for the balance of repulsive and attractive interaction forces which govern the form of the pair and high order correlation functions [32]. This implies β_T is directly related to the total correlation function h(r) [24] through:

$$\rho k_B T \beta_T = 1 + 4\pi\rho \int_0^\infty dr\, r^2 h(r) \tag{3}$$

where ρ is the average density measured in number of molecules per unit volume. The correlation function describes the correlating effect of the presence of one molecule on the position of a second molecule [24]. The parameter $\rho k_B T \beta_T$ is the structure factor as wave vector tends to zero, and characterizes the strength of intermolecular interactions, the regularity of liquid's structure and more generally the structural complexity per particle [33], [34]. More importantly, $\rho k_B T \beta_T$ characterizes the local microscopic volume fluctuations of liquids [35], providing a connection between microscopic many-body interactions of liquids and its macroscopic, thermodynamic properties [36]. Thus, volume fluctuations at microscopic scales are a specific signature of liquid structure.

2.3. Volume fluctuations

Multiple equations have been established to estimate fluctuations in volume and energy in a liquid. For example, Ploetz and Smith determined formulas to quantify macroscopic fluctuations of the spatial distribution of liquid density and fluctuations of the interaction energy from the isothermal-isobaric partition function [35], [37]:

$$\langle (\delta V)^2 \rangle_{NPT} = V k_B T \beta_T \tag{4}$$

$$\langle \delta V \delta (E + PV) \rangle_{NPT} = V k_B T^2 \alpha_p \tag{5}$$

$$\langle \left(\delta (E + PV) \right)^2 \rangle_{NPT} = N k_B T^2 C_{p,m} \tag{6}$$

where $\langle (\delta V)^2 \rangle_{NPT}$ is the mean square fluctuations in volume (V) for constant temperature (T), pressure (P), and number of molecules (N), $\langle \delta V \delta (E + PV) \rangle_{NPT}$ is the fluctuation correlation in volume and entropy for constant temperature, pressure, and number of molecules, and $\langle \left(\delta (E + PV) \right)^2 \rangle_{NPT}$ is the mean square fluctuations in entropy for constant temperature, pressure, and number of molecules.

The inconvenient of using these equations is that it is necessary to define a pertinent volume small enough to detect the fluctuations but large enough for the extensive thermodynamic quantities of the volume V and the entropy S to be evaluated. To circumvent this difficulty, Koga and coworkers defined the (volume-independent) mean-square amplitudes in fluctuations of volume, entropy and volume-entropy cross fluctuations:

$$^{V}\delta \equiv \frac{\langle (\Delta V)^2 \rangle}{(k \langle V \rangle)} = T \beta_T \tag{7}$$

$$^{S}\delta \equiv \frac{\langle (\Delta S)^2 \rangle}{(k \langle V \rangle)} = \frac{C_{p,m}}{V_m} \tag{8}$$

$$^{SV}\delta \equiv \frac{\langle (\Delta S)(\Delta V) \rangle}{(k \langle V \rangle)} = T \alpha_p \tag{9}$$

where $C_{p,m}$ and V_m are respectively the molar isobaric heat capacity and molar volume. Then, in order to qualitatively take into account the wavelength of fluctuations, *i.e.* the extensity, new equations have been defined that give an approximate idea of both amplitude of fluctuations in densities and fluctuation wavelengths [38], [39]:

$$^{V}\Delta \equiv \frac{RT \beta_T}{V_m} \tag{10}$$

$$^{S}\Delta \equiv \frac{R C_{p,m}}{{V_m}^2} \tag{11}$$

$$^{SV}\delta \equiv \frac{RT \alpha_p}{V_m} \tag{12}$$

Finally, Ploetz and Smith also provided formulas to appraise local microscopic fluctuation quantities of a liquid [37]:

$$1 + N_{11}^0 = \rho_1^0 RT\beta_T^0 \tag{13}$$

$$F_1^0 = PRT\beta_T^0 - RT^2\alpha_p^0 \tag{14}$$

$$\Delta_m^0 = RT^2 C_{p,m}^0 + PV_m^0\left(PRT\beta_T^0 - 2RT^2\alpha_p^0\right) \tag{15}$$

where $1 + N_{11}^0$ is essentially the fluctuations of the number of molecules, F_1^0 is the energy-number fluctuations and Δ_m^0 is the local excess energy fluctuations. The superscript (°) denotes the pure liquid values.

Several equations previously mentioned overlap and all are based on volumetric parameters such as the isothermal compressibility, the isobaric thermal expansion coefficient and the isobaric heat capacity.

Since β_T is a measure of volume fluctuations [35], [38], [39], Soper [13] recently suggested that a thermodynamic quantity f_V, strictly related to β_T, can be used to describe how large the density fluctuations are likely to be in any given volume of a liquid. [40].

$$f_V = \left(\frac{k_B T}{V K_T}\right)^{0.5} = \left(\frac{k_B T \beta_T}{V}\right)^{0.5} \tag{16}$$

The f_V quantity is not density dependent, is close to zero at macroscopic length scales, but display significant values at microscopic ones [40]. For example, for a water volume of 1 nm^3 at 298 K, $f_V = 4.3\%$.

Equation (16) will be an interest of Chapter II.

2.4. Gibbs free energy of cavity creation

On the basis of a statistical mechanical approach, the process of solvating a solute molecule in a solvent (e.g. AGPs in water) can exactly be separated in two sub-processes [24]: (a) formation of a cavity of the size of the solute molecule; (b) introduction of the solute molecule into the cavity, switching on solute-solvent attractive interactions [41], [42]. This theoretical construction is feasible because the Gibbs free energy is a state function of a thermodynamic system. In terms of Gibbs free energy this can be written as follows:

$$\Delta G_{sol} = \Delta G_c + \Delta G_{int} \tag{17}$$

where ΔG_c is the Gibbs free energy cost of cavity formation and depends solely on solvent properties. On the other hand, ΔG_{int} depends on solute-solvent attractive interactions.

The Gibbs free energy of cavity creation is a very fundamental parameter attesting the structure and stiffness of a liquid, such as creating a cavity in a highly structured liquid will lead to great energy cost and so, high ΔG_c. The "solubility" in water of a solute first depends on ΔG_c.

2.3. Particularities of aroma compound thermodynamic properties

Aromas are chemical substances having flavoring properties, *i.e.* imparting the odor and/or taste to food or modifies odor and/or taste of food (Regulation (EC) No 1334/2008) [43]. They are generally found as mixtures in essential oils, vegetables, meats and fishes, in plant extracts or in transformed food products and beverages. As an example, over 300 aroma compounds have been identified in strawberry [44]. Aroma compounds are low molecular weight molecules with the common properties of being partially volatile and odorous under normal conditions of pressure and temperature [45]. They are foremost hydrophobic organic compounds varying in chemical classes (e.g. terpenoids, hydrocarbures, esters, ketones, alcohols, phenols, pyrazines, aldehydes, acids, sulfurs). They offer a wide variety of physicochemical and thermodynamic properties, e.g. viscosity, solubility, diffusivity, hydrophobicity, fusion temperature, vapor pressure, compressibility. These specific characteristics and in particular the poor solubility, require to formulate aroma compounds as an emulsion to favor their incorporation in water rich media as beverage, sauces, or dairy products.

Most aroma compounds are in liquid form at room temperature or when mixed with each other. Therefore, in this Ph.D. they were considered as organic liquids. They were selected to cover a large category of chemical classes (alkane, terpene, ketone, ester and alcohol) and hydrophobicity (*i.e.* oil-water interfacial tension) (see Table I.2). The choice was also made to vary in viscosity and solubility in water.

Table I.2. Oil-water interfacial tension, oil log P, solubility in water, density, viscosity and vapor pressure at 25°C.

Oil type	Oil name	Structure	Oil-water interfacial tension ($mN.m^{-1}$)	Log P[a]	Solubility in water[a] ($mg.L^{-1}$)	Density[a] ($kg.m^{-3}$)	Viscosity [46] (10^{-3} Pa.s)	Vapor pressure[a] (Pa)
Alkane	n-Hexadecane	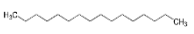	52-47 [47], [48]	8.20	2×10^{-5}	773	3.45*	0.2
Terpene	Myrcene		*n.d.*	4.17	6	796	*n.d.*	278.6
	d-Limonene		44* [49]	4.57	14	840	0.85	206.7
Ester	Ethyl octanoate	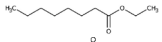	*n.d.*	3.84	70	865	1.41 [52]	29.9
	Methyl octanoate	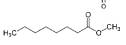	*n.d.*	3.33	64*	875	1.39* [53]	72.0
Ketone	Carvone		*n.d.*	2.54	1300	959 [51]	2.46 [51]	20.0
Alcohols	1-Decanol		9.5 [48]	4.57	37	826	10.97	1.1
	1-Octanol		8.5 [50]	3.00	540	822	7.21	10.7

**value at 20°C*
n.d.: no data available

d-Limonene and myrcene are monoterpenes, commonly found in citrus fruits [54]. They are the two most hydrophobic aroma compounds of this set. They are both characterized by a low solubility, high vapor pressure and weak viscosity but differ by their density. Regarding the interfacial tension, the least hydrophobic compounds are both linear alcohols, namely 1-octanol and 1-decanol. However, the C8 is 10 time more soluble than the C10. The carvone, a cyclic terpenic ketone, is also found in citrus or *Mentha spicata* essential oil [55] and is characterized by a strong solubility (C_S = 1300 $mg.L^{-1}$) and high density (ρ = 965 $kg.m^{-3}$). Regarding the viscosity, 1-decanol and d-limonene were found, respectively, the most (η = 10.97 mPa.s) and the least (η = 0.85 mPa.s) viscous compounds. The two esters only differ by the length of their carbon chain and possess quite similar properties except for the vapor pressure. n-Hexadecane is characterized by the lowest solubility in water ($C_S = 2 \times 10^{-5}$ $mg.L^{-1}$) and density (ρ = 773 $kg.m^{-3}$). It is not an aroma compound as previously defined but was selected as a reference of highly hydrophobic compound (log P = 8.20 and γ_{ow} = 52 $mN.m^{-1}$). Log P is a flavorists' criterion for classifying compounds according to their lipophilicity [56]. High log P value implies high lipophilicity. It is equal to the logarithm of the ratio of the concentrations of the substance in 1-octanol and in water. During this Ph.D. we used the oil-water interfacial tension as criterion to sort compounds according to their hydrophobicity [48], [57], [58].

[a]values from https://pubchem.ncbi.nlm.nih.gov/, data base of national library of medicine

3. Tensiometry

3.1. Concept of interfacial tension

The coexistence of two condensed phases (e.g. liquid and gas, two immiscible liquids) takes place if a stable boundary called an interface enables a separation. This separation interface is characterized according to Gibbs [59] by a free energy F_S associated with the formation of a contact surface area A between the two phases:

$$F_S = \frac{\partial F}{\partial A} A = \gamma A \tag{18}$$

where γ is the interfacial tension reflecting the variation in free energy F associated with a variation in surface area dA between the two media. Therefore, the interfacial tension γ represents the free energy per unit surface area that is required for creating an interface between two phases. γ can be defined either as an energy per unit area (in $J.m^{-2}$) or as a force per unit length (in $N.m^{-1}$).

Taking the example of an oil droplet surrounded of water, the interfacial tension depends on the oil-oil, water-water and oil-water intermolecular interactions [27], [60]. An oil molecule within the drop will tend to be attracted equally in all directions. On the other hand, an oil molecule at the interface will experience a net attraction by other molecules towards the interior of the drop (Fig. I.2). This is owed to the cohesive forces being greater than the adhesive forces, or in other words, to the supremacy of water-water and oil-oil interactions compared to oil-water interactions. As a result, there is a tangential stress that tends to minimize the interfacial area. This is the reason why dispersed drops of an emulsion are assumed to be spherical, as it is the smallest possible area for a given volume.

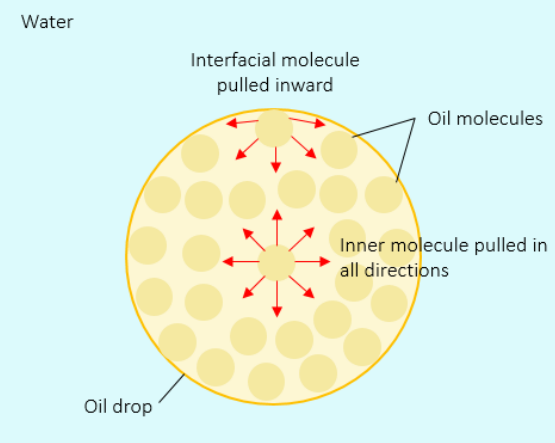

Fig. I.2. Oil cohesive forces defining the oil-water interfacial tension.

3.2. Methods of measurements of the interfacial tension

3.2.1. Oil-water interfacial tension

Various methods allow the measurement of the interfacial tension. One of them is the pendant or rising drop technique that consists in an automatic drop tensiometer. The shape of the drop results from the competition between the interfacial tension and the gravitational force (Fig. I.3). According to the drop weight (liquid density), the gravitational force can lead to changes of curvature of the drop interface in vertical direction. The density of the selected oils being lower than that of the aqueous phase, the "rising drop" configuration was used.

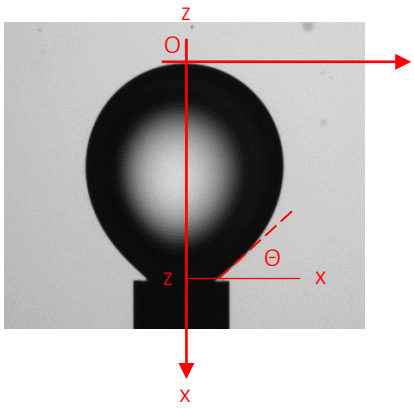

Fig. I.3. The oil droplet profile and (x, z) coordinate system.

The value of the interfacial tension can be determined using the profile of the drop. The calculation of the interfacial tension is based on Laplace Young's equation which expresses the pressure difference between the two phases, called the Laplace pressure ΔP as a function of the interfacial tension and the drop radius of curvature R [61].

$$\Delta P = \frac{2\gamma}{R} \tag{19}$$

The interfacial tension is also expressed as the balance of physical forces applying on the drop. This consists in the buoyant force acting on the upper part of the drop, the Laplace pressure force exerted on the straight section and the interfacial tension applied on the periphery of the section, which counterbalances the first two. Projecting onto the vertical axis Oz leads respectively to:

$$V_a(\rho_{GA} - \rho_a)g + \pi x^2 \Delta P = 2\pi x \gamma sin\theta \tag{20}$$

where g is the gravitational constant, ρ_{GA} and ρ_a the density of respectively GA dispersion and oil (aroma) compound, x and θ coordinates of the drop system and V_a the volume of the oil drop.

Thus, the interfacial tension can be expressed through:

$$\gamma = \frac{(\rho_{GA} - \rho_a)R^2 g}{w_b} \tag{21}$$

where w_b is the dimensionless Bond number, the ratio between the buoyant force and the interfacial tension.

$$w_b = \frac{2\pi x R(Rsin(\theta - x))}{V_a - z\pi x^2} \tag{22}$$

In practice, targeted Bond numbers were of order of ~0.15 to avoid too spherical drop shape leading to high uncertainties of γ (low w_b), and the dropping of the drop (high w_b).

3.2.2. Dilational rheology

The drop interface undergoes deformations consisting of a sinusoidal variation of the volume V leading to the deformation of the interfacial area A. Thus, the drop interface follows successive compression and dilation cycles resulting in variations of the interfacial tension with a phase angle Φ. Then, the dilational rheology can be characterized through the complex interfacial viscoelastic modulus E^*. The latter is derived from the change in interfacial tension γ resulting from the drop area fluctuation as followed:

$$\gamma = \gamma_0 \sin(\omega t + \Phi) \tag{23}$$

$$A = A_0 \sin(\omega t) \tag{24}$$

$$E^* = d\gamma/(dA/A) = d\gamma/dln(A) \tag{25}$$

with ω the oscillation frequency. The resulting interfacial viscoelastic modulus E^* is a complex number, with a real part E', corresponding to the stored elastic energy, and an imaginary part E", corresponding to the dissipative viscous energy.

$$E^* = |E|\cos(\Phi) + i|E|\sin(\Phi) \tag{26}$$

$$E' = |E|\cos(\Phi) \tag{27}$$

$$E'' = |E|\sin(\Phi) \tag{28}$$

4. Liquid – liquid interfaces: water in interaction with hydrophobic surfaces

4.1. The water interfacial depletion zone

A number of reviews and studies focused on water interactions with hydrophobic surfaces, e.g. [62]–[70]. They revealed the existence of a 1-6 Å water density depletion zone [69], [71], [72], occurring at the interface of water and of macroscopic hydrophobic solute. This so-called hydrophobic gap would show water vapor characteristics [64] and pronounced density fluctuations [70], [72]. This was recently supported through high-resolution Raman spectroscopy analyses of water around large solutes, revealing an increasing population of dangling OH bonds very similar to high temperature bulk water [73].

4.2. On the role of water in interfacial physics

4.2.1. Interest of volumetric properties

Dispersibility and interfacial properties of biopolymers, two significant functional properties of Acacia gums, are in general determined both by intrinsic properties of macromolecules (composition, accessibility and spatial division of charged, polar and nonpolar atomic groups, chain density, molar mass, molar volume, conformation, number, shape and dynamic of inner cavities) and their ability to dynamically interact with the solvent. On the other hand, volumetric properties are thermodynamic properties that have been linked to solute intrinsic molecular properties and solute-solvent interactions, more specifically solute flexibility and hydration [74]. Thus, volumetric properties of biopolymers are important determinants of their functionality. Another advantage is that they allow descriptions of thermodynamic macroscopic properties, such as the isothermal and adiabatic compressibility and the partial specific volume, in terms of microscopic volumes and their dynamic fluctuations [75].

4.2.2. The dynamic two-phase structure of water

Water is a transiently connected network of molecules through Lifshitz–van der Waals (LW), Lewis acid–base (AB) and electrical double layer (EL) non-covalent interactions [76]. The AB forces or electron–acceptor/electron–donor interactions are quantitatively predominant and are responsible for the hydrophobic effect, *i.e.* the molecular attraction caused by changes in

hydrogen bond-related (AB) free energy of cohesion between water molecules which surround molecules or particles when they are immersed in water [76]. Sun described a water model [77] with a two-phase structure, preferentially tetrahedrally-coordinated, and with a strong correlated and fluctuating network. Accordingly, the two structures share the same geometry but hold different H-O bond lengths transiting cooperatively as illustrated in Fig. I.4. The proton serves as the coordination origin of asymmetrical and short–range interactions with on the left side the intermolecular weaker O:H nonbond also called van der Waals bond with a ~10 kJ.mol^{-1} energy, and on the right side the intramolecular stronger H–O polar covalent bond with an energy of ~40 kJ.mol^{-1}.

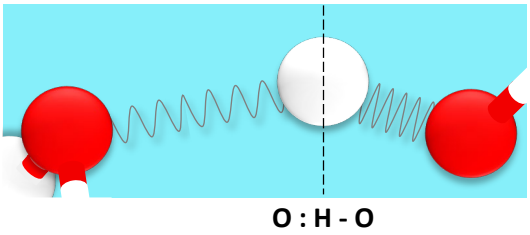

Fig. I.4. O:H-O intramolecular bonds according to Sun, on the left side the O:H nonbond, on the right side the H–O polar covalent bond.

According to this model, a H_2O molecular coordination number less than four will result in the H:O elongation associated with the H–O bond contraction (combined with a strong polarization of the H:O bond and vibration frequency transitions).

4.2.3. A 3D-approach of protein adsorption to hydrophobic interfaces

Vogler developed in 2012 a 3D-approach of the proteins adsorption process on hydrophobic surfaces that outline the role of the solvent, *i.e.* water [52]. The model divides in four main steps: (A) instantaneous creation of a thin pseudo-2D interface between adsorbent (physical surface) and protein dispersion (bulk solution); (B) rapid diffusion of proteins from solution into an inflating 3D-interphase region with concomitant displacement of interphase water; (C) reorganization and concentration of protein within an interphase that is shrinking by expulsion of interphase water (D) attainment of steady-state interphase protein concentration by entrapment of initially adsorbed protein in a minimal volume interphase (Fig. I.5).

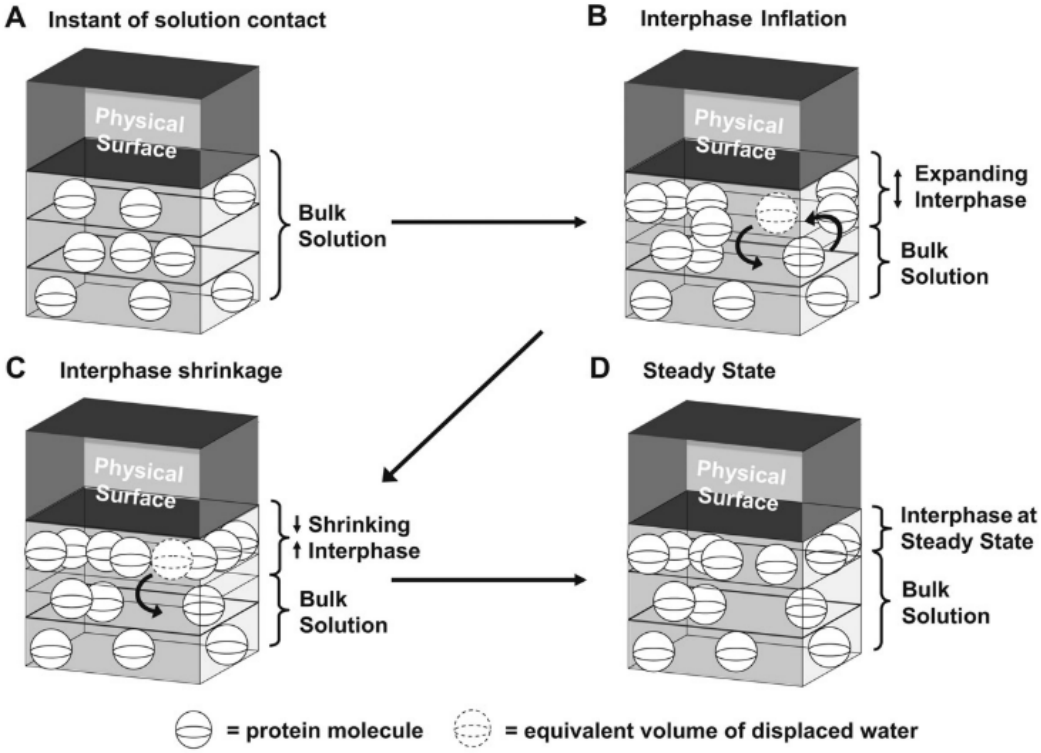

Fig. I.5. Graphical illustration of the kinetics of single-protein adsorption on a hydrophobic adsorbent interface. Adapted from Vogler 2012 [78].

The approach directly presupposes that changes in hydrogen-bonding structure induced by contact with surfaces have a significant effect on the interfacial water properties, which in turn influence the interfacial interaction dynamics of proteins.

5. Generalities on Acacia gum interfacial properties

5.1. GA interfacial rheological behavior and similarities with proteins, polymers and microgels

Interfacial properties of AGPs have been attributed to the protein moiety, high-molecular-weight AGP content as well as the structural accessibility of proteins, the molecular weight distribution, and the AGP flexibility [9], [10], [20], [79]. All these parameters allow interfacial AGPs adsorption and structural rearrangements and spreading. This leads to the decrease of the interfacial tension and the formation of a viscoelastic barrier [80], [81] that displays at equilibrium almost perfectly elastic structure [47], [81], [82]. Effect of physicochemical parameters such as pH, ionic strength, GA concentration and dispersion viscosity upon GA interfacial properties were thoroughly examined. This contributed to better understand interfacial structuring mechanism and interface structure [83], [84], [83], [85]–[89]. The

adsorption of GA can be compared to the adsorption of some proteins: globular proteins, such as β-lactoglobulin (BLG), bovine serum albumin (BSA), human serum albumin (HSA) and hen egg white lysozyme (LSZ), but also of random coil proteins, whey proteins or myofibrillar proteins [57], [58], [90]–[96]. All researches describe an adsorption process in three steps, which however does not mention any particular role of the solvent:

- the diffusion of the protein from the aqueous phase onto the interface driven by a concentration gradient,

- the penetration step,

- the aggregation step or rearrangement within the interfacial layer leading to a multilayer formation.

This 3-step rheological behavior has also been observed for other amphiphilic polymers such as microgels and polyelectrolytes, if the electrostatic interactions between the segments are shielded by the addition of inorganic salt [97]–[101]. Thus, although AGPs are mostly hydrophilic solutes due to their high sugar content [9] and the specific amino acid composition rich in hydrophilic species [9], [19], [20], they are sensitive to the hydrophobic effect. The last point was noticed by Goodrum et al. [102] who interrogate the possible implication of the secondary structure of hyperbranched sugar units in interfacial properties of the gums.

5.2. Oil hydrophobicity effect on interfacial properties

A few studies focused on the influence of the oil hydrophobicity on interfacial properties. For instance, the oil-GA-water interfacial tension has been examined and found to decrease with the decrease of the oil hydrophobicity until reaching a certain value insufficient for strong GA adsorption and resistance of droplets to coalescence [48]. Studies on globular and myofibrillar proteins also considered the impact of oil hydrophobicity on the structural rearrangement of interfacial proteins, revealing that larger oil hydrophobicity leads to stronger adsorption and elasticity of interfacial layers [57], [58], [90], [103]. They also highlighted a dependency between the interfacial tension and dilational rheology and the oil hydrophobicity for globular and flexible proteins [57], [58]. The former was also observed for surfactants and anisotropic charged nanoparticles [104]. Likewise, the surface load, the diffusion rate and the rearrangement rate were suggested to increase with the increase of the oil hydrophobicity [103].

6. Emulsion homogenization and stability

6.1. Emulsification process

Emulsions are produced by applying a mechanical energy to the two liquids involved. The interface between the two liquids is then deformed until droplets are formed. In order for droplet disruption to occur, the external stress applied must be of the same order of magnitude as the dispersed liquid cohesion forces. Several procedures can be used for emulsification. For instance, high-speed mixers, colloid mills, high-pressure homogenizers, and ultrasound generators [105], [106]. In addition, the selected choice of emulsification process is important as it plays a significant role on emulsification stability through its influence on the characteristic times of the emulsifier adsorption and its coverage degree of oil-water interfaces [107]. In addition, parameters of emulsification process such as the microfluidizer pressure and the number of passes are determining factors influencing the final droplet diameter [89], [108].

During this Ph.D., the oil-in-water emulsions were homogenized in two steps (Fig. I.6). The primary homogenization consisted of the conversion of two bulk liquids into a coarse emulsion. The secondary homogenization consisted of the reduction of droplets size (~1 µm) to obtain a fine emulsion.

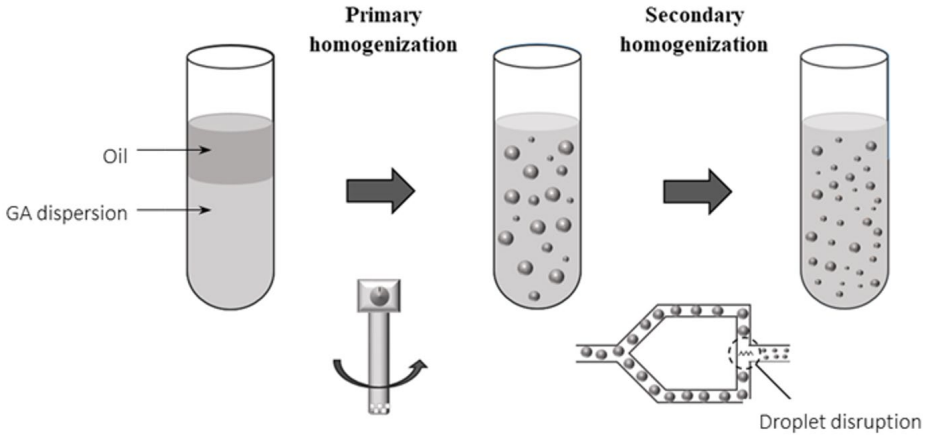

Fig I.6. Homogenization process of the Acacia gum stabilized oil-in-water emulsions; primary homogenization using a rotor/stator mixer, secondary homogenization using a microfluidizer.

The use of emulsifying agent allows the decrease of the interfacial tension between the two emulsion phases, leading to the decrease of the Laplace pressure and so, facilitating the creation of small droplets. Emulsifiers also result in the formation of an interfacial barrier, that can support droplets stabilization by limiting them to form larger droplets, or even separate out as

a bulk phase. In the aggregate, emulsifiers promote the emulsification and lead to the delay of destabilization mechanisms [85], [106], [109], [110].

6.2. Destabilization mechanisms

Destabilization mechanisms include both reversible and irreversible phenomena such as gravitational separation (creaming/sedimentation), flocculation, coalescence, Ostwald ripening, and phase inversion (see Fig. 1 from General Introduction) [106], [107].

Gravitational separation takes place as soon as a gap of density between the dispersed droplets and the surrounding liquid, exists [106]. A net gravitational force acts upon droplets which leads droplets to move upward (creaming) when the dispersed phase density is lower than the continuous phase density. Conversely, droplets move downward (sedimentation) if dispersed phase density is higher than the continuous phase density. Flocculation is the clustering of individual dispersed droplets together, without losing droplet individual identity [111]. It can also consist of the initial step leading to further aging of the emulsion (droplet coalescence, phase separation). Then, coalescence is the merging of two droplets into a single one, related to the thinning and rupture of the interfacial barrier [107]. Thus, it is strongly influenced by the interfacial properties of the adsorbed emulsifier layers. Coalescence in emulsions may occur when moving droplets get in contact or as consequent to their flocculation. Finally, the Ostwald ripening process originates from the higher Laplace pressure inside small droplets, driving the transfer of dispersed oil from small to large droplets [112]. It is therefore affected by the oil hydrophobicity, the solubility of the dispersed oil in the aqueous continuous phase, its diffusion coefficient and its density. For instance, oils which are slightly water-soluble can transfer between droplets at significant rates whereas Ostwald ripening can be negligibly slow for oils of sufficiently low aqueous phase solubility. This was supported experimentally [48].

The above destabilization processes are all interconnected and may influence each other during the emulsion aging [107]. Gravitational separation and flocculation tend to make more compact the droplet population and consequently may accelerate the processes of flocculation and coalescence. On the other side, flocculation, coalescence and Ostwald ripening tend to quicken the creaming process and eventually the complete destabilization of the emulsion. In the interest of improving Acacia gum emulsification conditions and the poor emulsion stability, SUPER GUMs, mixtures of emulsifiers and/or weighting agents are used [47], [110], [113]–[115].

6.3. Oil hydrophobicity effect

As for interfacial properties, a few studies focused on the role of the oil phase on emulsion formation and stabilization [13], [48], [85]. For instance, Chanamai and coworkers [48] evaluated the influence of oil polarity and solubility (hexadecane, decanol, decane, and decanol:hexadecane blends) on Oswald ripening and coalescence. They reported GA emulsions of nonpolar and water insoluble oil (hexadecane) were quite stable over time, while emulsions based on an oil phase having higher polarity and solubility (decanol) were very unstable with both Ostwald Ripening and coalescence occurring. Then, emulsions of low polarity but weaker solubility than decanol (decane) were stable to coalescence but not to Oswald Ripening. In addition, oil-water interfacial tension was also found to influence the droplet emulsion size, such as n-hexadecane-in-water emulsions displayed the smallest droplets compared to emulsions of lower oil-water interfacial tension oils, namely d-limonene and orange oil [13]. However, the oil viscosity is also a strong parameter affecting emulsions droplet size during homogenization and must not be forgotten [85], [110], [116].

7. References

[1] D. Verbeken, S. Dierckx, and K. Dewettinck, "Exudate gums: Occurrence, production, and applications," *Appl. Microbiol. Biotechnol.*, vol. 63, no. 1, pp. 10–21, 2003, doi: 10.1007/s00253-003-1354-z.

[2] D. M. W. Anderson, D. M. Brown Douglas, N. A. Morrison, and W. Weiping, "Specifications for gum arabic (Acacia senegal); analytical data for samples collected between 1904 and 1989," *Food Addit. Contam.*, vol. 7, no. 3, pp. 303–321, 1990, doi: 10.1080/02652039009373896.

[3] O. H. M. Idris, P. A. Williams, and G. O. Phillips, "Characterisation of gum from Acacia senegal trees of different age and location using multidetection gel permeation chromatography," *Food Hydrocolloids*, vol. 12, no. 4. pp. 379–388, 1998, doi: 10.1016/S0268-005X(98)00058-7.

[4] A. M. Islam, G. O. Phillips, A. Sljivo, M. J. Snowden, and P. A. Williams, "A review of recent developments on the regulatory, structural and functional aspects of gum arabic," *Food Hydrocoll.*, vol. 11, no. 4, pp. 493–505, 1997, doi: 10.1016/S0268-005X(97)80048-3.

[5] S. Al-Assaf, G. O. Phillips, and P. A. Williams, "Studies on acacia exudate gums. Part I: The molecular weight of Acacia senegal gum exudate," *Food Hydrocoll.*, vol. 19, no. 4, pp. 647–660, 2005, doi: 10.1016/j.foodhyd.2004.09.002.

[6] C. Sanchez *et al.*, "Acacia gum: History of the future," *Food Hydrocoll.*, vol. 78, pp. 140–160, 2018, doi: 10.1016/j.foodhyd.2017.04.008.

[7] L. Lopez-Torrez, M. Nigen, P. Williams, T. Doco, and C. Sanchez, "Acacia senegal vs. Acacia seyal gums - Part 1: Composition andstructure of hyperbranched plant exudates," *Food Hydrocoll.*, vol. 51, no. April, pp. 41–53, 2015, doi: 10.1016/j.foodhyd.2015.04.019.

[8] D. Renard, L. Lavenant-Gourgeon, A.

Lapp, M. Nigen, and C. Sanchez, "Enzymatic hydrolysis studies of arabinogalactan-protein structure from Acacia gum: The self-similarity hypothesis of assembly from a common building block," *Carbohydr. Polym.*, vol. 112, pp. 648–661, 2014, doi: 10.1016/j.carbpol.2014.06.041.

[9] A. Davantès, M. Nigen, C. Sanchez, A. d'Orlando, and D. Renard, "Adsorption of Hyperbranched Arabinogalactan-Proteins from Plant Exudate at the Solid–Liquid Interface," *Colloids and Interfaces*, vol. 3, no. 2, p. 49, 2019, doi: 10.3390/colloids3020049.

[10] M. Elmanan, S. Al-Assaf, G. O. Phillips, and P. A. Williams, "Studies on Acacia exudate gums: Part VI. Interfacial rheology of Acacia senegal and Acacia seyal," *Food Hydrocoll.*, vol. 22, no. 4, pp. 682–689, 2008, doi: 10.1016/j.foodhyd.2007.02.008.

[11] E. Dickinson, B. S. Murray, G. Stainsby, and D. M. W. Anderson, "Surface activity and emulsifying behaviour of some Acacia gums," *Top. Catal.*, vol. 2, no. 6, pp. 477–490, 1988, doi: 10.1016/S0268-005X(88)80047-X.

[12] R. Chanamai and D. J. McClements, "Comparison of gum arabic, modified starch, and whey protein isolate as emulsifiers: Influence of pH, CaCl2 and temperature," *J. Food Sci.*, vol. 67, no. 1, pp. 120–125, 2002, doi: 10.1111/j.1365-2621.2002.tb11370.x.

[13] E. Dickinson, V. B. Galazka, and D. M. W. Anderson, "Emulsifying behaviour of gum arabic. Part 1: Effect of the nature of the oil phase on the emulsion droplet-size distribution," *Carbohydr. Polym.*, vol. 14, no. 4, pp. 373–383, 1991, doi: 10.1016/0144-8617(91)90003-U.

[14] H. Mirhosseini, C. P. Tan, N. S. A. Hamid, and S. Yusof, "Effect of Arabic gum, xanthan gum and orange oil contents on ζ-potential, conductivity, stability, size index and pH of orange beverage emulsion," *Colloids Surfaces A Physicochem. Eng. Asp.*, 2008, doi: 10.1016/j.colsurfa.2007.07.007.

[15] C. Sanchez, C. Schmitt, E. Kolodziejczyk, A. Lapp, C. Gaillard, and D. Renard, "The acacia gum arabinogalactan fraction is a thin oblate ellipsoid: A new model based on small-angle neutron scattering and ab initio calculation," *Biophys. J.*, vol. 94, no. 2, pp. 629–639, 2008, doi: 10.1529/biophysj.107.109124.

[16] D. Renard, C. Garnier, A. Lapp, C. Schmitt, and C. Sanchez, "Structure of arabinogalactan-protein from Acacia gum: From porous ellipsoids to supramolecular architectures," *Carbohydr. Polym.*, vol. 90, no. 1, pp. 322–332, 2012, doi: 10.1016/j.carbpol.2012.05.046.

[17] D. Renard, C. Garnier, A. Lapp, C. Schmitt, and C. Sanchez, "Erratum: Structure of arabinogalactan-protein from Acacia gum: From porous ellipsoids to supramolecular architectures (Carbohydrate Polymers (2012) 90 (322-332))," *Carbohydr. Polym.*, vol. 97, no. 2, pp. 864–867, 2013, doi: 10.1016/j.carbpol.2013.05.006.

[18] D. Renard, E. Lepvrier, C. Garnier, P. Roblin, M. Nigen, and C. Sanchez, "Structure of glycoproteins from Acacia gum: An assembly of ring-like glycoproteins modules," *Carbohydr. Polym.*, vol. 99, pp. 736–747, 2014, doi: 10.1016/j.carbpol.2013.08.090.

[19] V. Mejia Tamayo *et al.*, "Flexibility and hydration of amphiphilic hyperbranched arabinogalactan-protein from plant exudate: A volumetric perspective," *Colloids and Interfaces*, vol. 2, no. 1, 2018, doi: 10.3390/colloids2010011.

[20] A. Davantès, M. Nigen, C. Sanchez, and D. Renard, "Adsorption Behavior of Arabinogalactan-Proteins (AGPs) fromAcacia senegalGum at a Solid-Liquid Interface," *Langmuir*, vol. 37, no. 35, pp. 10547–10559, 2021, doi: 10.1021/acs.langmuir.1c01619.

[21] L. Lopez Torrez, "Characterisation of acacia gum s and developm ent of heat-induced acacia gum /potato proteins m icroparticles," 2016.

[22] Verónica Meija Tamayo, "Propriétés volumétriques des Arabinogalactane-protéines d'exsudats de gommes d'Acacia,"

2018.

[23] J. Frenkel, "Kinetic Theory of Liquids," 1955.

[24] B. Widom, "Intermolecular Forces and the Nature of the Liquid State," *Science (80-.).*, vol. 157, no. 3787, pp. 375–382, 1967.

[25] D. Bolmatov, V. V. Brazhkin, and K. Trachenko, "The phonon theory of liquid thermodynamics," *Sci. Rep.*, vol. 2, pp. 1–6, 2012, doi: 10.1038/srep00421.

[26] D. Bolmatov, "The Phonon Theory of Liquids and Biological Fluids: Developments and Applications," *J. Phys. Chem. Lett.*, vol. 13, no. 31, pp. 7121–7129, 2022, doi: 10.1021/acs.jpclett.2c01779.

[27] J. N. Israelachvili, *Intermolecular and Surface Forces*. 2011.

[28] C. M. Lindsay and M. E. Fajardo, "The quest for greater chemical energy storage in energetic materials: Grounding expectations," *AIP Conf. Proc.*, vol. 1793, 2017, doi: 10.1063/1.4971517.

[29] Y. Marcus, *The Properties of Solvents*, John Wiley. The Hebrew University of Jerusalem, Israel, 1998.

[30] A. R. Van Buuren, S. J. Marrink, and H. J. C. Berendsen, "A molecular dynamics study of the decane/water interface," *J. Phys. Chem.*, vol. 97, no. 36, pp. 9206–9212, 1993, doi: 10.1021/j100138a023.

[31] J. S. Rowlinson and F. L. Swinton, *Liquids and liquid mixtures*, Butterwort. 1982.

[32] D. Stopper, H. Hansen-Goos, R. Roth, and R. Evans, "On the decay of the pair correlation function and the line of vanishing excess isothermal compressibility in simple fluids," *J. Chem. Phys.*, vol. 151, no. 1, pp. 1–13, 2019, doi: 10.1063/1.5110044.

[33] M. Chorazewski and E. B. Postnikov, "Thermal properties of compressed liquids: Experimental determination via an indirect acoustic technique and modeling using the volume fluctuations approach," *Int. J. Therm. Sci.*, vol. 90, pp. 62–69, 2015, doi: 10.1016/j.ijthermalsci.2014.11.028.

[34] M. J. Godfrey and M. A. Moore, "Absence of Hyperuniformity in Amorphous Hard-Sphere Packings of Nonvanishing Complexity," *Phys. Rev. Lett.*, vol. 121, no. 7, 2018, doi: 10.1103/PhysRevLett.121.075503.

[35] E. A. Ploetz and P. E. Smith, "Local fluctuations in solution: Theory and applications," *Adv. Chem. Phys.*, vol. 153, pp. 311–372, 2013, doi: 10.1002/9781118571767.ch4.

[36] K. Nygård *et al.*, "Density fluctuations of hard-sphere fluids in narrow confinement," *Phys. Rev. X*, vol. 6, no. 1, 2016, doi: 10.1103/PhysRevX.6.011014.

[37] E. A. Ploetz and P. E. Smith, "Local fluctuations in solution mixtures," *J. Chem. Phys.*, vol. 135, no. 4, pp. 1–8, 2011, doi: 10.1063/1.3615718.

[38] D. Siu and Y. Koga, "Fluctuation functions in aqueous NaCl and urea," *J. Phys. Chem. B*, vol. 109, no. 35, pp. 16886–16890, 2005, doi: 10.1021/jp0516792.

[39] Y. Koga, "Fluctuations in aqueous solutions of some hydrophobic solutes," *Chem. Phys. Lett.*, vol. 240, no. 4, pp. 340–344, 1995, doi: 10.1016/0009-2614(95)00531-8.

[40] A. . Soper, "Is water one liquid or two ?," *J. Chem. Phys.*, vol. 150, no. 234503, 2019, doi: 10.1063/1.5096460.

[41] G. Graziano, "Contrasting the hydration thermodynamics of methane and methanol," *Phys. Chem. Chem. Phys.*, vol. 21, no. 38, pp. 21418–21430, 2019, doi: 10.1039/c9cp03213d.

[42] R. A. Pierotti, "Aqueous Solutions of Nonpolar Gases," *J. Phys. Chem.*, vol. 69, pp. 281–288, 1965.

[43] European Commission, "Regulation (EC) No 1334/2008 on flavourings," *Off. J. Eur. Union, 2008*, vol. L 354/34, no. 1334, pp. 34–50, 2008.

[44] R. Watson, C. J. Wright, T. McBurney, A. J. Taylor, and R. S. T. Linforth, "Influence of harvest date and light integral on the development of strawberry flavour compounds," *J. Exp. Bot.*, vol. 53, no. 377, pp. 2121–2129, 2002, doi: 10.1093/jxb/erf088.

[45] H. Richard, "Arômes alimentaires," *Flavour Sci. Technol. (Proc. 5th Weurman Flavour Res. Symp.*, no. Figure 1, pp. 1–17, 1987, [Online]. Available: %5C%5CRobsrv-05%5Creference manager%5CArticles%5C4182.pdf.

[46] Viswanath, Ghosh, Prasad, Dutt, and Rani, *Viscosity of liquids*. 2007.

[47] O. Castellani, S. Al-Assaf, M. Axelos, G. O. Phillips, and M. Anton, "Hydrocolloids with emulsifying capacity. Part 2 - Adsorption properties at the n-hexadecane-Water interface," *Food Hydrocoll.*, vol. 24, no. 2–3, pp. 121–130, 2010, doi: 10.1016/j.foodhyd.2009.07.006.

[48] R. Chanamai, G. Horn, and D. J. McClements, "Influence of oil polarity on droplet growth in oil-in-water emulsions stabilized by a weakly adsorbing biopolymer or a nonionic surfactant," *J. Colloid Interface Sci.*, vol. 247, no. 1, pp. 167–176, 2002, doi: 10.1006/jcis.2001.8110.

[49] L. M. Pérez-Mosqueda, J. Maldonado-Valderrama, P. Ramírez, M. A. Cabrerizo-Vílchez, and J. Muñoz, "Interfacial characterization of Pluronic PE9400 at biocompatible (air-water and limonene-water) interfaces," *Colloids Surfaces B Biointerfaces*, vol. 111, pp. 171–178, 2013, doi: 10.1016/j.colsurfb.2013.05.029.

[50] A. H. Demond and A. S. Lindner, "Estimation of interfacial tension between organic liquid mixtures and water," *Environ. Sci. Technol.*, vol. 27, pp. 2318–2331, 1993, doi: 10.1021/es901061k.

[51] P. M. Florido *et al.*, "Viscosities and densities of systems involved in the deterpenation of essential oils by liquid-liquid extraction: New UNIFAC-VISCO parameters," *J. Chem. Thermodyn.*, vol. 72, pp. 152–160, 2014, doi: 10.1016/j.jct.2013.11.026.

[52] D. Li *et al.*, "Densities and viscosities for the ternary system of (ethylcyclohexane + 1-butanol + ethyl octanoate) and corresponding binary systems at T = (293.15–323.15) K," *J. Chem. Thermodyn.*, vol. 150, p. 106173, 2020, doi: 10.1016/j.jct.2020.106173.

[53] X. Wang *et al.*, "Viscosity measurement and correlation research of one biodiesel component (methyl octanoate) with five 1-alcohols," *Fuel*, vol. 324, no. PA, p. 124441, 2022, doi: 10.1016/j.fuel.2022.124441.

[54] F. A. Jabalpurwala, J. M. Smoot, and R. L. Rouseff, "A comparison of citrus blossom volatiles," *Phytochemistry*, vol. 70, no. 11–12, pp. 1428–1434, 2009, doi: 10.1016/j.phytochem.2009.07.031.

[55] Y. Shahbazi, "Chemical Composition and In Vitro Antibacterial Activity of Mentha spicata Essential Oil against Common Food-Borne Pathogenic Bacteria," *J. Pathog.*, 2015, doi: 10.1155/2015/916305.

[56] R. Mannhold and R. F. Rekker, "The hydrophobic fragmental constant approach for calculating log P in octanol/water and aliphatic hydrocarbon/water systems," *Perspect. Drug Discov. Des.*, vol. 18, pp. 1–18, 2000, doi: 10.1023/A:1008782809845.

[57] J. Bergfreund *et al.*, "Globular protein assembly and network formation at fluid interfaces: effect of oil," *Soft Matter*, pp. 1692–1700, 2021, doi: 10.1039/d0sm01870h.

[58] J. Bergfreund, P. Bertsch, and P. Fischer, "Adsorption of proteins to fluid interfaces: Role of the hydrophobic subphase," *J. Colloid Interface Sci.*, vol. 584, pp. 411–417, 2021, doi: 10.1016/j.jcis.2020.09.118.

[59] J. W. Gibbs, *The collected works of J.W. Gibbs. Longsmann*. Green and Co, 1931.

[60] C. Della Volpe and S. Siboni, "From van der Waals equation to acid-base theory of surfaces: A chemical-mathematical journey," *Rev. Adhes. Adhes.*, vol. 10, no. 1, pp. 47–97, 2022, doi: 10.47750/RAA/10.1.02.

[61] M. Rayner and P. Dejmek, *Engineering aspects of food emulsification and Homogenization*, CRC Press. 2015.

[62] S. Bekele and M. Tsige, "Characterizing the Hydrophobicity of Surfaces Using the Dynamics of Interfacial Water Molecules," *J. Phys. Chem. C*, vol. 122, no. 16, pp. 9015–9020, 2018, doi: 10.1021/acs.jpcc.8b01353.

[63] F. Bresme, E. Chacón, P. Tarazona, and K. Tay, "Intrinsic structure of hydrophobic surfaces: The oil-water interface," *Phys.*

Rev. Lett., vol. 101, no. 5, pp. 1–4, 2008, doi: 10.1103/PhysRevLett.101.056102.

[64] M. K. Coe, R. Evans, and N. B. Wilding, "Density Depletion and Enhanced Fluctuations in Water near Hydrophobic Solutes: Identifying the Underlying Physics," *Phys. Rev. Lett.*, vol. 128, no. 4, p. 45501, 2022, doi: 10.1103/physrevlett.128.045501.

[65] A. J. Patel, P. Varilly, D. Chandler, and S. Garde, "Quantifying Density Fluctuations in Volumes of All Shapes and Sizes Using Indirect Umbrella Sampling," *J. Stat. Phys.*, vol. 145, no. 2, pp. 265–275, 2011, doi: 10.1007/s10955-011-0269-9.

[66] R. Godawat, S. N. Jamadagni, and S. Garde, "Characterizing hydrophobicity of interfaces by using cavity formation, solute binding, and water correlations," *Proc. Natl. Acad. Sci. U. S. A.*, vol. 106, no. 36, pp. 15119–15124, 2009, doi: 10.1073/pnas.0902778106.

[67] N. B. Rego and A. J. Patel, "Understanding Hydrophobic Effects: Insights from Water Density Fluctuations," *Annu. Rev. Condens. Matter Phys.*, vol. 13, no. 1, pp. 303–324, 2022, doi: 10.1146/annurev-conmatphys-040220-045516.

[68] M. C. Bellissent-Funel *et al.*, "Water Determines the Structure and Dynamics of Proteins," *Chem. Rev.*, vol. 116, no. 13, pp. 7673–7697, 2016, doi: 10.1021/acs.chemrev.5b00664.

[69] U. Kumar Sur, "Behaviour of water at hydrophobic interfaces," *J. Mol. Liq.*, vol. 348, p. 118433, 2022, doi: 10.1016/j.molliq.2021.118433.

[70] S. N. Jamadagni, R. Godawat, and S. Garde, "Hydrophobicity of proteins and interfaces: Insights from density fluctuations," *Annu. Rev. Chem. Biomol. Eng.*, vol. 2, pp. 147–171, 2011, doi: 10.1146/annurev-chembioeng-061010-114156.

[71] V. R. Hande and S. Chakrabarty, "How Far Is 'Bulk Water' from Interfaces? Depends on the Nature of the Surface and What We Measure," *J. Phys. Chem. B*, vol. 126, no. 5, pp. 1125–1135, 2022, doi: 10.1021/acs.jpcb.1c08603.

[72] C. Sendner, D. Horinek, L. Bocquet, and R. R. Netz, "Interfacial water at hydrophobic and hydrophilic surfaces: Slip, viscosity, and diffusion," *Langmuir*, vol. 25, no. 18, pp. 10768–10781, 2009, doi: 10.1021/la901314b.

[73] V. Hande and S. Chakrabarty, "Size-Dependent Order–Disorder Crossover in Hydrophobic Hydration: Comparison between Spherical Solutes and Linear Alcohols," *ACS Omega*, vol. 7, no. 3, pp. 2671–2678, 2022, doi: 10.1021/acsomega.1c05064.

[74] T. V. Chalikian and R. Filfil, "How large are the volume changes accompanying protein transitions and binding?," *Biophys. Chem.*, vol. 104, no. 2, pp. 489–499, 2003, doi: 10.1016/S0301-4622(03)00037-1.

[75] T. V. Chalikian, J. Völker, A. R. Srinivasan, W. K. Olson, and K. J. Breslauer, "The hydration of nucleic acid duplexes as assessed by a combination of volumetric and structural techniques," *Biopolymers*, vol. 50, no. 5, pp. 459–471, 1999, doi: 10.1002/(SICI)1097-0282(19991015)50:5<459::AID-BIP1>3.0.CO;2-B.

[76] C. J. Van Oss, "Long-range and short-range mechanisms of hydrophobic attraction and hydrophilic repulsion in specific and aspecific interactions," *J. Mol. Recognit.*, vol. 16, no. 4, pp. 177–190, 2003, doi: 10.1002/jmr.618.

[77] C. Q. Sun, "Supersolidity of undercoordinated and hydrating water," *Phys. Chem. Chem. Phys.*, vol. 20, no. 48, pp. 30104–30119, 2018, doi: 10.1039/c8cp06115g.

[78] E. A. Vogler, "Protein adsorption in three dimensions," *Biomaterials*, vol. 33, no. 5, pp. 1201–1237, 2012, doi: 10.1016/j.biomaterials.2011.10.059.

[79] R. C. Randall, G. O. Phillips, and P. A. Williams, "Fractionation and characterization of gum from Acacia senegal," *Top. Catal.*, vol. 3, no. 1, pp. 65–75, 1989, doi: 10.1016/S0268-005X(89)80034-7.

[80] Q. Jin, X. Li, Z. Cai, F. Zhang, M. P. Yadav, and H. Zhang, "A comparison of

corn fiber gum, hydrophobically modified starch, gum arabic and soybean soluble polysaccharide: Interfacial dynamics, viscoelastic response at oil/water interfaces and emulsion stabilization mechanisms," *Food Hydrocoll.*, vol. 70, pp. 329–344, 2017, doi: 10.1016/j.foodhyd.2017.03.005.

[81] P. Erni *et al.*, "Interfacial rheology of surface-active biopolymers: Acacia senegal gum versus hydrophobically modified starch," *Biomacromolecules*, vol. 8, no. 11, pp. 3458–3466, 2007, doi: 10.1021/bm700578z.

[82] C. Sanchez *et al.*, "Acacia gum: History of the future," *Food Hydrocoll.*, vol. 78, pp. 140–160, 2018, doi: 10.1016/j.foodhyd.2017.04.008.

[83] S. R. Padala, P. A. Williams, and G. O. Phillips, "Adsorption of Gum Arabic, Egg White Protein, and Their Mixtures at the Oil-Water Interface in Limonene Oil-in-Water Emulsions," *J. Agric. Food Chem.*, vol. 57, no. 11, pp. 4964–4973, 2009, doi: 10.1021/jf803794n.

[84] M. Atgié, O. Masbernat, and K. Roger, "Emulsions Stabilized by Gum Arabic: Composition and Packing within Interfacial Films," *Langmuir*, vol. 35, no. 4, pp. 962–972, 2019, doi: 10.1021/acs.langmuir.8b02715.

[85] S. J. Reiner, G. A. Reineccius, and T. L. Peppard, "A comparison of the stability of beverage cloud emulsions formulated with different gum acacia- and starch-based emulsifiers," *J. Food Sci.*, vol. 75, no. 5, 2010, doi: 10.1111/j.1750-3841.2010.01625.x.

[86] R. M. A. Mansour and E. A. Hassan, "Effect of gum concentration and gum protein concentration on emulsifying properties of some Acacia gums," *Int. J. basic Appl. Chem. Sci.*, vol. 6, no. 2, pp. 23–35, 2016.

[87] C. Aphibanthammakit, "Propriétés interfaciales et émulsifiantes de gommes d'Acacia senegal, Acacia seyal et de leurs fractions," 2018.

[88] L. Han *et al.*, "Effect of arabinogalactan protein complex content on emulsification performance of gum arabic," *Carbohydr. Polym.*, vol. 224, no. August, p. 115170, 2019, doi: 10.1016/j.carbpol.2019.115170.

[89] J. Zhang, T. L. Peppard, and G. A. Reineccius, "Preparation and characterization of nanoemulsions stabilized by food biopolymers using microfluidization," *Flavour Fragr. J.*, vol. 30, no. 4, pp. 288–294, 2015, doi: 10.1002/ffj.3244.

[90] J. Bergfreund, P. Bertsch, S. Kuster, and P. Fischer, "Effect of Oil Hydrophobicity on the Adsorption and Rheology of β-Lactoglobulin at Oil-Water Interfaces," *Langmuir*, vol. 34, no. 16, pp. 4929–4936, 2018, doi: 10.1021/acs.langmuir.8b00458.

[91] E. H. Lucassen-Reynders, J. Benjamins, and V. B. Fainerman, "Dilational rheology of protein films adsorbed at fluid interfaces," *Curr. Opin. Colloid Interface Sci.*, vol. 15, no. 4, pp. 264–270, 2010, doi: 10.1016/j.cocis.2010.05.002.

[92] V. B. Fainerman *et al.*, "Dilational Viscoelasticity of Proteins Solutions in Dynamic Conditions," *Langmuir*, vol. 34, no. 23, pp. 6678–6686, 2018, doi: 10.1021/acs.langmuir.8b00631.

[93] N. A. Alexandrov *et al.*, "Interfacial layers from the protein HFBII hydrophobin: Dynamic surface tension, dilatational elasticity and relaxation times," *J. Colloid Interface Sci.*, vol. 376, no. 1, pp. 296–306, 2012, doi: 10.1016/j.jcis.2012.03.031.

[94] F. MacRitchie and A. Alexander, "Kinetics of adsorption of proteins at interfaces. Part I. The role of bulk diffusion in adsorption," *J. Colloid Sci.*, vol. 18, no. 5, pp. 458–463, 1963, [Online]. Available: http://www.sciencedirect.com/science/article/pii/0095852263900370%5Cnhttp://www.sciencedirect.com/science/article/pii/0095852263900369.

[95] E. M. Freer, K. S. Yim, G. G. Fuller, and C. J. Radke, "Shear and dilatational relaxation mechanisms of globular and flexible proteins at the hexadecane/water interface," *Langmuir*, vol. 20, no. 23, pp. 10159–10167, 2004, doi: 10.1021/la0485226.

[96] C. J. Beverung, C. J. Radke, and H. W. Blanch, "Protein adsorption at the oil/water interface: Characterization of

adsorption kinetics by dynamic interfacial tension measurements," *Biophys. Chem.*, vol. 81, no. 1, pp. 59–80, 1999, doi: 10.1016/S0301-4622(99)00082-4.

[97] B. A. Noskov, A. V. Akentiev, and R. Miller, "Dynamic surface properties of poly(vinylpyrrolidone) solutions," *J. Colloid Interface Sci.*, vol. 255, no. 2, pp. 417–424, 2002, doi: 10.1006/jcis.2002.8614.

[98] B. A. Noskov *et al.*, "Dynamic surface properties of poly(N-isopropylacrylamide) solutions," *Langmuir*, vol. 20, no. 22, pp. 9669–9676, 2004, doi: 10.1021/la048836t.

[99] B. A. Noskov, "Protein conformational transitions at the liquid-gas interface as studied by dilational surface rheology," *Adv. Colloid Interface Sci.*, vol. 206, pp. 222–238, 2014, doi: 10.1016/j.cis.2013.10.024.

[100] F. Pinaud *et al.*, "Adsorption of microgels at an oil-water interface: Correlation between packing and 2D elasticity," *Soft Matter*, vol. 10, no. 36, pp. 6963–6974, 2014, doi: 10.1039/c4sm00562g.

[101] N. Nussbaum, J. Bergfreund, J. Vialetto, L. Isa, and P. Fischer, "Microgels as globular protein model systems," *Colloids Surfaces B Biointerfaces*, vol. 217, no. May, p. 112595, 2022, doi: 10.1016/j.colsurfb.2022.112595.

[102] L. J. Goodrum, A. Patel, J. F. Leykam, and M. J. Kieliszewski, "Gum arabic glycoprotein contains glycomodules of both extensin and arabinogalactan-glycoproteins," *Phytochemistry*, vol. 54, no. 1, pp. 99–106, 2000, doi: 10.1016/S0031-9422(00)00043-1.

[103] W. Zhang, X. Xu, X. Zhao, and G. Zhou, "Insight into the oil polarity impact on interfacial properties of myofibrillar protein," *Food Hydrocoll.*, vol. 128, no. January, p. 107563, 2022, doi: 10.1016/j.foodhyd.2022.107563.

[104] J. Bergfreund, P. Bertsch, and P. Fischer, "Effect of the hydrophobic phase on interfacial phenomena of surfactants, proteins, and particles at fluid interfaces," *Curr. Opin. Colloid Interface Sci.*, vol. 56, p. 101509, 2021, doi: 10.1016/j.cocis.2021.101509.

[105] T. F. T. Ed, *Emulsion Science and Technology*, Tharwat F. 2009.

[106] D. J. McCLements, *Food Emulsions Principles, Practices, and Techniques*. 2010.

[107] F. Ravera, K. Dziza, E. Santini, L. Cristofolini, and L. Liggieri, "Emulsification and emulsion stability: The role of the interfacial properties," *Adv. Colloid Interface Sci.*, vol. 288, p. 102344, 2021, doi: 10.1016/j.cis.2020.102344.

[108] S. M. Jafari, Y. He, and B. Bhandari, "Production of sub-micron emulsions by ultrasound and microfluidization techniques," *J. Food Eng.*, vol. 82, no. 4, pp. 478–488, 2007, doi: 10.1016/j.jfoodeng.2007.03.007.

[109] E. Dickinson, V. B. Galazka, and D. M. W. Anderson, "Emulsifying behaviour of gum arabic. Part 2: Effect of the Gum Molecular Weight on the Emulsion Droplet-size," *Carbohydr. Polym.*, vol. 14, no. 4, pp. 373–383, 1991, doi: 10.1016/0144-8617(91)90003-U.

[110] R. Chanamai and D. J. McClements, "Impact of weighting agents and sucrose on gravitational separation of beverage emulsions," *J. Agric. Food Chem.*, vol. 48, no. 11, pp. 5561–5565, 2000, doi: 10.1021/jf0002903.

[111] A. Adamson and A. Gast, *Physical chemistry of surfaces*. 1997.

[112] I. Capek, "Degradation of kinetically-stable o/w emulsions," *Adv. Colloid Interface Sci.*, vol. 107, no. 2–3, pp. 125–155, 2004, doi: 10.1016/S0001-8686(03)00115-5.

[113] H. Aoki, T. Katayama, T. Ogasawara, Y. Sasaki, S. Al-Assaf, and G. O. Phillips, "Characterization and properties of Acacia senegal (L.) Willd. var. Senegal with enhanced properties (Acacia (sen) SUPER GUM^{TM}): Part 5. Factors affecting the emulsification of Acacia senegal and Acacia (sen) SUPER GUM^{TM}," *Food Hydrocoll.*, vol. 21, no. 3, pp. 353–358, 2007, doi: 10.1016/j.foodhyd.2006.04.014.

[114] Q. Wang, W. Burchard, S. W. Cui, X. Huang, and G. O. Phillips, "Solution properties of conventional gum arabic and

a matured gum arabic (Acacia (sen) SUPER GUM)," *Biomacromolecules*, vol. 9, no. 4, pp. 1163–1169, 2008, doi: 10.1021/bm7011696.

[115] X. Xu, Q. Sun, and D. J. McClements, "Enhancing the formation and stability of emulsions using mixed natural emulsifiers: Hydrolyzed rice glutelin and quillaja saponin," *Food Hydrocoll.*, vol. 89, no. September 2018, pp. 396–405, 2019, doi: 10.1016/j.foodhyd.2018.11.020.

[116] J. Zhang, T. L. Peppard, and G. A. Reineccius, "Preparation and characterization of nanoemulsions stabilized by food biopolymers using microfluidization," *Flavour Fragr. J.*, vol. 30, no. 4, pp. 288–294, 2015, doi: 10.1002/ffj.3244.

Chapter II: Thermodynamic properties of liquids

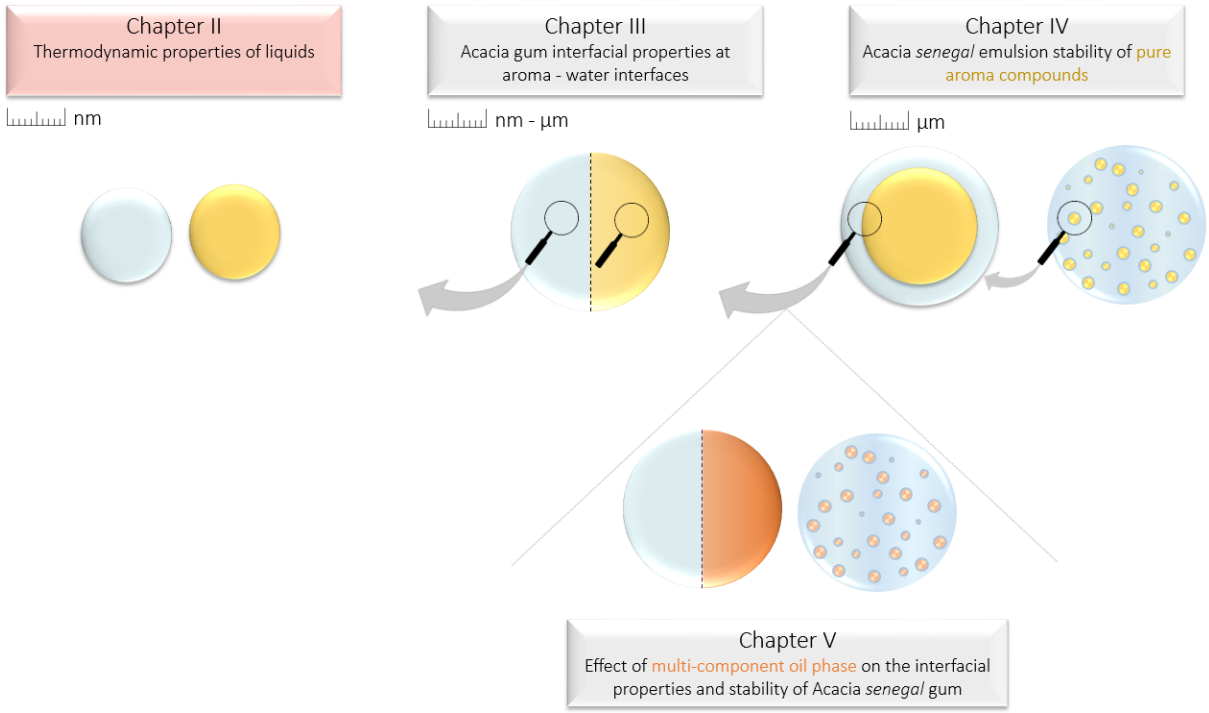

This chapter aimed to study the thermodynamic properties, in particular the volumetric properties of liquids in order to explore the fundamental differences between both phases of Acacia gum emulsions, *i.e.* water and hydrophobic compounds, in terms of volume fluctuations and interaction energy. To this end, we took interest in liquid structure through microscopic volume fluctuations. In addition, we intended to examine the relationship between volume fluctuations and the Gibbs free energy of cavity formation which is part of the solvation process. This led to the confirmation by calculations of the already foreseen relationship between the isothermal compressibility of liquids and the work of cavity formation.

Highlights

- Data gathering of the isothermal compressibility, the volume fluctuations and the work of cavity creation of 200 liquids.

- Identification of a relation between the work of cavity creation in liquids and the latter average density fluctuations.

- Modification proposition of the relation between the isothermal compressibility of liquids and the work of cavity creation.

On the relationship between volume fluctuations in liquids and the Gibbs free energy of cavity formation[1]

Camille Faucon[a], Pascale Chalier[a], Christian Sanchez[a]

[a] IATE, Univ Montpellier, INRAE, Institut Agro, Montpellier, France.

Abstract

Microscopic volume fluctuations in liquids are a reflection of their structure and intermolecular energy. Microscopic volume fluctuations in liquids are associated with cavity formation. The latter is considered of fundamental importance for the solvation process. The relationship between volume fluctuations and cavity formation is investigated in the present study. Scaled particle theory calculations provide a relationship between the Gibbs free energy of cavity formation and the average density fluctuations in volume at 298 K. The already foreseen correlation between the Gibbs free energy of cavity formation and the isothermal compressibility is confirmed and adjusted using no less than 200 liquids, covering a large category of organic compounds, plus water.

Keywords: liquids; isothermal compressibility; Gibbs free energy of cavity formation; microscopic volume fluctuations; Scaled Particle Theory

1. Introduction

Characterizing the structure of a liquid has long been of great interest to gain knowledge of the origin of many-body condensed-matter phenomena. At microscopic scales, attractive intermolecular interactions ensure liquid cohesion. The latter is generally represented by thermodynamic parameters such as the internal pressure P_i, or the cohesive energy density

[1]Article published in Journal of Molecular Liquids, https://doi.org/10.1016/j.molliq.2022.119845

CED [1]–[4]. P_i is defined as the resultant of attraction and repulsion forces between liquid molecules, while CED, which is based on the vaporization enthalpy and molar volume, is a measure of liquid stiffness. Another parameter that measures the liquid stiffness is the isothermal compressibility β_T. The latter accounts for volume fluctuations induced by pressure fluctuations [$\beta_T = -\frac{1}{V}\left(\frac{\delta V}{\delta P}\right)_T$]. Moreover, the isothermal compressibility accounts for the balance of repulsive and attractive interaction forces which govern the form of the pair and high order correlation functions [5]. Indeed, β_T is directly related to the total correlation function $h(r)$ (r being the distance between the centers of a pair of interacting molecules) through

$$\rho k_B T \beta_T = 1 + 4\pi\rho \int_0^\infty dr\, r^2 h(r) \tag{1}$$

The correlation function describes the correlating effect of the presence of one molecule on the position of a second molecule [6]. Note that $(\rho k_B T)^{-1}$ is the compressibility of an ideal gas. The parameter $\rho k_B T \beta_T$ is the structure factor as wave vector tends to zero, and characterizes the strength of intermolecular interactions, the regularity of fluid's structure and more generally the structural complexity per particle [7], [8]. More importantly, $\rho k_B T \beta_T$ characterizes the *local* microscopic volume fluctuations of liquids [9], providing a connection between microscopic many-body interactions of fluids and its macroscopic, thermodynamic properties [10]. So, it may be appreciated that volume fluctuations at microscopic scales are a specific signature of liquid structure that deserve attention.

Since β_T is a measure of volume fluctuations [9], [11], [12], Soper [13] suggested that a thermodynamic quantity f_V, strictly related to β_T (the relation is presented below), can be used to describe how large the density fluctuations are likely to be in any given volume of a liquid. [13]. The f_V quantity is not density dependent, is close to zero at macroscopic length scales, but display significant values at microscopic ones [13]. For example, for a water volume of 1 nm^3 at 298 K, f_V = 4.3 %. The study of volume fluctuations in liquids has proved useful for understanding solvent effects in chemical reactions [14] and the (local) hydrophobicity of a surface [15]. Various volumetric approaches arose: (a) the assumption of the existence of empty spaces emerging from fluctuations in local density has been applied to model the viscosity of ionic liquids [16]; (b) the free-volume model has been used to describe the viscosity of dense liquids and glasses, and the liquid-glass transition [17]; (c) measurements of the isothermal or adiabatic compressibility of globular proteins has been used to shed light on their conformational fluctuations and catalytic functions [18]–[20].

Several features of a liquid can be approached by means of the Scaled Particle Theory (SPT). The latter is a hard sphere theory in origin that allows the calculation of the Gibbs free energy cost of cavity formation, ΔG_c, in a liquid. Actually, it works well also in real liquids because it accounts, in a physically reliable way, for the packing features of a condensed state of the matter. For instance, SPT provides information on the width of the cavity size distribution in liquids and globular proteins, suggesting a link to the isothermal compressibility of the medium surrounding the cavity [21]. In addition, SPT allows an explanation of the hydrophobic effect, the poor solubility of nonpolar species in water, in terms of the higher ΔG_c in water than in other solvents [22]–[25]. On the basis of a statistical mechanical approach, the process of solvating a solute molecule in a solvent can exactly be separated in two sub-processes: (a) formation of a cavity of the size of the solute molecule; (b) introduction of the solute molecule into the cavity, switching on solute-solvent attractive interactions [26], [27]. This theoretical construction is feasible because the Gibbs free energy is a state function of a thermodynamic system. In terms of Gibbs free energy this can be written as follows

$$\Delta G_{sol} = \Delta G_c + \Delta G_{int} \tag{2}$$

where ΔG_c depends solely on solvent properties, while ΔG_{int} depends on solute-solvent attractive interactions.

The formation of a cavity is connected to the molecular-scale density fluctuations characterizing the ensemble of equilibrium configurations of a given liquid. This means that molecular dynamics or Monte Carlo simulations can be exploited to calculate ΔG_c. On the other hand, it is possible to account for molecular-scale density fluctuations looking at the packing properties of the liquid that depend upon density and molecular sizes [28], [29]. Pratt and co-workers [30], [31] were the first to point out the relationship between ΔG_c and β_T through an information theory approach developed to quantify hydrophobic hydration and interactions. The approach accounts for the link between the probability of cavity formation in bulk water, resulting from molecular-scale density fluctuations, and the hydration Gibbs free energy of the simplest hydrophobic solutes, *i.e.*, hard spheres. The result was that ΔG_c is inversely proportional to β_T, $\Delta G_c \sim 1/\beta_T$. Thus, rising the isothermal compressibility results in a decrease in the Gibbs free energy of cavity formation because a great number of packing arrangements can accommodate the cavity. Theoretical analyses indicate that the inverse relationship $\Delta G_c \sim 1/\beta_T$ should be valid only for very small cavities. Therefore, it should be important to test the occurrence of a

relationship between ΔG_c and β_T for atomic and molecular-sized cavities in a large number of liquids.

In this article, we study the relationship between the values of ΔG_c and f_V^*, calculated for 230 liquids covering a large category of organic compounds and water at 298 K. The occurrence of the relationship is investigated for both small-sized and molecular-sized cavities, allowing us to establish its general validity and robustness. Moreover, this finding leads to a general correlation between the ΔG_c magnitude and the liquid isothermal compressibility.

2. Methods of calculations

2.1. The isothermal compressibility

Values of β_T can be determined by measuring the adiabatic compressibility β_S, using the following equation [32]:

$$\beta_s = \beta_T - \frac{{\alpha_p}^2 T}{\rho C_{p,m}} \tag{3}$$

where α_p is the isobaric thermal expansion coefficient (K^{-1}), $C_{p,m}$ the isobaric heat capacity ($J.K^{-1}.kg^{-1}$), and ρ is the density of matter ($kg.m^{-3}$). β_s can be determined according to the Newton-Laplace equation:

$$v_s = \sqrt{\frac{1}{\rho \beta_s}} \tag{4}$$

where v_s is the sound velocity in the fluid ($m.s^{-1}$).

Determinations of β_T were done for 230 liquids, covering a large category of organic compounds (hydrocarbons, alcohols, esters, ethers, ketones, aldehydes, terpenes, acids, halogenated solvents) and water, see Table II.1. Values were collected from the literature when available, calculated using the Equation (3), or estimated using the existing power law between β_T and β_S, allowing us to obtain acceptable estimates of β_T when the first two options were not possible (results not shown).

When using Equation (3), the values of density, isobaric thermal expansion coefficient and isobaric heat capacity came from the literature, or measurements using a DSA 5000M

sonodensimeter (Anton Paar, France) for the density, and a differential scanning calorimetry (DSC) from T = 243.15 K to T = 303.15 K (Q200 modulated DSC from TA Instruments, New Castle, USA) for the isobaric thermal expansion coefficient.

2.2. The Gibbs free energy of cavity formation

SPT, originally developed by Reiss, Frisch and Lebowitz, has been employed in the study of a variety of liquid systems. It has often been used for the ΔG_c calculation in real liquids, using the experimental density at each temperature [23], [33]–[36]. SPT equations need the value of the effective hard sphere radius of liquid molecules. This approach implies two main assumptions: (a) liquid density is determined by the attractive interactions among its molecules; (b) molecules can be described as hard spheres. Following the SPT procedure to arrive at the ΔG_c analytic formula, it is clear that ΔG_c is a measure of the reduction in the size of the configuration space accessible to liquid molecules upon cavity formation at the given packing density. The pressure being fixed at 1 atm, SPT provides the following expression for ΔG_c [37]

$$\Delta G_c = RT\,.\{-\ln(1-\phi_{pd}) + U.(r_c/r) + (U/2).(U+2).(r_c/r)^2\} \quad (5)$$

where $\phi_{pd} = (4\Pi r^3.\mathrm{N}_{Av})/3V_m$, is the volume packing density of the liquid, the ratio of the physically occupied volume to the liquid molar volume V_m, r is the effective hard sphere radius of liquid molecules, r_c the cavity radius defined as the radius of the spherical region from which all parts of the solvent molecules are excluded [37], and $U = 3\phi_{pd}/(1-\phi_{pd})$.

For water, the effective hard-sphere radius is equal to 0.14 nm [22], [37]–[39]. However, the determination of the effective hard sphere radius is, in general, not a simple task. Reliable estimates of effective hard sphere radii can be calculated starting from the van der Waals volume of the liquid molecule. Values of V_{vdw} are readily available in literature [40], [41] or can be estimated using the Bondi method [42].

Calculations of ΔG_c were done for the same set of liquids considered for β_T determination at 298 K. In order to provide a comparison with simulation calculations from Sedov and Magsumov [37], r_C was set at 0.12 nm. In their work, Sedov and Magsumov compared results of ΔG_c at R = 0.31 nm, with R defined as the cavity radius of the spherical region from which the centers of the solvent molecules are excluded. For spherical cavities, $R = r_C + r_S$, r_S being

the solvent radius equal to 0.14 nm for water and to 0.19 nm (it is the radius of carbon atom) for organic compounds [43]–[45].

2.3. The average density fluctuations in number f_V and in volume f_V^*

f_V is defined as the ratio between the mean square deviation of the number of molecules in a specified volume V, and the average number of molecules in the same volume:

$$f_V = \frac{\sqrt{\langle (N - \langle N \rangle)^2 \rangle}}{\langle N \rangle} = \left(\frac{k_B T}{V K_T}\right)^{0.5} = \left(\frac{k_B T \beta_T}{V}\right)^{0.5} \quad (6)$$

where k_B is the Boltzmann constant, T is the temperature and β_T is the isothermal compressibility of the liquid [13]. f_V was determined for the same liquids as β_T and ΔG_c at 298 K, for a specific volume V of 1 nm^3. f_V is a dimensionless quantity, but we decided to convert it to nm^3 by multiplying for the molar volume normalized per molecule:

$$f_V^* = f_V * V_M \quad (7)$$

where V_M is obtained by dividing the liquid molar volume by the Avogadro's number ($V_M = V_m/N_{Av}$). The quantities f_V and f_V^* are called the average density fluctuations in number and in volume, respectively. Values of f_V and f_V^* are reported in % and nm^3, respectively, in Table II.2.

Correlations between the parameters were analyzed using the Residual Root Mean Square Error (RMSE) according to the following equation:

$$\mathrm{RMSE} = \sqrt{\frac{\sum_{i=1}^{n} (Pi - Oi)^2}{n}} \quad (8)$$

where Pi is the predicted value, Oi is the observed value, and n is the total number of observations.

3. Results and discussion

3.1. The Gibbs free energy of cavity formation and the average density fluctuations in volume of organic compounds and water

Table II.1.

V_{vdw} volume, isothermal compressibility and volume-independent mean-square amplitude in fluctuations of entropy ($^{S}\Delta$) of different organic compounds and water at 298 K.

Liquid	V_{vdw}[a] ($cm^3.mol^{-1}$)	β_T .10^{-9} (Pa^{-1})	$^{S}\Delta$ .10^{-12} ($J^2.K^{-2}.m^{-6}$)	Liquid	V_{vdw}[a] ($cm^3.mol^{-1}$)	β_T .10^{-9} (Pa^{-1})	$^{S}\Delta$ .10^{-12} ($J^2.K^{-2}.m^{-6}$)	Liquid	V_{vdw}[a] ($cm^3.mol^{-1}$)	β_T .10^{-9} (Pa^{-1})	$^{S}\Delta$ .10^{-12} ($J^2.K^{-2}.m^{-6}$)
1,1,1-trichloroethane	53.72	1.13	0.12	*acetic anhydride*	54.40	0.87	0.18	*di(2-chloroethyl)ether*	70.43	0.74	0.13
1,1,2,2-tetrachloroethane	62.52	0.68	0.12	*acetone*	39.04	1.27	0.19	*diacetyl*	54.23	0.86	0.14
1,1,2-trichloroethane	53.11	0.73	0.14	*acetonitrile*	28.37	1.10	0.28	*dibromomethane*	39.43	0.64	0.18
1,1-dichloroethane	44.93	1.07	0.15	*acetonyl acetone*	75.06	0.91	0.10	*dichloromethane*	34.71	0.99	0.20
1,2,4-trichlorobenzene	78.74	0.54	0.10	*acetophenone*	70.41	0.56	0.12	*diethanolamine*	65.08	0.35	0.21
1,2-diaminoethane	47.50	0.51	0.31	*acetyl chloride*	38.85	1.07	0.19	*diethyl carbonate*	66.70	0.98	0.12
1,2-dibromoethane	49.26	0.64	0.15	*acrolein*	38.52	1.05	0.23	*diethyl malonate*	88.43	0.74	0.10
1,2-dichloroethane	43.70	0.82	0.17	*acrylonitrile*	35.10	1.64	0.21	*diethyl phthalate*	119.92	0.61	0.08
1,2-dimethoxyethane	55.20	0.99	0.15	*allyl Chloride*	43.97	1.24	0.14	*diiodomethane*	50.93	0.45	0.17
1,2-ethanediol	36.54	0.37	0.40	*amyl acetate*	83.46	0.95	0.10	*diisopropyl ether*	71.94	1.73	0.09
1,2-propanediol	46.77	0.49	0.29	*amyl formate*	73.43	1.03	0.12	*dimethyl sulfoxide*	42.88	0.53	0.25
1,4-butanediol	57.00	0.44	0.21	*amyl propionate*	97.48	0.88	0.07	*dimethylacetamide*	57.04	0.65	0.17
1,4-dioxane	46.62	0.66	0.27	*aniline*	56.38	0.47	0.18	*dimethylformamide*	46.81	0.65	0.21
1,5-pentanediol	67.23	0.46	0.17	*anisole*	62.41	0.64	0.15	*di-n-butylamine*	96.80	1.09	0.08
1-bromobutane	58.76	1.03	0.12	*benzaldehyde*	60.98	0.59	0.14	*di-n-propyl ether*	71.95	1.32	0.10
1-chlorobutane	55.98	1.21	0.13	*benzene*	48.40	0.97	0.14	*diphenyl ether*	103.19	0.50	0.09
1-nitropropane	50.93	0.80	0.18	*benzonitrile*	60.54	0.62	0.13	*diphenyl methane*	103.02	0.54	0.07
1-nonene	97.31	1.16	0.08	*benzyl alcohol*	64.11	0.44	0.17	*ethanol*	31.94	1.06	0.27
1-octene	86.89	1.28	0.08	*bromobenzene*	60.16	0.65	0.12	*ethanolamine*	39.04	0.42	0.29
1-pentadecene	159.80	0.82	0.06	*bromoform*	49.98	0.57	0.14	*ethybenzene*	69.74	0.84	0.10
1-tridecene	138.97	0.91	0.06	*butyl acetate*	70.23	1.05	0.11	*ethyl acetate*	52.77	1.17	0.15
1-undecene	118.14	1.02	0.07	*butyl propionate*	83.46	1.01	0.09	*ethyl acetoacetate*	74.70	0.61	0.13
2,2,4-trimethyl pentane	88.69	1.57	0.07	*butyric acid*	53.87	0.88	0.18	*ethyl acrylate*	59.51	0.92	0.17
2-butanone	49.27	1.19	0.16	*caprylic acid*	97.48	0.82	0.08	*ethyl benzoate*	84.14	0.66	0.10
2-chloroethanol	40.12	0.60	0.20	*carbon disulfide*	31.20	0.97	0.17	*ethyl bromide*	38.30	1.09	0.16
2-ethoxyethanol	56.10	0.68	0.18	*carbon tetrachloride*	52.55	1.07	0.11	*ethyl chloride*	35.52	1.12	0.18
2-heptanone	79.96	0.96	0.10	*carvone*	96.72	0.63	0.09	*ethyl ether*	52.11	1.85	0.13
2-methoxyethanol	45.87	0.62	0.23	*chlorobenzene*	57.84	0.73	0.12	*ethyl formate*	42.74	1.18	0.18
2-methylbutane	58.02	2.45	0.10	*chloroform*	43.50	1.12	0.15	*ethyl iodide*	43.08	0.98	0.15
2-methylcyclohexanone	74.33	0.72	0.12	*cinnamaldehyde*	66.95	0.49	0.12	*ethyl isovalerate*	83.45	1.08	0.07
2-methylphenol	65.03	0.48	0.18	*cis-dichloroethylene*	40.18	1.02	0.17	*ethyl octanoate*	114.35	0.90	0.07
2-nitropropane	50.92	0.89	0.17	*crotonaldehyde*	48.93	0.81	0.18	*ethyl propanoate*	63.00	1.18	0.12
2-pentanone	59.50	1.09	0.13	*cumene*	79.96	0.84	0.09	*ethylene carbonate*	38.22	0.53	0.25
3-methylcyclohexanone	74.33	0.73	0.11	*cyclohexane*	61.40	1.07	0.11	*ethylene oxide*	29.69	0.59	0.30
3-pentanone	59.50	1.02	0.14	*cyclohexanol*	64.84	0.58	0.16	*ethyl-n-butyrate*	74.32	1.05	0.10
4-butyrolactone	45.89	0.50	0.20	*cyclohexanone*	62.85	0.66	0.14	*fluorobenzene*	50.84	0.97	0.14
4-methylcyclohexanone	74.33	0.73	0.11	*cyclohexene*	52.05	1.01	0.11	*formamide*	25.46	0.40	0.56
acetaldehyde	28.81	1.53	0.23	*cyclohexylamine*	66.83	0.73	0.12	*formic acid*	22.74	0.65	0.57
acetic acid	33.30	0.87	0.31	*cyclopentadiene*	40.05	0.93	0.14	*furfuric alcohol*	50.64	0.49	0.22

Table II.1 *(continued)*

V_{vdw} volume, isothermal compressibility and volume-independent mean-square amplitude in fluctuations of entropy ($^{S}\Delta$) of different organic compounds and water at 298 K.

Liquid	V_{vdw}[a] ($cm^3.mol^{-1}$)	β_T .10^{-9} (Pa^{-1})	$^{S}\Delta$ .10^{-12} ($J^2.K^{-2}.m^{-6}$)	Liquid	V_{vdw}[a] ($cm^3.mol^{-1}$)	β_T .10^{-9} (Pa^{-1})	$^{S}\Delta$ .10^{-12} ($J^2.K^{-2}.m^{-6}$)	Liquid	V_{vdw}[a] ($cm^3.mol^{-1}$)	β_T .10^{-9} (Pa^{-1})	$^{S}\Delta$ .10^{-12} ($J^2.K^{-2}.m^{-6}$)
glycerol	51.36	0.24	0.35	*n-butyl acrylate*	80.17	0.97	0.11	*pentachloroethane*	71.78	0.62	0.11
hexafluorobenzene	63.24	1.18	0.14	*n-butylamine*	54.90	1.14	0.16	*perchloroethylene*	61.04	0.76	0.12
hexamethyl phosphoramide	104.75	0.79	0.09	*n-butyronitrile*	48.83	1.02	0.17	*perfluoro-methyl-cyclohexane*	121.78	1.30	0.08
hexyl chloride	76.81	0.95	0.10	*n-decane*	109.18	1.08	0.07	*phenetole*	75.00	0.92	0.11
indene	64.53	0.59	0.12	*n-decanol*	113.78	0.69	0.08	*phenol*	53.80	0.49	0.21
iodobenzene	64.68	0.58	0.11	*n-dodecane*	129.64	0.99	0.06	*pinene*	92.13	0.89	0.08
iso-amyl butyrate	107.89	0.95	0.07	*n-dodecanol*	134.24	0.63	0.07	*piperidine*	59.23	0.92	0.16
isobutanol	52.39	0.97	0.18	*n-heptane*	78.49	1.37	0.09	*propanoic acid*	43.42	1.05	0.23
isobutyl-isobutyrate	93.67	1.07	0.08	*n-heptanol*	83.09	0.83	0.11	*propionitrile*	38.60	1.14	0.20
isopentane	58.02	2.29	0.10	*n-hexadecane*	170.56	0.86	0.05	*propyl acetate*	63.00	1.15	0.12
isopentanol	62.62	0.95	0.15	*n-hexane*	68.26	1.62	0.09	*propylene carbonate*	45.20	0.59	0.18
isopropanol	42.16	1.33	0.22	*n-hexanoic acid*	74.33	0.82	0.13	*p-xylene*	70.66	0.86	0.10
isopropyl acetate	62.99	1.17	0.12	*n-hexanol*	72.86	0.84	0.13	*pyridine*	45.50	0.68	0.17
limonene	95.24	0.87	0.07	*nicotine*	96.34	0.57	0.07	*pyrrole*	41.96	0.65	0.22
linalool	106.74	0.89	0.10	*nitrobenzene*	61.84	0.51	0.14	*pyrrolidine*	49.00	0.82	0.18
malonitrile	39.63	0.46	0.29	*nitroethane*	40.70	0.79	0.22	*quinoline*	71.10	0.44	0.12
mesitylene	81.83	0.70	0.09	*nitromethane*	30.47	0.72	0.30	*sulfolane*	61.22	0.43	0.17
methanol	21.71	1.25	0.41	*n-methylacetamide*	47.12	0.63	0.21	*t-butanol*	52.38	0.99	0.20
methyl acetate	42.54	1.11	0.19	*n-methylaniline*	66.79	0.50	0.13	*tetrabromoethane*	60.02	0.36	0.10
methyl acrylate	49.28	1.04	0.16	*n-methylformamide*	36.45	0.60	0.29	*tetraethylene glycol*	114.95	0.42	0.12
methyl benzoate	73.91	0.66	0.12	*n-methylpyrrolidone*	60.39	0.62	0.15	*tetrahydrofuran*	44.62	0.99	0.16
methyl bromide	28.07	1.24	0.24	*n-nonane*	98.95	1.15	0.07	*tetrahydropyran*	55.08	0.96	0.13
methyl cyclohexane	64.06	1.11	0.09	*n-octane*	88.72	1.26	0.08	*tetraline*	83.10	0.56	0.11
methyl diethanolamine	74.44	0.48	0.19	*n-octanol*	93.32	0.76	0.10	*tetramethylurea*	74.18	0.91	0.13
methyl formate	32.51	1.21	0.26	*n-pentane*	58.03	2.01	0.10	*thiophene*	40.78	0.79	0.17
methyl iodide	32.85	0.82	0.18	*n-pentanoic acid*	63.88	1.07	0.14	*toluene*	59.51	0.87	0.11
methyl metacrylate	59.49	1.00	0.14	*n-pentanol*	62.63	0.89	0.15	*t-pentanol*	62.62	1.08	0.17
methyl octanoate	103.49	0.89	0.08	*n-propanol*	42.17	0.99	0.22	*trans 1,2-dichloroethylene*	40.18	1.02	0.16
methyl propionate	55.81	1.02	0.16	*n-propyl acetate*	63.00	1.08	0.12	*trichloroethylene*	49.58	0.92	0.13
methylhexylketone	90.19	1.00	0.09	*n-propylbenzene*	79.97	0.83	0.09	*triethanolamine*	89.83	0.36	0.15
methyl-i-propyl ketone	59.49	1.08	0.13	*n-tetradecane*	150.10	0.91	0.05	*triethyl phosphate*	97.50	0.75	0.10
methyl-isopropyl benzene	90.54	0.82	0.08	*o-bromotoluene*	71.97	0.61	0.12	*triethylamine*	73.03	1.38	0.10
m-nitrotoluene	74.92	0.51	0.11	*o-chloroaniline*	66.44	0.45	0.15	*triethylene glycol*	88.82	0.41	0.15
morpholine	52.70	0.62	0.19	*octyl bromide*	100.09	0.78	0.07	*trifluoroacetic acid*	41.07	1.86	0.24
m-xylene	70.66	0.85	0.10	*octyl chloride*	97.64	0.90	0.06	*vinyl acetate*	49.28	1.65	0.15
myrcene	98.65	0.98	0.07	*o-dichlorobenzene*	67.30	0.61	0.14	*water*	10.45[b]	0.45	1.92
n-butanol	52.40	0.93	0.18	*oleic acid cis*	200.05	0.67	0.06				
n-butyl acetate	73.23	1.00	0.11	*o-nitrotoluene*	74.92	0.55	0.11				
				o-xylene	70.66	0.81	0.11				

a [40]–[42], b Hard sphere volume [37]

Table II.2

Calculated Gibbs free energy, ΔG_c, of a spherical cavity creation of radius $R = 0.31$ nm and average density fluctuations in number (f_V) and in volume (f_V^*) in 1 nm^3 of different organic compounds and water at 298 K. *a calculated with SPT method, b Sedov and Magsumov 2020* [43]

Liquid	ΔG_c [a] (kJ.mol^{-1})	ΔG_c [a] .10^{-20} (J.nm^{-3})	ΔG_c [b] .10^{-20} (J.nm^{-3})	f_V (%)	f_V^* .10^{-2} (nm^3)	Liquid	ΔG_c [a] (kJ.mol^{-1})	ΔG_c [a] .10^{-20} (J.nm^{-3})	ΔG_c [b] .10^{-20} (J.nm^{-3})	f_V (%)	f_V^* .10^{-2} (nm^3)
1,1,1-trichloroethane	10.01	9.94		6.85	1.14	*acetic anhydride*	12.09	12.74		6.01	0.95
1,1,2,2-tetrachloroethane	12.41	11.75		5.29	0.93	*acetone*	11.04	14.91	1.09	7.24	0.89
1,1,2-trichloroethane	12.02	12.90		5.51	0.85	*acetonitrile*	13.41	25.52		6.71	0.59
1,1-dichloroethane	10.51	12.41		6.62	0.93	*acetonyl acetone*	7.71	5.27		6.06	1.47
1,2,4-trichlorobenzene	13.69	10.97		4.66	0.97	*acetophenone*	12.39	10.55		4.81	0.94
1,2-diaminoethane	27.62	40.85		4.61	0.52	*acetyl chloride*	11.96	16.84		6.59	0.78
1,2-dibromoethane	12.26	14.16		5.11	0.74	*acrolein*	14.04	21.03		6.51	0.72
1,2-dichloroethane	11.75	14.73	18.60	5.84	0.77	*acrylonitrile*	11.66	17.58		8.23	0.91
1,2-dimethoxyethane	9.63	9.21		6.42	1.11	*allyl Chloride*	10.89	13.34		7.08	0.96
1,2-ethanediol	22.53	40.30		3.90	0.36	*amyl acetate*	9.33	6.31		6.17	1.52
1,2-propanediol	17.95	24.36		4.48	0.55	*amyl formate*	9.76	7.48		6.40	1.39
1,4-butanediol	16.95	19.04		4.26	0.63	*amyl propionate*	10.09	6.09		5.98	1.65
1,4-dioxane	11.10	12.96		5.20	0.74	*aniline*	14.84	16.24		4.39	0.67
1,5-pentanediol	15.84	15.01		4.41	0.77	*anisole*	11.24	10.29		5.13	0.93
1-bromobutane	10.06	9.31		6.51	1.17	*benzaldehyde*	12.98	12.74		4.91	0.83
1-chlorobutane	9.53	9.07		7.01	1.22	*benzene*	10.73	11.99		6.32	0.94
1-nitropropane	12.12	13.55		5.75	0.85	*benzonitrile*	12.38	12.01		5.07	0.87
1-nonene	8.83	5.11		6.85	1.97	*benzyl alcohol*	14.12	13.60		4.26	0.74
1-octene	9.00	5.77		7.19	1.86	*bromobenzene*	11.25	10.70		5.11	0.89
1-pentadecene	8.51	3.16		5.78	2.58	*bromoform*	12.15	13.87		4.81	0.70
1-tridecene	8.46	3.54		6.08	2.41	*butyl acetate*	8.72	6.59		6.57	1.44
1-undecene	8.83	4.32		6.41	2.18	*butyl propionate*	8.98	5.95		6.42	1.61
2,2,4-trimethyl pentane	8.15	5.00		7.84	2.12	*butyric acid*	12.61	13.75		5.94	0.90
2-butanone	10.89	11.90		7.12	1.08	*caprylic acid*	11.48	7.24		5.75	1.51
2-chloroethanol	14.82	21.81		4.93	0.56	*carbon disulfide*	11.38	18.78		6.30	0.63
2-ethoxyethanol	12.02	12.34		5.29	0.86	*carbon tetrachloride*	10.36	10.64		6.65	1.08
2-heptanone	9.98	7.10		6.28	1.47	*carvone*	11.72	7.46		5.09	1.33
2-methoxyethanol	13.31	16.78		5.06	0.67	*chlorobenzene*	11.24	11.05		5.46	0.92
2-methylbutane	7.98	6.79		10.08	1.97	*chloroform*	11.15	13.88	18.64	6.76	0.90
2-methylcyclohexanone	12.71	10.48		5.40	1.09	*cinnamaldehyde*	8.98	7.14		4.48	0.94
2-methylphenol	14.06	13.52		4.36	0.75	*cis-dichloroethylene*	11.15	14.83		6.46	0.81
2-nitropropane	11.66	12.87		6.06	0.91	*crotonaldehyde*	13.85	16.84		5.74	0.78
2-pentanone	10.50	9.76		6.72	1.20	*cumene*	10.19	7.29		5.89	1.37
3-methylcyclohexanone	12.23	9.97		5.43	1.11	*cyclohexane*	11.55	10.88	11.15	6.60	1.16
3-pentanone	10.79	10.15		6.48	1.15	*cyclohexanol*	14.36	13.84		4.82	0.83
4-butyrolactone	14.87	19.45		4.55	0.58	*cyclohexanone*	13.19	12.70		5.17	0.89
4-methylcyclohexanone	12.23	9.97		5.45	1.11	*cyclohexene*	8.92	8.79		6.39	1.08
acetaldehyde	11.42	20.43		7.80	0.72	*cyclohexylamine*	9.74	8.04		5.45	1.10
acetic acid	15.34	26.78		5.94	0.56	*cyclopentadiene*	8.73	10.59		6.14	0.84

Table II.2 *(continued)*

Calculated Gibbs free energy, ΔG_c, of a spherical cavity creation of radius $R = 0.31$ nm and average density fluctuations in number (f_V) and in volume (f_V^*) in 1 nm^3 of different organic compounds and water at 298 K. [a] *calculated with SPT method,* [b] *Sedov and Magsumov 2020* [43]

Liquid	ΔG_c [a] (kJ.mol^{-1})	ΔG_c [a] .10^{-20} (J.nm^{-3})	ΔG_c [b] .10^{-20} (J.nm^{-3})	f_V (%)	f_V^* .10^{-2} (nm^3)	Liquid	ΔG_c [a] (kJ.mol^{-1})	ΔG_c [a] .10^{-20} (J.nm^{-3})	ΔG_c [b] .10^{-20} (J.nm^{-3})	f_V (%)	f_V^* .10^{-2} (nm^3)
di(2-chloroethyl)ether	12.18	10.34		5.52	1.08	*glycerol*	25.86	35.30	1.99	3.16	0.38
diacetyl	15.57	17.85		5.96	0.86	*hexafluorobenzene*	9.85	8.54		6.94	1.33
dibromomethane	13.11	18.79		5.10	0.59	*hexamethyl*					
dichloromethane	11.92	18.54		6.28	0.67	*phosphoramide*	10.28	5.85		5.70	1.66
diethanolamine	19.56	20.29		3.80	0.61	*hexyl chloride*	9.53	6.94		6.20	1.42
diethyl carbonate	9.70	7.99		6.31	1.27	*indene*	10.00	8.59		4.90	0.95
diethyl malonate	10.14	6.65		5.53	1.40	*iodobenzene*	11.38	10.19		4.87	0.90
diethyl phthalate	9.92	5.00		4.95	1.63	*iso-amyl butyrate*	9.68	5.26		6.25	1.91
diiodomethane	16.55	20.55		4.24	0.57	*isobutanol*	11.57	12.53		6.24	0.96
diisopropyl ether	7.79	5.50		8.44	1.98	*isobutyl-isobutyrate*	8.70	5.16		6.59	1.85
dimethyl sulfoxide	15.45	21.67	27.20	4.66	0.55	*isopentane*	7.99	6.82		9.71	1.89
dimethylacetamide	14.54	15.69		5.14	0.79	*isopentanol*	11.53	10.56		6.32	1.15
dimethylformamide	15.20	19.64	21.43	5.17	0.66	*isopropanol*	11.87	15.43		7.43	0.95
di-n-butylamine	9.16	5.40		6.62	1.86	*isopropyl acetate*	9.44	8.06		6.93	1.35
di-n-propyl ether	8.33	6.05		7.36	1.68	*limonene*	13.10	8.08		5.96	1.60
diphenyl ether	13.70	8.58		4.59	1.22	*linalool*	10.08	5.60		5.76	1.72
diphenyl methane	11.32	6.74		4.73	1.32	*malonitrile*	31.08	55.15		4.41	0.41
ethanol	13.18	22.52	22.14	6.60	0.64	*mesitylene*	10.84	7.77		5.37	1.24
ethanolamine	21.15	35.06		4.16	0.42	*methanol*	14.77	36.28	32.15	7.17	0.48
ethybenzene	10.54	8.60		5.88	1.20	*methyl acetate*	10.87	13.65		6.74	0.89
ethyl acetate	10.07	10.27	15.35	6.89	1.12	*methyl acrylate*	10.77	11.89		6.53	0.98
ethyl acetoacetate	11.30	8.88		5.03	1.06	*methyl benzoate*	11.46	9.13		5.21	1.09
ethyl acrylate	10.07	9.24		6.16	1.12	*methyl bromide*	10.75	19.59		6.83	0.62
ethyl benzoate	10.48	7.33		5.15	1.22	*methyl cyclohexane*	7.78	6.10		6.71	1.42
ethyl bromide	10.17	13.72		6.59	0.81	*methyl diethanolamine*	15.44	13.45		4.40	0.84
ethyl chloride	9.50	13.54		6.51	0.76	*methyl formate*	11.70	18.90		7.04	0.72
ethyl ether	8.35	8.00		8.65	1.50	*methyl iodide*	11.67	18.74		5.74	0.59
ethyl formate	10.66	13.19		6.97	0.94	*methyl metacrylate*	10.64	9.99		6.38	1.13
ethyl iodide	10.68	13.28		6.27	0.84	*methyl octanoate*	9.13	5.04		6.04	1.82
ethyl isovalerate	9.17	6.10		6.66	1.66	*methyl propionate*	12.08	12.54		6.42	1.03
ethyl octanoate	8.85	4.43		6.10	2.02	*methylhexylketone*	9.77	6.19		6.46	1.69
ethyl propanoate	9.83	8.51		6.96	1.33	*methyl-i-propyl ketone*	10.60	9.91		6.67	1.19
ethylene carbonate	14.73	22.10		4.79	0.53	*methyl-isopropyl benzene*	10.14	6.49		5.85	1.52
ethylene oxide	16.88	33.84		4.79	0.40	*m-nitrotoluene*	14.09	11.90		4.53	0.89
ethyl-n-butyrate	9.82	7.41		6.56	1.44	*morpholine*	14.20	16.23		5.04	0.73
fluorobenzene	10.41	11.04		6.31	0.99	*m-xylene*	10.77	8.73		5.93	1.22
formamide	24.55	61.55	57.21	4.05	0.27	*myrcene*	9.37	5.43		6.36	1.82
formic acid	20.73	54.69		5.16	0.32	*n-butanol*	12.01	13.02	14.06	6.20	0.95
furfuric alcohol	12.84	14.79		4.45	0.64	*n-butyl acetate*	9.55	7.25		6.34	1.39

Table II.2 *(continued)*

Calculated Gibbs free energy, ΔG_c, of a spherical cavity creation of radius $R = 0.31$ nm and average density fluctuations in number (f_V) and in volume (f_V^*) in 1 nm^3 of different organic compounds and water at 298 K. [a] *calculated with SPT method,* [b] *Sedov and Magsumov 2020* [43]

Liquid	ΔG_c [a] (kJ.mol^{-1})	ΔG_c [a] .10^{-20} (J.nm^{-3})	ΔG_c [b] .10^{-20} (J.nm^{-3})	f_V (%)	f_V^* .10^{-2} (nm^3)	Liquid	ΔG_c [a] (kJ.mol^{-1})	ΔG_c [a] .10^{-20} (J.nm^{-3})	ΔG_c [b] .10^{-20} (J.nm^{-3})	f_V (%)	f_V^* .10^{-2} (nm^3)
n-butyl acrylate	9.54	6.65		6.33	1.51	*pentachloroethane*	11.81	9.81		5.01	1.00
n-butylamine	10.98	11.06		6.92	1.14	*perchloroethylene*	12.74	12.47		5.55	0.94
n-butyronitrile	11.47	13.20		6.35	0.92	*perfluoro-methyl-*					
n-decane	8.44	4.32		6.67	2.16	*cyclohexane*	11.05	5.65		7.30	2.37
n-decanol	9.95	5.20		5.33	1.69	*phenetole*	11.61	9.17		6.17	1.30
n-dodecane	8.13	3.60		6.24	2.34	*phenol*	15.02	16.87		4.63	0.68
n-dodecanol	9.45	4.20		5.11	1.91	*pinene*	9.87	6.19		6.06	1.60
n-heptane	8.53	5.80		7.51	1.83	*piperidine*	13.09	13.17		6.17	1.02
n-heptanol	10.58	7.41		5.85	1.39	*propanoic acid*	13.67	18.22		6.59	0.82
n-hexadecane	7.91	2.69		5.96	2.91	*propionitrile*	12.06	17.04		6.85	0.81
n-hexane	8.40	6.38		8.18	1.79	*propyl acetate*	9.80	8.48		6.88	1.32
n-hexanoic acid	11.43	9.08		5.79	1.21	*propylene carbonate*	10.79	12.67		5.00	0.71
n-hexanol	11.12	8.88		5.89	1.22	*p-xylene*	10.65	8.62		5.93	1.22
nicotine	10.66	6.63		4.79	1.28	*pyridine*	12.35	15.30	20.18	5.27	0.71
nitrobenzene	13.23	12.88	18.98	4.61	0.79	*pyrrole*	15.83	22.77		5.18	0.60
nitroethane	13.10	18.23		5.70	0.68	*pyrrolidine*	13.84	16.26		6.04	0.85
nitromethane	14.79	27.40	34.30	5.43	0.49	*quinoline*	12.32	10.41		4.26	0.84
n-methylacetamide	14.86	19.30		4.96	0.63	*sulfolane*	16.99	17.84		4.26	0.67
n-methylaniline	13.50	12.38		4.54	0.82	*t-butanol*	11.04	11.63	13.27	6.41	1.01
n-methylformamide	18.16	30.72	31.46	4.96	0.49	*tetrabromoethane*	8.51	7.30		3.84	0.74
n-methylpyrrolidone	15.02	15.58		5.02	0.80	*tetraethylene glycol*	14.31	8.32		4.14	1.18
n-nonane	8.46	4.74		6.83	2.02	*tetrahydrofuran*	11.31	13.90	17.53	6.32	0.85
n-octane	8.46	5.19		7.19	1.95	*tetrahydropyran*	11.22	11.43		6.28	1.02
n-octanol	10.55	6.66		5.59	1.47	*tetraline*	11.92	8.75		4.75	1.08
n-pentane	8.16	7.05		9.04	1.74	*tetramethylurea*	13.19	10.97		6.13	1.22
n-pentanoic acid	11.88	10.87		6.63	1.20	*thiophene*	10.09	12.79		5.65	0.74
n-pentanol	11.53	10.62		6.03	1.09	*toluene*	10.75	10.08	12.48	5.98	1.06
n-propanol	12.72	17.03		6.36	0.79	*t-pentanol*	11.24	10.26		6.66	1.21
n-propyl acetate	9.78	8.51		6.61	1.26	*trans 1,2-dichloroethylene*	10.26	13.26		6.44	0.83
n-propylbenzene	10.16	7.29		5.83	1.35	*trichloroethylene*	11.07	12.47		6.00	0.88
n-tetradecane	7.94	3.06		6.02	2.59	*triethanolamine*	16.87	12.67		3.86	0.85
o-bromotoluene	11.98	9.96		4.99	1.00	*triethyl phosphate*	9.46	5.57		5.55	1.57
o-chloroaniline	15.15	14.36		4.35	0.76	*triethylamine*	8.32	5.95		7.55	1.75
octyl bromide	9.38	5.37		5.66	1.64	*triethylene glycol*	16.14	12.11		4.08	0.90
octyl chloride	9.29	5.46		6.04	1.71	*trifluoroacetic acid*	11.07	14.37		8.76	1.12
o-dichlorobenzene	12.32	10.90		5.03	0.94	*vinyl acetate*	10.10	10.96		8.14	1.25
oleic acid cis	9.50	3.01		5.23	2.74	*water*	11.70	64.75	116.75	4.31	0.13
o-nitrotoluene	14.22	12.04		4.70	0.92						
o-xylene	11.30	9.35		5.75	1.15						

All calculated values are gathered in Table II.2. They indicate that creating a spherical cavity requires more energy in protic liquids such as water than in aprotic liquids such as alkanes. For instance, for R = 0.31 nm, ΔG_c(water) = 11.70 kJ.mol^{-1} and ΔG_c(n-hexadecane) = 7.91 kJ.mol^{-1}. This is supposed to be due to the presence of a strong dynamic network of hydrogen bonds [43], whose energetic strength (of the order of 10-40 kJ.mol^{-1} [46]) limits molecular-scale density fluctuations. In alkanes, the predominant interactions are dispersion forces whose energetic strength is much smaller, of the order of 1-10 kJ.mol^{-1} [47], and does not limit molecular-scale density fluctuations.

Sedov and Magsumov recently calculated the Gibbs free energy of cavity formation for a structurally diverse set of organic solvents [43]. Calculations were done using molecular dynamics simulations of solvent boxes and the Widom test-particle insertion method was applied [48]. Their ΔG_c values turned out to be of the same order of ours coming from simple SPT formulas, except in the case of water. The reason is that Sedov and Magsumov (SM) calculated ΔG_c for R = 0.31 nm, but with r_C = 0.17 nm for water and 0.12 nm for organic solvents [43]–[45]. In this work r_C was fixed at 0.12 nm in order to make a correct comparison among all the different solvents. Determining ΔG_c for water with Equation (5) and r_C = 0.17 nm leads to $\Delta G_{c,SPT}$ = 110.37×10^{-20} J.nm^{-3} close to $\Delta G_{c,SM}$ = 116.75×10^{-20} J.nm^{-3} [43]. ΔG_c values in formamide and glycerol (expressed in kJ.mol^{-1}) were found to be larger than in water. The result was considered surprising as the Gibbs free energies for apolar compound solvation in these two solvents are much lower than those in water. The explanation could be in the different magnitude of solvent reorganization upon placing real molecules into the cavity. Actually, this led to some discussions [44], [45]. In any case, looking at ΔG_c converted in energy per unit volume (J.nm^{-3}), water turns out to display the highest Gibbs free energy of cavity formation. The ΔG_c magnitude for alkanes and alcohols has a tendency to decrease on increasing the chain length. This can also be seen with the butanol isomers: V_M(t-butanol) = 157.55 Å^3 > V_M(isobutanol) = 153.33 Å^3 > V_M(n-butanol) = 153.15 Å^3; ΔG_c(t-butanol) = 11.63×10^{-20} J.nm^{-3} < ΔG_c(isobutanol) = 12.53×10^{-20} J.nm^{-3} < ΔG_c(n-butanol) = 13.02×10^{-20} J.nm^{-3}. Also the molecular shape affects ΔG_c [49], [50]: both limonene and n-octane have V_M close to 270 Å^3, but their ΔG_c is, respectively, 8.08×10^{-20} J.nm^{-3} and 5.19×10^{-20} J.nm^{-3}. Even though the size and shape are important, ΔG_c also depends on chemical features. For instance, the ΔG_c magnitude in dichloromethane, dibromomethane and diiodomethane increases even though the molecular size increases. The higher the electronegativity of the halogen element, the higher the interaction ability which favors the occurrence of molecular-scale density fluctuations, leading

to a lower ΔG_c. In other cases, strong intermolecular interactions may limit the occurrence of molecular-scale density fluctuations, leading to a greater ΔG_c. This can be noticed for alkenes in comparison to alkanes, or for molecules having the same number of carbons but different functional groups. The more polar the functional group, the more energy is needed for cavity formation. Overall, ΔG_c values depend on: the size of molecules, their shape and the strength of intermolecular interactions.

The $f_V{}^*$ quantity represents the average density fluctuations in volume and, according to Equations (6) and (7), it accounts for both the fluctuations in number of molecules occupying 1 nm^3, and the molar volume normalized per molecule. Its magnitude reflects structural features of the liquid: a lower f_V^* indicates a lower entity of molecular-scale density fluctuations. Of course, we expect a correlation between the ΔG_c values and the f_V^* values, as suggested by others [51].

3.2. The correlation between the Gibbs free energy of cavity formation and the average density fluctuations in volume

The expected correlation between the ΔG_c values, expressed in energy per volume, and the f_V ones results in $y = 0.04x^{-1.20}$, RMSE = ±5.06 (*i.e.*, ΔG_c proves to be roughly inversely proportional to f_V^*). The correlation is presented in the log-log plot of Fig. II.1a; a focus on data points in the range $f_V^* < 2\times10^{-2}$ nm^3 is shown in Fig. II.1b.

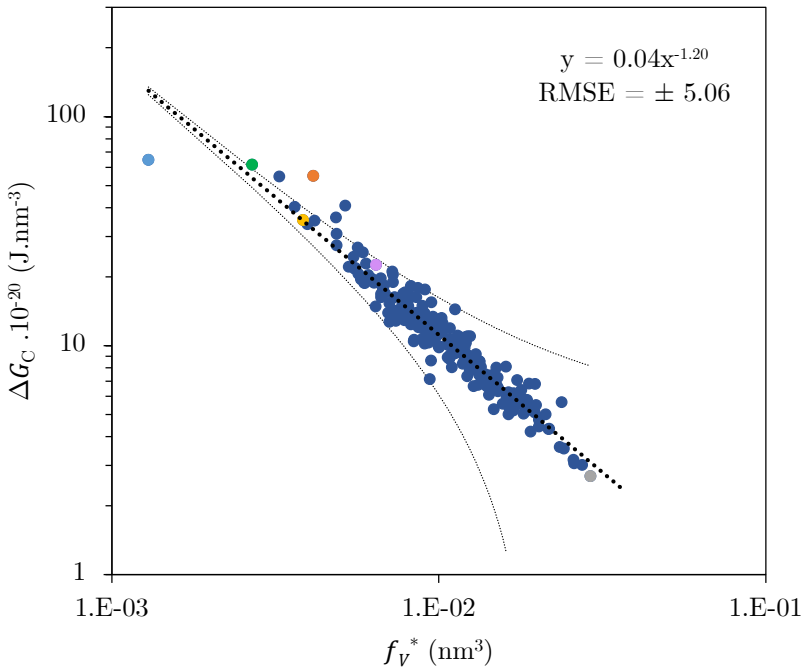

(a)

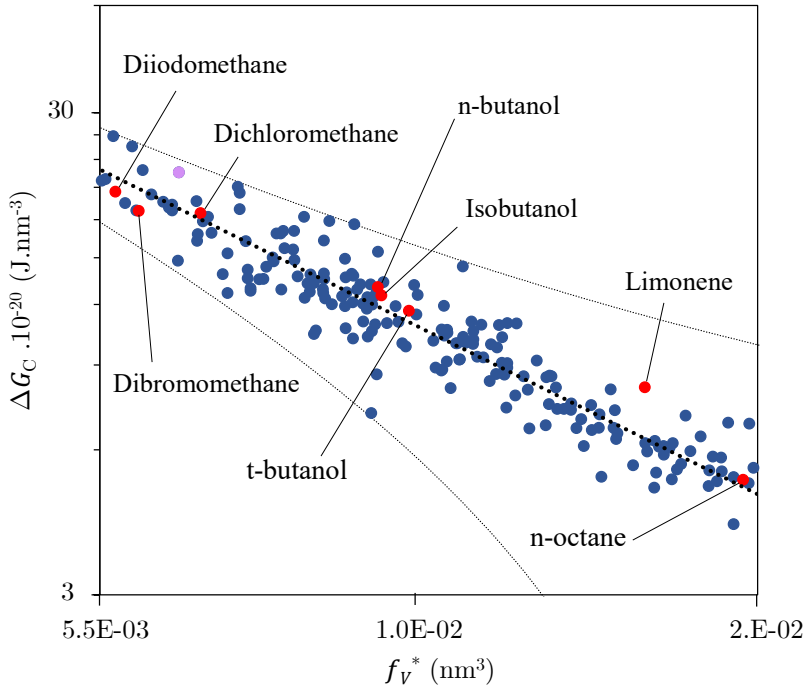

(b)

Fig. II.1. Log-log plot of the dependence of the Gibbs free energy (in the volumetric scale) of formation of a spherical cavity of radius R = 0.31 nm on the average density fluctuations in volume (at 298 K): **(a)** full scale with (●) water, (●) formamide, (●) malonitrile, (●) glycerol, (●) ethanol, (●) hexadecane and **(b)** liquids with $f_V^* < 2\times10^{-2}$ nm^3, ($y = 0.04x^{-1.20}$, RMSE = ±5.06).

This finding confirms that higher the average density fluctuations in volume, smaller the ΔG_c magnitude. Molecular-scale density fluctuations facilitate the accommodation of a cavity for the solute. The solubilisation of a real solute in a liquid needs a cavity of size larger than r_C = 0.12 nm. Thus, it is important to test the validity of the correlation for larger cavities. ΔG_c was calculated, via SPT formulas, for r_C = 0.4 nm, providing the correlation: $y = 0.15x^{-1.34}$. Moreover, the validity of the correlation was tested in extreme conditions, for r_C = 0.01 nm and for r_C = 50 nm. The finding is that the correlation still exists (see Fig. II.2), with the following boundaries:

$$a.x^{-0.88} \leq \Delta G_c = f(f_V^*) \leq b.x^{-1.41} \quad (9)$$

where a and b are constants. This, not only confirms the original suggestion of Pratt and co-workers, but greatly enlarges its validity.

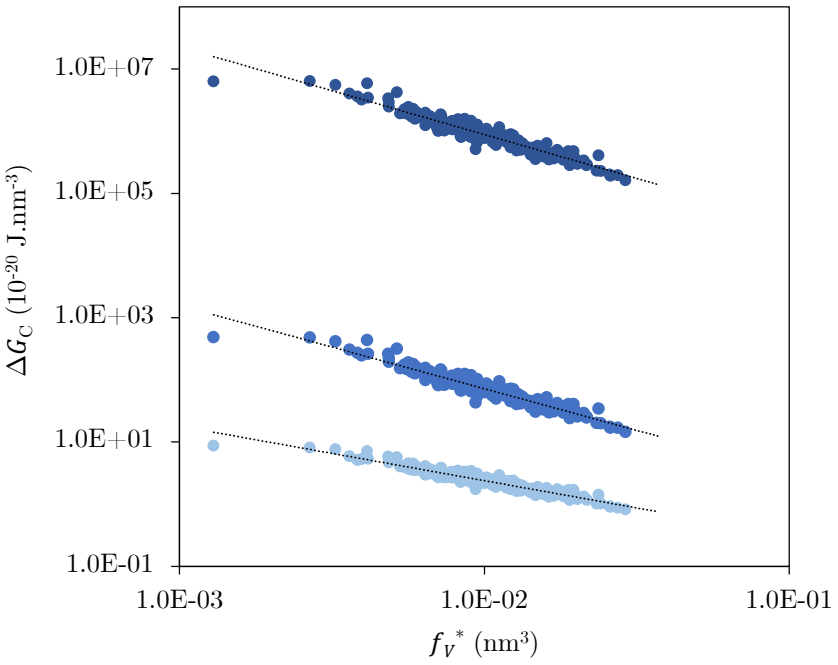

Fig. II.2. Log-log plot of the dependence of the Gibbs free energy (in the volumetric scale) of formation of a spherical cavity of radius (●) r_C = 0.1 Å ($y = 0.04x^{-0.88}$), (●) r_C = 0.4 nm ($y = 0.15x^{-1.34}$) and (●) r_C = 50 nm ($y = 1.33\times10^3\ x^{-1.41}$) upon the average density fluctuations in volume at 298 K.

Having verified the correlation between ΔG_c and f_V^*, and knowing that ΔG_c has a purely entropic origin [28], [29], one may wonder if the f_V^* quantity is related to entropy fluctuations. This possibility was tested using the (volume-independent) mean-square amplitude in entropy fluctuations $^S\Delta$ [11], [12]:

$$^{S}\Delta \equiv \frac{RC_{p,m}}{V_m{}^2} \tag{10}$$

where $C_{p,m}$ and V_m are, respectively, the molar isobaric heat capacity and molar volume of the liquid; $^{S}\Delta$ values are listed in Table II.1. A log-log plot is shown in Fig. II.3, providing the correlation y = 1.65×10^{-3} x$^{-0.97}$, RMSE = ±0.07. Since both f_V^* and $^{S}\Delta$ account for the number of particles/molecules that can fit into a defined volume, the correlation does not come as a surprise. It appears that both types of fluctuations are linked to molecular size. It is worth noting that the correlation still holds neglecting the point of water (y = 1.90×10^{-3} x$^{-0.93}$, RMSE = ±0.03).

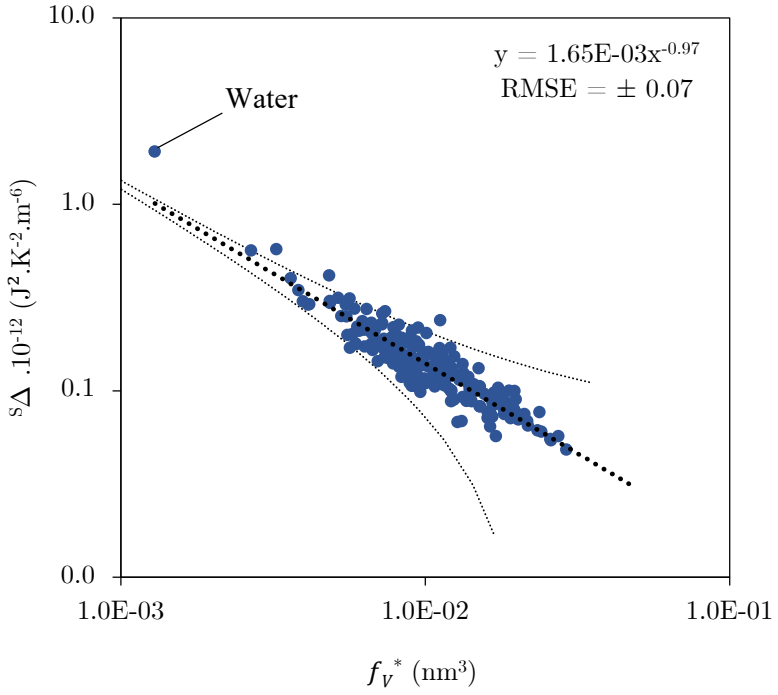

Fig. II.3. The log-log plot of the (volume-independent) mean-square amplitudes in entropy fluctuations $^{S}\Delta$ versus the average density fluctuations in volume at 298 K, (y = 1.65×10^{-3} x$^{-0.97}$, RMSE = ±0.07).

3.3. Critical evaluation of the SPT model

Sedov and Magsumov [43] calculated the Gibbs free energy of cavity formation for a structurally diverse set of organic solvents using computer simulations. We selected the solvents they used (except water in order to allow the comparison between liquids with the same cavity size r_C = 0.12 nm) and compared the correlations with the average density fluctuations in volume f_V^* (Fig. II.4).

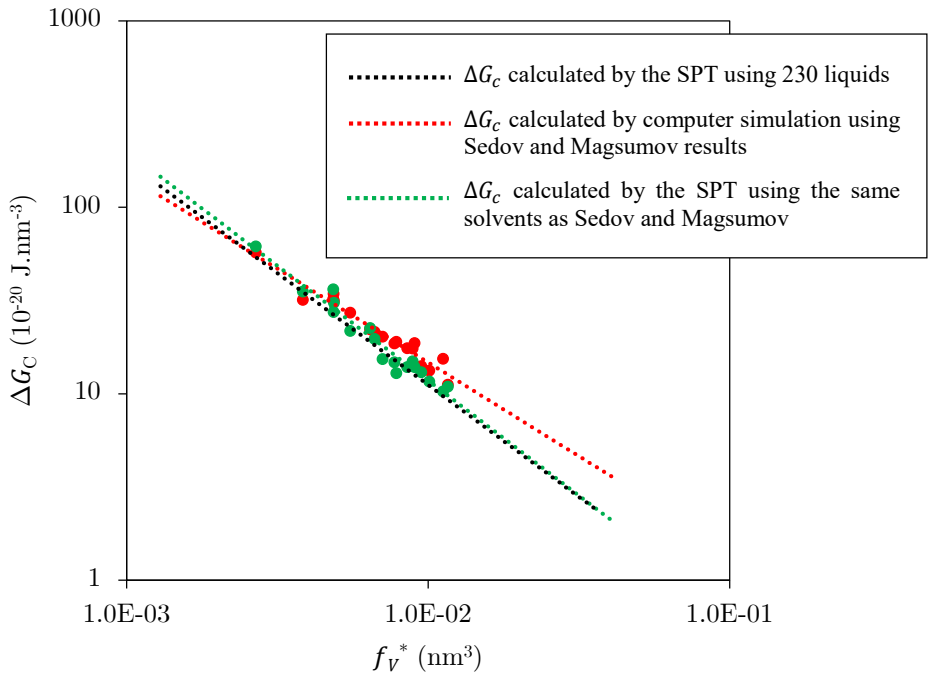

Fig. II.4. Comparison of the relationships between the Gibbs free energy of the formation of a spherical cavity (ΔG_c) of radius R = 0.31 nm and the average density fluctuations in volume f_V^* (at 298 K) given by the SPT model using 230 liquids (y = 0.04x$^{-1.20}$, RMSE = ±5.06, black dash line), by computer simulations using Sedov and Magsumov results (y = 0.13x$^{-1.02}$, RMSE = ±2.12, red dash line) and the SPT model using the same solvents as Sedov and Magsumov (y = 0.12x$^{-1.00}$, RMSE = ±4.49, green dash line).

The relationship obtained using Sedov and Magsumov ΔG_c values (y = 0.13x$^{-1.02}$, RMSE = ±2.12, red dash line) is close to the one obtained via SPT ΔG_c values (y = 0.12x$^{-1.00}$, RMSE = ±4.49, green dash line). The difference may be explained by the fact that Sedov and Magsumov selected the best fitting model for each solvent, obtaining more precise ΔG_c values. The OPLS and GAFF force fields used in their simulation calculations divide intermolecular interactions into different contributions, such as the energy between covalently bonded atoms, the energy due to the geometry of the covalent bonds, the torsional energy and the non-bonded energy. Moreover, some of the present data used to determine ΔG_c and f_V^*, such as β_T or V_{vdw}, were gathered from the literature or from approximations. This could explain a certain extent of point dispersion as observable in Fig. II.1b. It should also be reminded that the radius r used for ΔG_c calculations consisted of the radius of the sphere whose volume corresponds to V_{vdw} of the real molecule. Even considering these limits, the simple and analytic SPT formulas prove to be quite accurate.

Pratt and co-workers [30], [31] suggested, on theoretical grounds, that ΔG_c has to be inversely proportional to the isothermal compressibility, $\Delta G_c \sim 1/\beta_T$, for very small cavities. The present results lead to a more general relationship:

$$\frac{a}{f_V^{*\,0.9}} < \Delta G_c < \frac{b}{f_V^{*\,1.4}} \qquad a, b = \text{cts} \tag{11}$$

Using Equations (7) and then (6), one obtains:

$$a\left(\frac{1}{V_M f_V}\right)^{0.9} = a\left(\frac{\sqrt{V}}{V_M\sqrt{k_B T \beta_T}}\right)^{0.9} < \Delta G_c < b\left(\frac{1}{V_M f_V}\right)^{1.4} = b\left(\frac{\sqrt{V}}{V_M\sqrt{k_B T \beta_T}}\right)^{1.4} \tag{12}$$

That is

$$\frac{a'}{V_M{}^{0.9}\beta_T{}^{0.5}} < \Delta G_c < \frac{b'}{V_M{}^{1.4}\beta_T{}^{0.7}} \qquad a', b' = \text{cts} \tag{13}$$

The general relationship proves to be $\Delta G_c \sim 1/(V_M\sqrt{\beta}_T)$, as emphasized by the linearity of the log-log plot shown in Fig. II.5.

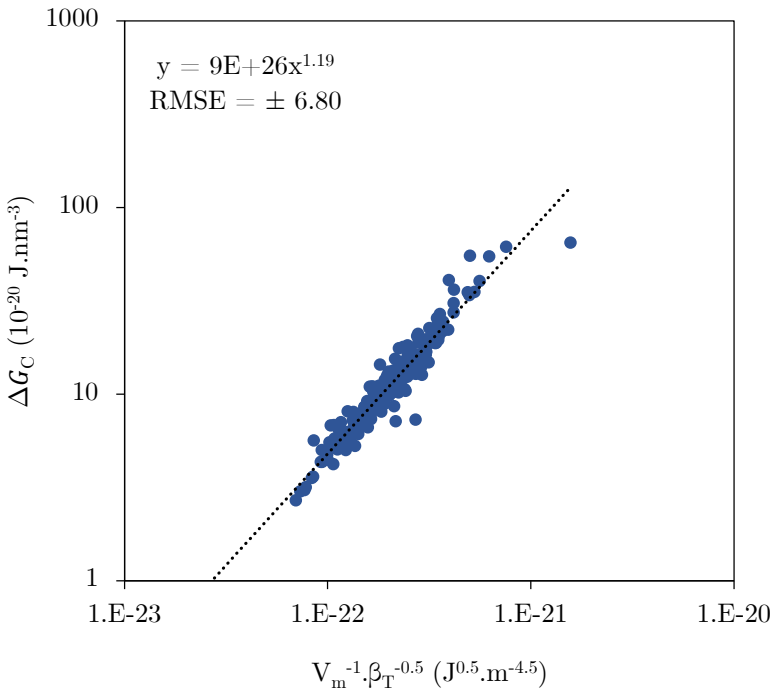

Fig. II.5. Log-log plot of the dependence of the Gibbs free energy (in the volumetric scale) of formation of a spherical cavity of radius R = 0.31 nm on the product of isothermal compressibility and the molecular volume of liquids at 298 K (y = 8.86×10^{26} $x^{1.19}$, RMSE = ±6.80).

4. Conclusions

The Gibbs free energy of cavity formation ΔG_c and the average density fluctuations in volume f_V^* were calculated for more than 200 liquids. The correlation between the two quantities is verified for both small-sized and molecular-sized cavities. This has led to an adjustment of the relationship between ΔG_c and the liquid isothermal compressibility β_T. Another interesting point is the correlation between f_V^* and entropy fluctuations. Moreover, the simple Scaled Particle Theory gives satisfactory results for ΔG_c, comparable to those obtained using computer simulations. This work leads to a description of liquid physics based on two quantities, ΔG_c and f_V^*, which are probes of the molecular-scale density fluctuations at equilibrium, characteristic of the liquid state.

5. Acknowledgements

The authors would like to thank ALLAND & ROBERT Company - Natural and organic gums (Port Mort, France) for financial support (Ph.D. C. Faucon), Sebastien Gaucel (UMR IATE) for his contribution on the mathematical aspects and the reviewers for the useful comments and suggestions incorporated in the revision.

6. References

[1] J. H. Hildebrand, "Solubility VI. Thermodynamic relation between solubility and internal pressure," *J. Am. Chem. Soc.*, vol. 43, no. 3, pp. 500–507, 1921, doi: 10.1021/ja01436a013.

[2] A. F. M. Barton, "Internal Pressure, A fundamental liquid property," *J. Chem. Educ.*, vol. 48, no. 3, pp. 156–162, 1971, doi: 10.1201/9781003091806-5.

[3] C. V. Suryanarayana Anna, "Ultrasound as a probe for assessing the internal pressure and molar cohesive energy of a liquid system: a new model," *Ultrasonics*, vol. 31, no. 4, pp. 281–287, 1993.

[4] M. R. J. Dack, "The importance of solvent internal pressure and cohesion to solution phenomena," *Chem. Soc. Rev.*, vol. 4, no. 2, pp. 211–229, 1975, doi: 10.1039/CS9750400211.

[5] D. Stopper, H. Hansen-Goos, R. Roth, and R. Evans, "On the decay of the pair correlation function and the line of vanishing excess isothermal compressibility in simple fluids," *J. Chem. Phys.*, vol. 151, no. 1, pp. 1–13, 2019, doi: 10.1063/1.5110044.

[6] B. Widom, "Intermolecular Forces and the Nature of the Liquid State," *Science (80-.).*, vol. 157, no. 3787, pp. 375–382, 1967.

[7] M. Chorazewski and E. B. Postnikov,

"Thermal properties of compressed liquids: Experimental determination via an indirect acoustic technique and modeling using the volume fluctuations approach," *Int. J. Therm. Sci.*, vol. 90, pp. 62–69, 2015, doi: 10.1016/j.ijthermalsci.2014.11.028.

[8] M. J. Godfrey and M. A. Moore, "Absence of Hyperuniformity in Amorphous Hard-Sphere Packings of Nonvanishing Complexity," *Phys. Rev. Lett.*, vol. 121, no. 7, 2018, doi: 10.1103/PhysRevLett.121.075503.

[9] E. A. Ploetz and P. E. Smith, "Local fluctuations in solution: Theory and applications," *Adv. Chem. Phys.*, vol. 153, pp. 311–372, 2013, doi: 10.1002/9781118571767.ch4.

[10] K. Nygård *et al.*, "Density fluctuations of hard-sphere fluids in narrow confinement," *Phys. Rev. X*, vol. 6, no. 1, 2016, doi: 10.1103/PhysRevX.6.011014.

[11] Y. Koga, "Fluctuations in aqueous solutions of some hydrophobic solutes," *Chem. Phys. Lett.*, vol. 240, no. 4, pp. 340–344, 1995, doi: 10.1016/0009-2614(95)00531-8.

[12] D. Siu and Y. Koga, "Fluctuation functions in aqueous NaCl and urea," *J. Phys. Chem. B*, vol. 109, no. 35, pp. 16886–16890, 2005, doi: 10.1021/jp0516792.

[13] A. . Soper, "Is water one liquid or two ?," *J. Chem. Phys.*, vol. 150, no. 234503, 2019, doi: 10.1063/1.5096460.

[14] W. Linert, M. Holzweber, and R. Schmid, *Effect of solvents on chemical reactions and reactivity*, Second Edi., vol. 1, no. April. ChemTec Publishing, 2014.

[15] S. N. Jamadagni, R. Godawat, and S. Garde, "Hydrophobicity of proteins and interfaces: Insights from density fluctuations," *Annu. Rev. Chem. Biomol. Eng.*, vol. 2, pp. 147–171, 2011, doi: 10.1146/annurev-chembioeng-061010-114156.

[16] A. P. Abbott, "Application of hole theory to the viscosity of ionic and molecular liquids," *ChemPhysChem*, vol. 5, no. 8, pp. 1242–1246, 2004, doi: 10.1002/cphc.200400190.

[17] M. H. Cohen and G. S. Grest, "Liquid-glass transition, a free-volume approach," *Phys. Rev. B*, vol. 20, no. 3, pp. 1077–1098, 1979, doi: 10.1103/PhysRevB.20.1077.

[18] T. V. Chalikian, M. Totrov, R. Abagyan, and K. J. Breslauer, "The hydration of globular proteins as derived from volume and compressibility measurements: Cross correlating thermodynamic and structural data," *J. Mol. Biol.*, vol. 260, no. 4, pp. 588–603, 1996, doi: 10.1006/jmbi.1996.0423.

[19] K. Gekko, "Compressibility gives new insight into protein dynamics and enzyme function," *Biochim. Biophys. Acta - Protein Struct. Mol. Enzymol.*, vol. 1595, no. 1–2, pp. 382–386, 2002, doi: 10.1016/S0167-4838(01)00358-2.

[20] F. Persson and B. Halle, "Compressibility of the protein-water interface," *J. Chem. Phys.*, vol. 148, no. 21, 2018, doi: 10.1063/1.5026774.

[21] G. Graziano, "Cavity size distribution in the interior of globular proteins," *Chem. Phys. Lett.*, vol. 434, no. 4–6, pp. 316–319, 2007, doi: 10.1016/j.cplett.2006.12.029.

[22] B. Lee, "Solvent reorganization contribution to the transfer thermodynamics of small nonpolar molecules," *Biopolymers*, vol. 31, no. 8, pp. 993–1008, 1991, doi: 10.1002/bip.360310809.

[23] M. Prévost, I. T. Oliveira, J. P. Kocher, and S. J. Wodak, "Free energy of cavity formation in liquid water and hexane," *J. Phys. Chem.*, vol. 100, no. 7, pp. 2738–2743, 1996, doi: 10.1021/jp952906a.

[24] B. Lee, "The physical origin of the low solubility of nonpolar solutes in water," *Biopolymers*, vol. 24, no. 5, pp. 813–823, 1985, doi: 10.1002/bip.360240507.

[25] A. Ben-Naim, "Statistical Mechanical Study of Hydrophobic Interaction. I. Interaction between Two Identical Nonpolar Solute Particles," *J. Chem. Phys.*, vol. 54, no. 3, pp. 1387–1404, 1971, doi: 10.1063/1.1674979.

[26] G. Graziano, "Contrasting the hydration thermodynamics of methane and methanol," *Phys. Chem. Chem. Phys.*, vol.

21, no. 38, pp. 21418–21430, 2019, doi: 10.1039/c9cp03213d.

[27] R. A. Pierotti, "Aqueous Solutions of Nonpolar Gases," *J. Phys. Chem.*, vol. 69, pp. 281–288, 1965.

[28] G. Graziano, "Comment on 'Reevaluation in interpretation of hydrophobicity by scaled particle theory,'" *J. Phys. Chem. B*, vol. 106, no. 31, pp. 7713–7717, 2002, doi: 10.1021/jp014558k.

[29] G. Graziano, "Relationship between cohesive energy density and hydrophobicity," *J. Chem. Phys.*, vol. 121, no. 4, pp. 1878–1882, 2004, doi: 10.1063/1.1766291.

[30] G. Hummer, S. Garde, A. E. Garcia, M. E. Paulaitis, and L. R. Pratt, "Hydrophobic Effects on a Molecular Scale," *J. Phys. Chemitry B*, vol. 102, no. 51, pp. 10469–10482, 1998, doi: 10.1177/074193258901000304.

[31] G. Graziano, "Cavity thermodynamics in the Gaussian model of particle density fluctuations," *Chem. Phys. Lett.*, vol. 446, no. 4–6, pp. 313–316, 2007, doi: 10.1016/j.cplett.2007.08.063.

[32] J. S. Rowlinson and F. L. Swinton, *Liquids and liquid mixtures*, Butterwort. 1982.

[33] H. Reiss, H. L. Frisch, and J. L. Lebowitz, "Statistical mechanics of rigid spheres," *J. Chem. Phys.*, vol. 31, no. 2, pp. 369–380, 1959, doi: 10.1063/1.1730361.

[34] E. Helfand, H. Reiss, H. L. Frisch, and J. L. Lebowitz, "Scaled particle theory of fluids," *J. Chem. Phys.*, vol. 33, no. 5, pp. 1379–1385, 1960, doi: 10.1063/1.1731417.

[35] M. J. Mandell and H. Reiss, "Scaled particle theory: Solution to the complete set of scaled particle theory conditions: Applications to surface structure and dilute mixtures," *J. Stat. Phys.*, vol. 13, no. 2, pp. 113–128, 1975, doi: 10.1007/BF01221372.

[36] K. E. S. Tang and V. A. Bloomfield, "Excluded volume in solvation: Sensitivity of scaled-particle theory to solvent size and density," *Biophys. J.*, vol. 79, no. 5, pp. 2222–2234, 2000, doi: 10.1016/S0006-3495(00)76470-8.

[37] G. Graziano, "Scaled particle theory study of the length scale dependence of cavity thermodynamics in different liquids," *J. Phys. Chem. B*, vol. 110, no. 23, pp. 11421–11426, 2006, doi: 10.1021/jp0571269.

[38] T. Head-gordon and G. Hura, "Water Structure from Scattering Experiments and Simulation," *Chem. Rev.*, no. 102, pp. 2651–2670, 2002, doi: 10.1021/cr0006831.

[39] G. Graziano, "Water: Cavity size distribution and hydrogen bonds," *Chem. Phys. Lett.*, vol. 396, no. 4–6, pp. 226–231, 2004, doi: 10.1016/j.cplett.2004.07.126.

[40] C. L. Yaws, "Thermophysical properties of chemicals and hydrocarbons," pp. 1–9, 2015, doi: 10.1016/B978-081551596-8.50024-9.

[41] Y. Marcus, *The Properties of Solvents*, John Wiley. The Hebrew University of Jerusalem, Israel, 1998.

[42] A. Bondi, "Van der waals volumes and radii," *J. Phys. Chem.*, vol. 68, no. 3, pp. 441–451, 1964, doi: 10.1021/j100785a001.

[43] I. Sedov and T. Magsumov, "The Gibbs free energy of cavity formation in a diverse set of solvents," *J. Chem. Phys.*, vol. 153, no. 13, 2020, doi: 10.1063/5.0021959.

[44] G. Graziano, "Comment on 'the Gibbs free energy of cavity formation in a diverse set of solvents'[J. Chem. Phys. 153, 134501 (2020)]," *J. Chem. Phys.*, vol. 154, no. 18, 2021, doi: 10.1063/5.0044991.

[45] I. Sedov, "Response to 'comment on "The Gibbs free energy of cavity formation in a diverse set of solvents"' (J. Chem. Phys. 154, 187101 (2021))," *J. Chem. Phys.*, vol. 154, no. 18, pp. 187101–187103, 2021, doi: 10.1063/5.0051746.

[46] P. Atkins and J. De Paula, *Physical Chemistry for the Life Sciences*, W. H. Free. New York, 2006.

[47] J. N. Israelachvili, *Intermolecular and Surface Forces*. 2011.

[48] B. Widom, "Potential-distribution theory and the statistical mechanics of fluids," *J. Phys. Chem.*, vol. 86, no. 6, pp. 869–872, 1982, doi: 10.1021/j100395a005.

[49] G. Graziano, "Shape effect on non-covalent dimer stability using classic scaled particle theory," *Chem. Phys. Lett.*, vol. 743, no. January, p. 137176, 2020, doi: 10.1016/j.cplett.2020.137176.

[50] A. J. Guseman, G. M. P. Goncalves, S. L. Speer, G. B. Young, and G. J. Pielak, "Protein shape modulates crowding effects," *Proc. Natl. Acad. Sci. U. S. A.*, vol. 115, no. 43, pp. 10965–10970, 2018, doi: 10.1073/pnas.1810054115.

[51] R. Godawat, S. N. Jamadagni, and S. Garde, "Characterizing hydrophobicity of interfaces by using cavity formation, solute binding, and water correlations," *Proc. Natl. Acad. Sci. U. S. A.*, vol. 106, no. 36, pp. 15119–15124, 2009, doi: 10.1073/pnas.0902778106.

Chapter III: Acacia gum interfacial properties at aroma – water interfaces

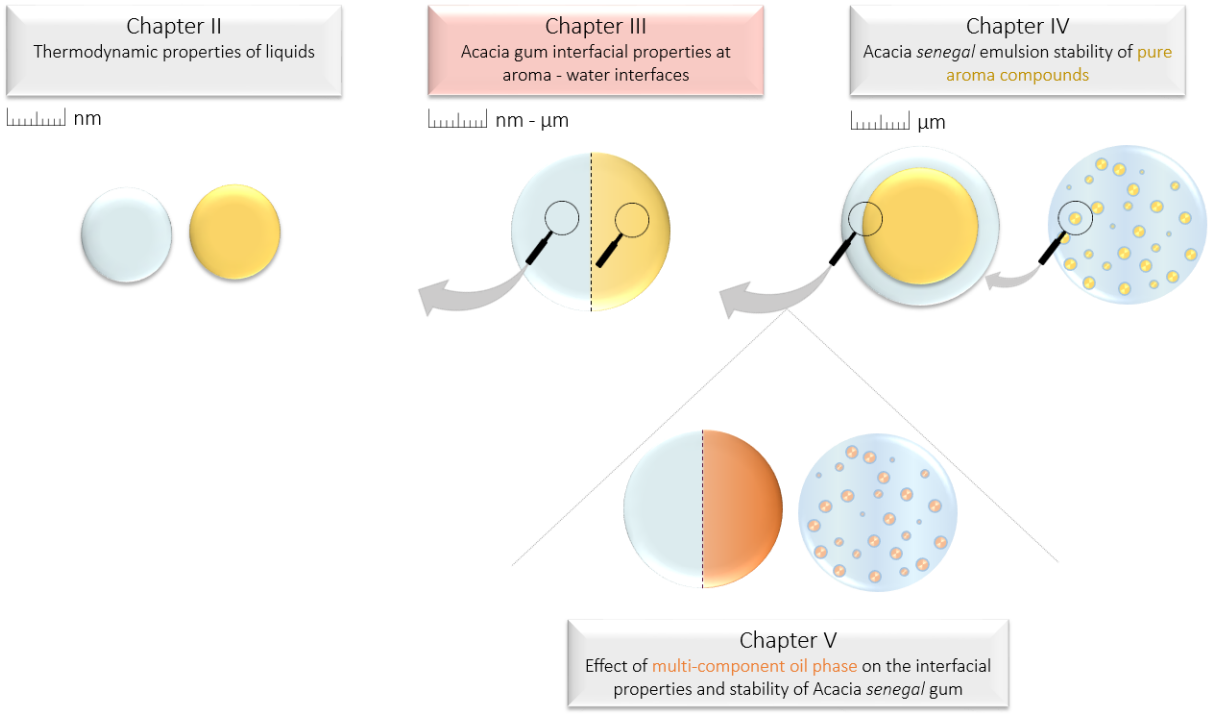

This chapter aimed to study the impact of the oil hydrophobicity on the thermodynamic mechanisms of the Acacia gum layer formation at the oil-water interface. Thus, interfacial properties of Acacia gum were examined using interfacial tension measurements and dilational rheological analyses.

Highlights

- Acacia gum is sensitive to water-induced hydrophobic effects due to the protein content, protein distribution, protein accessibility, and the presence of minerals (ions Ca) that screen charges. Methyl groups of sugars and buried polysaccharide-protein crosslinked

backbone may also contribute to the structure and dynamics of hydrophobic hydration water.

- Water-water, oil-water and AGP-water interactions constitute the driving force of the Acacia gum 3-phases adsorption to oil-water interface.

- Density fluctuations near a macroscopic hydrophobic interface along with the hydrophobic effect, lead AGPs to concentrate at the interface and form a dehydrated structured oil-gum-water interphase.

- Due to enhanced density fluctuations, AGPs preferentially adsorb to highly hydrophobic oils interfaces inducing high oil surface coverage, high interfacial layer elasticity and high ability to reduce the interfacial tension.

- A. *senegal* and A. *seyal* gums differ in protein content, structural conformation and hydration properties resulting in some divergence in interfacial kinetics and interfacial water composition. In turn, the thermodynamic mechanism at the origin of the formation of structured interphase does not depend on the type of gums.

- Oil-water interaction energy is the origin of the oil-water interfacial tension.

- A volumetric Acacia gum adsorption mechanism is proposed.

Natural hyperbranched biopolymer at liquid interfaces differing in oil-water interaction energy[1]

Camille Faucon[a], Pascale Chalier[a], Christian Sanchez[a]

[a] IATE, Univ Montpellier, INRAE, Institut Agro, Montpellier, France.

Abstract

Adsorption from Acacia gum of hyperbranched arabinogalactan-proteins (AGPs) to oil-water interfaces has been extensively studied and is known to contribute to colloidal stabilization of emulsions. Interfacial tension and rheological analyses revealed AGPs form a viscoelastic interfacial structure through a 3-phase mechanism. Yet, the role of water is generally not considered, even though it is the most dynamic component of the oil-gum-water structure. This article aimed to explore the importance of oil-water interactions on the ability of hydrated Acacia gum to form a dehydrated structured oil-gum-water interphase. To this end, interfacial tension and dilational rheological measurements are performed using different classes of oil and so, varying oil-water interactions. First, it is shown adsorption of AGPs is favored near highly hydrophobic interfaces, like proteins, despite its largely predominant hydrophilic characteristics. Then, a volumetric Acacia gum adsorption mechanism is proposed based on the assumptions i) favored interaction energy between water and oil, in particular OH-containing oils involving hydrogen-bond, limits the AGPs interfacial properties, and ii) the surface pressure is a direct measure of the change in the interfacial thermodynamic activity of water molecules.

Keywords: Acacia gum; adsorption; hydrophobic interfaces; interfacial tension; dilational rheology; water interactions

[1]Article submitted to Journal of Molecular Liquids

1. Introduction

The study of liquid interfacial properties is of great interest for many natural and industrial processes involving systems characterized by immiscible phases and high specific area such as emulsions, foams or colloidal systems in general [1]–[3]. Proteins and various types of polysaccharide-rich proteoglycan or protein-rich glycoprotein may form structured interfaces, contributing to the decrease of the interfacial tension and to the formation of a stabilizing interfacial viscoelastic barrier. This results in the delay of thermodynamic instability of emulsions such as the droplet flocculation, coalescence, or Ostwald ripening [4], [5]. Among proteoglycans, Acacia gum (GA) is a natural surface-active biopolymer widely used for colloidal stabilization purpose. It is obtained from the trunk and branches of Acacia trees [6], [7]. Acacia *senegal* (A. *senegal*) and Acacia *seyal* (A. *seyal*) are two varieties whose differences in interfacial properties have been related to their biochemical composition and structure [8]–[10]. Both gums are mainly composed by hyperbranched proteoglycans, namely highly glycosylated hydroxyproline-rich arabinogalactan-proteins or peptides (AGPs). These biopolymers are essentially made of sugars D-galactose, L-arabinose, L-rhamnose, D-glucuronic acid, and 4-O-methyl-D-glucuronic acid [6]. In addition, AGPs contain about 1-3% of proteins, 3-4% of minerals and around 1% polyphenols, relative proportions that may vary according to the specie, the origin (*i.e.* the tree location, the age), and the environmental and harvest conditions [6]. Generally, AGPs can be described as heavily branched neutral and charged sugars forming polysaccharide blocks covalently bonded to a polypeptide backbone rich in hydroxyproline and serine aminoacids [11], [12]. This protein/polysaccharide duality typically confers amphiphilic properties allowing the interfacial concentration of GA to gas–liquid, liquid–liquid, and solid–liquid interfaces [13]. The formation of oil-GA-water structure has already been studied and reported to behave similarly to pure protein interfaces [14]–[16]. In particular, high molar mass protein-rich AGPs that are present in Acacia gum were found responsible for providing the interfacial properties in relation to the protein content, its distribution and accessibility [13], [16]–[20].

Interfacial tension and rheology are widely used to investigate the stabilization mechanisms induced by these biopolymers [16], [19], [21]–[23]. For instance, dilational rheological measurements showed AGPs form a viscoelastic interfacial structure of a given thickness [24], [25] that displays at equilibrium almost perfectly elastic structure [6], [19], [25]. Physicochemical

parameters such as pH, ionic strength, GA concentration and dispersion viscosity changed the structuring mechanism and interface structure [26], [27], [8], [10], [26], [28]–[30]. In contrast, fewer studies considered these questions regarding the role of the oil phase [28], [30]–[32]. Recent work on proteins however concluded larger oil hydrophobicity leads to more elastic interfacial layers [33]–[36].

Curiously, the role of water, *i.e.* the major component and the most dynamic one, has been mainly omitted when discussing the interfacial structuring mechanism of biopolymers. Yet interactions with water are necessarily implied in these interfacial phenomena since hydration-dependent volumetric properties of proteins have been related to their hydrophobicity and surface properties [37]–[42]. A volumetric 3D model of the hydrated protein adsorption process on hydrophobic surfaces was then proposed in 2012 by Vogler [43]. It is based on the assumption that changes in hydrogen bond interaction energy induced by contact with surfaces have a significant effect on the interfacial water properties, which in turn influence the interfacial interaction dynamics of proteins. The first step is the hydration of the hydrophobic surface when brought into contact with an aqueous-protein dispersion. A thin, pseudo-2D interface between the adsorbent and protein dispersion is then immediatly formed. Thereafter the diffusion of protein molecules into this newly formed interface occurs by displacing an equivalent volume of interfacial water (interfacial dehydration). This leads to the creation of a truly 3D interphase that inflates with arriving proteins. However, the energy required for the displacement of interfacial water strongly depends on the interactions between the adsorbent surface and water. The volumetric model of protein interfaces predict more difficult interfacial concentration of proteins in case of stronger attractive water-surface interactions, in line with the increased stiffness of protein interfaces with low oil-water attractive interactions [33]–[36].

On the same vein, the air-water interfacial tension was defined as a change in water molecule free energy [44]. Importantly, this means the surface pressure is a direct measure of the change in the interfacial thermodynamic activity of water molecules a_w^s. In this theory, the reduction in interfacial water activity occurs as a result of two molecular processes, namely anchoring of the protein to the interface and its aggregation. Furthermore, this supposed correlation between the interfacial water activity and the air-water interfacial tension has been experimentally validated [45]. In addition, there is a strong correlation between surface activity of proteins and the extent of protein volume fluctuations [44], that only depends on the intrinsic compressibility of protein and its hydration level [46]. The Vogler's thermodynamic model of

protein interfaces associated to the interfacial thermodynamic activity of water molecules seems promising to describe interfacial properties of hydrated arabinogalactan-proteins or hydrated biopolymers in general.

In the present work, we explored the importance of oil-water van der Waals and hydrogen bond interactions on the ability of hydrated Acacia gum to form a dehydrated and structured oil-gum-water interphase. These interactions were examined by varying the oil hydrophobicity. Different classes of oil were used, e.g. alkane, terpene, ketone, ester and alcohol. We first confirmed adsorption of AGPs is favored near highly hydrophobic interfaces. In the discussion, we then proposed a volumetric Acacia gum adsorption mechanism based on the following hypotheses i) favored interaction energy between water and oil, in particular OH-containing oils involving hydrogen-bond, affects the AGPs interfacial properties [43], and ii) the surface pressure is a direct measure of the change in the interfacial thermodynamic activity of water molecules [44]. Throughout the article the assumption is made that the oil-water adsorption driving forces are similar to those of the air-water adsorption. The GA interfacial properties were investigated through interfacial tension and dilational rheological measurements. One may note the interfacial viscoelastic moduli in this article need to be considered as apparent parameters due to the known limitations of the used method (details are discussed later). Lastly, the term interphase will be used to better refer to the 3D-volumetric interfacial zone between oil and water.

2. Materials and methods

2.1. Materials

Acacia senegal (Batch n° OF110676, A. *senegal*) and Acacia *seyal* (Batch n° OF110724, A. *seyal*) gums were provided by Alland & Robert Company - Natural and organic gums (Port mort, France). Both gum powders were obtained with the same process. Their biochemical composition and basic structural properties were previously characterized [11], [12] and are presented in Table III.1. Acacia gum dispersions were obtained by dissolving the gum powders in a pH 5 sodium acetate buffer (10 mM; Milli-Q-water; acetic acid Sigma-Aldrich; $C_2H_3NaO_2{\cdot}3H_2O$, Sigma-Aldrich), by stirring overnight at room temperature, and then by centrifuging at 12 000 rpm for 30 minutes at 25°C for removing insoluble materials.

n-Hexadecane (≥99%), d-limonene (≥97%), carvone (≥98%), 1-octanol (≥99%), 1-decanol (≥98%), myrcene (≥95%), ethyl octanoate (≥99%), methyl octanoate (≥99%) were purchased from Sigma-Aldrich. The purity of the organic volatile d-limonene was improved through an additional purification step using Florisil® resins ($MgO{\cdot}SiO_2$, 60–100 mesh, Sigma-Aldrich). The method used is reported in literature [8], [47].

Table III.1. Biochemical compositions and structural parameters of A. *senegal* and A. *seyal*. Adapted from Lopez-Torrez et al. 2016 [48].

	A. *senegal* (Batch n° OF110676)	A. *seyal* (Batch n° OF110724)
Total dry matter ($mg.g^{-1}$)	899.3 (±0.4)	888.4 (±4.2)
Moisture (%)	10.1	11.1
Sugar ($mg.g^{-1}$)*	940.0	950.0
Arabinose (%)	30.3 (±2.5)	47.6 (±0.6)
Galactose (%)	35.8 (±1.2)	36.9 (±1.1)
Rhamnose (%)	15.5 (±0.4)	3.0 (±0.3)
Glucuronic acid (%)	17.4 (±1.2)	6.7 (±0.4)
4-O-Me-Glucuronic acid (%)	1.0 (±0.1)	5.8 (±0.6)
Uronic acid/neutral sugar ratio	0.23	0.14
Protein ($mg.g^{-1}$)	27.0 (±0.0)	10.0 (±0.0)
Mineral ($mg.g^{-1}$)	33.0 (±0.2)	40.0 (±0.1)
Average molar mass (M_w, $g.mol^{-1}$)	$6.8{\times}10^5$	$8.2{\times}10^5$
Polydispersity index (M_w/M_n)	2.0	1.5
Branching degree (%)	78.2	59.2
Intrinsic viscosity ($mL.g^{-1}$)	22.8	16.5

* Total content of sugars calculated from the difference of proteins and minerals from 1 000 $mg.g^{-1}$.

2.2. Methods

The interfacial tension and dilational rheological properties of Acacia gums (GA) at the oil-water interface were measured by the rising drop technique using an automatic drop tensiometer (Tracker™, Teclis Scientific, Civrieux d'Azergues, France) equipped with a CCD camera (640x480 pixels resolution, max 60 fps) and a cuvette surrounded with a thermostatic envelop. Drops of 3–10 µL of organic compound were formed from a 500 µL syringe with a stainless steel needle immersed in the cuvette containing a 5 wt% gum dispersion. Equipment and set up are illustrated in Fig. III.1. The measurements were performed at 25°C (±0.3°C),

the temperature being controlled for both the cuvette and the syringe using a circulating bath (Witeg, Germany). The drop profiles were monitored by the CCD camera for a 7h or 24h time.

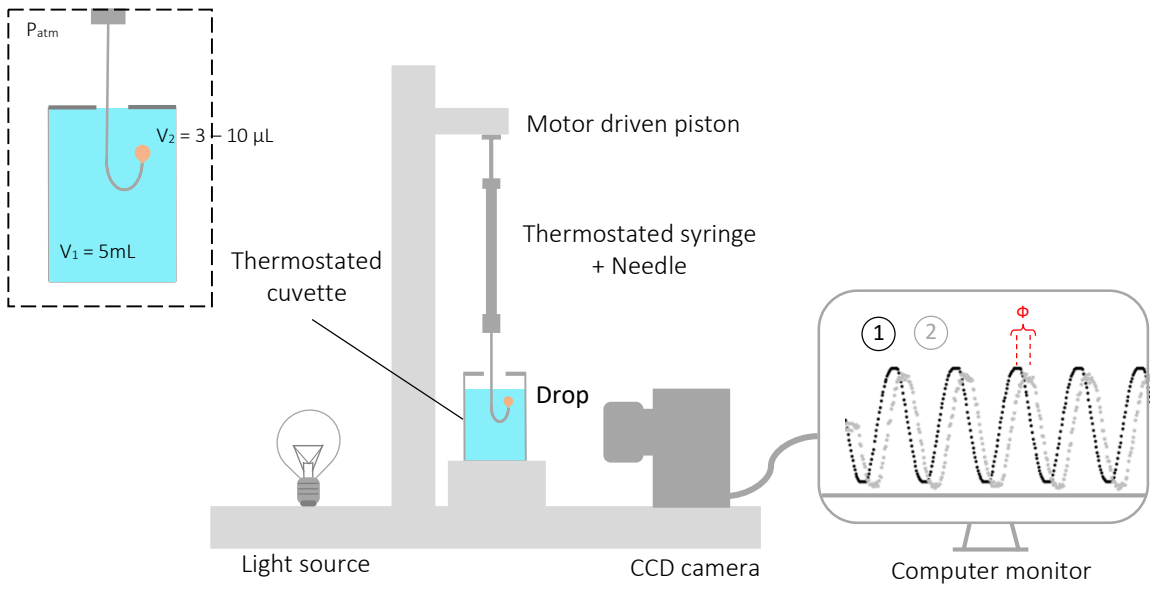

Fig. III.1. Schematic representation of the dynamic drop tensiometer. 1: Input (drop surface area), 2: Output (oil-GA dispersion interfacial tension).

The dynamic interfacial tension between the two immiscible liquids (GA dispersion and oil) was determined by a numerical analysis of the drop shape and a fit with models based on the Young-Laplace equation. The drop interface underwent deformations consisting of a sinusoidal variation of the volume V leading to the deformation of the interfacial area A. The oscillation ($\Delta V/V$) was performed with a 10% amplitude and an oscillation frequency (ω) of 0.1 s^{-1}. The drop interface followed successive compression and dilation cycles as illustrated on the computer monitor Fig. III.1 with the black signal. The response of this deformation manifested by a variation in the interfacial tension illustrated by the grey signal.

The interfacial viscoelastic modulus $E^*$and the phase angle Φ (Fig. III.1.) were derived from the change in interfacial tension γ resulting from the drop area fluctuation as followed:

$$\gamma = \gamma_0 \sin(\omega t + \Phi) \quad (1)$$

$$A = A_0 \sin(\omega t) \quad (2)$$

$$E^* = d\gamma/(dA/A) = d\gamma/dln(A) \quad (3)$$

The resulting interfacial viscoelastic modulus E^* is a complex number, with a real part E', corresponding to the stored elastic energy, and an imaginary part E", corresponding to the dissipative viscous energy.

$$E^* = |E|\cos(\Phi) + \mathrm{i}|E|\sin(\Phi) \quad (4)$$

$$E' = |E|\cos(\Phi) \quad (5)$$

$$E'' = |E|\sin(\Phi) \quad (6)$$

Referring to the definition, the elastic modulus E' represents the resistance of the drop surface layer to a change in surface area A (Equation 7). In this article, the word 'layer' will be used instead of 'film' in order to avoid any confusion with a 2D plate-notion the word 'film' can bring. The analogy can be made with another thermodynamic parameter, namely the isothermal compressibility β_T. The latter is defined as $\beta = -\frac{1}{V}\left(\frac{\delta V}{\delta P}\right)$ and qualify changes in volume V in response to changes in pressure P (Equation 8). The inverse of the isothermal compressibility is called the isothermal bulk modulus K_T and refers to the elastic resistance of a change in volume. The 2D-parameter E' is then the thermodynamic equivalent of the 3D-parameter K_T. Interfacial elastic modulus E' changes should be formally interpreted as fluctuations in surface density [49], [50].

$$E' = \mathrm{A}\frac{\Delta\gamma}{\Delta\mathrm{A}} \quad \text{2D-parameter} \quad (7)$$

$$\beta_T = -\frac{1}{\mathrm{V}}\frac{\Delta\mathrm{V}}{\Delta\mathrm{P}} \quad ; \quad \frac{1}{\beta_T} = K_T = -\mathrm{V}\frac{\Delta\mathrm{P}}{\Delta\mathrm{V}} \quad \text{3D-parameter} \quad (8)$$

3. Results

3.1 Effect of oil hydrophobicity on thermodynamic properties of interfacial water and interfacial viscoelastic properties

Mutual water molecule attraction leads to the segregation of oil from water in order to minimize unfavorable oil-water interactions [51]. In reality, interactions between water and oil are not unfavorable but water-water interactions are preferred over water-oil interactions due to the prohibitive cost to create in water a cavity for a large extended hydrophobic body. This results in an effective oil-oil attraction, commonly called the hydrophobic interaction. A thermodynamic parameter that may describe the extent of oil hydrophobicity is the oil-water

interfacial tension γ_{ow} [33], [35], [36], [52], [53]. The γ_{ow} parameter obtained on various hydrophobic liquids is presented in Table III.2.

Table III.2. Oil-water interfacial tension (γ_{ow}) with oils varying in hydrophobicity, maximum dilational elastic modulus (E'_{max}) obtained in a 5 wt% A. *senegal* or A. *seyal* dispersion and calculated surface concentration of 5 wt% A. *senegal* gum at 25°C according to the a model developed for amphiphilic copolymers [54], [55].

Oil type	Oil name	γ_{ow} (mN.m^{-1})	E'_{max} A. *senegal* (mN.m^{-1})	E'_{max} A. *seyal* (mN.m^{-1})	Γ^a A. *senegal* (mg.m^{-2})
Alkane	n-Hexadecane	47.2 (±1.4)	67.1 (±4.8)		7.3 (±0.2)
		*44.8 (±0.4)		55.0 (±5.0)	
Terpenes	d-Limonene	38.5 (±1.4)	46.3 (±3.4)	50.1 (±4.3)	6.7 (±0.3)
	d-Limonene 97%	*24.0 (±0.2)	31.9 (±2.0)	*26.7 (±3.5)	*4.3 (±0.3)
		30.0 (±0.4)		41.9 (±0.5)	
	Myrcene	36.4 (±0.1)	46.1 (±1.8)		5.7 (±0.2)
		*27.8 ± (1.0)		*36.3 (±2.6)	
Alcohols	1-Octanol	8.4 (±0.5)	14.4 (±0.3)	10.2 (±0.7)	1.1 (±0.1)
	1-Decanol	9.1 (±0.2)	15.5 (±0.1)	14.1 (±1.7)	1.1 (±0.1)
Ketone	Carvone	16.5 (±0.1)	23.3 (±0.8)	24.3 (±2.2)	2.8 (±0.1)
Esters	Methyl octanoate	21.3 (±0.2)	33.6 (±2.9)		3.1 (±0.1)
		*19.9 (±0.1)		*29.1 (±2.4)	
	Ethyl octanoate	23.9 (±0.2)	31.6 (±2.0)		3.6 (±0.1)
		*22.0 (±0.1)		*34.9 (±1.9)	

**moderately altered n-hexadecane, d-limonene 97%, myrcene, methyl octanoate and ethyl octanoate*
[a]estimations of GA surface concentrations using a model described in Supplemental Info 6.3

The results are fully consistent with the literature [22], [33]. In our set, n-hexadecane was found the most hydrophobic compound (γ_{ow} = 47.2 mN.m^{-1}) while 1-octanol was the least hydrophobic one (γ_{ow} = 8.4 mN.m^{-1}). The equilibrium interfacial pressures $\Pi_\infty = \gamma_{ow} - \gamma_\infty$ were calculated for both types of gums and plotted over the oil-water interfacial tension γ_{ow} (Fig. III.2). In parallel, the dilational rheological properties of interfaces were determined as presented in Table III.2. Then, Fig. III.3 reports the illustrative results for the most and the least hydrophobic oils of the evolution of elastic (E') and viscous (E") dilational moduli. It also displays the loss tangent (tan δ = E"/E') for both gums together with the maximum elastic modulus E'_{max} of all oils as a function of time. A better visualization of n-hexadecane and 1-octanol viscous moduli can be found in Supplemental Info 6.1. All rheological profiles can be found in annex B.

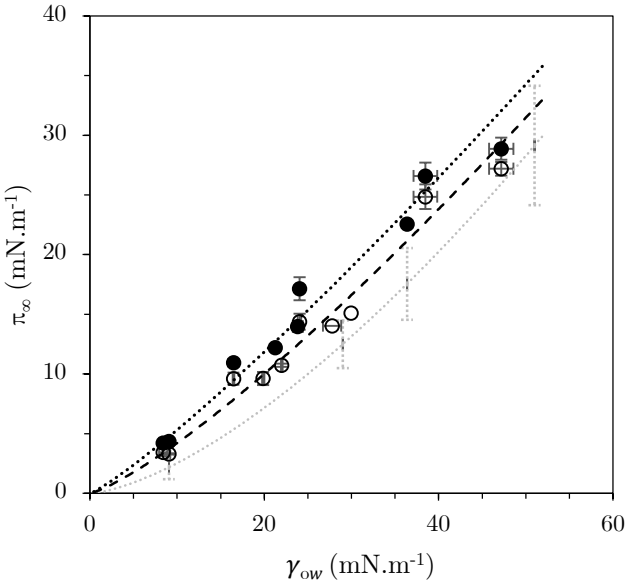

Fig. III.2. Dependency of the equilibrium oil-GA-water interfacial pressure Π_∞ on the oil-water interfacial tension γ_{ow}. Black dotted or dashed line represents respectively the fits for the 5 wt% A. *senegal* dispersion (filled label) ($y = 0.36x^{1.16}$) and for the 5 wt% A. *seyal* dispersion (open label) ($y = 0.24x^{1.25}$); the grey dotted line comes from Bergfreund and al. work and represents the fit for 10 mg.L^{-1} BSA, BLG, LSZ and some other protein values from literature ($y = 0.08x^{1.5}$) [35].

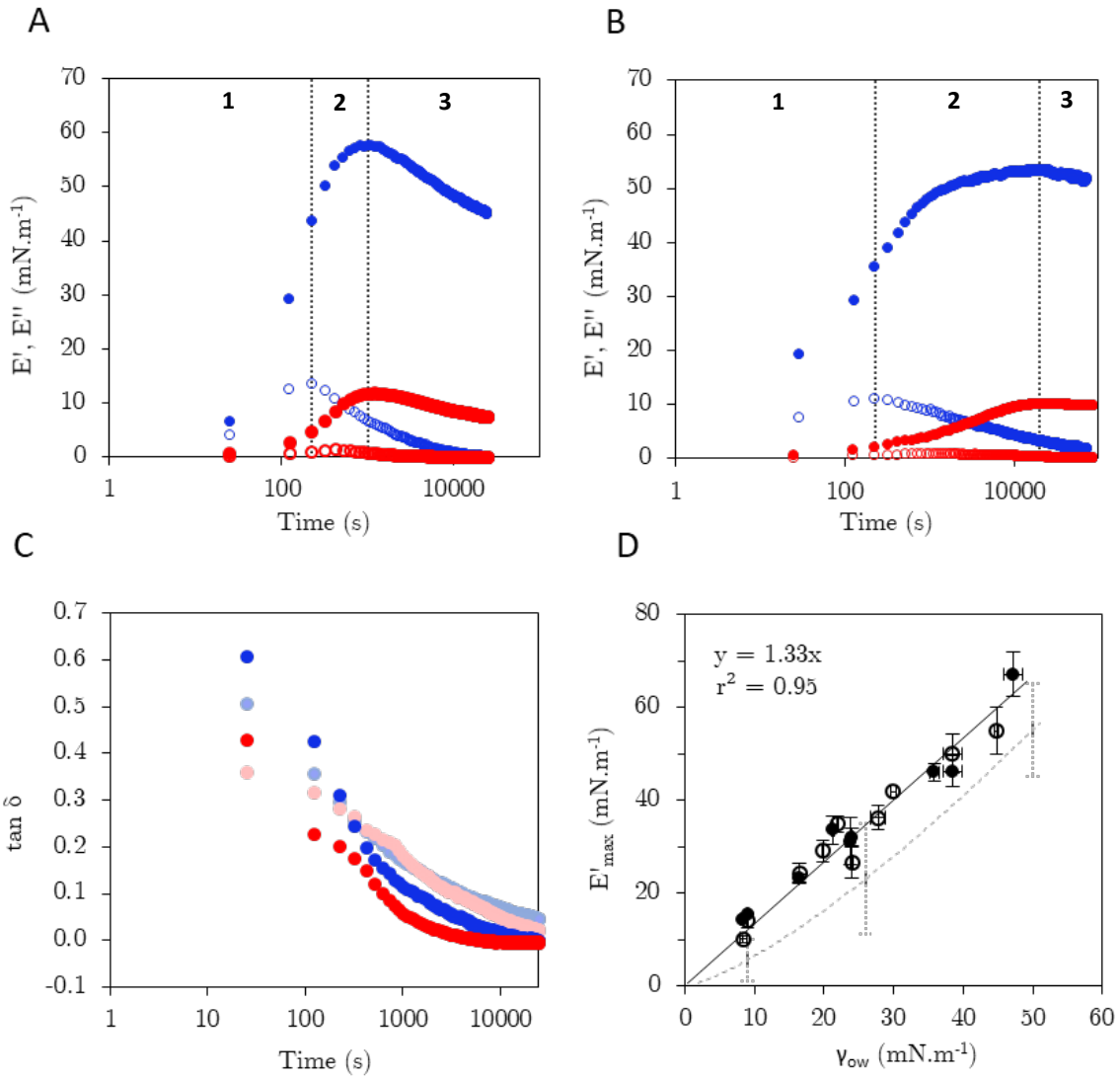

Fig. III.3. Interfacial viscoelastic properties at 25°C of 5 wt% Acacia gum at the oil-water interface. **(A, B)** Temporal evolution of dilational elastic (E', filled label) and viscous (E", open label) moduli at the oil-GA-water interphase (**A.** 5 wt% A. *senegal*, **B.** 5 wt% A. *seyal*, blue dots are for n-hexadecane and red dots are for 1-octanol). Numbers 1-3 refer to the three identified phases during formation of an interfacial gum structure. **(C)** (tan δ = E"/E'). **(D)** Dependency of the maximum dilatational elastic modulus E' on the oil-water interfacial tension γ_{ow}. The black line represents the fit for both 5 wt% A. *senegal* (filled) and 5 wt% A. *seyal* (open) gums (y = 1.33x); the grey dashed line comes from Bergfreund and al. work and represents the fit for 10 mg.L^{-1} BSA, BLG, LSZ and some other protein values from literature [34].

Both gums allow the decrease of the interfacial tension (Fig. III.2) and the formation of an interfacial viscoelastic layer (Fig. III.3). The rheological profiles are similar for all the analyzed oils listed in Table III.2. Profiles are also similar to those obtained with some proteins,

polymers, microgels and polyelectrolytes [33], [34], [63]–[65], [35], [56]–[62], and can be roughly described according to a common 3-phase mechanism:

- The phase 1 corresponds to the rapid increase of both elastic and viscous moduli until the latter reaches a maximum, more pronounced for the most hydrophobic compound, n-hexadecane.

- The phase 2 corresponds to the clear decrease of the viscous modulus simultaneously with the increase of the elastic modulus until it reaches a maximum.

- During the phase 3, the elastic modulus decreases while the viscous modulus approaches 0.

The phase 1 suggests the formation of a viscoelastic interphase due to gum molecules concentrating by dehydration near the interface. In addition, E' was larger than E" for both gums and all the oils, suggesting oil-GA-water interphases were predominantly elastic. This can also be observed through the sharp decrease of the loss tangent for all the analyzed oils, at the very beginning of adsorption (Fig. III.3C). However, the loss tangent at t_0 was higher for highly hydrophobic oils than for weakly hydrophobic ones. For instance, the tan δ obtained with A. *senegal* and n-hexadecane or 1-octanol equals respectively, 0.61 and 0.43. This suggest enhanced volume fluctuations and energy dissipation at n-hexadecane interface which is in accordance with computer simulation studies upon water near hydrophobic interfaces [66]–[69]. The phase 2 implies the interfacial layer thickening that becomes more rigid until it reaches a maximum. The maximum of viscous modulus E" attests the manifestation of a state transition in which the system moves from a dominant viscous state with dissipation of energy to a prevailing elastic (see Supplemental Info 6.2). Then, although E' decreases during phase 3, the loss tangent tends towards 0. This suggest that after aging, the formed viscoelastic layer exhibits a solid-like structure. Due to the modulus definition (see Materials and Methods) and the emergence of wrinkles on the surface droplet (see Supplemental Info 6.2), the decrease in E' is believed to be an indirect probe of the emergence of an elastic interfacial crosslinked network presenting fluctuations in density. This would lead to a super elastic structure with heterogeneities that no longer meet the requirements of the fitting model of the dynamic drop tensiometry (see Supplemental Info 6.2). Thus, the decrease of E' may principally come from limitations of the method [70].

One can notice the equilibrium interfacial pressure Π_∞ and the oil-water interfacial tension γ_{ow} are correlated (Fig. III.2), demonstrating a dependency of the equilibrium interfacial tension on the oil hydrophobicity. In addition, a linear relation was obtained ($y = 1.33x$, $r^2 = 0.95$) between the maximum dilational elastic modulus E' and γ_{ow} (Fig. III.3D). These dependencies have already been observed for three different globular proteins (lysozyme LSZ, β-lactoglobulin BLG and bovine serum albumin BSA) [35], confirming proteins adsorb stronger to highly hydrophobic interfaces. In addition, the increase of surface concentration with the increase of oil-water interfacial tension was noticed with myofibrillar protein [36]. Similarly, AGPs preferably adsorb to n-hexadecane and myrcene hydrophobic interfaces rather than to low hydrophobic ones such as 1-octanol, 1-decanol or carvone [13], [20], [71]. The decrease in interfacial tension is then larger for highly hydrophobic interfaces leading to larger interfacial pressures. This is further attested by estimations of GA surface load (see Table III.2 and Supplemental Info 6.3). Likewise, the hydrophobicity of the oil is contributing to the GA interfacial rheology. The overall value of the elastic modulus of the n-hexadecane-GA-water structure was almost 5 times higher than the elastic modulus of the 1-octanol-GA-water one (Table III.2). Therefore, A. *senegal* and A. *seyal* display the same adsorption behavior than proteins (a slight difference between the two gum varieties is discussed later). This comes from the similarity in volumetric properties between proteins and AGP-like proteoglycans that suggest equivalent role of dehydration on the emergence of inner cavity volume fluctuations [12].

3.2. Effect of water interactions on AGPs interfacial adsorption

3.2.1. Initial oil-GA-water interactions

The initial interfacial tension in presence of GA was measured with all oils and both gums. They are presented in Table III.3.

Table III.3. Oil-GA-water interfacial tension at t_0 and interfacial water activity a_w^s at t_0 of oils in a 5 wt% A. *senegal* or A. *seyal* dispersion at 25°C.

Oil type	Oil name	γ_{t0} A. *senegal* (mN.m^{-1})	γ_{t0} A. *seyal* (mN.m^{-1})	a_w^s A. *senegal*	a_w^s A. *seyal*
Alkane	n-Hexadecane	43.4 (±0.6)		0.42	
			*41.7 (±1.8)		*0.40
Terpenes	d-Limonene	35.7 (±0.4)	36.4 (±0.4)	0.57	0.59
	d-Limonene 97%	*23.3 (±0.8)	*23.2 (±0.3)	*0.81	*0.75
			29.5 (±0.5)		0.68
	Myrcene	34.7 (±0.6)		0.65	
			*26.9 (±2.6)		*0.70
Alcohols	1-Octanol	8.4 (±0.3)	8.2 (±0.3)	0.98	0.95
	1-Decanol	8.9 (±0.1)	8.5 (±0.1)	0.98	0.95
Ketone	Carvone	15.9 (±0.2)	15.1 (±0.3)	0.89	0.83
Esters	Methyl octanoate	20.8 (±0.3)		0.91	
			*19.2 (±0.1)		*0.82
	Ethyl octanoate	22.7 (±0.3)		0.87	
			*21.5 (±0.2)		*0.79

**moderately altered n-hexadecane, d-limonene 97%, myrcene, methyl octanoate and ethyl octanoate*

Plotting the initial interfacial tension in presence of GA over the corresponding oil-water interfacial tensions γ_{ow} leads to a clear linear correlation (y = 0.93x, r^2 = 0.99) (Fig. III.4). This correlation implies that at the initial time, when the drop is created into the GA-water dispersion, first interactions arise between oil and water molecules.

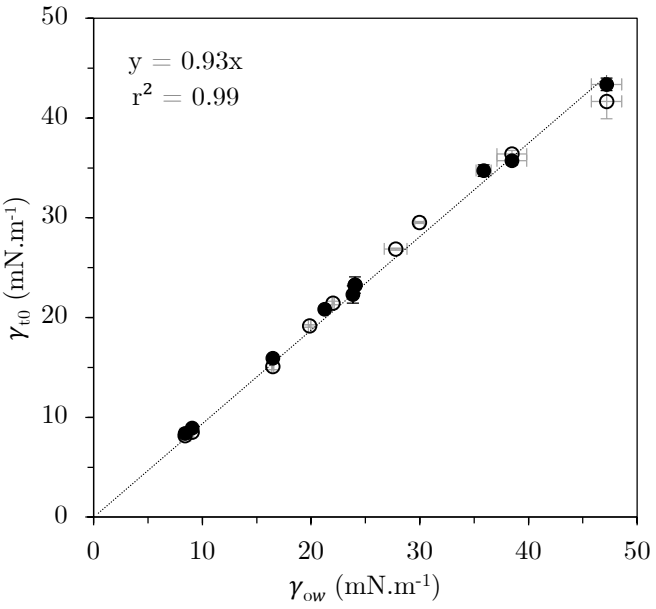

Fig. III.4. Oil-GA-water interfacial tension at t_0 plotted over oil-water interfacial tension γ_{ow}. Oil-GA-water interfacial tensions were obtained with 5 wt% A. *senegal* (filled label) or 5 wt% A. *seyal* (open label) at 25°C.

The way oils perturb the dynamic energetic structure of water may be estimated through the calculation of the interfacial water activity a_w^s (Table III.3). a_w^s can be estimated using the following equation [44], [72]:

$$\Pi = -RT\,\Gamma_w\,ln\,a_w^s \quad (9)$$

with Π ($\Pi = \gamma - \gamma_{ow}$) the interfacial pressure, R the gas constant, T the temperature, Γ_w the moles of water per unit area of the interfacial phase and a_w^s the interfacial water activity. Γ_w can be determined as follow:

$$\Gamma_w = 2\,H^s/E_{coh} \quad (10)$$

where H^s is the heat of formation of water surface and E_{coh} is the cohesive density energy of the bulk water, that is notably dependent on the evaporation enthalpy of water and its molar volume. At 25°C, $\Gamma_w = 5.7 \times 10^{-10}$ mol.cm^{-2}.

The interfacial water activity a_w^s is defined as the ratio between the vapor pressure of water at the interface and the saturation vapor pressure of water in the bulk. This parameter reflects the extent of perturbation of the water network within an interphase. If a_w^s is close to 1, properties of interfacial water are similar to the bulk water properties, *i.e.* the water molecular interfacial organization is not disturbed by the presence of solute. On the other hand, dry interfaces with water vapor phase result in a_w^s being close to 0. As mentioned in the introduction, the correlation between the interfacial water activity and the air-water interfacial tension has been experimentally proven [45]. The air-water interfacial tension, *i.e.* the surface tension, was studied at different temperatures and for different air relative humidities (RH). Accordingly, the air-water surface tension at 20°C decreased with an increase of air RH. Large air RH leads to large number of water molecules in the air phase and so, to high similarities with the water network in the bulk. That is why the interfacial water activity of a highly humid air and water is close to 1, leading to a low air-water interfacial tension. Consequently, the interfacial water activity a_w^s may be a pertinent thermodynamic parameter characterizing the oil hydrophobicity, thus defining oil-water interactions.

As one could expect, 1-octanol and 1-decanol are characterized by the highest interfacial water activity since they display the lowest oil-water interfacial tension. Water molecules are less disturbed within the interphase of weakly hydrophobic liquids (e.g. alcohols) than water molecules within the interphase of highly hydrophobic oils (e.g. n-hexadecane). In more volumetric terms, water displays reduced volume fluctuations near low hydrophobic surfaces.

It could also be noted a_w^s obtained with A. *senegal* gum are often moderately larger than with A. *seyal*, suggesting the oil-A. *senegal*-water interphase is slightly more hydrated, less disturbed, than the oil-A. *seyal*-water interphase. Further details are discussed below.

3.2.2. AGP-water interactions contributing to the differences between A. senegal and A. seyal

The main difference between the two varieties of gums lies in the adsorption kinetic. Within the analyzed time windows, the interfacial pressures reached by A. *seyal* are lower than those displayed by A. *senegal*, *i.e.* the A. *seyal* kinetic is slower (Fig. III.2). For instance, for a 5 wt% A. *senegal* dispersion, Π(n-hexadecane) = 28.9 mN.m^{-1} and Π(1-octanol) = 4.2 mN.m^{-1}, while in a 5 wt% A. *seyal* dispersion Π(n-hexadecane) = 27.2 mN.m^{-1} and Π(1-octanol) = 3.4 mN.m^{-1}. Regarding the interfacial dilational viscoelasticity, both gums reach an equivalent maximum of interfacial layer elasticity E'_{max} with a delay in time in favor of A. *senegal* (Fig. III.3A, B and D). This is particularly noticeable during the phase 2 and 3 which are longer for the A. *seyal* (Fig. III.3A and B). The strong diminution of elasticity during phase 3 of A. *senegal* can also be observed with A. *seyal* but over longer times. This implies that the interfacial structures formed by both gums are characterized by the same driving forces and rearrangement but with a kinetic difference.

This delay in interface formation was already mentioned in the literature [9], [10] and could be due to a difference in the biochemical composition or/and AGPs conformation. The protein content of A. *senegal* (Batch n° OF110676) and A. *seyal* (Batch n° OF110724) are respectively 27.0 mg.g^{-1} and 10.0 mg.g^{-1}. Moreover, the gums also show differences in structure, A. *senegal* gum being characterized by an average molar mass of 6.8×10^5 g.mol^{-1} and a branching degree of 78% while A. *seyal* gum is defined by an average molar mass of 8.2×10^5 g.mol^{-1} and a branching degree of 59%. Therefore, the lower protein content together with the more compact structure of A. *seyal* that lower the accessibility of high molar mass protein-rich AGPs, could be responsible for the low interfacial properties of A. *seyal* compared to A. *senegal* [8], [9]. However, the reduction of the interfacial tension can be interpreted as a manifestation of a change in water molecule free energy (a_w^s) [44] caused by the dehydration of the interphase [43]. We noticed in the above section slight differences between the interfacial water activities

of both gums, thus suggesting they also differ in hydration properties. As reported in Table III.1, A. *seyal* is characterized by a larger concentration of arabinose (47.6%) and a lower concentration of rhamnose (3.0%) than A. *senegal* (respectively 30.3 and 15.5%) [11]. Both arabinose and rhamnose are monosaccharides composed of five carbon atoms (pentose) and 4 hydroxyl groups. The main difference is the presence of a methyl group in rhamnose contributing to an increase of hydrophobicity. This suggests A. *seyal* greater affinity with water could limit and/or delay the interfacial dehydration step during the adsorption compared to A. *senegal*.

The interfacial water contents were estimated at the maximum of the layer elasticity and are presented in Fig. III.5. Method of calculation is provided in Supplemental Info 6.4.

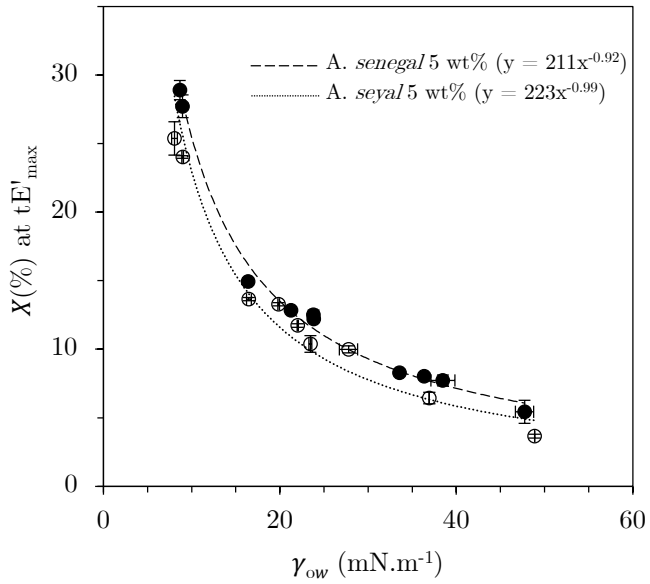

Fig. III.5. Interfacial water content $X(\%)$ of 5 wt% A. *senegal* (filled label) and 5 wt% A. *seyal* (open label) interfaces at their maximum of dilational elasticity depending on the oil-water interfacial tension γ_{ow}.

Results call for several observations. First, interphases formed at low hydrophobic oil interfaces are characterized by higher interfacial water contents. Secondly, estimations indicated water contents in the range of 5-30%, which is far lower than described in recent studies of AGPs adsorption at solid-liquid interfaces [13], [73]. Authors gave approximations of water contents around 90% [13], [73]. These different results may come from assumptions used for a_w^s estimations, in particular that adsorbed GA forms a monolayer at the interface and behaves

as an ideal two-dimensional solution [74]. This hypothesis is likely at the very initial adsorption time, where the oil-GA-water structure still displays viscoelastic behavior, but as GA adsorbed layer matures, the interphase tends to behave as a rigid three-dimensional system [43]. Another assumption in the Damodaran model is the magnitude of attractive forces from the bulk phase acting on water molecules at the interface, supposed to be one-half of that present in the bulk phase [74]. We then performed a_w^s calculations extending the range of magnitude of attractive forces from 30% to 70%. This did not result in values close to Davantès and al. work, e.g. the initial assumption (50% of magnitude) led to a 30% water content for the 1-octanol-A. *senegal*-water interphase, while the assumption extension (30 to 70% of magnitude) led to a water content range of 21-36%. It is also relevant to remark isotherms used in Fig. III.5 to approach water content values were obtained analyzing water sorption onto gum powder, whereas in this work the gum is solvated. Yet, the water hydration of a solute through a gas or a liquid phase involve different contributions of interactions [75] leading to different water contents. Second, Davantès and al. studied the gum adsorption onto gold hydrophilic surface [13], [73]. They also consider the adsorption of the whole AGP, *i.e.* both protein and polysaccharide parts. Here, the protein moiety is believed to mainly contribute to the gum adsorption. This may explain the range of water concentrations founded in Fig. III.5 since we found in a previous work the same order of value for AGP hydration number per protein moiety (0.3 g_{H2O}/g_{AGP}) [12].

Although Fig. III.5 values may not be quantitative, they are qualitative and informative. They confirm elastic structures formed by A. *seyal* gum are less hydrated than those formed by A. *senegal* gum even though differences are subtle and need complementary confirmation. According to Fig. III.2 and Fig. III.5, A. *seyal* not only dehydrates more slowly but also has to further dehydrate the interface in order to reach the same interfacial elasticity than A. *senegal*. A study on the flexibility and hydration of both Acacia gums through the characterization of their volumetric properties [12] described that bulk A. *senegal* was more flexible and less hydrated than bulk A. *seyal* according to the higher protein content and the greater value of partial specific volume of the former. In addition, the proportion of arabinose-containing polymers, which have high flexibility and capacity of water absorption, was reported to be decisive for leaf rehydration after the drying period [76]–[80]. This suggests A. *seyal*, due to its high arabinose content, should have a better affinity with water. Thus, A. *seyal* is less prone to dehydration than A. *senegal,* as it requires more energy, and so time, to displace sufficient water to form an elastic structure. In the aggregate, A. *senegal* and A. *seyal* gums differ in

protein content, structural conformation and hydration properties resulting in some divergence in interfacial kinetics and water composition.

3.2.3. The influence of oil-water van der Waals and hydrogen bond interaction energy on interfacial pressure and rheology

The equilibrium interfacial pressure of oil-GA-water was determined for n-hexadecane and 1-octanol oils for different A. *seyal* bulk concentrations (Fig. III.6). The shape of concentration isotherms displayed by both oils is sigmoidal and identical. This suggests the general mechanism of AGPs interfacial structuring is not affected by the oil hydrophobicity, *i.e.* by oil-water interactions. Difference lies in the stronger GA adsorption to highly hydrophobic interfaces.

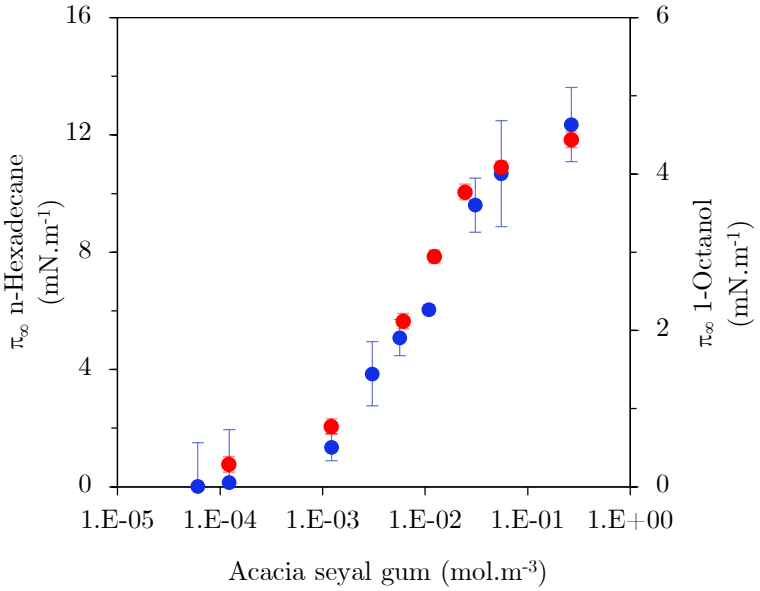

Fig. III.6. Equilibrium interfacial pressures of n-hexadecane (blue dots) and 1-octanol (red dots) over the A. *seyal* bulk concentration. Vertical bars onto points are standard deviation (3 experiments).

However, two master curves were obtained when plotting the normalized elastic modulus E'/E'_{max} over the normalized interfacial tension γ/γ_{ow} (Fig. III.7). A first one is observed for the most hydrophobic oils, *i.e.* n-hexadecane, myrcene, purified d-limonene, d-limonene 97%, ethyl octanoate, methyl octanoate and carvone. A second master curve is grouping alcohols, *i.e.* the least hydrophobic oils. The difference between both master curves was then dependent

on the presence of chemical groups enhancing interactions with water, namely OH groups. Although this main distinction, a certain dispersion of the hydrophobic master curve can be noted. This indicates that in addition to the dominant OH effect, van der Waals interactions between aroma and water (e.g. esters/ketone/oxide-water interactions > alkane/terpenes-water interactions), slightly impact the gum adsorption. This was however independent of the gum type as the same behavior was observed with A. *seyal* gum (results not shown).

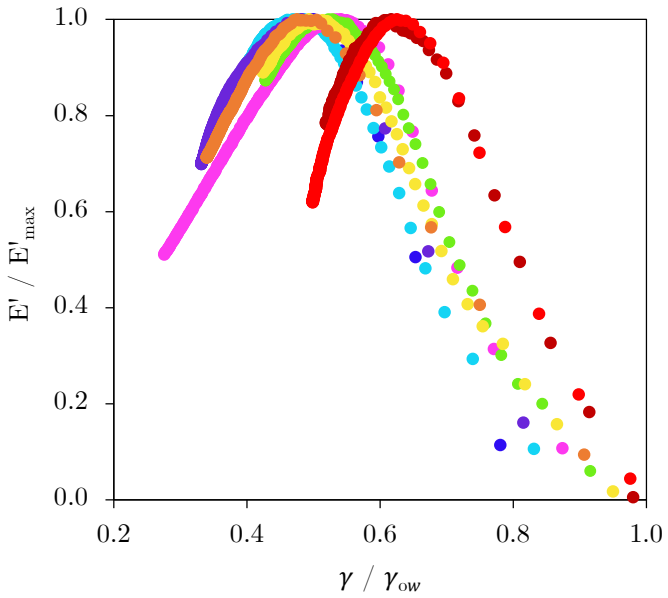

Fig. III.7. Dilational elastic modulus E' normalized by E'_{max} over the oil-GA-water interfacial tension normalized by γ_{ow} for a 5 wt% A. *senegal* dispersion at 25°C. (●) n-Hexadecane, (●) Myrcene, (●) purified d-Limonene, (●) d-Limonene 97%, (●) Ethyl octanoate, (●) Methyl octanoate, (●) Carvone, (●) 1-Decanol, (●) 1-Octanol.

Hydrogen bond interactions and London dispersion forces are enhanced at low temperatures [81]–[84]. Therefore, one may expect that changes in bulk temperatures affect the AGPs adsorption behavior. Dilational rheological measurements were performed at 4 (temperature of water maximum density), 10, 20 and 25°C at 1-octanol and myrcene interfaces for a 5 wt% A. *seyal* dispersion. Results of 1-octanol-A.*seyal* interface are presented in Fig. III.8.

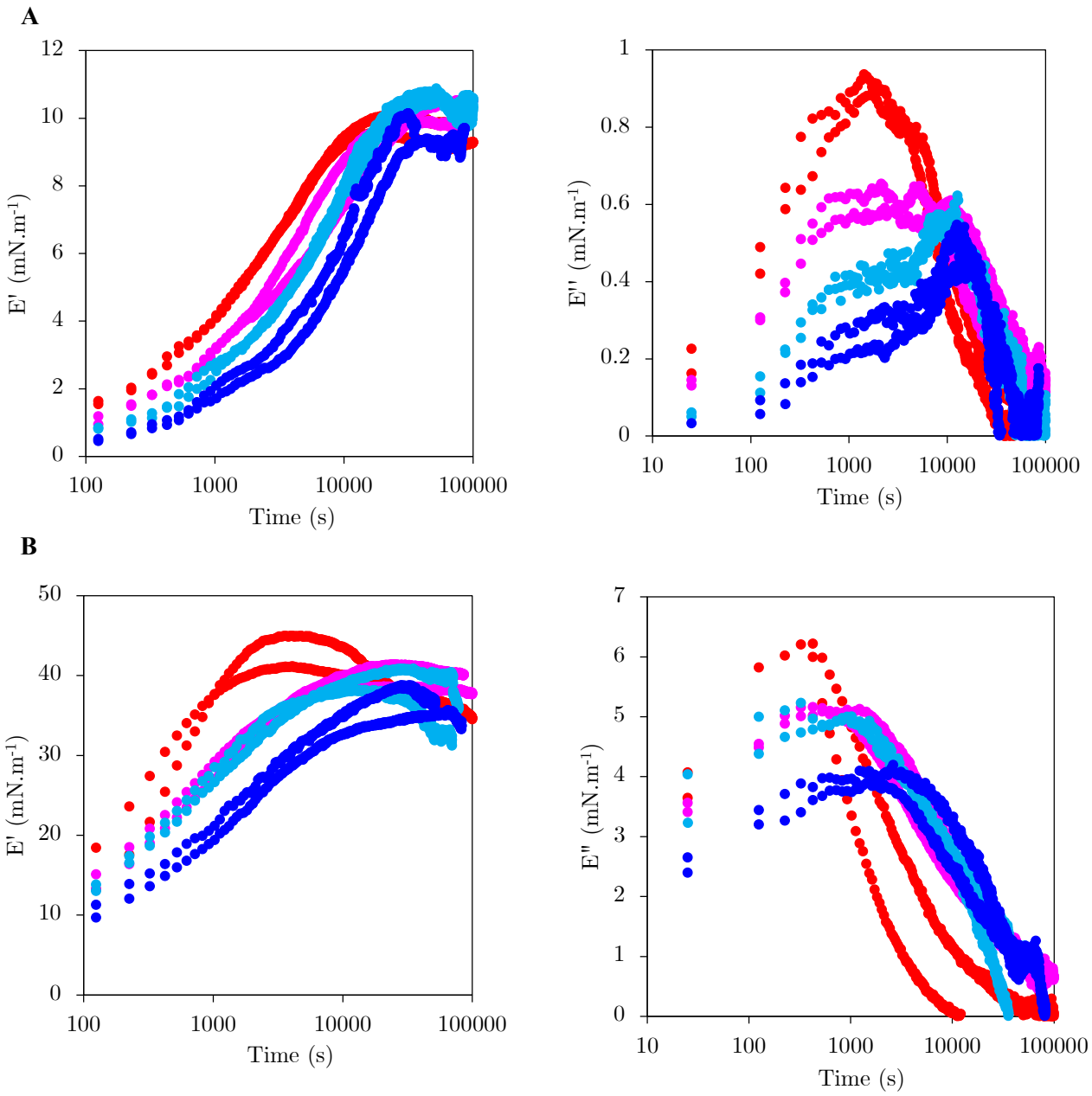

Fig. III.8. Evolution of the elastic modulus E' (on the left) and the viscous modulus E" (on the right) at the **(A)** 1-octanol – A. *seyal* and **(B)** myrcene – A. *seyal* interfaces at (●) 25°C, (●) 20°C, (●) 10°C and (●) 4°C. Two experiments per temperature are shown.

The maximum of elasticity was not dramatically impacted in this range of temperatures. However, the kinetic was slower at lower temperatures. An important effect of temperature may be observed with the loss modulus E". Decreasing the temperature led to a decrease of the maximum of loss modulus E" and a slowdown of the kinetic. This indicates dissipation of energy is more difficult at low temperatures, where hydrogen bond interaction energy (and dispersion forces) are stronger. A plateau can be seen in the loss modulus of 1-octanol at 4, 10 and 20°C.

At 25°C, the plateau turns into a peak, indicating a more rapid state transition where volume fluctuations are larger. For the lowest temperatures, the plateau seems first stable then the modulus increases before tending toward 0. This means that the dissipative structure (see Supplemental Info 6.2) preceding the change of state is more stable at 4°C than at 25°C. In addition, these results highlight the presence of an initial two-stage structuring mechanism during the first phase of gum adsorption (from 0 to maximum of E"), that is not detectable at 25°C. Furthermore, this two-stage mechanism is less significant for the myrcene-A. *seyal* interface. The first phase of gum adsorption appears then related to a dynamic and dissipative organized structure, partially stabilized through a hydrogen bond interaction network.

Apparent activation energies E_a of the increase of E' and E" with temperature were estimated at the fixed time of 400 s where the interfacial structure begins to emerge. For 1-octanol and myrcene oils, dissipative E_a (E_a related to E") were respectively of 41 and 13 kJ.mol^{-1}. On the other hand, E_a related to E' were respectively 28 and 17 kJ.mol^{-1}. These energies are compatible with van der Waals interactions (~1-10 kJ.mol^{-1}) [85], [86] and/or hydrogen interactions (~10-40 kJ.mol^{-1}) [86]. Myrcene being a highly hydrophobic compound, no hydrogen interactions with water can be considered. Thus, the apparent activation energies of 13 kJ.mol^{-1} and 17 kJ.mol^{-1} can be identified as van der Waals interactions. Regarding 1-octanol, the presence of the hydroxyl group enables hydrogen interactions with water. Therefore, the apparent activation energies of 41 kJ.mol^{-1} and 28 kJ.mol^{-1} can be considered as the combination of both hydrogen and van der Waals interactions with water molecules. This could account for the greater thermal sensitivity of both E' and E" for 1-octanol compared to myrcene.

In addition, the thermal sensitivity of the dissipative modulus E" of 1-octanol is about twice that of the elastic modulus E'. This means the impact of the presence of OH functional group is highly significant during the conception phase of the interfacial structure, *i.e.* during the dissipative state subsequently leading to the organized elastic structure.

4. Discussion

The principal aim of the present work was to propose a volumetric Acacia gum adsorption mechanism based on the assumption that interfacial thermodynamic properties of water near

hydrophobic surfaces are correlated to the AGPs thermodynamic interfacial properties. This requires first to be clear on the main physical characteristics of water and the used water model. Water is a transiently connected network of molecules through Lifshitz–van der Waals (LW), Lewis acid–base (AB) and electrical double layer (EL) non-covalent interactions [87], [88]. The AB forces or electron–acceptor/electron–donor interactions are quantitatively predominant and are responsible for the "hydrophobic effect". By "hydrophobic effect" we mean the molecular attraction caused by changes in hydrogen bond-related (AB) free energy of cohesion between water molecules which surround molecules or particles when they are immersed in water [87]. Introducing a hydrophobic solute of significant size into water, typically above 1 nm radius, leads to significant perturbation of the hydrogen-bonded network and a severe reduction in the entropy [89]. Thus, water tends to exclude the solute from the solution in order to minimize the entropic penalty, as suggested for globular proteins [90]. A number of reviews and studies focused on water interactions with hydrophobic surfaces, e.g. [66], [68], [89], [91]–[96]. They revealed the existence of a 1-6 Å water density depletion zone [96]–[98], occurring at the interface of water and a macroscopic hydrophobic solute. This so-called hydrophobic gap would show vapor characteristics [93] and pronounced density fluctuations [66], [98]. This was recently supported through high-resolution Raman spectroscopy analyses of water around large solutes, revealing an increasing population of dangling OH bonds very similar to higher temperature bulk water [99].

Here we used the water model of Sun [100], that describes a two-phase structure, preferentially tetrahedrally-coordinated, with a strong correlated and fluctuating network. This model is interesting because, i) it is based on quantum mechanics calculation then it describes water at the scale required to understand molecular phenomena, ii) it defines the hydrogen bond interaction as a correlated directional interaction composed by van der Waals forces and a covalent bond, iii) it allows to easily explain the supersolidity of air-water interfaces, the blue shift of infrared spectra of heated water and, more importantly for this Discussion, the local fluctuations in volume [100], [101]. Accordingly, the two structures share the same geometry but hold different H-O bond lengths transiting cooperatively as illustrated in Fig. III.9. The proton serves as the coordination origin of asymmetrical and short–range interactions with on the left side the intermolecular weaker O:H nonbond also called van der Waals bond with a ~1-10 kJ.mol^{-1} energy, and on the right side the intramolecular stronger H–O polar covalent bond with an energy of ~10-40 kJ.mol^{-1}.

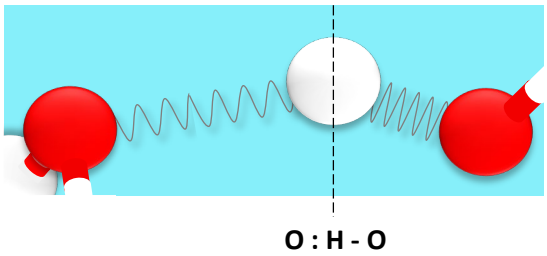

Fig. III.9. Water O:H-O intramolecular bonds according to Sun's model [100], on the left side the O:H nonbond, on the right side the H–O polar covalent bond.

According to this model, a H_2O molecular coordination number less than four will result in the H:O elongation associated with the H–O bond contraction (combined with a strong polarization of the H:O bond and vibration frequency transitions). A consequence of the H–O bond contraction is the deepening of the H–O potential well. The electrons of the H_2O molecule get denser and are entrapped in both the H–O bond and the core orbitals of oxygen. Thus, the reduction of the water coordination number results in the increase of the charge localized in the adjacent oxygen anions O^{2-} further enhancing the O–O repulsion. Subsequently, hydrophobic effects are stated to originate from the structural competition between hydrogen bonding in bulk water and that in interfacial water [101].

It is well known oils are hydrophobic liquids. Thus, the water dynamic structure at the interface of a drop of oil, pictured as a planar surface at the microscopic scale, is necessarily changed. The perturbation amplitude of the interfacial water structure depends on the presence and distribution of highly or weakly hydrophobic elements in the oil molecule. For instance, interactions between 1-octanol and H_2O molecules are favored through the polar functional group (see the schematic representation in Fig. III.10). Electron exchanges with the surface are facilitated leading to a H_2O coordination number close or equals to four. On the other hand, in the case of water near a highly hydrophobic macroscopic surface, such as a drop of n-hexadecane, interactions between the surface and H_2O molecules tend to be disadvantaged. As discussed earlier, a vapor-like interphase is formed in the vicinity of a hydrophobic surface [92], [93], [96]. The transition of liquid interfacial water molecules into the vapor phase results in the elongation of the H:O bond and the contraction of the H–O bond [102]. Consequently, changes in local hydrogen bond interaction energy are coupled to local changes in volume [103]–[106]. The hypothesis can be made that in a high hydrophobic interphase, H:O bonds are preferentially adopted, with H pointing to the interface [107], [108] as illustrated in Fig. III.10. In the absence of interactions with the surface, water molecules constituting the first hydrated

layers are strongly impacted in such way their coordination number is reduced. The latter induces the polarization of the H_2O electrons, their densification and their delocalization toward the H–O bonds and oxygen anions, pointing to the bulk. As a consequence, the H–O bonds become shorter and stiffer, enhancing the water molecules network in the bulk close to the interphase and creating a repulsive force [100]. Then, increasing the hydrophobicity of a surface leads to the further delocalization and densification of H_2O electrons, resulting in the increase of the interfacial tension.

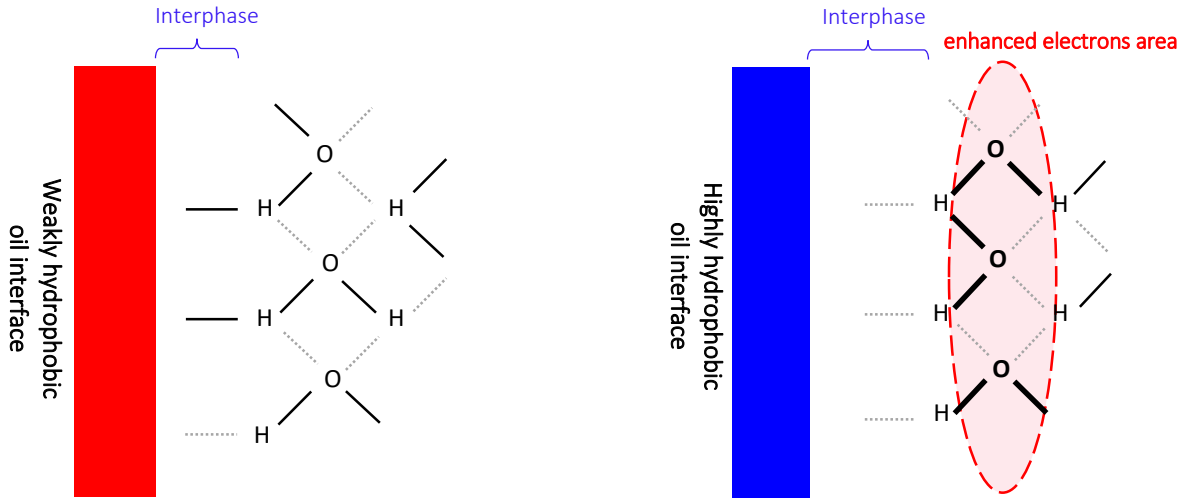

Fig. III.10. Schematic representation of the water molecules network at the interface of oil of different hydrophobic degree, e.g. 1-octanol as the weakly hydrophobic oil and n-hexadecane as the highly hydrophobic oil. The dotted line are for H:O bonds, black line are for H-O bonds, bold black lines for electron-concentrated H-O bonds. (Lengths are not to scale).

The Lewis acid–base (AB) forces or electron–acceptor/electron–donor interactions are quantitatively predominant in water and are responsible for the hydrophobic effect [87]. When a drop of oil is formed in water, the surface may bear a variable surface density of Lewis acid/base functional groups capable of hydrogen bonding with water, increasing from 0 functional groups/nm^2 (a 'hydrophobic' oil as n-hexadecane) to a surface packed with functional groups (a 'hydrophilic' oil as 1-octanol) [43], [109]. The strength of the Lewis acid/base surface functional groups can vary from relatively strong to weak for ion-exchange functionalities. For example, alcohols such as 1-decanol and 1-octanol are Lewis bases, *i.e.* that can donate an electron pair resulting in reactions involving the formation of coordinated polar covalent bonds with a transitory water H:O bond. Thus, they are characterized by a low interfacial tension with water of respectively 9.06 mN.m^{-1} and 8.43 mN.m^{-1}. Then, ketones and esters present stronger exchange functionalities than alkanes or any other organic compound

having no polar group such as n-hexadecane, purified d-limonene and myrcene. That is why the latter possess a great interfacial tension γ_{ow} of 47.18, 38.47 and 36.37 mN.m^{-1} respectively. It is interesting to note that this model stays in agreement with the classic definition of interfacial tension. By considering a flat surface, the interfacial tension can be defined as the difference of pressure exerted on each side of the surface, that is to say, as the resultant of the forces applied to the surface. This includes a force normal to the plane as well as tangential forces. The latter forces are generated through the interactions with water molecules along with interactions between water molecules and so, through the electron exchanges.

Highly hydrophobic oil enhances the vapor-structure water within the interphase, inducing a predominance of H:O nonbonds. The analogy can be made with the strong presence of density fluctuations near macroscopic hydrophobic interface discussed earlier in the introduction [66], [98]. In addition, Jamadagni and al. stated that enhanced density fluctuations, *i.e.* volume fluctuations, are correlated to a decrease of the work of cavity formation, ΔG_c, in a fluid [66] which has been recently attested by calculations (Chapter II) [110]. This thermodynamic parameter is involved in a statistical mechanical approach of the process of solvating a solute in a solvent. The latter can exactly be separated in two sub-processes: (a) formation of a cavity of the size of the solute molecule; (b) introduction of the solute molecule into the cavity, switching on solute-solvent attractive interactions [111], [112]. In terms of free energy cost this can be written as follows [66], [94], [113]:

$$\Delta G_{sol} = \Delta G_c + \Delta G_{int} \quad (11)$$

with ΔG_c involving solvent-solvent interactions and ΔG_{int} involving solute-solvent interactions.

Based on Vogler 3D-approach [43] and the previous results, the following model illustrated in Fig. III.11 is proposed as the description of the GA adsorption process to oil-water interfaces emphasizing the water interactions contribution.

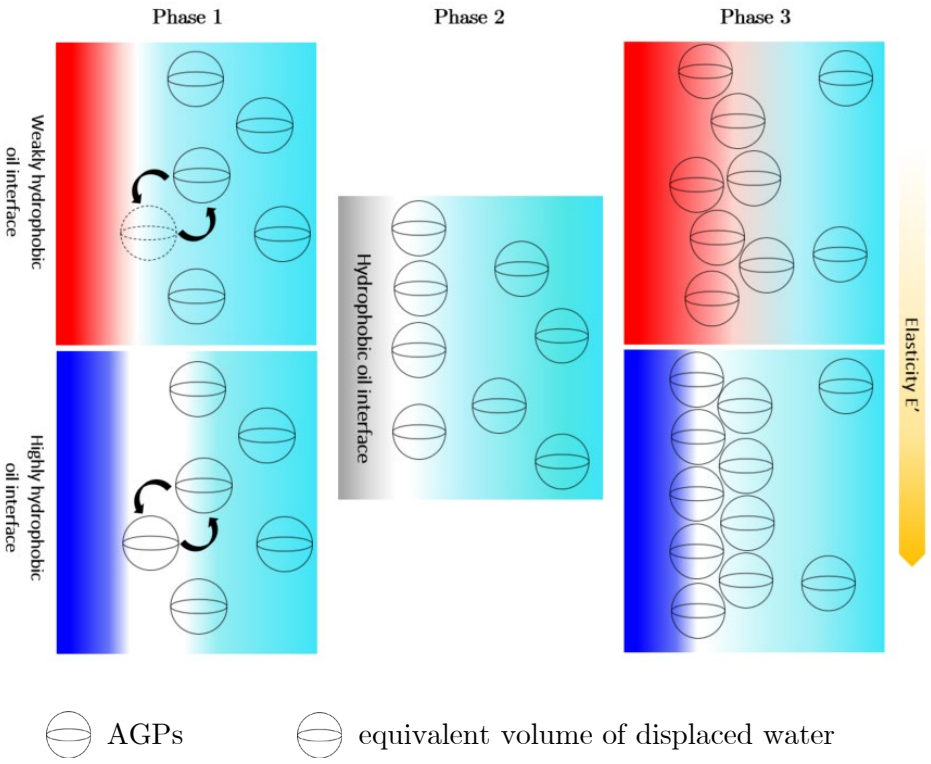

Fig. III.11. Schematic representation of the GA adsorption to oil-water interfaces. The light blue zone represents the bulk water; the white zone represents the interfacial water (the depth of the interphase region and the depth over which interfacial water properties might be different than bulk solution, are not known and therefore, are not to scale).

Phase 1: Hydration of the oil interface leading to the formation of an immediate interphase composed of vapor-like water structure. As illustrated in the schematic representation Fig. III.10, H:O bonds are preferentially adopted in the interfacial zone of the oil interface. AGPs are mostly hydrophilic solutes due to their sugar composition [11]. However, AGPs are known to adsorb at interfaces. In particular, the third fraction of the gum, HIC-F3, obtained by hydrophobic interaction chromatography (HIC), presents the highest protein content (~14%) and molecular weight of 16×10^5 g.mol^{-1}, and is believed to contribute the most to the gum adsorption in opposition to the first fraction HIC-F1 (lowest protein content ~0.5% and molecular weight of 3.5×10^5 g.mol^{-1}) [12], [13], [73]. HIC-F3 peptide part is predominantly composed of proline, hydroxyproline, serine and threonine [6], [114], [115]. Serine and threonine are classified as polar according to Zhu and al. amino acid hydrophobicity scale [116]. Therefore, simply looking to specific amino acid composition does not allow to explain the hydrophobic characteristic of Acacia gum. However, AGPs are characterized by a fractal structure [114] with a core enclosing part of amino acids and hindering their accessibility [115]. In addition,

the existence of minerals, such as ions Ca, in the gum, contributes to the electrostatic screening of charges, especially on carboxylic acids [117]. These effects impair the hydrophilicity of the AGP protein part, thus explaining its sensitivity to hydrophobic effect. Consequently, AGPs are 'expelled' out of the solution in order to minimize unfavorable interactions with water. In parallel, a macroscopic hydrophobic surface brought into contact with water induces an interphase of water molecules of weaker hydrogen bonding-network than the one in the bulk. Therefore, the interphase is characterized by enlarged volume fluctuations, *i.e.* significant amount of void. It is then energetically more favorable to form a cavity capable of accommodating AGPs inside the interphase than in the bulk [110]. The latter along with the existence of hydrophobic effect inside the bulk water constitute the driving forces for AGPs to move into the interphase by displacing first an equivalent volume of water as illustrated in Fig. III.11. Then, AGPs diffuse into this newly formed interface and a one-or-more adsorbed layers develop, inducing a 3D-interphase that depends on AGPs size, GA concentration, and the oil interface. This 3D-interphase is constituting the viscoelastic layer around the oil drop.

The impact of oil hydrophobicity noticed on Fig. III.2, 3D and 7, further support the significant role of water in GA adsorption dynamics. As discussed earlier, one can assume highly hydrophobic oil induces a predominance of H:O nonbonds within the interphase and so high volumes fluctuations. This is supported by the loss tangent at n-hexadecane-GA-water interphases being greater than the loss tangent at 1-octanol-GA-water interphases (Fig. III.3C). Highly hydrophobic interfaces ease AGPs movements and accumulation within the interphase. Moreover, H:O bonded water are weaker than H-O bonded water. Adsorption to highly hydrophobic interfaces is then energetically facilitated. This was further attested in Fig. III.8 as enhanced oil-water hydrogen interactions led to the stabilization of the gum dissipative structure and to the delay of change of state into a prevailing elastic structure. The differences of configuration of phase 1 are illustrated in Fig. III.11.

Phase 2: The dehydration at the oil interface continues in order for AGPs to concentrate and organize. The formed interfacial layer undergoes a transition state from a structure where some of the energy is dissipated into a structure where all energy is stored (tan $\delta \sim 0$) (gel-like transition state). The interphase slowly shrinks in volume by expelling interphase water and/or initially adsorbed AGPs, causing them to concentrate into closely-packed arrangements until reaching a maximum of elasticity. Fig. III.5 results further attest the impact of the oil

hydrophobicity and so the role of water in the adsorption mechanisms. Dehydrating and accumulating into the interphase is more difficult for AGPs as it requires more energy to displace water. This explains the water composition $X(\%)$ of weakly hydrophobic oil interphase being greater than of highly hydrophobic oil interphase. Promoted interfacial dehydration together with promoted interfacial volume fluctuations are then contributing to the decrease of the energy cost of the GA adsorption, explaining the greater ability to reduce the interfacial tension (Fig. III.2), the higher surface coverage (Table III.2) and the greater interfacial elasticity observed at highly hydrophobic oils (Fig. III.3D).

Phase 3: The oil interface is saturated but AGPs continue to accumulate into the interphase leading to the formation of wrinkles (see Supplemental Info 6.2) [6], [118]. This phase is characterized by low but substantial dissipative energy before maturing into a solid-like structure (Fig. III.3C). One can assume that the AGPs accumulation formation induces compression of the AGPs. They pack within the interphase, leading to a decrease of the dissipative energy and to a super elastic structure with distribution heterogeneities that no longer meet the requirements of the dynamic drop tensiometry method (see Supplemental Info 6.2). The loss modulus E" values being greater for highly hydrophobic interfaces such as n-hexadecane, one may suppose AGPs can reorganize and well arrange within the interphase. This results in a better packing of AGPs and a high surface concentration inducing a large maximum of elasticity E'. With weakly hydrophobic interfaces such as 1-octanol, the oil-water interactions induce an interfacial zone less prone to adsorption. AGPs require more energy to concentrate within the interphase resulting in a less packed and ordered AGPs network. Moreover, AGPs could adsorb into a zone where the separation between water and oil molecules is less distinct than within an interfacial zone of water and highly hydrophobic oil, leading to an interfacial layer with incorporated oil molecules as illustrated in Fig. III.11. This analysis is similar to the theory made in Bergfreund and al. work, supported by molecular dynamic simulation on globular proteins [33], [35], [119]. For example, β-lactoglobulin is said to adsorb in a random orientation and inserted itself partly into the oil phase without conformational changes.

Finally, this adsorption model that considers the significant role of water is supported by the study of the effect of the temperature on the interfacial properties (Fig. III.8). Researches

highlighted increase of the temperature resulted in acceleration of the reorientation of the water solvating molecules [81], increase of fluctuations [82], increase of the molecules kinetic energy and breaking of hydrogen bonds [83]. This contributes to improve connectivity between the hydration water and bulk water at high temperatures, mostly due to the Debye-Keesom part of van der Waals interactions [86], making the surface of the macrosolute effectively more hydrophobic [84]. Consequently, the hydrogen bond interactions and London dispersion forces between oil and water are enhanced and strengthened when decreasing the temperature. The displacement of a volume of water equivalent to the volume of AGPs then requires more energy at 4°C than at 25°C.

5. Conclusions

Water-water, oil-water and AGPs-water interactions constitute the driving force of the Acacia gum 3-phases adsorption. The enhanced dehydration of macroscopic hydrophobic interfaces along with the hydrophobic effect inside the bulk water, lead AGPs to concentrate in the interphase by displacing first an equivalent volume of water. Then, AGPs accumulate, interact and constitute a network at the macroscopic scale resulting in the formation of a viscoelastic layer. As the adsorption proceeds the number of molecules and the interactions increase until a threshold is reached and a transition state is observed. Thereafter, the most effective structure is achieved at the maximum of elasticity but the system continues to develop. AGPs pack at the interface. Interfacial fluctuations in density result in the loss of the elasticity and the wrinkling of the drop surface.

The favoring adsorption of AGPs molecules to highly hydrophobic oils interfaces was confirmed. In addition, the oil hydrophobicity strongly influences the Acacia gum adsorption as it is directly related to the water interactions at the interface. It has significant consequences on the phase 1 of Acacia gum adsorption and also affects the rearrangement during phase 2 and phase 3. Oil-water interactions are also important through van der Waals interactions, coupled or not to hydrogen bond interactions according to the nature of the oil. In the absence of hydrogen interactions, *i.e.* for highly hydrophobic oil, the strength of the hydrogen bond-network of water molecules within the interphase decreases. This results in partial vaporization of water. The latter together with promoted water interfacial volume fluctuations, contribute to the decrease of the energy cost of AGP adsorption. In addition, the oil hydrophobicity also

impacts the AGPs rearrangement within the interphase as low oil hydrophobicity induces less packed and ordered layer network with oil molecule incorporation. Thus, a sufficient oil hydrophobicity is required to enhance the efficiency of the gum adsorption. This better efficiency induces in turn high oil surface coverage, high interfacial layer elasticity and ability to reduce the interfacial tension. Finally, the drop shape analysis method may not be fitted for studying super elastic structure with a heterogeneous distribution of AGPs, then of stresses. Other techniques such as Langmuir trough and capillary pressure tensiometry may be more appropriated [70] and should be considered for the study of the Acacia gum interfacial properties in the future.

6. Supplemental info

6.1. Viscous modulus of n-hexadecane and 1-octanol

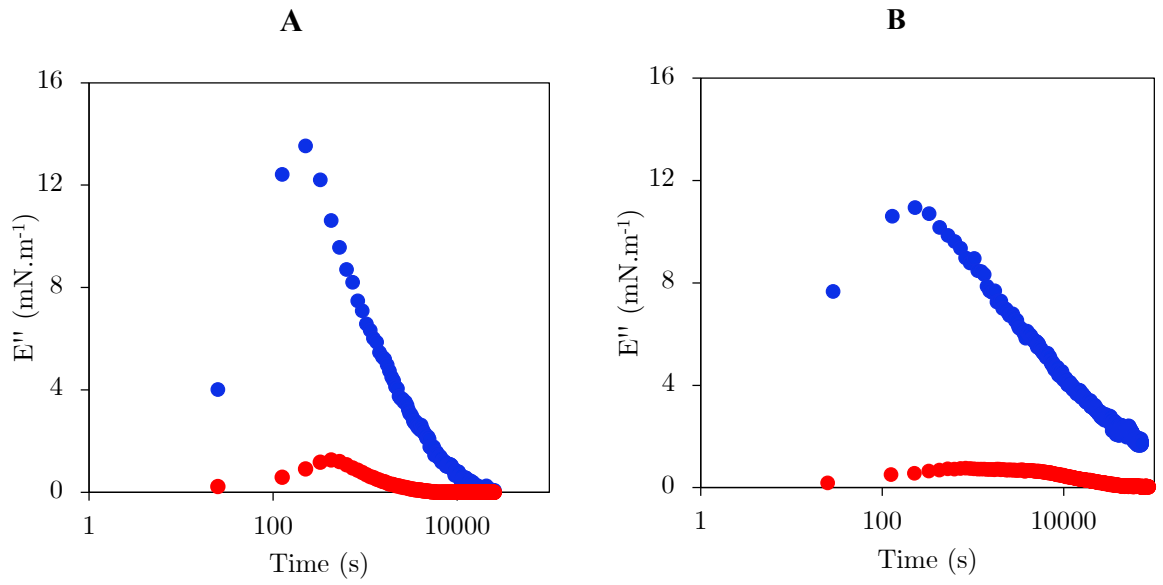

Fig. III.12. Evolution of the viscous modulus E" at the oil-GA interface **(A)** 5 wt% A. *senegal*, **(B)** 5 wt% A. *seyal*, blue dots are for n-hexadecane and red dots are for 1-octanol).

6.2. Elastic modulus decrease during phase 3

Another characteristic that can be observed in the dilational analyses is the genesis of a dissipative structure and its evolution. This is particularly noticeable in the sinusoidal oscillations of the interfacial tension between n-hexadecane and a 5 wt% A. *senegal* dispersion

as reported in Fig. III.13. Until reaching the transition between phase 1 and phase 2, *i.e.* when the loss modulus E" is at its maximum, the signal of the interfacial tension highly fluctuates. Then the fluctuations slowly fade during phases 2 and 3. This reflects a transition under nonequilibrium conditions from an unstable state into an organized structure, which is typical of dissipative structures [120], [121]. Here, the maximum of viscous modulus E" attests the manifestation of a state transition in which the system moves from a viscoelastic state with dissipation of energy ($E" \neq 0$) to an elastic state with no longer energy dissipation ($E" \sim 0$). Then, a new thermodynamical equilibrium is approached during phase 3, forming a structure with pure elastic features [121], [122]. This is consistent with the ability of GA to form highly cohesive elastic interfacial multilayer (gel-like) layers that is long known [123]–[127].

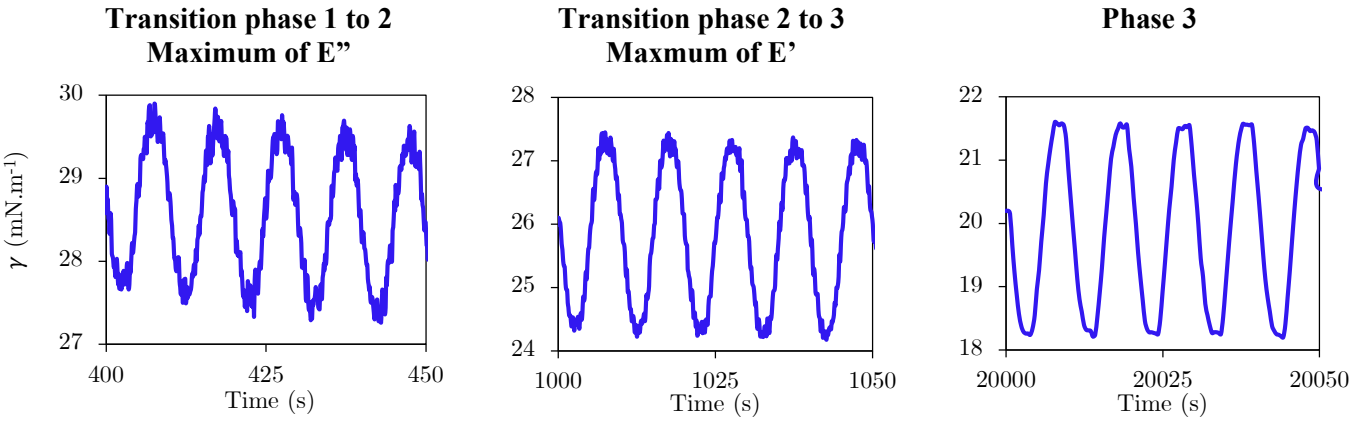

Fig. III.13. Sinusoidal oscillations of the interfacial tension between n-hexadecane and a 5 wt% A. *senegal* dispersion at different times. First during the transition of phase 1 into phase 2 corresponding to the maximum of viscous modulus E", then during the transition of phase 2 into phase 3 corresponding to the maximum of elastic modulus E', and during phase 3.

During the dilational rheology measurements, the volume deformation $\Delta V/V$ has been noticed not to be constant and deviate from the applied value of 10%. This could be due to the mass transfer of the oil through the water phase, causing the evolution of the drop over time [128], [129]. Consequences on the decrease of elastic modulus during the phase 3 were checked performing a deformation scan ranging from $\Delta V/V = 2\%$ to 20% (Fig. III.14). Results show that before the viscous modulus E" reaches its maximum, *i.e.* during phase 1, the layer structure presents linear viscoelastic features from a 2% to approximatively 13% volume deformation, *i.e.* the stress response is not dependent on the strain. However, as soon as the phase 2 starts, the interfacial layer response shows nonlinear viscoelastic characteristics. This means that

under our measuring conditions, the material has changed its properties under the deformation. In order to compare the viscoelastic responses of all the analyzed systems, the moduli of phases 2 and 3 were normalized to a deformation value of $\Delta V/V = 10\%$. As may be seen in Fig. III.14 (right), deviations in the volume deformation tend to lower the values of moduli but can not explain alone the decrease of elasticity during phase 3.

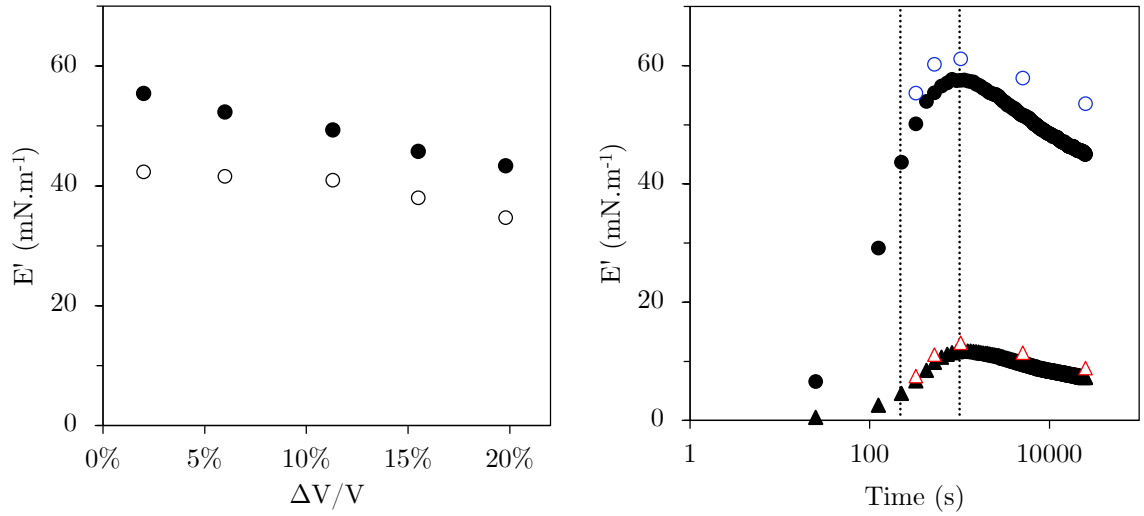

Fig. III.14. On the left: the scan deformation of a drop of n-hexadecane in a 5 wt% A. *senegal* dispersion at $t=t_{E'max}$ (opened) and $t=t_{E'max}$ (filled). On the right: evolution of the elastic modulus E' of n-hexadecane (filled black circles) and 1-octanol (filled black triangles) and in a 5 wt% A. *senegal* dispersion and their normalized elastic modulus, respectively opened blue circles and opened red triangles.

As the interfacial layer matures over time, the shape of the drop also changes. Initially the drop is formed with a rather spherical shape (Fig. III.15a), before lengthening (Fig. III.15b).

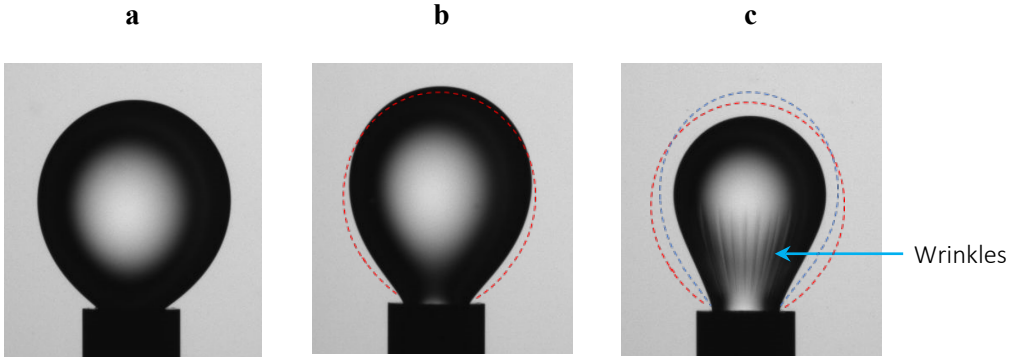

Fig. III.15. Drop of d-limonene formed in a 5 wt% A. *senegal* dispersion during phase 1 **(a)**, phase 2 **(b)** and a compressing cycle occurring in phase 3 **(c)**.

High elastic structure features were earlier identified (Fig. III.3C). In addition, a wrinkling phenomenon was observed upon the drop surface area whatever the oil-type (Fig. III.15c). The existence of such anisotropic structures highlights the presence of non-homogeneous elasticity areas resulting in the interfacial layer folding, *i.e.* wrinkles. Surface heterogeneities have also been noticed on highly elastic saponin [70] or hydrophobin [99] interfaces. As well, A. *senegal* and A. *seyal* gums adsorbed on solid gold surfaces present a non-uniform surface coverage upon dehydration, with large localized aggregates [13]. The existence of a heterogeneous AGPs distribution is in fact naturally attested by the theoretical meaning of the 2D-parameter E', *i.e.* the pressure-induced density fluctuations of the interface [49], [50]. As explained in the section 2.2, the E' parameter is the 2D equivalent of the bulk elastic modulus K_T, and must be considered as the resistance to surface density fluctuations. In case AGP becomes heterogeneously distributed at the interface, one could expect an increase of density fluctuations and then a decrease of the dilational elastic modulus [130]–[133]. This is what we observed. However, the real cause of the drop of E' during the phase 3 is probably the nonhomogeneous stress distribution, that render the used Laplace method inadequate [70]. Indeed, the Young–Laplace equation was stated to be valid for fluid surfaces having no shear strength [134]. Otherwise, corrections of the Young–Laplace fitting model may be required taking into account the anisotropic interfacial stresses leading to deviations of the drop shape and in some case to the wrinkling of the interface [135], [136]. We may see the buckling is mainly localized in the neck of the drop rather than on the apex (Fig. III.15c), also leading to the rising of the drop bond number. The heterogeneity of stress distribution is at the origin of anisotropic wrinkles, allowing the concentrated solid elastic structure to adapt to the drop shrinking [128], [86].
In the aggregate, the decrease in E' may be an indirect probe of the emergence of an elastic interfacial crosslinked network presenting fluctuations in density.

6.3. The surface concentration of AGPs

An analogy can be made between AGPs that consist of a protein part and a polysaccharide part, and amphiphilic polymers. In the frame of the wattle-blossom model, it is supposed that the most hydrophobic protein chain anchors at the interface while the protruding hydrophilic carbohydrate blocks attached to this chain provide a strong steric barrier towards flocculation and coalescence [123], [137], [138]. Under the increasing compression induced by the AGPs concentration at the interface, the polysaccharide grafts could be squeezed out of the proximal

region. The 'expelled' segments are then forming tails in the distal zone [62]–[64]. This assumption could be supported by electronic spin resonance data indicating GA adsorbed at solid-liquid interface with approximately half of its segments close to the surface in trains and the other half in loops and tails extending away from the surface into solution [123], [139]. Consequently, calculations of the AGPs surface concentration (Γ) were conducted using a model developed for amphiphilic copolymers. In a regime where the hydrophobic parts are adsorbed to the air/water interface and the hydrophilic parts form stretched loops in solution, the surface pressure of a copolymer layer can be expressed as follow [54], [55]:

$$\Pi = k_B T \alpha N \Gamma \quad (12)$$

where k_B is the Bolztman constant, T the temperature and αN the number of grafts in the polymer chain, presumed to be the number of loops [55].

If we assume the most hydrophobic part of the gum is adsorbed to the oil-water interface and the least hydrophobic parts are protruded in the dispersion [123], [139], Equation (9) can be used to determine the surface concentration of AGPs at oil-water interfaces. The number of AGPs segments localized in the dispersion was determined using the description of elementary structural building blocks by Renard et al. work [114]. In the proposed structural model, AGPs are made of the assembly of 6 building blocks of category 1 and 8 building blocks of category 2. Grafts of blocks 1 consist in 17 arabinoside oligomers and 6 polysaccharide blocks while grafts of blocks 2 consist in 87 arabinoside oligomers and 32 polysaccharide blocks. The total number of grafts is then in theory $\alpha N = 1090$. Using this number, the surface concentration of AGPs were estimated (Table III.2).

Depending on the oil hydrophobicity, we found surface concentration of AGPs in the 1-7 mg.m^{-2} range (Table III.2), which may be compared to the 1-10 mg.m^{-2} values reported in the literature both for Acacia gums or proteins [17], [23], [27], [140]–[143]. The surface load is seen to increase with the increase of oil-water interfacial tension, further attesting GA adsorbs preferentially to highly hydrophobic interfaces such as n-hexadecane (Γ = 7.3 mg.m^{-2}) rather than weaker hydrophobic interfaces such as 1-octanol (Γ = 1.1 mg.m^{-2}). A similar correlation was recently found while studying the oil polarity impact on interfacial properties of myofibrillar protein [36].

6.4. Hydration isotherms determination

For A. *senegal* and A. *seyal* gums, the curves were determined experimentally at 25°C and data were fitted using the TSS (three stage sorption) model [48] that gave the best fit results :

$$X(\%) = Xm\frac{Cka_w^s H(a_w^s)H'(a_w^s)}{(1-ka_w^s)[1+(CH(a_w^s)-1)ka_w^s]} \quad (13)$$

$$H(a_w^s) = 1 + \frac{(1-k)(ka_w^s)h}{f(1-a_w^s)} \quad (14)$$

$$H'(a_w^s) = 1 + \frac{(H(a_w^s)-1)(1-ka_w^s)}{H(a_w^s)(1-a_w^s)}[h+(1-h)a_w^s] \quad (15)$$

where Xm is the monolayer moisture content (%), C is the energy constant, k is the characteristic constant correcting the properties of the multilayer molecules with respect to the bulk liquid, and h is the TSS isotherm constant. All fitting parameters are presented in Table III.4.

Table III.4. Three stage sorption fitted parameters. Adapted from Lopez-Torrez et al. 2016 [48].

Model parameters	A. *senegal*	A. *seyal*
Xm (% db.)	8.7	10.3
C	7.7	4.0
k	0.9	0.8
h	28.1	20.8

Xm is expressed in % dry basis.

7. Acknowledgements

The authors would like to thank ALLAND & ROBERT Company - Natural and organic gums (Port Mort, France) for financial support (Ph.D. C. Faucon).

8. Complementary studies

8.1. Determination of gum surface concentration using a protein model

Surface properties of Acacia gums being related to the presence of protein-rich high molecular weight AGPs and their accessibility, it is interesting to estimate surface loads using a model that is commonly applied to proteins. Then, results can be compared to estimations from the model described in Supplemental Info 6.3. The following equation of state was used [144]

$$-\frac{\Pi\omega_0}{RT} = \ln(1-\theta_p) + \theta_p(1-\omega_0/\omega_p) + a_p\theta_p{}^2 \quad (16)$$

where $\Gamma_p = \sum_{i=1}^{n}\Gamma_{pi}$ is the total adsorption of proteins in all n states ($1 \leq i \leq n$), $\theta_p = \omega_p\Gamma_p$ the total surface coverage by protein molecules, ω_p is average molar area of the adsorbed protein, ω_0 is the molar area of the solvent, a_p is the intermolecular interaction parameter.

Since the gum adsorption states are unknown, the assumption is made that the gum is adsorbing in a single state. HIC-F3 fraction is believed to contribute the most to the gum adsorption [12], [13], [73] and was determined to have in average a 25 nm hydrodynamic radius when solubilized in a 10 mM sodium acetate buffer solution [145]. HIC-F3 molecules were considered as spheres leading to an average molar area of 4.7×10^9 $m^2.mol^{-1}$. We also take the intermolecular interaction parameter supposed in the quoted study for β-casein and serum bovine albumin, *i.e.* $a_p = 1$. The model was applied to n-hexadecane and 1-octanol interfaces. Surface concentrations of respectively 0.40 $mg.m^{-2}$ and 0.35 $mg.m^{-2}$ were found. Although the GA surface concentration at n-hexadecane interface is greater than at 1-octanol interface as observed in Table III.2, the values are quite low.

The model considers that the all AGP surface adsorbs at the interface. However, AGPs being packed, it is possible only a part of their surface is in contact with the oil interface. Therefore, calculations were made to determine the average molar area of the adsorbed AGPs, ω_{p*}, that would be needed in order to achieve a surface load of 7.27 and 1.06 $mg.m^{-2}$ for n-hexadecane and 1-octanol respectively. It results in $\omega_{p*} = 2\%\,\omega_p$ for n-hexadecane and in $\omega_{p*} = 36\%\,\omega_p$ for 1-octanol. Although assumptions were required for applying this model, results are informative. They support the assumption AGPs within the interphase of a weakly hydrophobic oil (1-octanol), are less packed and ordered than within the interphase of a highly hydrophobic oil (n-hexadecane) (see Fig. III.11). This leads to an interfacial layer with incorporated oil

molecules, *i.e.* with AGPs in greater contact with oil molecules (36% for 1-octanol compared to 2% for n-hexadecane).

8.2. Alternative hypothesis for the decrease of E' during phase 3

As discussed in section 6.3, an analogy can be made between AGPs that consist of a protein part and a polysaccharide part, and amphiphilic polymers [123], [137], [138]. Under the increasing compression induced by the multilayers formation, the polysaccharide grafts could be squeezed out of the proximal region and the 'expelled' segments are then forming tails in the distal zone [62]–[64]. These structural interfacial rearrangements are supposed to produce motions and energy dissipation (E"≠0), that should be visible on loss modulus results. However, under the used experimental conditions, E" values are decreasing until approaching 0. This may invalidate the suggestion. It should be noted that the energy dissipation could appear at frequencies lower from the one selected in our measurements (0.1 Hz).

9. References

[1] L. L. Schramm, *Emulsions, Foams and Suspensions*, Wiley-VCH. 2005.

[2] D. J. McCLements, *Food Emulsions Principles, Practices, and Techniques*. 2010.

[3] T. F. T. Ed, *Emulsion Science and Technology*, Tharwat F. 2009.

[4] T. C. Botti, A. Hutin, E. Quintella, and M. S. Carvalho, "Effect of interfacial rheology on drop coalescence in water-oil emulsion," *Soft Matter*, vol. 18, no. 7, pp. 1423–1434, 2022, doi: 10.1039/d1sm01382c.

[5] F. Ravera, K. Dziza, E. Santini, L. Cristofolini, and L. Liggieri, "Emulsification and emulsion stability: The role of the interfacial properties," *Adv. Colloid Interface Sci.*, vol. 288, p. 102344, 2021, doi: 10.1016/j.cis.2020.102344.

[6] C. Sanchez *et al.*, "Acacia gum: History of the future," *Food Hydrocoll.*, vol. 78, pp. 140–160, 2018, doi: 10.1016/j.foodhyd.2017.04.008.

[7] FAO, "Gum arabic," 1999. https://www.fao.org/3/W6355E/w6355e0g.htm (accessed Jul. 12, 2022).

[8] C. Aphibanthammakit, "Propriétés interfaciales et émulsifiantes de gommes d'Acacia senegal, Acacia seyal et de leurs fractions," 2018.

[9] C. Flindt, S. Al-Assaf, G. O. Phillips, and P. A. Williams, "Studies on acacia exudate gums. Part V. Structural features of Acacia seyal," *Food Hydrocoll.*, vol. 19, no. 4, pp. 687–701, 2005, doi: 10.1016/j.foodhyd.2004.09.006.

[10] R. M. A. Mansour and E. A. Hassan, "Effect of gum concentration and gum protein concentration on emulsifying properties of some Acacia gums," *Int. J.*

basic Appl. Chem. Sci., vol. 6, no. 2, pp. 23–35, 2016.

[11] L. Lopez-Torrez, M. Nigen, P. Williams, T. Doco, and C. Sanchez, "Acacia senegal vs. Acacia seyal gums - Part 1: Composition andstructure of hyperbranched plant exudates," *Food Hydrocoll.*, vol. 51, no. April, pp. 41–53, 2015, doi: 10.1016/j.foodhyd.2015.04.019.

[12] V. Mejia Tamayo *et al.*, "Flexibility and hydration of amphiphilic hyperbranched arabinogalactan-protein from plant exudate: A volumetric perspective," *Colloids and Interfaces*, vol. 2, no. 1, 2018, doi: 10.3390/colloids2010011.

[13] A. Davantès, M. Nigen, C. Sanchez, A. d'Orlando, and D. Renard, "Adsorption of Hyperbranched Arabinogalactan-Proteins from Plant Exudate at the Solid–Liquid Interface," *Colloids and Interfaces*, vol. 3, no. 2, p. 49, 2019, doi: 10.3390/colloids3020049.

[14] E. Bouyer *et al.*, "Stabilization mechanism of oil-in-water emulsions by β-lactoglobulin and gum arabic," *J. Colloid Interface Sci.*, vol. 354, no. 2, pp. 467–477, 2011, doi: 10.1016/j.jcis.2010.11.019.

[15] P. Erni *et al.*, "Interfacial rheology of surface-active biopolymers: Acacia senegal gum versus hydrophobically modified starch," *Biomacromolecules*, vol. 8, no. 11, pp. 3458–3466, 2007, doi: 10.1021/bm700578z.

[16] E. Dickinson, B. S. Murray, G. Stainsby, and D. M. W. Anderson, "Surface activity and emulsifying behaviour of some Acacia gums," *Top. Catal.*, vol. 2, no. 6, pp. 477–490, 1988, doi: 10.1016/S0268-005X(88)80047-X.

[17] R. C. Randall, G. O. Phillips, and P. A. Williams, "The role of the proteinaceous component on the emulsifying properties of gum arabic," *Top. Catal.*, vol. 2, no. 2, pp. 131–140, 1988, doi: 10.1016/S0268-005X(88)80011-0.

[18] A. K. Ray, P. B. Bird, G. A. Iacobucci, and B. C. Clark, "Functionality of gum arabic. Fractionation, characterization and evaluation of gum fractions in citrus oil emulsions and model beverages," *Top. Catal.*, vol. 9, no. 2, pp. 123–131, 1995, doi: 10.1016/S0268-005X(09)80274-9.

[19] O. Castellani, S. Al-Assaf, M. Axelos, G. O. Phillips, and M. Anton, "Hydrocolloids with emulsifying capacity. Part 2 - Adsorption properties at the n-hexadecane-Water interface," *Food Hydrocoll.*, vol. 24, no. 2–3, pp. 121–130, 2010, doi: 10.1016/j.foodhyd.2009.07.006.

[20] C. Aphibanthammakit, M. Nigen, S. Gaucel, C. Sanchez, and P. Chalier, "Surface properties of Acacia senegal vs Acacia seyal films and impact on specific functionalities," *Food Hydrocoll.*, vol. 82, pp. 519–533, 2018, doi: 10.1016/j.foodhyd.2018.04.032.

[21] O. Castellani, D. Guibert, S. Al-Assaf, M. Axelos, G. O. Phillips, and M. Anton, "Hydrocolloids with emulsifying capacity. Part 1 - Emulsifying properties and interfacial characteristics of conventional (Acacia senegal (L.) Willd. var. senegal) and matured (Acacia (sen) SUPER GUM™) Acacia senegal," *Food Hydrocoll.*, vol. 24, no. 2–3, pp. 193–199, 2010, doi: 10.1016/j.foodhyd.2009.09.005.

[22] R. Chanamai, G. Horn, and D. J. McClements, "Influence of oil polarity on droplet growth in oil-in-water emulsions stabilized by a weakly adsorbing biopolymer or a nonionic surfactant," *J. Colloid Interface Sci.*, vol. 247, no. 1, pp. 167–176, 2002, doi: 10.1006/jcis.2001.8110.

[23] S. Xiang *et al.*, "Gum Arabic-stabilized conjugated linoleic acid emulsions: Emulsion properties in relation to interfacial adsorption behaviors," *Food Hydrocoll.*, vol. 48, pp. 110–116, 2015, doi: 10.1016/j.foodhyd.2015.01.033.

[24] Q. Jin, X. Li, Z. Cai, F. Zhang, M. P. Yadav, and H. Zhang, "A comparison of corn fiber gum, hydrophobically modified starch, gum arabic and soybean soluble polysaccharide: Interfacial dynamics, viscoelastic response at oil/water interfaces and emulsion stabilization mechanisms," *Food Hydrocoll.*, vol. 70, pp. 329–344, 2017,

doi: 10.1016/j.foodhyd.2017.03.005.

[25] P. Erni *et al.*, "Interfacial rheology of surface-active biopolymers: Acacia senegal gum versus hydrophobically modified starch," *Biomacromolecules*, vol. 8, no. 11, pp. 3458–3466, 2007, doi: 10.1021/bm700578z.

[26] S. R. Padala, P. A. Williams, and G. O. Phillips, "Adsorption of Gum Arabic, Egg White Protein, and Their Mixtures at the Oil-Water Interface in Limonene Oil-in-Water Emulsions," *J. Agric. Food Chem.*, vol. 57, no. 11, pp. 4964–4973, 2009, doi: 10.1021/jf803794n.

[27] M. Atgié, O. Masbernat, and K. Roger, "Emulsions Stabilized by Gum Arabic: Composition and Packing within Interfacial Films," *Langmuir*, vol. 35, no. 4, pp. 962–972, 2019, doi: 10.1021/acs.langmuir.8b02715.

[28] S. J. Reiner, G. A. Reineccius, and T. L. Peppard, "A comparison of the stability of beverage cloud emulsions formulated with different gum acacia- and starch-based emulsifiers," *J. Food Sci.*, vol. 75, no. 5, 2010, doi: 10.1111/j.1750-3841.2010.01625.x.

[29] L. Han *et al.*, "Effect of arabinogalactan protein complex content on emulsification performance of gum arabic," *Carbohydr. Polym.*, vol. 224, no. August, p. 115170, 2019, doi: 10.1016/j.carbpol.2019.115170.

[30] J. Zhang, T. L. Peppard, and G. A. Reineccius, "Preparation and characterization of nanoemulsions stabilized by food biopolymers using microfluidization," *Flavour Fragr. J.*, vol. 30, no. 4, pp. 288–294, 2015, doi: 10.1002/ffj.3244.

[31] E. Dickinson, V. B. Galazka, and D. M. W. Anderson, "Emulsifying behaviour of gum arabic. Part 1: Effect of the nature of the oil phase on the emulsion droplet-size distribution," *Carbohydr. Polym.*, vol. 14, no. 4, pp. 373–383, 1991, doi: 10.1016/0144-8617(91)90003-U.

[32] R. Chanamai and D. J. McClements, "Comparison of gum arabic, modified starch, and whey protein isolate as emulsifiers: Influence of pH, CaCl2 and temperature," *J. Food Sci.*, vol. 67, no. 1, pp. 120–125, 2002, doi: 10.1111/j.1365-2621.2002.tb11370.x.

[33] J. Bergfreund, P. Bertsch, S. Kuster, and P. Fischer, "Effect of Oil Hydrophobicity on the Adsorption and Rheology of β-Lactoglobulin at Oil-Water Interfaces," *Langmuir*, vol. 34, no. 16, pp. 4929–4936, 2018, doi: 10.1021/acs.langmuir.8b00458.

[34] J. Bergfreund *et al.*, "Globular protein assembly and network formation at fluid interfaces: effect of oil," *Soft Matter*, pp. 1692–1700, 2021, doi: 10.1039/d0sm01870h.

[35] J. Bergfreund, P. Bertsch, and P. Fischer, "Adsorption of proteins to fluid interfaces: Role of the hydrophobic subphase," *J. Colloid Interface Sci.*, vol. 584, pp. 411–417, 2021, doi: 10.1016/j.jcis.2020.09.118.

[36] W. Zhang, X. Xu, X. Zhao, and G. Zhou, "Insight into the oil polarity impact on interfacial properties of myofibrillar protein," *Food Hydrocoll.*, vol. 128, no. January, p. 107563, 2022, doi: 10.1016/j.foodhyd.2022.107563.

[37] K. Gekko and H. Noguchi, "Compressibility of globular proteins in water at 25°C," *J. Phys. Chem.*, vol. 83, no. 21, pp. 2706–2714, 1979, doi: 10.1021/j100484a006.

[38] K. Gekko and Y. Hasegawa, "Compressibility-Structure Relationship of Globular Proteins," *Biochemistry*, vol. 25, no. 21, pp. 6563–6571, 1986, doi: 10.1021/bi00369a034.

[39] M. Bánó and J. Marek, "How thick is the layer of thermal volume surrounding the protein?," *Biophys. Chem.*, vol. 120, no. 1, pp. 44–54, 2006, doi: 10.1016/j.bpc.2005.09.024.

[40] T. V. Chalikian, "Volumetric properties of proteins," *Annu. Rev. Biophys. Biomol. Struct.*, vol. 32, no. February 2003, pp. 207–235, 2003, doi: 10.1146/annurev.biophys.32.110601.141709.

[41] T. V. Chalikian, M. Totrov, R. Abagyan,

and K. J. Breslauer, "The hydration of globular proteins as derived from volume and compressibility measurements: Cross correlating thermodynamic and structural data," *J. Mol. Biol.*, vol. 260, no. 4, pp. 588–603, 1996, doi: 10.1006/jmbi.1996.0423.

[42] V. P. Voloshin, N. N. Medvedev, N. Smolin, A. Geiger, and R. Winter, "Disentangling volumetric and hydrational properties of proteins," *J. Phys. Chem. A*, vol. 119, no. 5, pp. 1881–1890, 2015, doi: 10.1021/jp510891b.

[43] E. A. Vogler, "Protein adsorption in three dimensions," *Biomaterials*, vol. 33, no. 5, pp. 1201–1237, 2012, doi: 10.1016/j.biomaterials.2011.10.059.

[44] C. S. Rao and S. Damodaran, "Is surface pressure a measure of interfacial water activity? Evidence from protein adsorption behavior at interfaces," *Langmuir*, vol. 16, no. 24, pp. 9468–9477, 2000, doi: 10.1021/la0007168.

[45] J. L. Pérez-Díaz, M. A. Álvarez-Valenzuela, and J. C. García-Prada, "The effect of the partial pressure of water vapor on the surface tension of the liquid water-air interface," *J. Colloid Interface Sci.*, vol. 381, no. 1, pp. 180–182, 2012, doi: 10.1016/j.jcis.2012.05.034.

[46] T. V. Chalikian, M. Totrov, R. Abagyan, and K. J. Breslauer, "The hydration of globular proteins as derived from volume and compressibility measurements: Cross correlating thermodynamic and structural data," *J. Mol. Biol.*, vol. 260, no. 4, pp. 588–603, 1996, doi: 10.1006/jmbi.1996.0423.

[47] L. M. Pérez-Mosqueda, J. Maldonado-Valderrama, P. Ramírez, M. A. Cabrerizo-Vílchez, and J. Muñoz, "Interfacial characterization of Pluronic PE9400 at biocompatible (air-water and limonene-water) interfaces," *Colloids Surfaces B Biointerfaces*, vol. 111, pp. 171–178, 2013, doi: 10.1016/j.colsurfb.2013.05.029.

[48] L. Lopez Torrez, "Characterisation of acacia gum s and developm ent of heat-induced acacia gum /potato proteins m icroparticles," 2016.

[49] N. W. Tschoegl, "Elastic moduli in monolayers," *J. Colloid Sci.*, pp. 500–507, 1958, doi: 10.1016/0095-8522(58)90058-8.

[50] J. B. Rosenholm, P. Ihalainen, and J. Peltonen, "Thermodynamic characterization of Langmuir monolayers of thiolipids: A conceptual analysis," *Colloids Surfaces A Physicochem. Eng. Asp.*, vol. 228, no. 1–3, pp. 119–130, 2003, doi: 10.1016/S0927-7757(03)00301-7.

[51] D. Chandler, "Two faces of water," *Nature*, vol. 417, no. 6888, p. 491, 2002, doi: 10.1038/417491a.

[52] M. El-Mahrab-Robert, V. Rosilio, M. A. Bolzinger, P. Chaminade, and J. L. Grossiord, "Assessment of oil polarity: Comparison of evaluation methods," *Int. J. Pharm.*, vol. 348, no. 1–2, pp. 89–94, 2008, doi: 10.1016/j.ijpharm.2007.07.027.

[53] J. Maldonado-Valderrama, R. Miller, V. B. Fainerman, P. J. Wilde, and V. J. Morris, "Effect of gastric conditions on β-lactoglobulin interfacial networks: Influence of the oil phase on protein structure," *Langmuir*, vol. 26, no. 20, pp. 15901–15908, 2010, doi: 10.1021/la102294u.

[54] V. Aguié-Béghin, E. Leclerc, M. Daoud, and R. Douillard, "Asymmetric multiblock copolymers at the gas-liquid interface: Phase diagram and surface pressure," *J. Colloid Interface Sci.*, vol. 214, no. 2, pp. 143–155, 1999, doi: 10.1006/jcis.1999.6144.

[55] C. Trégouët *et al.*, "Adsorption dynamics of hydrophobically modified polymers at an air-water interface," *Eur. Phys. J. E*, vol. 41, no. 9, 2018, doi: 10.1140/epje/i2018-11711-y.

[56] E. H. Lucassen-Reynders, J. Benjamins, and V. B. Fainerman, "Dilational rheology of protein films adsorbed at fluid interfaces," *Curr. Opin. Colloid Interface Sci.*, vol. 15, no. 4, pp. 264–270, 2010, doi: 10.1016/j.cocis.2010.05.002.

[57] V. B. Fainerman *et al.*, "Dilational Viscoelasticity of Proteins Solutions in Dynamic Conditions," *Langmuir*, vol. 34, no. 23, pp. 6678–6686, 2018, doi: 10.1021/acs.langmuir.8b00631.

[58] N. A. Alexandrov *et al.*, "Interfacial layers from the protein HFBII hydrophobin: Dynamic surface tension, dilatational elasticity and relaxation times," *J. Colloid Interface Sci.*, vol. 376, no. 1, pp. 296–306, 2012, doi: 10.1016/j.jcis.2012.03.031.

[59] F. MacRitchie and A. Alexander, "Kinetics of adsorption of proteins at interfaces. Part I. The role of bulk diffusion in adsorption," *J. Colloid Sci.*, vol. 18, no. 5, pp. 458–463, 1963, [Online]. Available: http://www.sciencedirect.com/science/article/pii/0095852263900370%5Cnhttp://www.sciencedirect.com/science/article/pii/0095852263900369.

[60] E. M. Freer, K. S. Yim, G. G. Fuller, and C. J. Radke, "Shear and dilatational relaxation mechanisms of globular and flexible proteins at the hexadecane/water interface," *Langmuir*, vol. 20, no. 23, pp. 10159–10167, 2004, doi: 10.1021/la0485226.

[61] C. J. Beverung, C. J. Radke, and H. W. Blanch, "Protein adsorption at the oil/water interface: Characterization of adsorption kinetics by dynamic interfacial tension measurements," *Biophys. Chem.*, vol. 81, no. 1, pp. 59–80, 1999, doi: 10.1016/S0301-4622(99)00082-4.

[62] B. A. Noskov, A. V. Akentiev, and R. Miller, "Dynamic surface properties of poly(vinylpyrrolidone) solutions," *J. Colloid Interface Sci.*, vol. 255, no. 2, pp. 417–424, 2002, doi: 10.1006/jcis.2002.8614.

[63] B. A. Noskov *et al.*, "Dynamic surface properties of poly(N-isopropylacrylamide) solutions," *Langmuir*, vol. 20, no. 22, pp. 9669–9676, 2004, doi: 10.1021/la048836t.

[64] B. A. Noskov, "Protein conformational transitions at the liquid-gas interface as studied by dilational surface rheology," *Adv. Colloid Interface Sci.*, vol. 206, pp. 222–238, 2014, doi: 10.1016/j.cis.2013.10.024.

[65] F. Pinaud *et al.*, "Adsorption of microgels at an oil-water interface: Correlation between packing and 2D elasticity," *Soft Matter*, vol. 10, no. 36, pp. 6963–6974, 2014, doi: 10.1039/c4sm00562g.

[66] S. N. Jamadagni, R. Godawat, and S. Garde, "Hydrophobicity of proteins and interfaces: Insights from density fluctuations," *Annu. Rev. Chem. Biomol. Eng.*, vol. 2, pp. 147–171, 2011, doi: 10.1146/annurev-chembioeng-061010-114156.

[67] P. Varilly, D. Chandler, A. J. Patel, and S. Garde, "Fluctuations in water and their relation to the hydrophobic effect near model surfaces and proteins," 2013.

[68] A. J. Patel, P. Varilly, D. Chandler, and S. Garde, "Quantifying Density Fluctuations in Volumes of All Shapes and Sizes Using Indirect Umbrella Sampling," *J. Stat. Phys.*, vol. 145, no. 2, pp. 265–275, 2011, doi: 10.1007/s10955-011-0269-9.

[69] R. Godawat, S. N. Jamadagni, and S. Garde, "Characterizing hydrophobicity of interfaces by using cavity formation, solute binding, and water correlations," *Proc. Natl. Acad. Sci. U. S. A.*, vol. 106, no. 36, pp. 15119–15124, 2009, doi: 10.1073/pnas.0902778106.

[70] R. Stanimirova, K. Marinova, S. Tcholakova, N. D. Denkov, S. Stoyanov, and E. Pelan, "Surface rheology of saponin adsorption layers," *Langmuir*, vol. 27, no. 20, pp. 12486–12498, 2011, doi: 10.1021/la202860u.

[71] O. Castellani *et al.*, "Hydrocolloids with emulsifying capacity. Part 3 - Adsorption and structural properties at the air-water surface," *Food Hydrocoll.*, vol. 24, no. 2–3, pp. 131–141, 2010, doi: 10.1016/j.foodhyd.2009.07.009.

[72] L. Ter-Minassian-Saraga, "Protein denaturation on adsorption and water activity at interfaces: an analysis and suggestion," *J. Colloid Interface Sci.*, vol. 80, no. 2, pp. 393–401, 1981, doi: 10.1016/0021-9797(81)90198-3.

[73] A. Davantès, M. Nigen, C. Sanchez, and D. Renard, "Adsorption Behavior of Arabinogalactan-Proteins (AGPs) fromAcacia senegalGum at a Solid-Liquid Interface," *Langmuir*, vol. 37, no. 35, pp. 10547–10559, 2021, doi: 10.1021/acs.langmuir.1c01619.

[74] S. Damodaran, "Water activity at interfaces and its role in regulation of interfacial enzymes: A hypothesis," *Colloids Surfaces B Biointerfaces*, vol. 11, no. 5, pp. 231–237, 1998, doi: 10.1016/S0927-7765(98)00040-X.

[75] S. Shimizu and N. Matubayasi, "Sorption: A Statistical Thermodynamic Fluctuation Theory," *Langmuir*, vol. 37, no. 24, pp. 7380–7391, 2021, doi: 10.1021/acs.langmuir.1c00742.

[76] J. P. Moore, M. Vicré-Gibouin, J. M. Farrant, and A. Driouich, "Adaptations of higher plant cell walls to water loss: Drought vs desiccation," *Physiol. Plant.*, vol. 134, no. 2, pp. 237–245, 2008, doi: 10.1111/j.1399-3054.2008.01134.x.

[77] J. P. Moore *et al.*, "Arabinose-rich polymers as an evolutionary strategy to plasticize resurrection plant cell walls against desiccation," *Planta*, vol. 237, no. 3, pp. 739–754, 2013, doi: 10.1007/s00425-012-1785-9.

[78] J. P. Moore, J. M. Farrant, and A. Driouich, "A role for pectin-associated arabinans in maintaining the flexibility of the plant cell wall during water deficit stress," *Plant Signal. Behav.*, vol. 3, no. 2, pp. 102–104, 2008, doi: 10.4161/psb.3.2.4959.

[79] E. A. Vieira, K. R. Silva, A. Oriani, C. F. Moro, and M. R. Braga, "Mechanisms of desiccation tolerance in the bromeliad Pitcairnia burchellii Mez: biochemical adjustments and structural changes," *Plant Physiol. Biochem.*, vol. 121, no. October, pp. 21–30, 2017, doi: 10.1016/j.plaphy.2017.10.002.

[80] J. P. Moore *et al.*, "Response of the leaf cell wall to desiccation in the resurrection plant Myrothamnus flabellifolius," *Plant Physiol.*, vol. 141, no. 2, pp. 651–662, 2006, doi: 10.1104/pp.106.077701.

[81] C. Petersen, K. J. Tielrooij, and H. J. Bakker, "Strong temperature dependence of water reorientation in hydrophobic hydration shells," *J. Chem. Phys.*, vol. 130, no. 21, 2009, doi: 10.1063/1.3142861.

[82] Q. Huang, J. M. Rodgers, R. J. Hemley, and T. Ichiye, "Effects of pressure and temperature on the atomic fluctuations of dihydrofolate reductase from a psychropiezophile and a mesophile," *Int. J. Mol. Sci.*, vol. 20, no. 6, pp. 1–13, 2019, doi: 10.3390/ijms20061452.

[83] P. G. Brewer and E. T. Peltzer, "The Molecular Basis for the Heat Capacity and Thermal Expansion of Natural Waters," *Geophys. Res. Lett.*, vol. 46, no. 22, pp. 13227–13233, 2019, doi: 10.1029/2019GL085117.

[84] A. Oleinikova, I. Brovchenko, and G. Singh, "The temperature dependence of the heat capacity of hydration water near biosurfaces from molecular simulations," *Epl*, vol. 90, no. 3, 2010, doi: 10.1209/0295-5075/90/36001.

[85] A. R. Van Buuren, S. J. Marrink, and H. J. C. Berendsen, "A molecular dynamics study of the decane/water interface," *J. Phys. Chem.*, vol. 97, no. 36, pp. 9206–9212, 1993, doi: 10.1021/j100138a023.

[86] J. N. Israelachvili, *Intermolecular and Surface Forces*. 2011.

[87] C. J. Van Oss, "Long-range and short-range mechanisms of hydrophobic attraction and hydrophilic repulsion in specific and aspecific interactions," *J. Mol. Recognit.*, vol. 16, no. 4, pp. 177–190, 2003, doi: 10.1002/jmr.618.

[88] C. Della Volpe and S. Siboni, "From van der Waals equation to acid-base theory of surfaces: A chemical-mathematical journey," *Rev. Adhes. Adhes.*, vol. 10, no. 1, pp. 47–97, 2022, doi: 10.47750/RAA/10.1.02.

[89] N. B. Rego and A. J. Patel, "Understanding Hydrophobic Effects: Insights from Water Density Fluctuations," *Annu. Rev. Condens. Matter Phys.*, vol. 13, no. 1, pp. 303–324, 2022, doi: 10.1146/annurev-conmatphys-040220-045516.

[90] E. A. Vogler, "Structure and reactivity of water at biomaterial surfaces," *Adv. Colloid Interface Sci.*, vol. 74, no. 1–3, pp. 69–117, 1998, doi: 10.1016/S0001-

8686(97)00040-7.

[91] S. Bekele and M. Tsige, "Characterizing the Hydrophobicity of Surfaces Using the Dynamics of Interfacial Water Molecules," *J. Phys. Chem. C*, vol. 122, no. 16, pp. 9015–9020, 2018, doi: 10.1021/acs.jpcc.8b01353.

[92] F. Bresme, E. Chacón, P. Tarazona, and K. Tay, "Intrinsic structure of hydrophobic surfaces: The oil-water interface," *Phys. Rev. Lett.*, vol. 101, no. 5, pp. 1–4, 2008, doi: 10.1103/PhysRevLett.101.056102.

[93] M. K. Coe, R. Evans, and N. B. Wilding, "Density Depletion and Enhanced Fluctuations in Water near Hydrophobic Solutes: Identifying the Underlying Physics," *Phys. Rev. Lett.*, vol. 128, no. 4, p. 45501, 2022, doi: 10.1103/physrevlett.128.045501.

[94] R. Godawat, S. N. Jamadagni, and S. Garde, "Characterizing hydrophobicity of interfaces by using cavity formation, solute binding, and water correlations," *Proc. Natl. Acad. Sci. U. S. A.*, vol. 106, no. 36, pp. 15119–15124, 2009, doi: 10.1073/pnas.0902778106.

[95] M. C. Bellissent-Funel *et al.*, "Water Determines the Structure and Dynamics of Proteins," *Chem. Rev.*, vol. 116, no. 13, pp. 7673–7697, 2016, doi: 10.1021/acs.chemrev.5b00664.

[96] U. Kumar Sur, "Behaviour of water at hydrophobic interfaces," *J. Mol. Liq.*, vol. 348, p. 118433, 2022, doi: 10.1016/j.molliq.2021.118433.

[97] V. R. Hande and S. Chakrabarty, "How Far Is 'Bulk Water' from Interfaces? Depends on the Nature of the Surface and What We Measure," *J. Phys. Chem. B*, vol. 126, no. 5, pp. 1125–1135, 2022, doi: 10.1021/acs.jpcb.1c08603.

[98] C. Sendner, D. Horinek, L. Bocquet, and R. R. Netz, "Interfacial water at hydrophobic and hydrophilic surfaces: Slip, viscosity, and diffusion," *Langmuir*, vol. 25, no. 18, pp. 10768–10781, 2009, doi: 10.1021/la901314b.

[99] V. Hande and S. Chakrabarty, "Size-Dependent Order–Disorder Crossover in Hydrophobic Hydration: Comparison between Spherical Solutes and Linear Alcohols," *ACS Omega*, vol. 7, no. 3, pp. 2671–2678, 2022, doi: 10.1021/acsomega.1c05064.

[100] C. Q. Sun, "Supersolidity of undercoordinated and hydrating water," *Phys. Chem. Chem. Phys.*, vol. 20, no. 48, pp. 30104–30119, 2018, doi: 10.1039/c8cp06115g.

[101] Q. Sun, "The physical origin of hydrophobic effects," *Chem. Phys. Lett.*, vol. 672, pp. 21–25, 2017, doi: 10.1016/j.cplett.2017.01.057.

[102] C. Q. Sun, X. Zhang, J. Zhou, Y. Huang, Y. Zhou, and W. Zheng, "Density, elasticity, and stability anomalies of water molecules with fewer than four neighbors," *J. Phys. Chem. Lett.*, vol. 4, no. 15, pp. 2565–2570, 2013, doi: 10.1021/jz401029z.

[103] E. S. Minina, E. S. Pyanzina, E. V. Novak, and S. S. Kantorovich, "Compressibility of ferrofluids: Towards a better understanding of structural properties," *Eur. Phys. J. E*, vol. 41, no. 5, 2018, doi: 10.1140/epje/i2018-11678-7.

[104] M. Klähn, A. Martin, D. W. Cheong, and M. V. Garland, "Variation and decomposition of the partial molar volume of small gas molecules in different organic solvents derived from molecular dynamics simulations," *J. Chem. Phys.*, vol. 139, no. 24, 2013, doi: 10.1063/1.4854135.

[105] E. L. Ratkova and M. V. Fedorov, "On a relationship between molecular polarizability and partial molar volume in water," *J. Chem. Phys.*, vol. 135, no. 24, 2011, doi: 10.1063/1.3672094.

[106] S. A. Blair and A. J. Thakkar, "Relating polarizability to volume, ionization energy, electronegativity, hardness, moments of momentum, and other molecular properties," *J. Chem. Phys.*, vol. 141, no. 7, 2014, doi: 10.1063/1.4893178.

[107] C. J. van Oss and R. J. Good, "Orientation of the water molecules of hydration of human serum albumin," *J. Protein Chem.*,

vol. 7, no. 2, pp. 179–183, 1988, doi: 10.1007/BF01025248.

[108] S. M. Sarhangi, M. M. Waskasi, S. M. Hashemianzadeh, and D. V. Matyushov, "Effective Dielectric Constant of Water at the Interface with Charged C 60 Fullerenes," *J. Phys. Chem. B*, vol. 123, no. 14, pp. 3135–3143, 2019, doi: 10.1021/acs.jpcb.9b00901.

[109] S. H. Lee and P. J. Rossky, "A comparison of the structure and dynamics of liquid water at Hydrophobic and hydrophilic surfaces - A molecular dynamics simulation study," *J. Chem. Phys.*, vol. 100, no. 4, pp. 3334–3345, 1994, doi: 10.1063/1.466425.

[110] C. Faucon, P. Chalier, and C. Sanchez, "On the relationship between volume fluctuations in liquids and the Gibbs free energy of cavity formation," *J. Mol. Liq.*, vol. 364, p. 119845, 2022, doi: 10.1016/j.molliq.2022.119845.

[111] G. Graziano, "Contrasting the hydration thermodynamics of methane and methanol," *Phys. Chem. Chem. Phys.*, vol. 21, no. 38, pp. 21418–21430, 2019, doi: 10.1039/c9cp03213d.

[112] R. A. Pierotti, "Aqueous Solutions of Nonpolar Gases," *J. Phys. Chem.*, vol. 69, pp. 281–288, 1965.

[113] M. Prévost, I. T. Oliveira, J. P. Kocher, and S. J. Wodak, "Free energy of cavity formation in liquid water and hexane," *J. Phys. Chem.*, vol. 100, no. 7, pp. 2738–2743, 1996, doi: 10.1021/jp952906a.

[114] D. Renard, L. Lavenant-Gourgeon, A. Lapp, M. Nigen, and C. Sanchez, "Enzymatic hydrolysis studies of arabinogalactan-protein structure from Acacia gum: The self-similarity hypothesis of assembly from a common building block," *Carbohydr. Polym.*, vol. 112, pp. 648–661, 2014, doi: 10.1016/j.carbpol.2014.06.041.

[115] D. M. W. Anderson and F. J. McDougall, "Degradative Studies of Gum Arabic (Acacia Senegal (L.) Willd.) with Special Reference to the Fate of the Amino Acids Present," *Food Addit. Contam.*, vol. 4, no. 3, pp. 247–255, 1987, doi: 10.1080/02652038709373633.

[116] C. Zhu *et al.*, "Characterizing hydrophobicity of amino acid side chains in a protein environment via measuring contact angle of a water nanodroplet on planarpeptide network," *Proc. Natl. Acad. Sci. U. S. A.*, vol. 113, no. 46, pp. 12946–12951, 2016, doi: 10.1073/pnas.1616138113.

[117] M. L. Jayme, D. E. Dunstan, and M. L. Gee, "Zeta potentials of gum arabic stabilised oil in water emulsions," *Food Hydrocoll.*, vol. 13, no. 6, pp. 459–465, 1999, doi: 10.1016/S0268-005X(99)00029-6.

[118] J. B. Li, "Multilayer formation on a curved drop surface," *Angew. Chemie - Int. Ed.*, vol. 40, no. 5, pp. 891–894, 2001, doi: 10.1002/1521-3773(20010302)40:5<891::AID-ANIE891>3.0.CO;2-K.

[119] D. Zare, J. R. Allison, and K. M. McGrath, "Molecular Dynamics Simulation of β-Lactoglobulin at Different Oil/Water Interfaces," *Biomacromolecules*, vol. 17, no. 5, pp. 1572–1581, 2016, doi: 10.1021/acs.biomac.5b01709.

[120] D. K. Kondepudi, B. De Bari, and J. A. Dixon, "Dissipative structures, organisms and evolution," *Entropy*, vol. 22, no. 11, pp. 1–19, 2020, doi: 10.3390/e22111305.

[121] I. Prigogine and R. Lefever, "Theory of Dissipative Structures," *Synergetics*, pp. 124–135, 1973, doi: 10.1007/978-3-663-01511-6_10.

[122] G. Nicolis, "Biological order, structure and instabilities," *Q. Rev. Biophys.*, vol. 4, no. 2–3, pp. 107–148, 1971, doi: 10.1017/S0033583500000615.

[123] C. Sanchez *et al.*, "Acacia gum: History of the future," *Food Hydrocoll.*, vol. 78, pp. 140–160, 2018, doi: 10.1016/j.foodhyd.2017.04.008.

[124] T. R. Briggs and H. F. Schmidt, "Experiments on emulsions. II," *J. Phys. Chem.*, vol. 19, no. 6, pp. 478–499, 1915, doi: 10.1021/j150159a002.

[125] J. A. Serrallach and J. Owex, "Strength of

Emulsifier Films a t Liquid- Liquid Interfaces," pp. 816–819.

[126] E. Shotton and K. Wibberley, "Interfacial Films Between Benzene and Solutions of Salts of Arabic Acid," *J. Pharm. Pharmacol.*, vol. 11, no. 1 S, pp. 120T-126T, 1959, doi: 10.1111/j.2042-7158.1959.tb10421.x.

[127] K. Wibberley, "Some Physical Properties of Interfacial Films of Potassium Arabate," *J. Pharm. Pharmacol.*, vol. 14, no. 1 S, pp. 87T-92T, 1962, doi: 10.1111/j.2042-7158.1962.tb10536.x.

[128] P. Erni, H. A. Jerri, K. Wong, and A. Parker, "Interfacial viscoelasticity controls buckling, wrinkling and arrest in emulsion drops undergoing mass transfer," *Soft Matter*, vol. 8, no. 26, pp. 6958–6967, 2012, doi: 10.1039/c2sm25438g.

[129] B. P. Binks, P. D. I. Fletcher, B. L. Holt, O. Kuc, P. Beaussoubre, and K. Wong, "Compositional ripening of particle- and surfactant-stabilised emulsions: A comparison," *Phys. Chem. Chem. Phys.*, vol. 12, no. 9, pp. 2219–2226, 2010, doi: 10.1039/b918812f.

[130] E. A. Ploetz and P. E. Smith, "Local fluctuations in solution: Theory and applications," *Adv. Chem. Phys.*, vol. 153, pp. 311–372, 2013, doi: 10.1002/9781118571767.ch4.

[131] D. Siu and Y. Koga, "Fluctuation functions in aqueous NaCl and urea," *J. Phys. Chem. B*, vol. 109, no. 35, pp. 16886–16890, 2005, doi: 10.1021/jp0516792.

[132] Y. Koga, "Fluctuations in aqueous solutions of some hydrophobic solutes," *Chem. Phys. Lett.*, vol. 240, no. 4, pp. 340–344, 1995, doi: 10.1016/0009-2614(95)00531-8.

[133] A. . Soper, "Is water one liquid or two ?," *J. Chem. Phys.*, vol. 150, no. 234503, 2019, doi: 10.1063/1.5096460.

[134] A. Yeung and L. Zhang, "Shear effects in interfacial rheology and their implications on oscillating pendant drop experiments," *Langmuir*, vol. 22, no. 2, pp. 693–701, 2006, doi: 10.1021/la051795w.

[135] M. Nagel, T. A. Tervoort, and J. Vermant, "From drop-shape analysis to stress-fitting elastometry," *Adv. Colloid Interface Sci.*, vol. 247, no. May, pp. 33–51, 2017, doi: 10.1016/j.cis.2017.07.008.

[136] J. D. Berry, M. J. Neeson, R. R. Dagastine, D. Y. C. Chan, and R. F. Tabor, "Measurement of surface and interfacial tension using pendant drop tensiometry," *J. Colloid Interface Sci.*, vol. 454, pp. 226–237, 2015, doi: 10.1016/j.jcis.2015.05.012.

[137] R. C. Randall, G. O. Phillips, and P. A. Williams, "Fractionation and characterization of gum from Acacia senegal," *Top. Catal.*, vol. 3, no. 1, pp. 65–75, 1989, doi: 10.1016/S0268-005X(89)80034-7.

[138] A. M. Islam, G. O. Phillips, A. Sljivo, M. J. Snowden, and P. A. Williams, "A review of recent developments on the regulatory, structural and functional aspects of gum arabic," *Food Hydrocoll.*, vol. 11, no. 4, pp. 493–505, 1997, doi: 10.1016/S0268-005X(97)80048-3.

[139] M. J. Snowden, G. O. Phillips, and P. A. Williams, "Functional characteristics of gum arabic," *Top. Catal.*, vol. 1, no. 4, pp. 291–300, 1987, doi: 10.1016/S0268-005X(87)80017-6.

[140] T. Katayama *et al.*, "Estimation of Concentration and Performance of AGPs in Emulsion Systems Using Gum Arabic," *Foods food Ingredients J. Jpn.*, vol. 211, no. 3, pp. 222–227, 2006.

[141] M. Nakauma *et al.*, "Comparison of sugar beet pectin, soybean soluble polysaccharide, and gum arabic as food emulsifiers. 1. Effect of concentration, pH, and salts on the emulsifying properties," *Food Hydrocoll.*, vol. 22, no. 7, pp. 1254–1267, 2008, doi: 10.1016/j.foodhyd.2007.09.004.

[142] A. Schröder, C. Berton-Carabin, P. Venema, and L. Cornacchia, "Interfacial properties of whey protein and whey protein hydrolysates and their influence on O/W emulsion stability," *Food Hydrocoll.*, vol. 73, pp. 129–140, 2017, doi: 10.1016/j.foodhyd.2017.06.001.

[143] M. A. B. Bos and T. van Vliet, "Interfacial rheological properties of adsorbed protein layers and surfactants: a review," *Adv. Colloid Interface Sci.*, vol. 91, pp. 437–471, 2001, doi: https://doi.org/10.1016/S0001-8686(00)00077-4.

[144] V. B. Fainerman, R. Miller, and E. V. Aksenenko, "Thermodynamics of adsorption at liquid interfaces," *Comput. Methods Complex Liq. Interfaces*, pp. 3–40, 2015, doi: 10.1201/b19337.

[145] Verónica Meija Tamayo, "Propriétés volumétriques des Arabinogalactane-protéines d'exsudats de gommes d'Acacia," 2018.

Chapter IV: Stability of Acacia gum oil-in-water emulsions

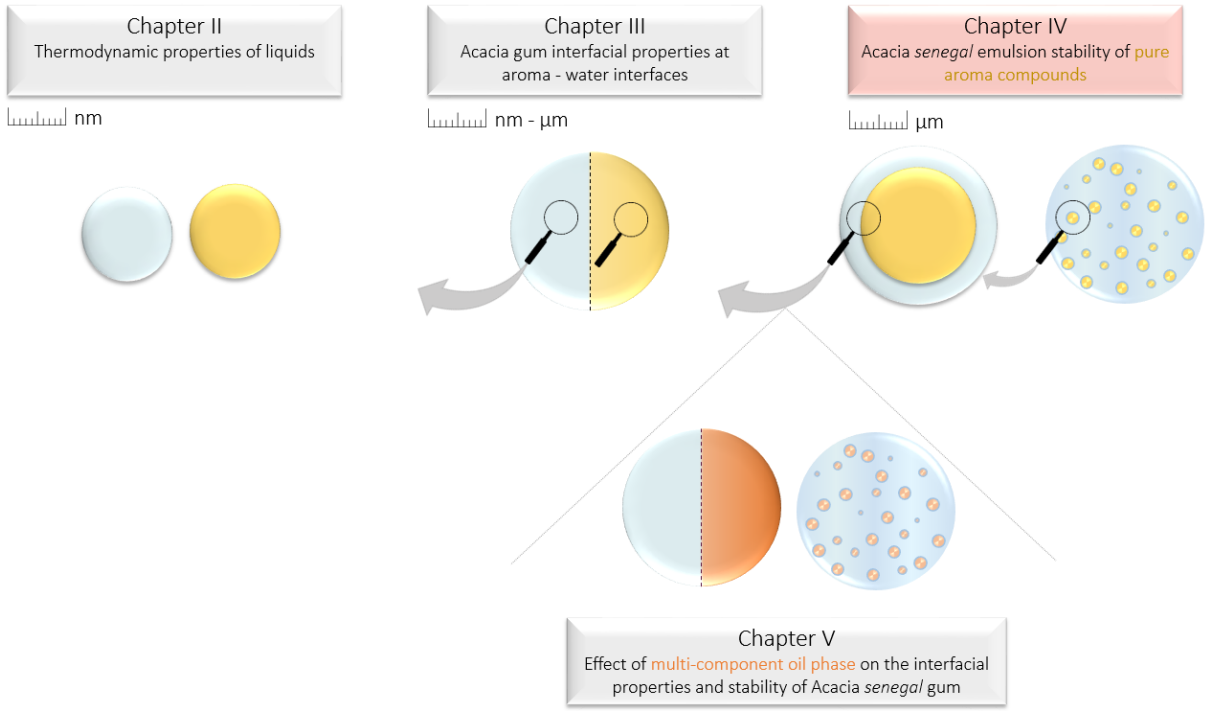

This chapter aimed to study the impact of the oil hydrophobicity on the size of droplets during homogenization and on the stability of resulting emulsions. To this end, droplet size distribution analyses and monitoring of destabilization phenomena were performed on Acacia *senegal* emulsions of five types of oil (n-hexadecane, d-limonene, ethyl octanoate, 1-decanol, 1-octanol). In addition, the effect of the gum type using another variety of Acacia gum (Acacia *seyal*) on the emulsion stability was studied.

Highlights

- The increase of the oil hydrophobicity (*i.e.* oil-water interfacial tension) leads to the increase of the coarse emulsion droplet size and to the decrease of creaming and of initial droplet growth.

- A. *senegal* provides smaller droplet size for both coarse and fine emulsions of the least hydrophobic oils (1-decanol and 1-octanol) than A. *seyal*.

- The weaker interfacial properties of A. *seyal*, due to its supposed but not demonstrated greater affinity with water [1]–[4] together with its lower flexible conformation, decrease the AGPs adsorption rate during emulsification. This leads to the enlargement of the droplet recoalescence during homogenization.

- The low apparent viscosity of A. *seyal* dispersion enhances the creaming rate as compared to the emulsions produced with A. *senegal*.

Effect of the oil hydrophobicity on the stability and structure of Acacia *senegal* gum oil-in-water emulsion[1]

Camille Faucon[a], Pascale Chalier[a], Christian Sanchez[a]

[a] IATE, Univ Montpellier, INRAE, Institut Agro, Montpellier, France.

Abstract

Emulsions based on five types of oils (n-hexadecane, d-limonene, ethyl octanoate, 1-decanol, 1-octanol), Acacia *senegal* gum and water were studied to examine the role of the oil hydrophobicity on their stability and physicochemical characteristics . The results indicated the droplet size of emulsions after the first stage of the high shear homogenization was dependent on the oil hydrophobicity. The second homogenization step provided oil droplets of the same order of size, allowing the comparison of the aging stability. Emulsions based on the most hydrophobic oils (e.g. n-hexadecane, d-limonene) were found more stable to creaming and showed better resistance to coalescence during the first hours of storage. This mostly originates from how interfaces and viscoelasticity of AGPs interfacial layer are modified by the adsorption process (details are given in Chapter III).

Keywords: emulsions; stability; Acacia gum; oil hydrophobicity; interfacial tension.

1. Introduction

Acacia *senegal* gum (A. *senegal*) is a natural emulsifier obtained from the trunk and branches of Acacia trees [5], [6]. It is commonly used to stabilize oil-in-water emulsions, in particular aroma compounds in beverages. GA is composed by a continuum of arabinogalactan-proteins (AGPs) that are essentially made of sugars D-galactose, L-arabinose, L-rhamnose, D-glucuronic acid, and 4-O-methyl-D-glucuronic acid. In addition, AGPs contain about 1-3%

[1]Article in preparation

of proteins, 3-4% of minerals and around 1% polyphenols [8]. Its chemical composition and structural complexity induces amphiphilic characteristics allowing the gum to reduce the interfacial tension between the dispersed and the continuous phases. This is the result of the formation of an interfacial viscoelastic barrier, promoting the formation of a more stable emulsion by producing droplet size distribution with limited span. The interfacial properties of AGPs have been mainly attributed to the proteinaceous moiety of high molar mass AGPs [3], [7], [8]. On the other hand, the emulsion stabilization is mainly related to the hydrated charged and polar carbohydrate portion, contributing to viscosity, steric, and electrostatic effects and acting against flocculation and coalescence [9]–[12]. Aromas, that constitute the dispersed phase of oil-in-water beverage emulsions, are small organic compounds having high volatility and flavoring properties. They vary in chemical classes, terpenoids, hydrocarbures, esters, ketones, alcohols, phenols, pyrazines, aldehydes, acids, sulfurs and so long. In the terpene family, compounds with different chemical function are found, e.g. d-limonene, the main component of citrus oil, is classified as a monoterpene, citronellal giving the distinctive lemon scent to citronella oil is a monoterpenoid aldehyde, or linalool from lavender (*Lavandula angustifolia*) oil is a terpene alcohol. They offer a wide variety of physicochemical and thermodynamic properties, e.g. vapor pressure, hydrophobicity, viscosity, diffusivity and compressibility, which may contribute to the emulsion instability phenomena such as coalescence, creaming or Ostwald ripening. The stability of GA-based oil-in-water emulsions has been widely studied [13], [14] through the characteristics and the physicochemical properties of the continuous phase, e.g. the nature and the concentration of the emulsifier [7], [10], [15]–[19], the pH of the solvent [12], [20] and the concentration of salts [12], [20]. In addition, the volume fraction [21], [22] and viscosity of the oil dispersed phase are also important physical characteristics. These parameters are important in determining Reynolds and Weber numbers, promoting variations of flows and balance between shear, local static pressure and cavitation effects. Thus, they impact the initial emulsion droplet average size and size distribution and ergo, the stability. However, the importance of the nature of the dispersed phase composition on emulsion stability were much less explored [12], [18], [23], [24]. For instance, Chanamai and others determined for a set of more or less hydrophobic oils how their solubility and hydrophobicity modified the emulsion instability mechanisms through coalescence and Oswald ripening [25]. Similarly, in the case of emulsions stabilized with low surfactants [26], less hydrophobic oils were found highly unstable to droplet growth during storage. Other studies demonstrated that low

interfacial tensions between oil and aqueous phase limited as well the droplet fragmentation using surfactants or proteins [27]–[29]. Chapter III highlighted the substantial impact of the oil hydrophobicity on an oil-gum-water interphase model. Therefore, the present study aimed to examine the effect of the oil hydrophobicity under practical conditions, by drawing or not correlations between oil hydrophobicity and droplet size and growth of A. *senegal*-stabilized emulsions. In our approach, oil was first dispersed using a high shear mixer to obtain coarse emulsions, then finer emulsions were obtained using high-pressure microfluidization. The impact of hydrophobicity was studied using similar and further classes of oils, namely alkane, terpene, ketone, ester and alcohol, as compared to the work of Chanamai and al. research [25]. The droplet size distribution of emulsions was analyzed after the two homogenization steps and the temporal stability over time was followed during 28 days of storage using light scattering method.

2. Materials and methods

2.1. Materials

Acacia senegal (Batch n° OF152413) gum was provided by Alland & Robert Company - Natural and organic gums (Port mort, France). The biochemical composition and structural properties of the gum were previously characterized, showing in particular a 2.2 wt% protein content [2], [30]. Dispersions of 20 wt% Acacia gum were done stirring gum powders in Milli-Q-water overnight at room temperature, followed by sample centrifugation for removing insoluble materials (5 000 rpm for 20 minutes at 25°C). n-Hexadecane (≥99%), d-limonene (≥97%), carvone (≥98%), 1-octanol (≥99%), 1-decanol (≥98%) and ethyl octanoate (≥99%) were purchased from Sigma-Aldrich. The hydrophobicity of oils, transcribed by the oil-water interfacial tension, the density and the viscosity are presented in Table IV.1. The oil solubility in water came from the literature. In this set, the most hydrophobic compound was n-hexadecane (γ_{ow}= 47.2 mN.m^{-1}) and the least hydrophobic one was 1-octanol (γ_{ow}= 8.4 mN.m^{-1}). n-Hexadecane is also characterized by the lowest solubility in water ($C_S = 2 \times 10^{-5}$ mg.L^{-1}) and density (ρ = 770 kg.m^{-3}) in opposition with carvone (C_S = 1300 mg.L^{-1}, ρ = 957 kg.m^{-3}). Regarding the viscosity, 1-decanol and d-limonene were found, respectively, the most (η = 11.85 mPa.s) and the least (η = 0.87 mPa.s) viscous compound.

Table IV.1. Oil-water interfacial tension, oil solubility in water and oil viscosity at 25°C. Oil-water interfacial tensions were measured using an automatic drop tensiometer through the rising drop technique (see Chapter III).

Oil type	Oil name	Oil-water interfacial tension ($mN.m^{-1}$)	Solubility in water ($mg.L^{-1}$)[2]	Density ($kg.m^{-3}$)	Viscosity ($.10^{-3}$ Pa.s)
Alkane	n-Hexadecane	47.2 (±1.4)	$2x10^{-5}$	770	2.98
Terpene	d-Limonene	28.0 (±0.2)	14	834	0.87
Ester	Ethyl octanate	22.7 (±0.3)	70	862	1.41
Ketone	Carvone	16.5 (±0.1)	1300	957	2.42
Alcohols	1-Decanol	9.1 (±0.1)	37	827	11.85
	1-Octanol	8.4 (±0.1)	540	823	7.85

2.2 Methods

2.2.1. Emulsification process

The oil-in-water emulsions were obtained using a two stage homogenization process. The primary homogenization consists of the conversion of two bulk liquids into a coarse emulsion. To this end, 5 g of oil were added to 95 g of Acacia gum dispersion in order to obtain a 20 wt% gum concentrated emulsion containing 5 wt% oil concentration. Coarse emulsions were prepared using a rotor/stator homogenizer (Silverson L4RT, Evry, France) equipped with a square hole high shear screen stator at a 7500 rpm speed for 5 min at room temperature (~25°C). The secondary homogenization consists of the reduction of coarse droplet size to obtain a smaller drop emulsion using a microfluidizer (F12Y diamond interaction chamber; LM20, Microfluidics Corporation, MA, USA) at a pressure of 45 MPa (450 bars) for 2 passes.

2.2.3. Mean volumetric droplet diameter $D_{4,3}$ of emulsion

The mean volumetric droplet diameter $D_{4,3}$, together with the droplet size distribution of the emulsions, were determined by laser diffraction using a Beckman Coulter LS 13 320 XR (Beckman Coulter, Villepinte, France). Five cycles of measurements were performed 15 minutes after the emulsification step, using an obscuration value of ~10%. The $D_{4,3}$ was calculated from:

[2]values from https://pubchem.ncbi.nlm.nih.gov/, data base of national library of medicine

$$D_{4,3} = \frac{\sum n_i d_i^4}{\sum n_i d_i^3} \quad (1)$$

where n_i is the number of droplets of diameter d_i.

2.2.3. Emulsion structure and stability measurements

The droplet size was determined as described above. The emulsion colloidal stability was monitored using a vertical scan light scattering analyzer type Turbiscan® Tower (Formulaction Company, France) equipped with a pulsed near infrared light source (λ = 880 nm) and two synchronous transmission (T) and backscattering (BS) detectors. About 15 ml emulsion sample (equivalent to ~4 cm height) were loaded into cylindrical glass tubes 5 minutes after emulsification and scanned throughout its entire height. Backscattered (BS) and transmitted (T) light were recorded every 5 minutes during the first 24h, and then after 2, 3, 7, 14, 21 and 28 days of storage at 25°C. Instability phenomena such as creaming, sedimentation and coalescence of oil droplets were analyzed through the differences in backscattering (BS) and in transmittance (T) profiles between the initial scan and scans over time (ΔBS and ΔT expressed in %). In addition, the Turbiscan® stability index (TSI) corresponding to the signal variation at definite positions (h) throughout various height (H) ranges of the sample between the $scan_i$ and the $scan_{i-1}$ was calculated. TSI was determined through Equation (2).

$$TSI = \sum_i \frac{\sum_h |scan_i(h) - scan_{i-1}(h)|}{H} \quad (2)$$

where $scan_i$ is the average backscattering intensity of the i-th scan, $scan_{i-1}$ is the average backscattering intensity of the (i-1)-th scan and H is the scan numbers in the whole measurement. This parameter was calculated over the entire tube height and takes into account the ensemble of destabilization phenomena occurring during storage (creaming, flocculation/coalescence, clarification).

3. Results and discussion

3.1. Oil hydrophobicity and droplet size distribution of Acacia gum-based emulsions

The droplet size distribution and the $D_{4,3}$ diameter of both coarse and fine emulsions stabilized by 20 wt% A. *senegal* were measured (Fig. IV.1 and Table IV.2). For all emulsions, the first

homogenization step led to the dispersion of the oil into droplets (light blue profile of Fig. IV.1) and the second homogenization steps allowed the decrease of the droplet size, as expected (dark blue profile of Fig. IV.1). The droplet distribution shape and span varied according to the dispersed oil. For instance, 1-octanol droplet distribution was bimodal for both coarse and fine emulsion. d-Limonene and 1-decanol fine emulsions displayed a small population of fine drops disconnected from the main droplet distribution.

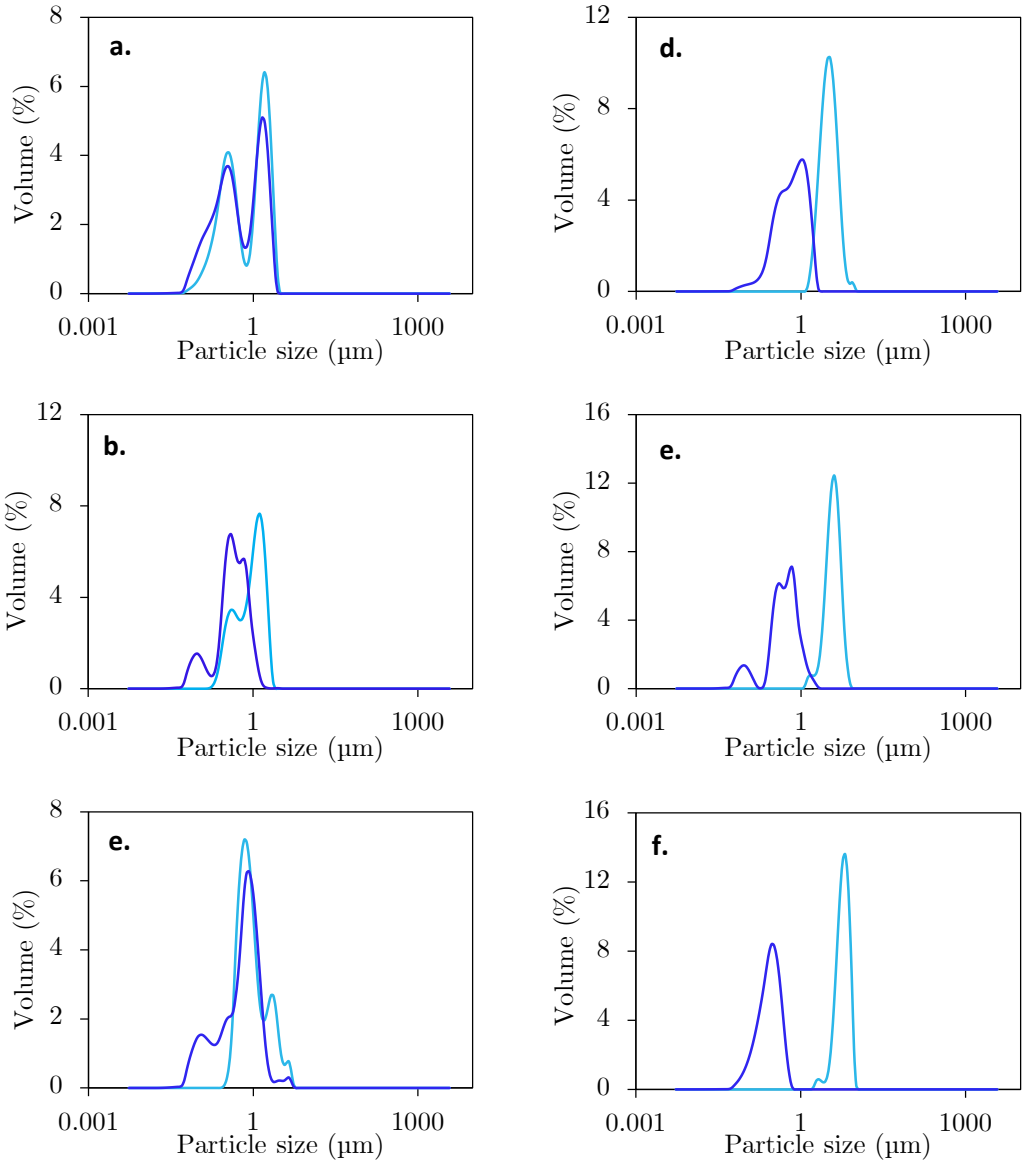

Fig. IV.1. Droplet size distribution of 20 wt% A. *senegal* stabilized oil-in-water emulsion. Light blue is for coarse emulsions signals and dark blue for fine emulsion signals. Oil load was set at 5 wt%. **(a)** 1-octanol, **(b)** 1-decanol, **(c)** carvone, **(d)** ethyl octanoate, **(e)** d-limonene, **(f)** n-hexadecane.

Table IV.2. Volumetric droplet diameters $D_{4,3}$ in oil-in-water coarse and fine emulsions containing 20 wt% A. *senegal* gum.

Oil type	Oil name	$D_{4,3}$ coarse (µm)	$D_{4,3}$ fine (µm)	%difference fine - coarse
Alkane	n-Hexadecane	5.94 (±0.15)	0.29 (±0.01)	95
Terpene	d-Limonene	4.01 (±0.13)	0.54 (±0.02)	87
Ester	Ethyl octanoate	3.35 (±0.05)	0.77 (±0.01)	77
Ketone	Carvone	2.42 (±0.20)	0.61 (±0.05)	75
Alcohols	1-Decanol	0.98 (±0.01)	0.49 (±0.01)	50
	1-Octanol	0.99 (±0.04)	0.79 (±0.01)	20

According to the oil-water interfacial tension scale, n-hexadecane-water is the most hydrophobic system. Then, n-hexadecane also appeared the most difficult liquid to homogenize using a simple mixer system, with droplets $D_{4,3}$ of about 6 µm. This is significantly larger than those obtained with 1-octanol (~1.3 µm), a clearly less hydrophobic compound with an oil-water interfacial tension of 8.4 mN.m^{-1} (Table IV.1). A linear correlation was found when plotting the $D_{4,3}$ diameter of the coarse emulsion and the initial oil-water interfacial tension (Fig. IV.2). This obviously implies larger droplet diameters are obtained in coarse emulsions with more hydrophobic oils.

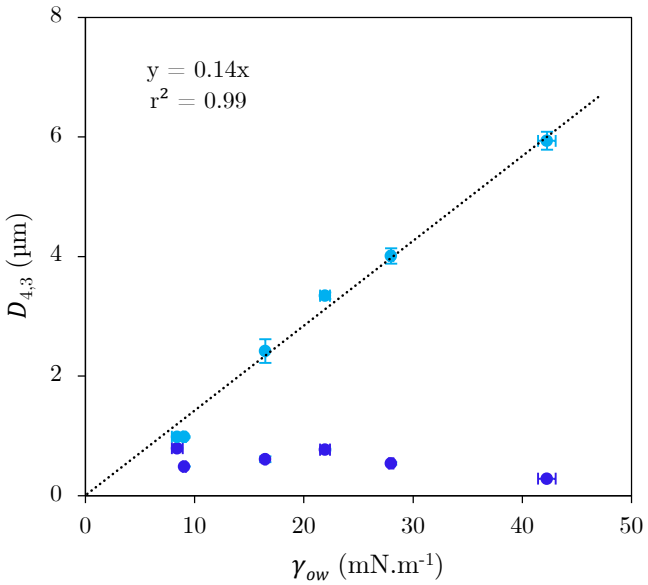

Fig. IV.2. Dependency at 25°C of emulsion droplet diameter $D_{4,3}$ on the initial oil-water interfacial tension γ_{ow}. Dark blue dots are for diameter of fine emulsion droplets; light blue dots are for diameter of coarse emulsion droplets. Emulsions were stabilized by 20 wt% A. *senegal* gum. Oil load was set at 5 wt%.

On the contrary, no dependency on the oil interfacial tension was observed regarding the $D_{4,3}$ of final emulsion droplets, emphasizing the different transport mechanism and hydrodynamic conditions of the two process stages. However, it can be observed the efficiency of the second homogenization stage increases with the increase of the oil hydrophobicity. For instance, the droplet size of n-hexadecane and d-limonene emulsions is reduced respectively by 95% and 87% after the second stage, while the droplet size of 1-decanol and 1-octanol is only reduced by 50% and 20% respectively. The difference in resulted correlations could be due to variations of types on flow (laminar vs elongational) and mechanism of droplets disruption (planar shear, elongation shear, turbulent fluctuations, pressure gradients and cavitation [14], [31]–[33]) according to the homogenization step.

3.2. Impact of hydrodynamic-mechanical fragmentation mechanisms on droplet size

The fragmentation of oil droplets under turbulent flow is assumed to occur if the disruptive forces exceed the cohesive ones. In dilute liquid–liquid systems with low viscosity such as those we used, viscous stresses are negligible, therefore only cohesive forces are stabilizing the droplets [34], [35]. The Weber number We is dimensionless and describes the droplet deformation. It represents the ratio of the fluid's inertia and the internal coherent stress [32].

$$We = \frac{Inertial\ forces}{Cohesion\ forces} \tag{3}$$

The cohesion forces are due to interfacial tension attempting to minimize surface area by forcing the deformed drop to return to its original spherical shape [36].

3.2.1. High shear mixer

During the first homogenization, shear stress is mainly responsible for mixing the two fluids through the motion of the rotating and stationary parts of the mixer. The rotor rotation provides a pressure gradient, drawing the fluid towards the center in the axial direction and out through stator holes in the axial, radial and tangential directions [37]. Shear stress is mainly caused by energy dissipation between interacting fluid molecules (viscosity effect) but also between the fluids and the rotor parts. The viscosity of A. *senegal* dispersions being low, *i.e.* 51 mPa.s., high shear mixer is a valuable process equipment for homogenization [37]. Under turbulent flow conditions, the Weber number can be expressed through [34], [35]:

$$We = \frac{\rho_C N^2 D_o^3}{\gamma} \quad (4)$$

with ρ_C the density of the continuous phase (kg.m^{-3}), N the rotor speed (s^{-1}), D_o the outer rotor diameter (m) and γ the interfacial tension of dispersive phase (N.m^{-1}).

For all types of oil, the same mixing conditions were applied, *i.e.* 7500 rpm for the speed and 5 min of residence time. Herein, it can be seen from Equation (4) that the main variable affecting the droplet disruption mechanism is the oil-water interfacial tension. Therefore, incrementing in Equation (4) the relation obtained from Fig. IV.2, $D_{4,3} = a\gamma_{ow}$ with a being a constant, leads to:

$$We = \frac{b}{D_{4,3}} \quad (5)$$

with b a constant. Thus, plotting the volumetric droplet diameter over the Weber number leads to the following dependency (Fig. IV.3).

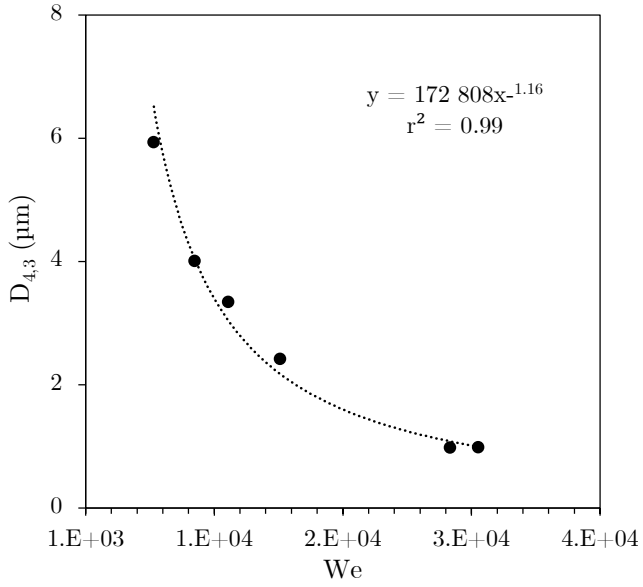

Fig. IV.3. Dependency of the droplet diameter $D_{4,3}$ of coarse emulsions of 5 wt% oil load and stabilized by 20 wt% A. *senegal* gum on the Weber number We.

As well documented [34], [38], reducing the interfacial tension results in the increase of the Weber number, lowering the energy needed to cause droplet disruption. The reason is that interfacial forces acting to keep the droplets together are inversely proportional to the droplet radius. This resistance to drop deformation and breakup is called the Laplace pressure ΔP [31]. It is defined as the pressure difference between the inside and the outside of a drop dispersed in a continuous phase and is proportional to the interfacial tension.

$$\Delta P = \frac{2\gamma}{R_d} \quad (6)$$

with R_d the radius of the spherical drop.

Thus, the Laplace pressure increases with decreasing drop diameter. Producing successively smaller drops requires successively higher external stresses applied by mechanical means and/or successively higher concentrations of surfactant to lower the interfacial tension [31]. As previously demonstrated, GA interfacial concentration is dependent on the oil hydrophobicity (Chapter III) such that increasing the oil hydrophobicity results in the increase of the surface coverage. Therefore, increasing the applied mechanical stress could be the only way to further reduce the droplet size of highly hydrophobic oil. To this purpose, an effective way is to use a secondary homogenization step through, for instance high-pressure homogenizers.

Incrementing Equations (4) and (6) gives the following relation between the Weber number We and the droplet radius R_d.

$$R_d = \frac{2\rho_C N^2 {D_o}^3}{We\Delta P} \quad (7)$$

This explains the correlation observed at outlet homogenization in Fig. IV.3, *i.e.* Equation (5) with $b = \frac{4\rho_C N^2 {D_o}^3}{\Delta P}$.

3.2.2. High pressure microfluidizer

In the case of the secondary homogenization, the coarse emulsion droplets are accelerated to a high velocity within an interaction chamber containing two microchannels. The liquids are made to collide with each other, generating intense static and shear forces which cause the large droplets to be disrupted [14]. Mechanical stresses acting on droplet disruption when using high-pressure homogenization are due to turbulent microeddies, stress fluctuations inside turbulent jets and cavitation, associated to shear [14], [31], [32]. The formation of microeddies within the liquid occurs at relatively high flow rates when fluid flow tends to be irregular, chaotic, and ill-defined. Cavitation appears when the liquid presents highly fluctuating pressure variations. Small cavities violently implode and generate shock waves defined by high Mach's number, contributing to the reduction in droplet sizes [14].

Droplet breakup in turbulent flow has been described by the Kolmogorov–Hinze theory [39] and two different fragmentation mechanisms were identified, turbulent inertial (TI) and turbulent viscous (TV) fragmentations. For the TI mechanism, drops are fragmented by

pressure fluctuations induced by small eddies while for the TV mechanism they are fragmented by shearing of larger eddies [39], [40]. Here, the physical parameters describing the ratio between disruptive forces and cohesion forces are denoted by the Weber number We_{TI} for TI fragmentation and the Capillary number Ca_{TV} for TV fragmentation [33], [40], [41]:

$$We_{TI} = \frac{\rho_C \varepsilon_d{}^{2/3} d^{5/3}}{4\gamma} \tag{8}$$

$$Ca_{TV} = \frac{\eta_C \varepsilon_d{}^{1/3} d^{1/3}}{2\gamma} \tag{9}$$

where ρ_C is the continuous phase density, η_C the continuous phase dynamic viscosity, d the final emulsion drop diameter, γ the interfacial tension, and ε_d the local turbulent dissipation rate in the chamber ($\varepsilon_d = \eta_C G^2$, with G the local velocity gradient).

Whether in turbulent flow viscous or inertial forces are predominant depends on the drop Reynolds number Re_{dr}, where the characteristic length equals drop diameter d, and the velocity is that of the drop relative to the adjacent liquid. The transition occurs for $Re_{dr} \approx 1$. Re_{dr} can be calculated through [42]:

$$Re_{dr} = \frac{\gamma^{1/2} \rho^{1/2} d^{1/2}}{\eta_C} \tag{10}$$

For the analyzed emulsions $0.05 \leq Re_{dr} \leq 0.27$, with Re_{dr} the ratio between viscous and inertial forces [42]. Thus, $Re_{dr} < 1$ means the flow near the drop is laminar and drop disruption occurs under TV regime.

From Equation (9), it can be seen the oil-water interfacial tension is not the only parameter affecting the final emulsion droplet size. The energy dissipation rate of the flow depends on local velocity fluctuations cause by pressure fluctuations [42]. Therefore, it is rather a correlation of effects between the oil density, the oil viscosity, the oil hydrophobicity and the liquid velocity, which itself is influenced by the viscosity of the continuous and dispersed phases. Fluctuations in the size of the eddies formed in the chamber combined with rapid droplet recoalescence occurring in the chamber result in the variation of the mean volumetric diameter.

Drops are deformed and may or may not be broken up. Moreover, drops frequently encounter each other, leading sometimes to their (re)coalescence [36], [42], [43]. In the meantime, emulsifier adsorbs, which affects the result of the various processes. Each of these processes has

its own time scale and mass transport phenomena. For instance, emulsifier adsorption in high shear mixer is diffusion-driven while it is convection-driven in the microfluidizer chamber [79]. All of the processes occur numerous when homogenizing, and large drops progressively give rise to smaller ones. Finally, a steady state may be reached, in which disruption and recoalescence balance each other, although in practice such a state is generally not quite reached.
Nevertheless, the microfluidizer homogenization step provides comparable droplet sizes between emulsified oils, thus enables the analysis of the oil hydrophobicity effect on the emulsion aging.

3.3. Effect of oil hydrophobicity on the emulsion stability

During storage, emulsions faced destabilization phenomena, sometimes leading to phase separation. Generally, a top opaque layer (creaming), a turbid layer in the middle (more or less coalescing emulsion) and a bottom transparent layer (clarification) were observed. An example of the backscattering (BS) profile obtained within 28 days of storage for 1-decanol and n-hexadecane emulsions stabilized by 20 wt% A. *senegal* is shown in Fig. IV.4. Similar 1-decanol global profiles were observed for d-limonene, ethyl octanoate, carvone and 1-octanol emulsions stabilized by 20 wt% A. *senegal* with subtle oil-depending differences in behavior. All changes of backscattered (ΔBS) and transmitted light profiles (ΔT) can be found in annex D.

Changes in backscattered light (ΔBS) is directly dependent on the droplet mean diameter and the droplet volume fraction. Changes in the backscattering profile of emulsions are thus related to changes in droplet size and droplet transport properties. Usually, positive ΔBS values are evidence of the migration of oil droplets, while negative ΔBS values implies changes in droplet size [44].

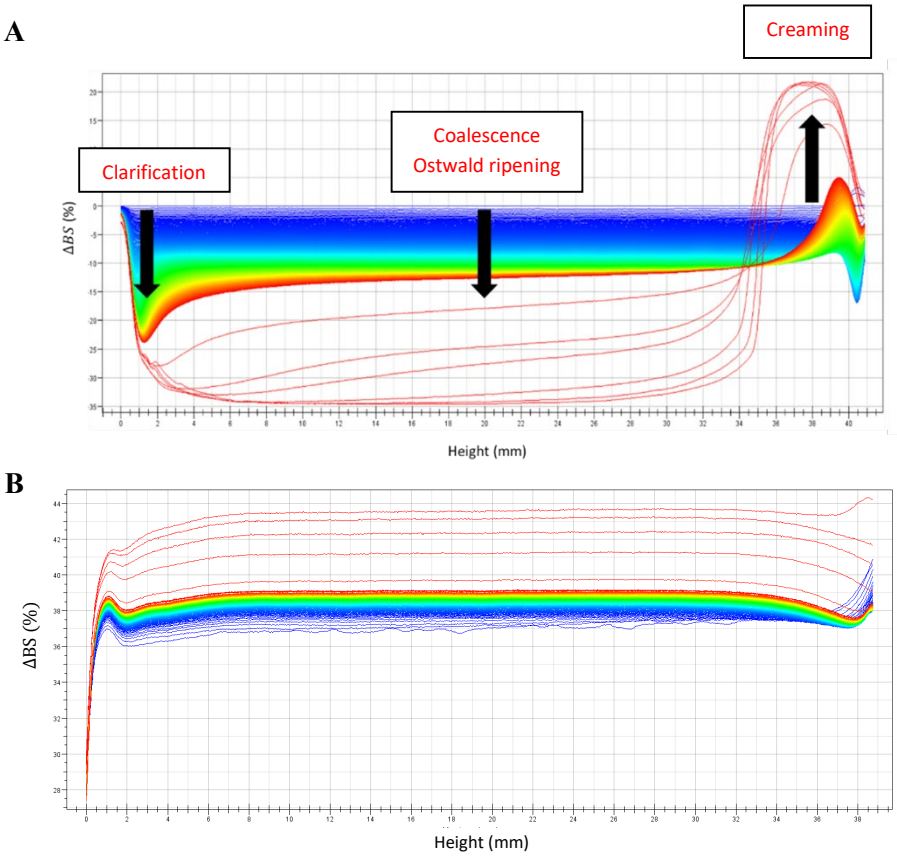

Fig. IV.4. Changes of light backscattering (ΔBS) profiles during 28 days of storage at 25°C of **(A)** 1-decanol emulsion and **(B)** n-hexadecane emulsion both containing 5 wt% oil and stabilized by 20 wt% A. *senegal*. Blue curve represents the earliest time point and red curve the latest time point.

In Fig. IV.4A, the signal decreases with time in the lower part of the measurement cell, *i.e.* in the height range of 0 mm to 34 mm, resulting in negative ΔBS values. This indicates that emulsion particles grew in size during storage which could be promoted by flocculation, coalescence and/or Ostwald ripening. In the upper part of the emulsion, from 34 to 40 mm, ΔBS gradually decreases within the first hours, suggesting as well an increase in droplet diameters. However, ΔBS signal starts to increase after a few hours along with an accentuation of the decrease in the bottom part of the emulsion (from 0 mm to 3 mm). This indicates that the emulsion undergoes phase separation, leading to a decrease in the oil droplet concentration, in turn reducing the intensity of the backscattered light. This is typical of the oil droplet migration, leading to creaming in the top and clarification in the lower part of the emulsion. The induced difference of oil volume fraction in the lower and upper parts of the emulsion results in a sudden change of the ΔBS signal. An approximate vertical line appears delimiting the negative signal area from the positive area. This vertical line progressively gets more

pronounced as time increases, indicating a further oil droplet concentration within the creaming phase.

The ΔBS of the n-hexadecane-stabilized emulsion (Fig. IV.4B) presented positive values during the 28 days of storage, implying oil droplet concentration. However, no clear front or BS variations were observed. This suggests the absence of droplet migration, highlighting the stability of this emulsion during our time window compared to the other homogenized oils. It may be noticed ΔBS signal increased by approximatively 6%. A possible explanation could be the emulsion droplets experienced coalescence or flocculation leading to expose droplets that were initially too small for Turbiscan® detection.

The *TSI* (Turbiscan® Scanning Index) is another qualitative parameter corresponding to the sum of all destabilization phenomena, that can be used to estimate the whole emulsion stability. The lower the *TSI* value is, the better the system stability [44], [45]. The *TSI* was recorded over 28 days of storage at 25°C. Fig. IV.5 shows the values for all emulsions within the first 24h. Except for the emulsion with n-hexadecane, all systems quickly exhibit high *TSI* values, especially d-limonene, carvone, 1-octanol, 1-decanol and ethyl octanoate emulsions. This is indicative of a high instability and a high probability of phase separation.

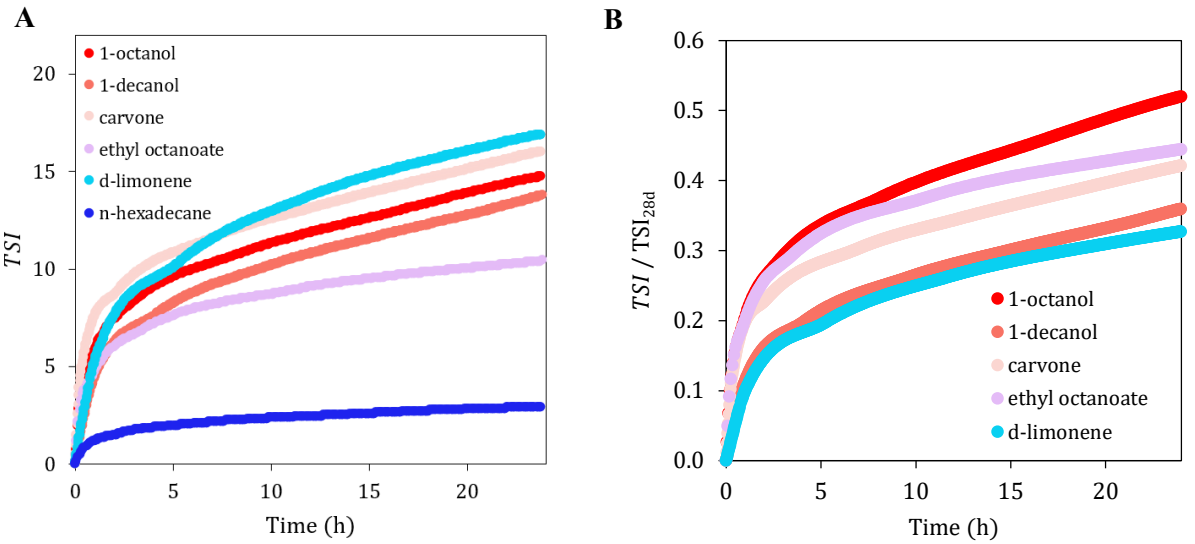

Fig. IV.5. Evolution of **(A)** *TSI* and **(B)** normalized *TSI* (right) signals over a 24h-storage at 25°C of 1-octanol, 1-decanol, carvone, ethyl octanoate, d-limonene and n-hexadecane emulsions containing 5 wt% of oil stabilized by 20 wt% A. *senegal*.

Emulsions appeared to the naked eye whitish right after homogenization. However, 1-octanol, ethyl octanoate or 1-decanol GA-stabilized emulsions initially tended toward yellow. The intensity of an emulsion color is known to give an indication on its stability such as higher the white intensity, higher the stability [46]. Oil GA-emulsions differing in color white intensity thus implies a difference in state of initial stability and so, in BS and T (light transmitted signal) initial outcomes. As discussed in Materials and Methods, TSI signal relies on variations between i-th scan and i-1-th scan (see Equation (2)). The initial scan, *i.e.* the first Turbiscan® measurement, is then decisive for the next scan calculations. For instance, outlet homogenization of the 1-octanol emulsion actually corresponded to a state that was already very unstable and close to final phase separation (TSI plateau). Thus, the subsequent emulsion stability evolved slowly compared to d-limonene emulsion whose outlet homogenization state was distant from instability plateau. TSI signal of 1-octanol emulsion then displayed low apparent values, no consistent with reality. Consequently, the TSI parameter in its raw form cannot be a correct parameter to compare the impact of oil hydrophobicity. However, after 28 days of storage, all emulsions except n-hexadecane showed nearly complete phase separation (see Fig. IV.6 below). Therefore, by normalizing TSI signals by the TSI value after 28 days, comparison of emulsions of d-limonene, ethyl octanoate, carvone, 1-decanol and 1-octanol can now be made properly (Fig. IV.5B).

Thus, d-limonene emulsion showed the highest stability followed respectively by 1-decanol, carvone, ethyl octanoate and 1-octanol emulsions. Accordingly, the aging of emulsions cannot be related to the oil hydrophobicity as normalized TSI of 1-decanol (γ_{ow} = 9.1 mN.m^{-1}) and d-limonene (γ_{ow} = 28.0 mN.m^{-1}) emulsions appeared similar as well as 1-octanol (γ_{ow} = 8.4 mN.m^{-1}) and ethyl octanoate (γ_{ow} = 22.7 mN.m^{-1}) emulsions during the first 8 hours. Destabilization phenomena were also studied separately using BS and T signals. Fig. IV.6 shows the evolution of BS and T as a function of the height of the emulsion sample after 24 hours and 28 days of storage at 25°C. It reflects the microscopic characteristic of growth or migration of oil droplets at a given time.

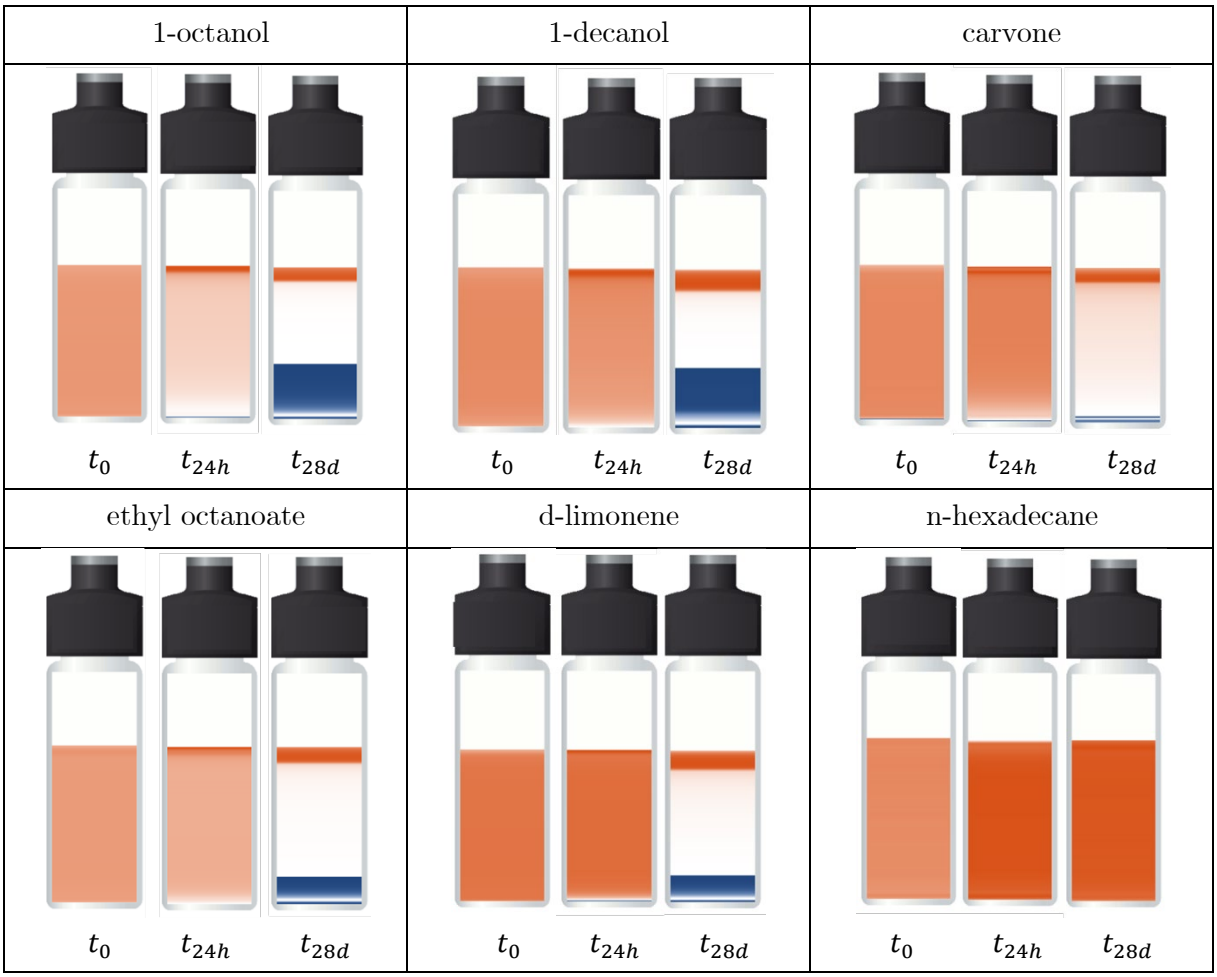

Fig. IV.6. Evolution of the emulsion stability of 5 wt% 1-octanol, 1-decanol, carvone, ethyl octanoate, d-limonene and n-hexadecane in 20 wt% A. *senegal*. Blue is for the transmittance signal intensity; orange is for the back scattering signal intensity.

1-Octanol, 1-decanol, carvone, ethyl octanoate and d-limonene GA-stabilized emulsions slowly started to cream after 24h of storage. This seems more pronounced for the least hydrophobic oils, *i.e.* 1-octanol, 1-decanol and carvone. After 28 days of storage the phase separation progressed. A layer of clarification intensified in the bottom of the sample and the creaming thickened. No creaming was observed in n-hexadecane GA-stabilized emulsion. Only the BS signal intensity slightly increased. Droplet migration and droplet growth were then examined separately.

3.3.1. Creaming of droplets

The creaming index CI of fine emulsions was calculated after 28 days according to the following equation [47]:

$$CI(\%) = \frac{H_S}{H_T} \times 100 \quad (11)$$

where H_S is the serum (transparent and turbid) layer from T signal and H_T the total height of emulsion. Results are reported in Table IV.3.

Table IV.3. Creaming index CI of 1-octanol, 1-decanol, carvone, ethyl octanoate, d-limonene and n-hexadecane fine emulsions stabilized by 20 wt% A. *senegal* gum after 28 days of storage at 25°C.

Oil type	Oil name	CI (%)
Alkane	n-Hexadecane	Not detected
Terpene	d-Limonene	16.5 (±4.8)
Ester	Ethyl octanoate	22.8 (±2.1)
Ketone	Carvone	6.3 (±1.0)
Alcohols	1-Decanol	39.2 (±2.6)
	1-Octanol	41.7 (±2.7)

All emulsions showed creaming after 28 days of storage except the n-hexadecane emulsion. The 1-octanol emulsion displayed the largest creaming phase (41.7%) while carvone emulsion displayed the smallest one (6.3%). CI results after 28 days of storage were plotted over the oil hydrophobicity in Fig. IV.7.

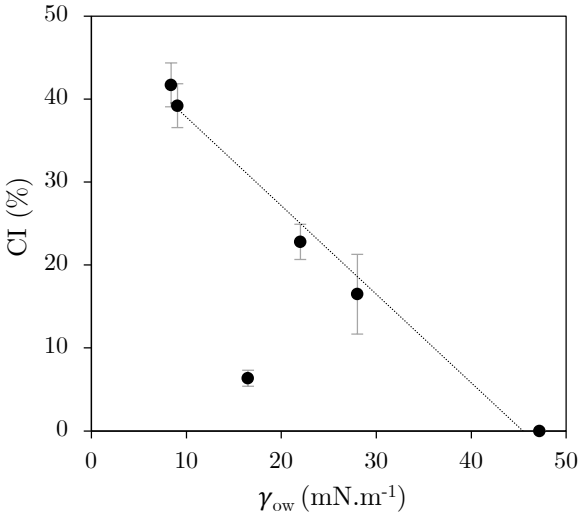

Fig. IV.7. Creaming index CI after 28 days of storage at 25°C of 5 wt% 1-octanol, 1-decanol, carvone, ethyl octanoate, d-limonene and n-hexadecane fine emulsions stabilized by 20 wt% A. *senegal* gum over the oil-water interfacial tension γ_{ow}.

A negative linear tendency ($y = -1.1x + 47.2$, $r^2 = 0.98$) appeared for n-hexadecane, d-limonene, ethyl octanoate, 1-decanol and 1-octanol emulsions. For this set, low hydrophobic oils exhibited larger creaming phases. The carvone emulsion was an outlier point meaning the droplet migration progressed at a slower pace than expected from the linear correlation.

The rate at which gravitational separation occurs in an infinitely diluted emulsion can be predicted using Stokes' law [14], [38]:

$$v = \frac{2gR_d{}^2(\rho_d - \rho_c)}{9\eta_c} \quad (12)$$

where g is the gravitational acceleration, R_d the droplet radius, ρ_d and ρ_c the density of the dispersed and continuous phases and η_c the viscosity of the continuous phase.

The dispersed phase being prepared with 20 wt% A. *senegal* gum, the variation of gum concentration due to AGPs adsorption to oil interfaces can be neglected. The parameters of the continuous phase can be considered constant and similar for all emulsions. Therefore, only parameters from the oil phase can explain Fig. IV.7 results. From Equation (12), large droplet size and high density difference between dispersed and continuous phases can promotes large creaming rate, as also described in [48]. Carvone aroma stands out from the other compounds because of its high density, *i.e.* 957 $kg.m^{-3}$ as compared to 823 $kg.m^{-3}$ for 1-octanol for instance. Therefore, the density difference between the aqueous phase and the oil phase is less important for the carvone emulsion. This could explain the gap between the carvone CI and the linear tendency. Comparing oils with densities of the same order of magnitude (n-hexadecane, d-limonene, ethyl octanoate, 1-decanol and 1-octanol) leads to the suggestion the oil hydrophobicity, aka the initial oil-water interfacial tension, is the driving force of the gravitational separation. The carvone emulsion data point underlines the interest in using weighting agents to reduce the density gap between phases and thus, to delay droplet migration phenomena. The correlation between the oil hydrophobicity and the instability mechanism affecting the droplet growth is studied below.

3.3.2. Growth of oil droplets

The growth of oil droplets can be caused by coalescence and/or Ostwald ripening. Coalescence is the merging of two droplets into a single larger one. It is correlated to the thinning and the

rupture of the two adsorbed layers of interacting droplets, and is strongly influenced by the interface mechanical properties [13], [49]. Ostwald ripening consists in the partial dissolution of the dispersed phase resulting in a mass transfer from small to big droplets. Though mainly driven by the solubility of the dispersed phase and strongly dependent on the size of the droplets, this phenomenon is also affected by the rheological properties of the interfacial layers [13].

Coalescence and Ostwald ripening (OR) of emulsions can be approached using the evolution of the back scattering intensity ΔBS in the middle of the emulsion sample. ΔBS measured at half of the sample height after 1 hour, 24 hours and 28 days of storage at 25°C were plotted over the initial oil-water interfacial tension (Fig. IV.8).

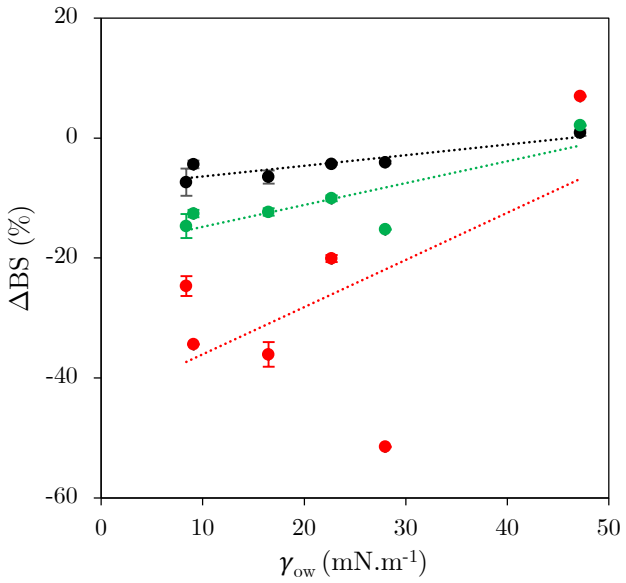

Fig. IV.8. Changes in light backscattering intensity ΔBS measured at half of fine emulsion height over the oil-water interfacial tension. The emulsion stability was determined at 25°C after 1h (black dot), 24h (green dot) and 28 days (red dot). Oil-in-water emulsions contained 5 wt% of oil and were stabilized by 20 wt% A. *senegal* gum.

The coalescence/Ostwald ripening of emulsions linearly rises with oil hydrophobicity after 1h of storage ($r^2 = 0.81$). Some studies highlighted droplet growth mechanisms were closely linked to the strong elasticity of the interfacial barrier formed by the emulsifier [13], [50]–[54]. Therefore, the linear tendency between ΔBS signal and γ_{ow} after 1h was mainly expected as a linear correlation was found between the oil hydrophobicity and the maximum elasticity of GA interfaces (Chapter III).

However, this linear correlation weakens as storage time increases and completely vanishing at day 28 of emulsion storage. It is important to note all the destabilization processes are interconnected and may influence each other during the emulsion aging. Creaming and flocculation do not modify the starting individual drop size distribution, which is instead affected by coalescence and Ostwald ripening, but tends to make the droplet population more dense (increase of local oil volume ratio) and consequently may accelerate the processes of flocculation and coalescence [13]. On the other side, both flocculation and the increase of the average droplet sizes induced by coalescence and Ostwald ripening, tend to quicken the creaming process and eventually the complete phase separation [13]. Thus, this could explain the lack of correlation with the oil hydrophobicity found after 28 days of storage. As time progresses, the ΔBS signal does not only inform on the droplet size growth, but also on droplet population concentration areas (creaming).

The differentiation between Ostwald ripening and coalescence is often difficult as both instability mechanisms cause an increase in the mean size of the droplets over time. However, OR can be theoretically approached through the Lifshitz, Slyozov and Wagner (LSW) theory that gives an estimation of the characteristic time τ_{OR} for the increase of the droplet size caused by the OR process [13], [55], [56]:

$$\tau_{OR} = \frac{3{R_d}^3}{2\Omega} \tag{13}$$

where R_d the droplet radius and Ω the growth rate which can be calculated through:

$$\Omega = \frac{8D\gamma MC_S}{9RT{\rho_d}^2} \tag{14}$$

where M is the molar mass, ρ_d the density of the disperse phase, D the diffusion coefficient of the dispersed phase, γ the interfacial tension, C_S the dispersed phase solubility, R the gas constant and T the absolute temperature.

Diffusion coefficients were determined using the Stokes-Einstein law:

$$D = \frac{k_B T}{6\pi\eta r_m} \tag{15}$$

where k_B is the Boltzmann constant, T the temperature, η the dynamic viscosity and r_m the radius of the oil molecule.

Then, τ_{OR} was calculated for all emulsions and plotted over the oil-water interfacial tension (Fig. IV.9). Values of diffusion coefficients and OR characteristic times are reported in Table IV.4.

Table IV.4. Theoretical diffusion coefficients and Ostwald Ripening characteristic times of oils at 25°C.

Oil type	Oil name	D $.10^{-10}$ ($m^2.s^{-1}$)	τ_{OR} (min)
Alkane	n-Hexadecane	1.5	7118
Terpene	d-Limonene	6.3	32
Ester	Ethyl octanoate	3.6	41
Ketone	Carvone	2.3	3
Alcohols	1-Decanol	0.4	290
	1-Octanol	0.7	0.02

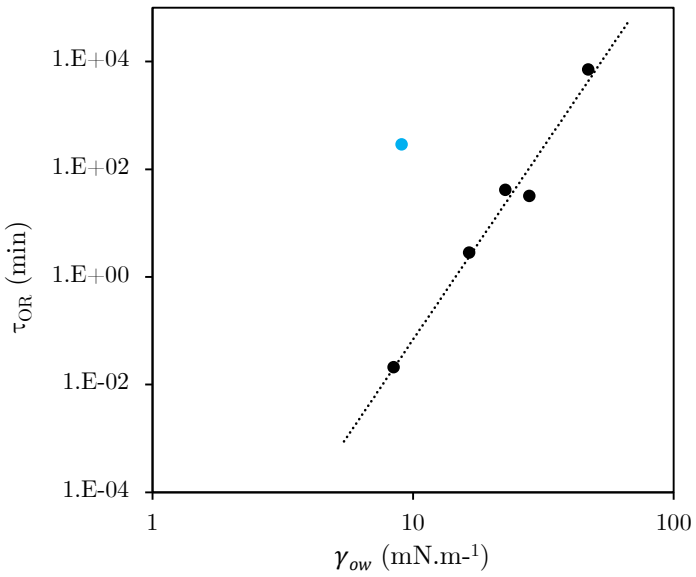

Fig. IV.9. Log-log plots of the OR characteristic time τ_{OR} over the oil-water interfacial tension γ_{ow}. Blue dot is for 1-decanol.

A main tendency seems to appear but not all the points could be included. This means the driving forces leading to Ostwald ripening cannot only be reduced to oil hydrophobicity. 1-Decanol is characterized by a low oil-water interfacial tension (γ_{ow} = 9.1 $mN.m^{-1}$) resulting in the low elasticity of the GA adsorbed layers (Chapter III). However, the OR occurs at a later time than the correlation (Fig. IV.9) would predict. This could be due to its low oil solubility (C_S = 37 $mg.L^{-1}$) compensating the limited interfacial rheological properties. As well,

the high viscosity of 1-decanol (η = 11.85 mPa.s) could interfere by limiting the deformability of the drops and slowing down the coalescence phenomena.

In brief, the oil hydrophobicity constitutes the main driving force leading to the droplet growth during the first hours of storage. However, several other effects such as the oil density, the solubility and the diffusion in the continuous phase, rapidly come into play. Thus, no correlation can be drawn using only the oil hydrophobicity. In addition, the destabilization processes are interdependent and may influence each other during the emulsion aging [13]. For instance, creaming and flocculation do not alter the droplet size distribution, but coalescence and Ostwald ripening do. Creaming and flocculation increase the compactness of the droplet population thus, accelerating the processes of coalescence or flocculation. On the other side, the increase of the average droplet sizes induced by coalescence and Ostwald ripening, may accelerate the creaming of emulsion which eventually may reach the complete phase separation.

4. Conclusions

The study aimed to examine the effect of the oil hydrophobicity on A. *senegal* emulsion practical conditions. To this end, emulsion droplet size distribution after two homogenization steps and emulsion stability over a 28-days storage were analyzed. Results showed the oil hydrophobicity impacts the droplets size of emulsions homogenized with a high shear mixer. It also influences the emulsion aging, especially during the first hours of storage. Chiefly, the increase of oil-water interfacial tension (oil hydrophobicity), leads to the increase of coarse emulsion droplet size, but also to the decrease of creaming and of initial droplet growth.

5. Complementary Information and Study

5.1. Principle of laser diffraction to measure particle size

When a beam of light (laser) strikes a particle it is either diffracted, refracted, reflected and/or absorbed (Fig. IV.10).

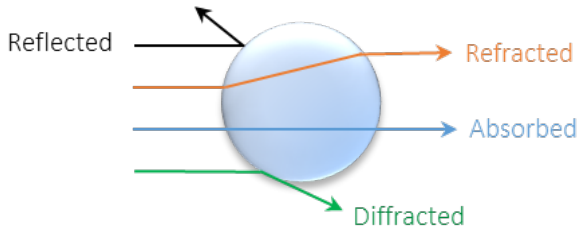

Fig. IV.10. Schematic representation of light paths through a particle.

Information about the size of a particle can be obtained using the widest possible range of angles and intensity of scattered light. Diffracted and refracted light are then recorded using detectors (Fig. IV.11). Absorbed and reflected light must be taken into account during measurement and size calculation.

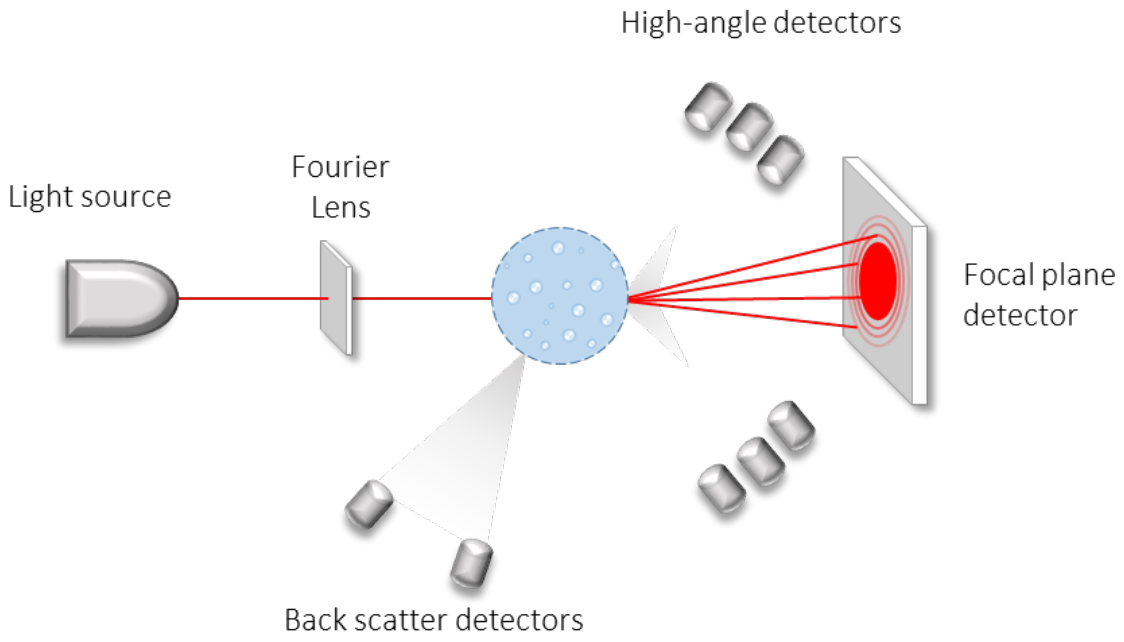

Fig. IV.11. Work principle of the Laser Diffraction Particle Analyzer.

The particle size distribution of a sample is determined by measuring the angular variation in intensity of light scattered. The scattered light data are then transformed into particle size information using the Mie Scattering Theory [57].

The evaluation of this signal is based on the principle that large particles preferentially scatter light at small angles, while small particles have their maximum scattered light at large angles.

5.2. Principle of light scattering measurement

When a light source projects photons into the outer surface of an emulsion, they are repeatedly scattered upon the dispersed droplets. Some of the photons are then transmitted and some are reflected [14]. The relative proportions of both transmitted and reflected photons depend on the geometry, the composition, and the microstructure of the emulsion [14]. During a Turbiscan® analysis, a measurement head moves over the cell height and works with two synchronous photodetectors localized at 0° and 135°. They acquire the scattered photons to determine the transport photon mean free path ℓ^* through the sample, and the photon mean free path ℓ that represents the mean distance traveled by photons before undergoing a scattering phenomenon. The collected signals are respectively known as backscattering (BS) and transmission (T) (Fig. IV.12).

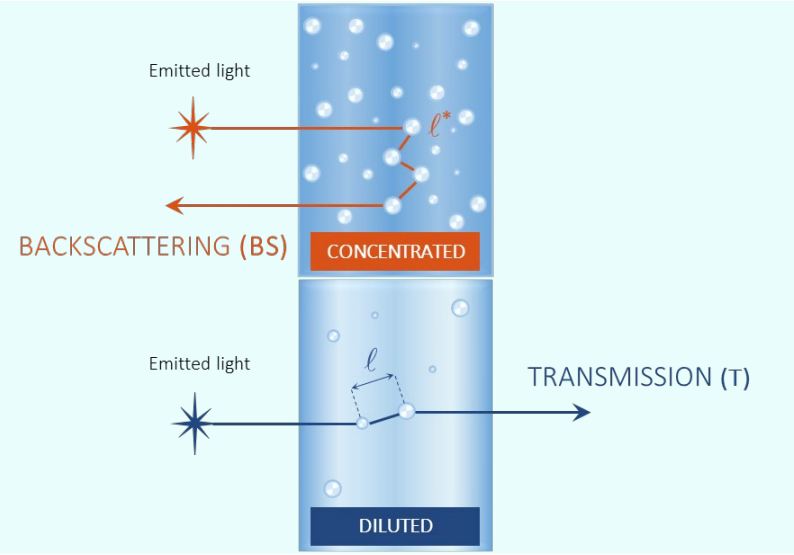

Fig. IV.12. Work principle of Turbiscan® stability analyzer.

The relationship between BS and ℓ^* and between T and ℓ are as follows:

$$BS = 1/\sqrt{\ell^*} \tag{16}$$

$$T = T_0 e^{-2r_i/\ell} \tag{17}$$

with BS the flux (intensity) of backscattered light, T the flux (intensity) of transmitted light, r_i is the measurement cell internal radius and T_0 the transmission of the continuous phase.

The transport photon mean free path and the photon mean free path can be determined through Equations (18) and (19):

$$\ell^*(\phi, d) = \frac{2d}{3\phi(1-g)Q_s} \quad (18)$$

$$\ell(\phi, d) = \frac{2d}{3\phi Q_s} \quad (19)$$

with ϕ the volume fraction of the dispersed phase, d the particle size of the dispersed phase, g and Qs the optical parameters given by the Mie theory [58]–[61].

T and BS signals are related to the droplet size and the concentration. Therefore, any BS or T variation is an indication of the emulsion destabilization.

5.3. Effect of the gum type (A. senegal vs A. seyal) on the emulsion stability

Emulsions of d-limonene, carvone, 1-decanol and 1-octanol were realized using another commercially available Acacia gum, *i.e.* Acacia *seyal,* under the same homogenization conditions as A. *senegal*. The idea was to study the effect of the gum nature on the emulsions stability. Acacia *seyal* (A. *seyal*, Batch n° OF183377) gum was provided by Alland & Robert Company - Natural and organic gums (Port mort, France). The protein content of A. *senegal* and A. *seyal* are respectively 2.2 wt% and 1.0 wt% [2], [30]. The gums also show differences in structural conformations, A. *senegal* gum is characterized by an average molar mass of 6.8×10^5 g.mol^{-1} and a branching degree of 78% while A. *seyal* gum is defined by an average molar mass of 8.2×10^5 g.mol^{-1} and a branching degree of 59%. In the aggregate, A. *senegal* and A. *seyal* gums differ in protein content, structural conformation and hydration properties resulting in some divergence in interfacial kinetics in favor of *A. senegal* (Chapter III) [2], [15], [16], [30], [62].

The volumetric droplet diameters $D_{4,3}$ of A. *seyal* stabilized emulsions were measured 15 minutes after the emulsification step, using an obscuration value of ~10%, and compared to the droplet size of A. *senegal* stabilized emulsions (Fig. IV.13).

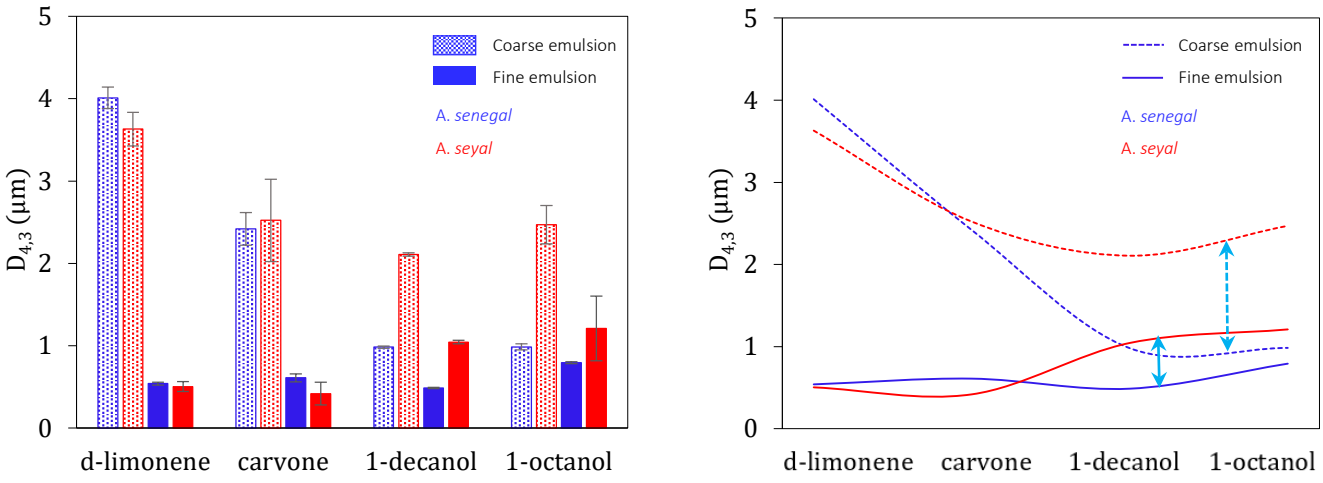

Fig. IV.13. Volumetric droplet diameters $D_{4,3}$ of the oil-in-water coarse emulsions (dotted bars and lines) and fine emulsions (full bars and lines) stabilized by 20 wt% of A. *senegal* (blue) and 20 wt% of A. *seyal* (red).

Significant differences (see light blue arrows) in the droplet $D_{4,3}$ between the coarse and fine emulsions can be observed for the two least hydrophobic oils, namely 1-decanol and 1-octanol. A. *senegal* provided smaller droplets size than A. *seyal*. Droplet size of 1-decanol and 1-octanol coarse A. *senegal* emulsions are respectively 0.98 and 0.99 µm (see Table IV.2), while with A. *seyal* droplet size are of about 2.11 and 2.47 µm. Similarly, fine emulsions of 1-decanol and 1-octanol stabilized by A. *senegal* provided respectively droplet sizes of about 0.49 and 0.79 µm while those stabilized by A. *seyal* were 1.04 and 1.21 µm. Two main points were demonstrated in Chapter III. First, the gum adsorption is favored at more hydrophobic oil-water interfaces. This leads to interfacial layers with larger elasticity, surface coverage and surface pressure. Secondly, A. *senegal* and A. *seyal* differences in protein content, distribution and accessibility, as well as structural conformation and hydration properties are supposed to be the origin of the divergence in water composition and interfacial kinetics [1], [3], [10], [63]–[65]. A. *senegal* adsorbs faster than A. *seyal*. These differences could also lead to droplet size difference between A. *senegal* and A. *seyal*. For instance, Dickinson et al. also evidenced a good correlation between the Acacia gum protein content, distribution and accessibility, and its emulsifying properties [10], [66]. More generally, the weaker interfacial properties of A. *seyal*, due to its supposed but not demonstrated greater affinity with water [1]–[4] together with its lower flexible conformation [2], [30], decrease the AGPs adsorption rate during emulsification. This could be particularly disturbing for low hydrophobic oils which are prone to (re)coalescence.

In addition to the study of droplet size after emulsification, the colloidal stability of emulsions was investigated by measuring the changes in backscattering (BS) and transmittance (T) intensity with time at 25°C using a Turbiscan® Tower. The gum varieties were compared using the *TSI* for each aroma compound (Fig. IV.14). Changes of backscattered (ΔBS) and transmitted light profiles (ΔT) of emulsions stabilized by 20 wt% A. *seyal* can be found in annex E.

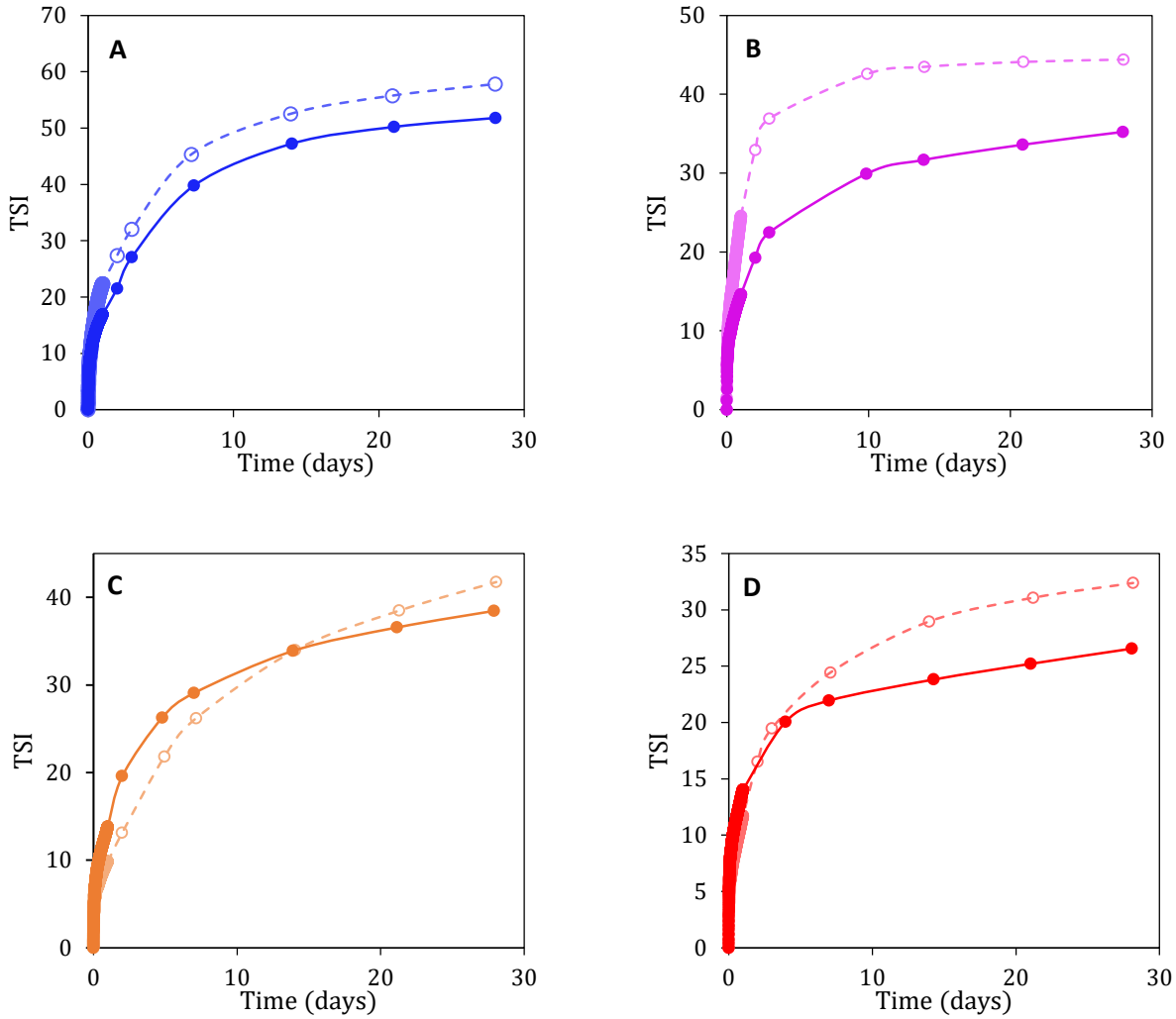

Fig. IV.14. Evolution of *TSI* signals over a 28 days-time at 25°C of **(A)** 5 wt% d-limonene, **(B)** 5 wt% carvone, **(C)** 5 wt% 1-decanol, and **(D)** 5 wt% 1-octanol emulsions stabilized by 20 wt% A. *senegal* (filled label, full line) and 20 wt% A. *seyal* (open label, dashed line).

The *TSI* signals of d-limonene or carvone A. *seyal* emulsions are higher than the A. *senegal* ones. The stability of A. *senegal* emulsions is then better than A. *seyal* emulsions. In contrast, the stability of A. *seyal* emulsions exceeds the stability of A. *senegal* emulsions for the two low hydrophobic oils, 1-octanol and 1-decanol, until respectively days 4 and 14. The believed greater

affinity with water of A. *seyal* gum compared to A. *senegal* [1]–[4] could lead to a better affinity with weakly hydrophobic oils as 1-decanol, preventing the flocculation or the coalescence compared to A. *senegal* gum. Creaming is supposed to appear rapidly due to the limited viscosities of 20 wt% A. *senegal* and 20 wt% A. *seyal* dispersions (respectively 51 mPa.s and 38 mPa.s). In addition, the larger size of droplets combined to the low apparent viscosity of A. *seyal* dispersion enhances the creaming rate as compared to the emulsions produced by A. *senegal*, thus explaining the stability crossovers observed at day 4 and 14 of storage of 1-octanol and 1-decanol emulsions.

Fig. IV.15 shows the evolution of BS and T as a function of the height of the d-limonene and 1-octanol emulsions stabilized by 20 wt% A. *senegal* or 20 wt% A. *seyal* after homogenization, 24 hours and 28 days of storage at 25°C.

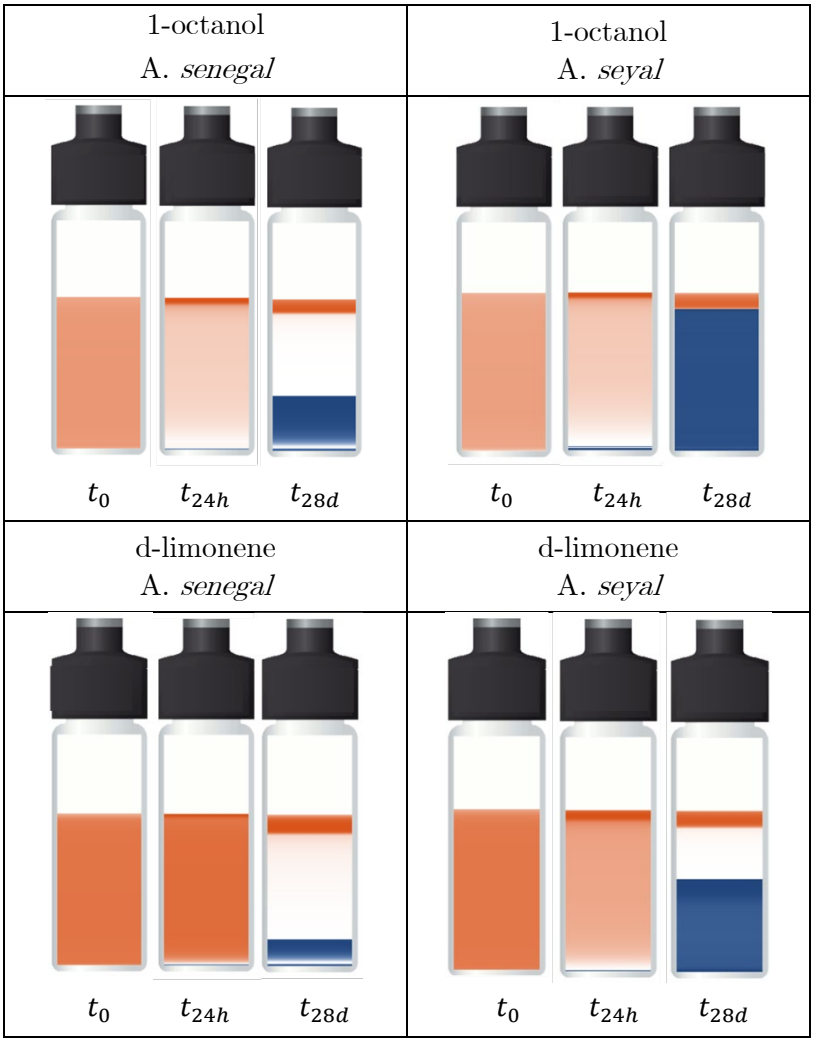

Fig. IV.15. Evolution of the emulsion stability of 5 wt% 1-octanol and d-limonene in 20 wt% A. *senegal* and 20 wt% A. *seyal.* Blue is for the transmittance signal intensity; orange is for the back scattering signal intensity.

After homogenization the signals are similar for both gums. However, after only 24h of storage differences are noticeable and deepen over time. The creaming index CI of final emulsions was calculated after 28 days of storage according to Equation (11). Results are reported in Table IV.5.

Table IV.5. Creaming index CI of 5 wt% 1-octanol and d-limonene emulsions stabilized by 20 wt% A. *senegal* and 20 wt% A. *seyal* after 28 days of storage at 25°C.

Oil type	Oil name	A. *senegal* CI (%)	A. *seyal* CI (%)
Terpene	d-Limonene	16.5 (±4.8)	66.0 (±1.0)
Alcohol	1-Octanol	41.7 (±2.7)	88.5 (±1.2)

For both d-limonene and 1-octanol emulsions, A. *seyal* provided larger CI values. This confirms the prevalent impact of the bulk apparent viscosity in the long-term stability of emulsions [45]. A. *senegal* gum improved the stability of emulsions by both delaying the instability mechanism and reducing the creaming index (CI).

6. Acknowledgements

The authors would like to thank ALLAND & ROBERT Company - Natural and organic gums (Port Mort, France) for financial support (Ph.D. C. Faucon).

7. References

[1] C. Aphibanthammakit, M. Nigen, S. Gaucel, C. Sanchez, and P. Chalier, "Surface properties of Acacia senegal vs Acacia seyal films and impact on specific functionalities," *Food Hydrocoll.*, vol. 82, pp. 519–533, 2018, doi: 10.1016/j.foodhyd.2018.04.032.

[2] V. Mejia Tamayo *et al.*, "Flexibility and hydration of amphiphilic hyperbranched arabinogalactan-protein from plant exudate: A volumetric perspective," *Colloids and Interfaces*, vol. 2, no. 1, 2018, doi: 10.3390/colloids2010011.

[3] A. Davantès, M. Nigen, C. Sanchez, A. d'Orlando, and D. Renard, "Adsorption of Hyperbranched Arabinogalactan-Proteins from Plant Exudate at the Solid–Liquid Interface," *Colloids and Interfaces*, vol. 3, no. 2, p. 49, 2019, doi: 10.3390/colloids3020049.

[4] A. Davantès, M. Nigen, C. Sanchez, and D. Renard, "Adsorption Behavior of Arabinogalactan-Proteins (AGPs) fromAcacia senegalGum at a Solid-Liquid Interface," *Langmuir*, vol. 37, no. 35, pp. 10547–10559, 2021, doi: 10.1021/acs.langmuir.1c01619.

[5] C. Sanchez *et al.*, "Acacia gum: History of the future," *Food Hydrocoll.*, vol. 78, pp. 140–160, 2018, doi: 10.1016/j.foodhyd.2017.04.008.

[6] FAO, "Gum arabic," 1999. https://www.fao.org/3/W6355E/w6355e0g.htm (accessed Jul. 12, 2022).

[7] M. Elmanan, S. Al-Assaf, G. O. Phillips, and P. A. Williams, "Studies on Acacia exudate gums: Part VI. Interfacial rheology of Acacia senegal and Acacia seyal," *Food Hydrocoll.*, vol. 22, no. 4, pp. 682–689, 2008, doi: 10.1016/j.foodhyd.2007.02.008.

[8] R. C. Randall, G. O. Phillips, and P. A. Williams, "Fractionation and characterization of gum from Acacia senegal," *Top. Catal.*, vol. 3, no. 1, pp. 65–75, 1989, doi: 10.1016/S0268-005X(89)80034-7.

[9] A. M. Islam, G. O. Phillips, A. Sljivo, M. J. Snowden, and P. A. Williams, "A review of recent developments on the regulatory, structural and functional aspects of gum arabic," *Food Hydrocoll.*, vol. 11, no. 4, pp. 493–505, 1997, doi: 10.1016/S0268-005X(97)80048-3.

[10] E. Dickinson, B. S. Murray, G. Stainsby, and D. M. W. Anderson, "Surface activity and emulsifying behaviour of some Acacia gums," *Top. Catal.*, vol. 2, no. 6, pp. 477–490, 1988, doi: 10.1016/S0268-005X(88)80047-X.

[11] L. Bai, S. Huan, J. Gu, and D. J. McClements, "Fabrication of oil-in-water nanoemulsions by dual-channel microfluidization using natural emulsifiers: Saponins, phospholipids, proteins, and polysaccharides," *Food Hydrocoll.*, vol. 61, pp. 703–711, 2016, doi: 10.1016/j.foodhyd.2016.06.035.

[12] R. Chanamai and D. J. McClements, "Comparison of gum arabic, modified starch, and whey protein isolate as emulsifiers: Influence of pH, CaCl2 and temperature," *J. Food Sci.*, vol. 67, no. 1, pp. 120–125, 2002, doi: 10.1111/j.1365-2621.2002.tb11370.x.

[13] F. Ravera, K. Dziza, E. Santini, L. Cristofolini, and L. Liggieri, "Emulsification and emulsion stability: The role of the interfacial properties," *Adv. Colloid Interface Sci.*, vol. 288, p. 102344, 2021, doi: 10.1016/j.cis.2020.102344.

[14] D. J. McCLements, *Food Emulsions Principles, Practices, and Techniques*. 2010.

[15] R. M. A. Mansour and E. A. Hassan, "Effect of gum concentration and gum protein concentration on emulsifying properties of some Acacia gums," *Int. J. basic Appl. Chem. Sci.*, vol. 6, no. 2, pp. 23–35, 2016.

[16] C. Aphibanthammakit, "Propriétés interfaciales et émulsifiantes de gommes d'Acacia senegal, Acacia seyal et de leurs fractions," 2018.

[17] P. Erni *et al.*, "Interfacial rheology of surface-active biopolymers: Acacia senegal gum versus hydrophobically modified starch," *Biomacromolecules*, vol. 8, no. 11, pp. 3458–3466, 2007, doi: 10.1021/bm700578z.

[18] S. J. Reiner, G. A. Reineccius, and T. L. Peppard, "A comparison of the stability of beverage cloud emulsions formulated with different gum acacia- and starch-based emulsifiers," *J. Food Sci.*, vol. 75, no. 5, 2010, doi: 10.1111/j.1750-3841.2010.01625.x.

[19] E. Dickinson, V. B. Galazka, and D. M. W. Anderson, "Emulsifying behaviour of gum arabic. Part 2: Effect of the Gum Molecular Weight on the Emulsion Droplet-size," *Carbohydr. Polym.*, vol. 14, no. 4, pp. 373–383, 1991, doi: 10.1016/0144-8617(91)90003-U.

[20] M. Atgié, O. Masbernat, and K. Roger, "Emulsions Stabilized by Gum Arabic: Composition and Packing within Interfacial Films," *Langmuir*, vol. 35, no. 4, pp. 962–972, 2019, doi: 10.1021/acs.langmuir.8b02715.

[21] V. Paramita, T. Furuta, and H. Yoshii, "High-Oil-Load Encapsulation of Medium-Chain Triglycerides and d-Limonene Mixture in Modified Starch by Spray Drying," *J. Food Sci.*, vol. 77, no. 2, pp. 38–44, 2012, doi: 10.1111/j.1750-3841.2011.02534.x.

[22] J. Zhang, T. L. Peppard, and G. A. Reineccius, "Preparation and characterization of nanoemulsions stabilized by food biopolymers using microfluidization," *Flavour Fragr. J.*, vol. 30, no. 4, pp. 288–294, 2015, doi: 10.1002/ffj.3244.

[23] K. Abdolmaleki, M. A. Mohammadifar, Z. Sheikhi, G. Matinfar, and K. Nayebzadeh, "The Role of Oil Phase in the Stability and Physicochemical Properties of Oil-in-Water Emulsions in the Presence of Gum Tragacanth," *JAOCS, J. Am. Oil Chem. Soc.*, vol. 96, no. 7, pp. 795–803, 2019, doi: 10.1002/aocs.12248.

[24] E. Dickinson, V. B. Galazka, and D. M. W. Anderson, "Emulsifying behaviour of gum arabic. Part 1: Effect of the nature of the oil phase on the emulsion droplet-size distribution," *Carbohydr. Polym.*, vol. 14, no. 4, pp. 373–383, 1991, doi: 10.1016/0144-8617(91)90003-U.

[25] R. Chanamai, G. Horn, and D. J. McClements, "Influence of oil polarity on droplet growth in oil-in-water emulsions stabilized by a weakly adsorbing biopolymer or a nonionic surfactant," *J. Colloid Interface Sci.*, vol. 247, no. 1, pp. 167–176, 2002, doi: 10.1006/jcis.2001.8110.

[26] J. Rao and D. J. McClements, "Impact of lemon oil composition on formation and stability of model food and beverage emulsions," *Food Chem.*, vol. 134, no. 2, pp. 749–757, 2012, doi: 10.1016/j.foodchem.2012.02.174.

[27] S. Van Der Graaf, C. G. P. H. Schroën, R. G. M. Van Der Sman, and R. M. Boom, "Influence of dynamic interfacial tension on droplet formation during membrane emulsification," *J. Colloid Interface Sci.*, vol. 277, no. 2, pp. 456–463, 2004, doi: 10.1016/j.jcis.2004.04.033.

[28] W. Zhang, Y. Qin, S. Chang, H. Zhu, and Q. Zhang, "Influence of oil types on the formation and stability of nano-emulsions by D phase emulsification," *J. Dispers. Sci. Technol.*, vol. 42, no. 8, pp. 1225–1232, 2021, doi: 10.1080/01932691.2020.1737538.

[29] W. Zhang, X. Xu, X. Zhao, and G. Zhou, "Insight into the oil polarity impact on interfacial properties of myofibrillar protein," *Food Hydrocoll.*, vol. 128, no. January, p. 107563, 2022, doi: 10.1016/j.foodhyd.2022.107563.

[30] L. Lopez-Torrez, M. Nigen, P. Williams, T. Doco, and C. Sanchez, "Acacia senegal vs. Acacia seyal gums - Part 1: Composition andstructure of hyperbranched plant exudates," *Food Hydrocoll.*, vol. 51, no. April, pp. 41–53, 2015, doi: 10.1016/j.foodhyd.2015.04.019.

[31] M. Rayner and P. Dejmek, *Engineering aspects of food emulsification and Homogenization*, CRC Press. 2015.

[32] K. Schroën, J. de Ruiter, and C. Berton-Carabin, "The importance of interfacial tension in emulsification: Connecting scaling relations used in large scale preparation with microfluidic measurement methods," *ChemEngineering*, vol. 4, no. 4, pp. 1–22, 2020, doi: 10.3390/chemengineering4040063.

[33] F. Innings, L. Fuchs, and C. Trägårdh, "Theoretical and experimental analyses of drop deformation and break-up in a scale model of a high-pressure homogenizer," *J. Food Eng.*, vol. 103, no. 1, pp. 21–28, 2011, doi: 10.1016/j.jfoodeng.2010.09.016.

[34] S. Hall, A. W. Pacek, A. J. Kowalski, M. Cooke, and D. Rothman, "The effect of scale and interfacial tension on liquid-liquid dispersion in in-line Silverson rotor-stator

mixers," *Chem. Eng. Res. Des.*, vol. 91, no. 11, pp. 2156–2168, 2013, doi: 10.1016/j.cherd.2013.04.021.

[35] S. Hall, M. Cooke, A. W. Pacek, A. J. Kowalski, and D. Rothman, "Scaling up of silverson rotor-stator mixers," *Can. J. Chem. Eng.*, vol. 89, no. 5, pp. 1040–1050, 2011, doi: 10.1002/cjce.20556.

[36] D. E. Leng, R. V. Calabrese, and L. P. Edward, *Immiscible liquid liquid systems*. 2003.

[37] V. Vashisth, K. D. P. Nigam, and V. Kumar, "Design and development of high shear mixers: Fundamentals, applications and recent progress," *Chem. Eng. Sci.*, vol. 232, p. 116296, 2021, doi: 10.1016/j.ces.2020.116296.

[38] L. L. Schramm, *Emulsions, Foams and Suspensions*, Wiley-VCH. 2005.

[39] J. O. Hinze, "Fundamentals of the hydrodynamic mechanism of splitting in dispersion processes," *AIChE J.*, vol. 1, no. 3, pp. 289–295, 1955, doi: 10.1002/aic.690010303.

[40] A. Håkansson, L. Fuchs, F. Innings, J. Revstedt, C. Trägårdh, and B. Bergenståhl, "High resolution experimental measurement of turbulent flow field in a high pressure homogenizer model and its implications on turbulent drop fragmentation," *Chem. Eng. Sci.*, vol. 66, no. 8, pp. 1790–1801, 2011, doi: 10.1016/j.ces.2011.01.026.

[41] A. Håkansson, C. Trägårdh, and B. Bergenståhl, "Dynamic simulation of emulsion formation in a high pressure homogenizer," *Chem. Eng. Sci.*, vol. 64, no. 12, pp. 2915–2925, 2009, doi: 10.1016/j.ces.2009.03.034.

[42] P. Walstra, *Physical Chemistry of Foods*. 2002.

[43] O. Robin, V. Blanchot, J. C. Vuillemard, and P. Paquin, "Microfluidization of dairy model emulsions. I. Preparation of emulsions and influence of processing and formulation on the size distribution of milk fat globules," *Lait*, vol. 72, no. 6, pp. 511–531, 1992, doi: 10.1051/lait:1992637.

[44] Y. Liu *et al.*, "Comparison of the effects of different food-grade emulsifiers on the properties and stability of a casein-maltodextrin-soybean oil compound emulsion," *Molecules*, vol. 25, no. 3, 2020, doi: 10.3390/molecules25030458.

[45] C. Aphibanthammakit, R. Barbar, M. Nigen, and P. Chalier, "Emulsifying properties of Acacia senegal gum : Impact of high molar mass," *Food Chem. X*, p. 100090, 2020, doi: 10.1016/j.fochx.2020.100090.

[46] M. Kharat, G. Zhang, and D. J. McClements, "Stability of curcumin in oil-in-water emulsions: Impact of emulsifier type and concentration on chemical degradation," *Food Res. Int.*, vol. 111, no. March, pp. 178–186, 2018, doi: 10.1016/j.foodres.2018.05.021.

[47] Y. S. Gu, E. A. Decker, and D. J. McClements, "Influence of pH and carrageenan type on properties of β-lactoglobulin stabilized oil-in-water emulsions," *Food Hydrocoll.*, vol. 19, no. 1, pp. 83–91, 2005, doi: 10.1016/j.foodhyd.2004.04.016.

[48] R. Chanamai and D. J. McClements, "Impact of weighting agents and sucrose on gravitational separation of beverage emulsions," *J. Agric. Food Chem.*, vol. 48, no. 11, pp. 5561–5565, 2000, doi: 10.1021/jf0002903.

[49] K. Dziza *et al.*, "Interfacial properties and emulsification of biocompatible liquid-liquid systems," *Coatings*, vol. 10, no. 4, 2020, doi: 10.3390/coatings10040397.

[50] M. B. J. Meinders and T. Van Vliet, "The role of interfacial rheological properties on Ostwald ripening in emulsions," *Adv. Colloid Interface Sci.*, vol. 108–109, pp. 119–126, 2004, doi: 10.1016/j.cis.2003.10.005.

[51] D. J. Burgess and J. K. Yoon, "Influence of

Interfacial Properties of Lipophilic Surfactants on Water-in-Oil Emulsion Stability," *Colloids Surfaces B Biointerfaces*, vol. 4, no. 5, pp. 297–308, 1995, [Online]. Available: http://linkinghub.elsevier.com/retrieve/pii/0927776594011799.

[52] C. Dicharry, D. Arla, A. Sinquin, A. Graciaa, and P. Bouriat, "Stability of water/crude oil emulsions based on interfacial dilatational rheology," *J. Colloid Interface Sci.*, vol. 297, no. 2, pp. 785–791, 2006, doi: 10.1016/j.jcis.2005.10.069.

[53] T. C. Botti, A. Hutin, E. Quintella, and M. S. Carvalho, "Effect of interfacial rheology on drop coalescence in water-oil emulsion," *Soft Matter*, vol. 18, no. 7, pp. 1423–1434, 2022, doi: 10.1039/d1sm01382c.

[54] M. Geng *et al.*, "Effects of different nut oils on the structures and properties of gel-like emulsions induced by ultrasound using soy protein as an emulsifier," *Int. J. Food Sci. Technol.*, vol. 56, no. 4, pp. 1649–1660, 2021, doi: 10.1111/ijfs.14786.

[55] P. Taylor, "Ostwald ripening in emulsions," *Adv. Colloid Interface Sci.*, vol. 75, no. 2, pp. 107–163, 1998, doi: 10.1016/S0001-8686(98)00035-9.

[56] I. M. Lifshits and V. V Slezov, "Kinetics of the diffusion decomposition of supersaturated solid solutions," *Zhurnal Eksp. i Teor. Fiz.*, vol. 35, no. 2, pp. 479–492, 1958.

[57] W. Hergert and T. Wriedt, *The Mie Theory Basic and Applications*, vol. 169, no. 10. Springer Series in Optical Sciences, 1981.

[58] Y. Lu *et al.*, "Study on the stabilization mechanism of crude oil emulsion with an amphiphilic polymer using the β-cyclodextrin inclusion method," *RSC Adv.*, vol. 7, no. 14, pp. 8156–8166, 2017, doi: 10.1039/c6ra28528g.

[59] K. Wang, G. Li, and B. Zhang, "Opposite results of emulsion stability evaluated by the TSI and the phase separation proportion," *Colloids Surfaces A Physicochem. Eng. Asp.*, vol. 558, no. August, pp. 402–409, 2018, doi: 10.1016/j.colsurfa.2018.08.084.

[60] P. Bru *et al.*, "Particle Size and Rapid Stability Analyses of Concentrated Dispersions: Use of Multiple Light Scattering Technique," no. June, pp. 45–60, 2004, doi: 10.1021/bk-2004-0881.ch003.

[61] A. Ishimaru and Y. Kuga, "Attenuation Constant of a Coherent Field in a Dense Distribution of Particles.," *J. Opt. Soc. Am.*, vol. 72, no. 10, pp. 1317–1320, 1982, doi: 10.1364/josa.72.001317.

[62] C. Flindt, S. Al-Assaf, G. O. Phillips, and P. A. Williams, "Studies on acacia exudate gums. Part V. Structural features of Acacia seyal," *Food Hydrocoll.*, vol. 19, no. 4, pp. 687–701, 2005, doi: 10.1016/j.foodhyd.2004.09.006.

[63] R. C. Randall, G. O. Phillips, and P. A. Williams, "The role of the proteinaceous component on the emulsifying properties of gum arabic," *Top. Catal.*, vol. 2, no. 2, pp. 131–140, 1988, doi: 10.1016/S0268-005X(88)80011-0.

[64] A. K. Ray, P. B. Bird, G. A. Iacobucci, and B. C. Clark, "Functionality of gum arabic. Fractionation, characterization and evaluation of gum fractions in citrus oil emulsions and model beverages," *Top. Catal.*, vol. 9, no. 2, pp. 123–131, 1995, doi: 10.1016/S0268-005X(09)80274-9.

[65] O. Castellani, S. Al-Assaf, M. Axelos, G. O. Phillips, and M. Anton, "Hydrocolloids with emulsifying capacity. Part 2 - Adsorption properties at the n-hexadecane-Water interface," *Food Hydrocoll.*, vol. 24, no. 2–3, pp. 121–130, 2010, doi: 10.1016/j.foodhyd.2009.07.006.

[66] D. E., "Hydrocolloids at interfaces and the influence on the properties of dispersed systems," *Food Hydrocoll.*, vol. 17, p. 25, 2003, [Online]. Available: www.elsevier.com/locate/foodhyd.

Chapter V: Effect of multi-component oil phase on the interfacial properties and stability of Acacia *senegal* gum oil-in-water emulsions

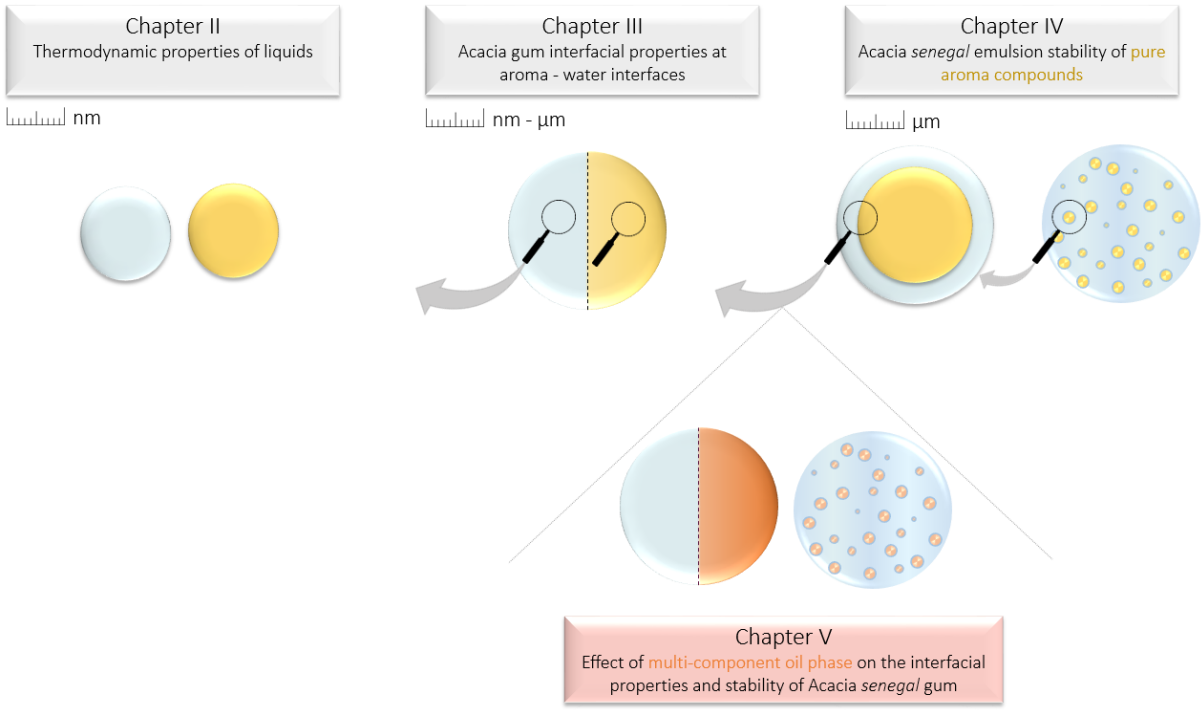

This chapter aimed to study the influence of multicomponent oil phase on oil-Acacia *senegal*-water interfacial structure and on the homogenization and stability of Acacia *senegal* oil-in-water emulsions. To this end, a mixture of two aroma compounds differing in oil-water interaction energy is used, namely d-limonene and 1-octanol. Then, assumptions drawn on oil-Acacia *senegal*-water interfacial structure are further attested through the study of another aroma binary mixture, d-limonene and carvone, and the study of an oil phase of more than two compounds including a weighting agent.

Highlights

- The oil-water interfacial tension is highly sensitive to the presence of minor amounts of weakly hydrophobic oils.

- Dependency of the equilibrium interfacial tension and interfacial rheology on the oil hydrophobicity remains valid for a mixture of two aroma compounds.

- Acacia gum interfacial structures at the interface of two-component oil phase are similar to Acacia gum interfacial structures at one-component oil interface.

- Independently of the number of constituents in the oil phase, the adsorption at the oil-water interface is driven by the weakest hydrophobic compound of the mixture.

- The dependency of coarse emulsion droplet size on the oil hydrophobicity stays valid for a mixture of two aroma compounds.

- Adding a compound producing stable emulsions to another compound producing unstable emulsions, improves both initial and over time stability.

Effect of a mixture of two oils of different hydrophobicity on the interfacial properties of Acacia *senegal* gum at oil-water interfaces[1]

Camille Faucon[a], Nathan Thoulouze[a], Pascale Chalier[a], Christian Sanchez[a]

[a] IATE, Univ Montpellier, INRAE, Institut Agro, Montpellier, France.

Abstract

The oil phase in liquid mixtures is often given little attention in interfacial and emulsion experiments. Yet, the oil composition and in particular the presence of multiple components (e.g. aroma compounds, carrier oil, weighting agents, additives, conservatives) are determinant factors influencing the structure and the properties of the oil phase. Consequently, they may improve or limit the emulsion homogenization and stability. In addition, multicomponent aqueous phase is known to involve preferential adsorption and potential variations of the interfacial composition. One may then wonder how multicomponent oil phase impact the oil-water interface in the presence or absence of an emulsifier. Therefore, the present study aims to examine how a mixture of two aroma compounds differing in hydrophobicity affects the adsorption of an amphiphilic biopolymer at oil-water interfaces. In particular, how the presence of OH chemical groups in the aroma mixture impact the interface structure. To this end interfacial tension and dilational rheological measurements are performed and Acacia gum is used as emulsifier. A high sensitivity of the oil-water interfacial tension to the presence of minor amounts of weakly hydrophobic oils is measured. It is believed to come from the lowest hydrophobic compounds preferential adsorption at the oil-water interface in order to lessen unfavorable oil-water interactions. In addition, the dependency of the equilibrium interfacial tension and interfacial rheology on the oil hydrophobicity is found unchanged for a mixture of two aroma compounds.

Keywords: aromas mixture; hydrophobicity; interfacial tension; oil–water interfaces; Acacia gum; adsorption; interfacial composition.

[1]Article in preparation

1. Introduction

Oil-in-water (O/W) emulsions are extensively used in food industry to encapsulate, protect, and deliver various types of lipophilic active ingredients [1], [2]. Conditions of emulsions preparation differ according to the targeted dispersed compound. Emulsions involving aroma compounds generally require other molecules of different specificities and properties which contribute to the improvement of emulsion quality and stability [3]–[5]. For instance, aroma compound having low density and viscosity, are mixed with weighting agents before production of the emulsion [4]. They allow to reduce the density contrast between the oil and water phases, thus delaying the gravitational separation. Understanding O/W emulsions stability has long been important for developing and optimizing formulations, operating conditions and shelf life of emulsion-based food products under a variety of environmental conditions. Physicochemical properties of the continuous phase, e.g. the pH of the solvent [6], [7] and the concentration of salts [6], [7] as well as the concentration [8], [9] viscosimetric behavior and nature of the oil that constitutes the dispersed phase are known to be important parameters impacting emulsions stability [7], [10], [11] (Chapter IV). Emulsifiers are first added in the aqueous phase to decrease the oil-water interfacial tension and facilitate the dispersion of oil droplets, then to form an interfacial viscoelastic barrier that slows down destabilization mechanisms such as droplet coalescence. The nature and the concentration of the emulsifier impact the initial morphology of the emulsions, *i.e.* the droplet size distribution and ergo, the stability [11]–[16]. Likewise, the process of emulsification plays a significant role as it may influence the characteristic times of the emulsifier adsorption and its coverage degree of oil-water interfaces [17]. In addition, preferential adsorption and competitive displacement between different types of emulsifiers alter the interfacial composition, and therefore emulsion stability and performance [18]–[20].

Until recently, the effect of the composition of the dispersed phase and in particular the presence of multiple components on interfacial properties received limited attention [4], [21], [22]. For instance, studies of the influence of weighting agents and carrier oil on emulsification and gravitation separation revealed the emulsion stability was positively correlated with the oil density but negatively related to the oil viscosity [4], [21]. Bergfreund and al. [22] suggested experimental guidelines for using oils in interfacial experiments, aiming to harmonize results and protocols for enabling comparability and generic description of interface science. They also

wisely highlighted only one oil phase is generally considered and that information on mixtures of oils is lacking. As multicomponent aqueous phase can lead to preferential adsorption and changes of the interfacial composition, it is legitimate to ask if this also applies to multicomponent oil phase. Therefore, the present study aimed to examine how a mixture of two aroma compounds differing in hydrophobicity affects the adsorption of an amphiphilic biopolymer at oil-water interfaces. To structure interfaces or stabilize aroma mixtures, we used as emulsifier Acacia *senegal* (A. *senegal*) gum. It is a well-known natural surface-active biopolymer aiding colloidal stabilization in food industry (E414) [23]. A. *senegal* gum is mainly composed by hyperbranched proteoglycans, namely highly glycosylated hydroxyproline-rich arabinogalactan-proteins (AGPs). These biopolymers are essentially made of sugars D-galactose, L-arabinose, L-rhamnose, D-glucuronic acid, and 4-O-methyl-D-glucuronic acid. AGPs also contain about 1-3% of proteins, 3-4% of minerals and around 1% polyphenols [8]. In this work, interfaces of formulations based on d-limonene:1-octanol mixtures were studied and compared to pure d-limonene and 1-octanol. These two aroma compounds are, respectively, highly and weakly hydrophobic, due in particular to the presence of OH chemical groups in 1-octanol. The presence of OH groups favors the interactions with water molecules and profoundly change interfacial tension and interface thermodynamic properties, as described in Chapter III. Resulting assumptions were then confronted to the multi-aroma compounds orange essential oil.

2. Materials and methods

2.1. Materials

Acacia senegal gum (Batch n°OF152413) and orange essential oil were provided by Alland & Robert Company - Natural and organic gums (Port mort, France). The biochemical composition and the structural properties of the gum were previously characterized, showing in particular a 2.2 wt% protein content [24], [25]. For the study of interfacial properties, 20 wt% A. *senegal* dispersions were obtained by dispersing the gum powder in a pH 5 sodium acetate buffer (10 mM; Milli-Q-water; acetic acid Sigma-Aldrich; $C_2H_3NaO_2{\cdot}3H_2O$, Sigma-Aldrich), stirring overnight at room temperature, and then by centrifuging at 12 000 rpm for 30 minutes at 25°C for removing insoluble materials. d-Limonene (≥97%) and 1-octanol (≥99%) were purchased from Sigma-Aldrich. Regarding the emulsion stability study, semi-concentrated

A. *senegal* gum dispersions (20 wt%) were made by dispersing the gum powders in Milli-Q-water, stirring overnight at room temperature, and then by centrifuging at 5 000 rpm for 20 minutes at 25°C. Basic physicochemical properties of selected oils are presented in Table V.1.

Table V.1. Oil-water interfacial tension, oil solubility in water, density, viscosity refractive index and sound velocity at 25°C.

Oil type	Oil name	Oil-water interfacial tension ($mN.m^{-1}$)	Oil solubility in water ($mg.L^{-1}$)[2]	Density ($kg.m^{-3}$)	Viscosity (10^{-3} Pa.s)	Refractive index	Vs ($m.s^{-1}$)
Terpene	d-Limonene	30.0 (±0.5)	14	834	0.9	1.467291	1319
Alcohols	1-Octanol	8.4 (±0.1)	540	823	7.9	1.425391	1348

The oil density, sound velocity, dynamic viscosity and refractive index were measured using a DSA 5000M sonodensimeter (Anton Paar, France), a capillary micro-viscometer LOVIS 2000M (Anton Paar, Graz, Austria), and an Abbemat Refractometer (Anton Paar, France). The oil-water interfacial tension was determined using an automatic drop tensiometer (Tracker™, Teclis Scientific, Civrieux d'Azergues, France). The oil solubility in water came from the database of the national library of medicine[2]. Considering the oil-water interfacial tension or the oil solubility in water as thermodynamic signatures of hydrophobicity, d-limonene appears to be the most hydrophobic oil, γ_{ow} = 30.0 $mN.m^{-1}$ and C_S = 14 $mg.L^{-1}$, as compared to γ_{ow} = 8.4 $mN.m^{-1}$ and C_S = 540 $mg.L^{-1}$ for 1-octanol. d-Limonene also displays a low viscosity, mainly due to large volume fluctuations and dissipation of energy [26]. Chapter II highlighted for d-limonene and 1-octanol respectively, a Gibbs free energy of cavity creation of 13.10×10^{-20} and 6.66×10^{-20} $J.nm^{-3}$, as well as 1.60×10^{-2} and 1.47×10^{-2} of volume fluctuations for a 1 nm^3 volume [27].

2.2. Methods

2.2.1. Preparation of the oil phase

The d-limonene:1-octanol mixtures were prepared from pure aroma compounds, stirred for 1h and stored during a maximum of 48h at 4°C. The stability of oil mixtures was controlled

[2]values from https://pubchem.ncbi.nlm.nih.gov/, data base of national library of medicine

through measurements of density and ultrasound velocity and refractive index at 25°C. The x_1 ratio is defined as the molar fraction of d-limonene in the d-limonene:1-octanol mixture.

2.2.2. Interfacial tension and dilational viscoelastic measurements

The interfacial tension and dilational viscoelastic properties of Acacia gums (GA) at the oil-water interface were measured by the rising drop technique using an automatic drop tensiometer (Tracker™, Teclis Scientific, Civrieux d'Azergues, France). The method is reported in details in Chapter III. In brief, drops of 3–10 µL of organic compound were formed from a 500 µL syringe with a stainless steel needle immersed in the cuvette containing a 5 wt% gum dispersion. Measurements were performed at 25°C (±0.3°C) for a 24h time. The dynamic interfacial tension between GA dispersion and the oil phase was determined by numerical analysis of the drop shape and a fit with models based on the Young-Laplace equation. The drop interface underwent deformations consisting of a sinusoidal variation of the volume of 10% amplitude at an oscillation frequency of 0.1 s^{-1}, so that the drop interfacial area followed successive compression and dilation cycles.

2.2.3. GC-MS analysis

Orange essential oil qualitative composition was characterized by a GC-MS (GC-2010 plus, MS QP2020, Shimadzu corporation, Tokyo, Japan) equipped with a DB-WAX polar capillary column (30 m, 0.25 mm i.d. x 0.25 µm of thickness) and a quadrupole detector. Helium was used as carrier gas with a flow rate of 1.2 ml/min. The GC-MS oven temperature was kept at 40°C for 5 min and programed to 250°C at a rate of 2°C.min^{-1}. One µL of diluted orange essential oil (1/100, v/v, in hexane) was injected via an injector maintained at 250°C in split mode (ratio of 1:20). Spectra were obtained in the electron impact mode with 70 eV of ionization energy, in full scan mode with a scan range between 40-500 amu. The identification of components was based on the comparison of the determined LRI and those reported in the literature and mass spectra of libraries (NIST 17/Wiley). The quantification (expressed as a percentage) of each identified compound was done by comparing their peak area to the total area of the identified peaks.

3. Results

3.1. Oil – water interfacial tension

The oil-water interfacial tensions of pure d-limonene and 1-octanol and their mixtures are reported in Table V.2. The evolution of the oil-water interfacial tension (γ_{ow}) as a function of the molar fraction of d-limonene is presented in Fig. V.1.

Table V.2. Effect at 25°C of d-limonene:1-octanol ratio on the oil-water interfacial tension, interfacial pressures Π_∞ and maximum elastic modulus E' in presence of a 5 wt% A. *senegal* dispersion.

x_1 (d-limonene)	γ_{ow} (mN.m^{-1})	Π_∞ 5 wt% A. *senegal* (mN.m^{-1})	E'_{max} 5 wt% A. *senegal* (mN.m^{-1})
0.00	8.4 (±0.5)	4.45 (±0.6)	10.7 (±0.1)
0.20	10.1 (±0.2)	-	-
0.40	11.6 (±0.1)	-	-
0.60	13.2 (±0.2)	6.8 (±0.2)	16.5 (±0.5)
0.80	15.2 (±0.1)	-	-
0.86	*15.0 (±0.1)	9.7 (±0.1)	17.9 (±0.5)
0.95	19.6 (±0.1)	11.1 (±0.1)	25.1 (±0.2)
0.98	21.7 (±0.1)	13.3 (±0.3)	26.4 (±0.6)
1.00	30.0 (±0.5)	17.5 (±0.8)	38.3 (±1.7)

**moderately altered d-limonene*

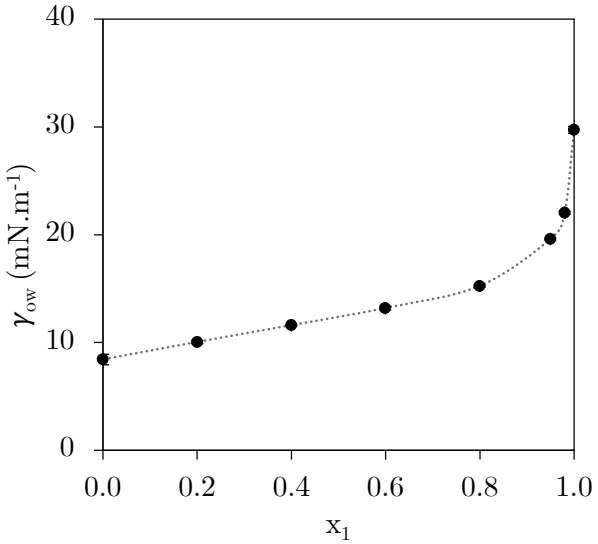

Fig. V.1. Oil-water interfacial tension (γ_{ow}) as a function of the molar fraction of d-limonene (x_1).

Increasing from 0 to about 0.2 the molar fraction of 1-octanol ($x_2 = 1 - x_1$) into the aroma mixture leads to a strong nonlinear decrease of the mixture interfacial tension aka hydrophobicity (Fig. V.1.). It suffices of 2% of 1-octanol in d-limonene to observe a 25% decrease of the interfacial tension. A high sensitivity of the oil-water interfacial tension in presence of minor amounts of weakly hydrophobic oil is then observed at high d-limonene volume fractions. In presence of A. *senegal* gum, the equilibrium interfacial pressures $\Pi_\infty = \gamma_{ow} - \gamma_\infty$ at oil ratios (x_1): 0, 0.6, 0.86, 0.95, 0.98 and 1 were calculated and plotted over the initial oil-water interfacial tension (Fig. V.2). The Π_∞ values may be found in Table V.2.

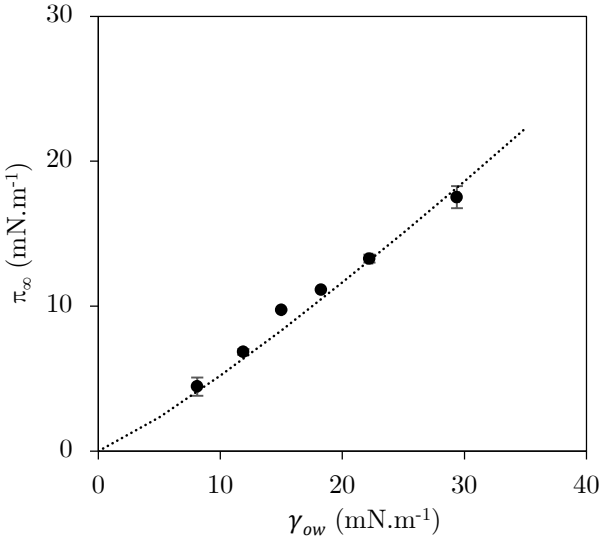

Fig. V.2. Dependency of the equilibrium oil-gum-water interfacial pressure Π_∞ on the oil-water interfacial tension γ_{ow}. The A. *senegal* gum concentration was 5 wt%. The oil phase was composed by d-limonene:1-octanol mixtures at ratios (x_1): 0, 0.6, 0.86, 0.95, 0.98 and 1. The black dotted line represents the fit obtained in Chapter III with a large range of pure oils and 5 wt% A. *senegal* dispersion ($y = 0.36x^{1.16}$).

As observed in Chapter III, the two interfacial parameters are correlated and overlap with the fit obtained with a large range of pure aroma compounds and 5 wt% A. *senegal* dispersion ($y = 0.36x^{1.16}$). This suggests the correlation between the equilibrium interfacial tension and the oil hydrophobicity stays valid for a mixture of two aroma compounds. High oil hydrophobicity (*i.e.* high ratio x_1) leads to large increase in the interfacial pressure. Thus, a binary mixture of components in the oil phase does not affect the dependency of AGPs adsorption on the oil hydrophobicity, nor their ability to reduce the interfacial tension.

3.2. Dilational surface rheology

The dilational viscoelastic properties of oil-gum-water interphases were recorded for oil mixtures with molar fractions (x_1): 0, 0.6, 0.86, 0.95, 0.98 and 1. To facilitate the global analysis, we only present in Fig. V.3. the evolution of the elastic (E') and viscous (E") dilational moduli as a function of time for oils at ratios (x_1): 0, 0.6, 0.98 and 1. Rheological profiles for oils at ratios (x_1): 0.86 and 0.95 can be found in annex C.

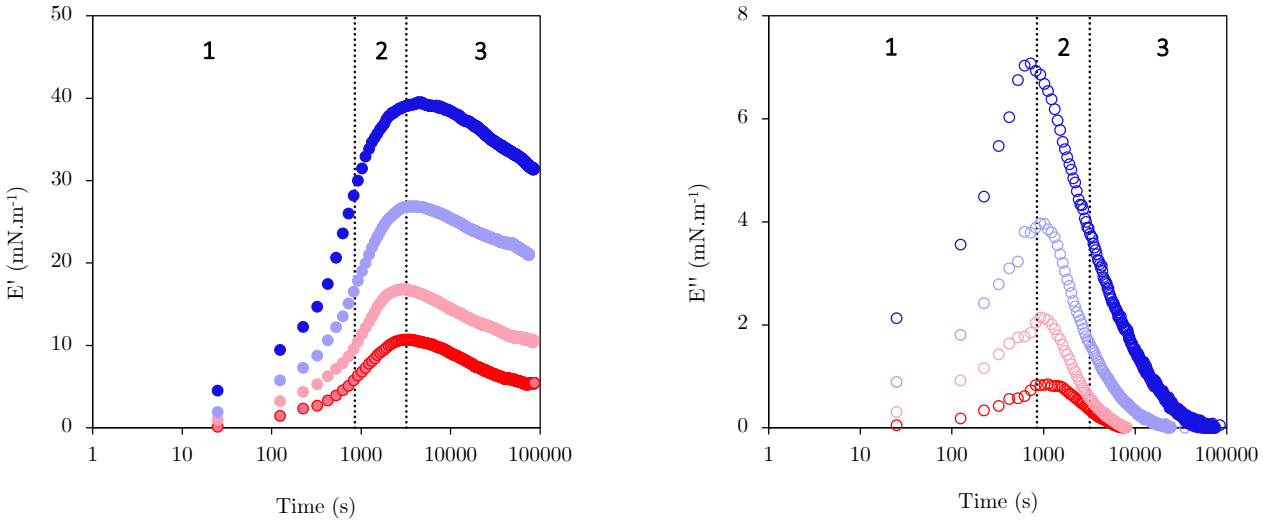

Fig. V.3. Evolution of the elastic (E', left) and viscous (E", right) moduli at the oil-gum-water interphase. The A. *senegal* gum concentration was 5 wt%. The oil phase was composed by d-limonene:1-octanol mixtures at ratios (x_1): 0 (red), 0.6 (light red), 0.98 (light blue) and 1 (blue).

The viscoelastic profiles of A. *senegal* at d-limonene:1-octanol-water interfaces are similar than the ones obtained at pure aroma interfaces. The 3-phase interface structuring mechanism described for gum AGPs in Chapter III also applies to composite oil phases. Enhanced density fluctuations near hydrophobic interface tend to facilitate the interphase dehydration necessary for interfacial AGPs accumulation [27], (Chapter III). Therefore, the work needed for AGPs interfacial concentration and stiffening is lower when the hydrophobicity of the oil mixture is larger. The first interface structuring phase, delimited by the maximum viscous modulus E" (Fig. V.3), consists essentially in an entropy-controlled dehydration-induced AGPs concentration, resulting in the formation of a viscoelastic structure. The second phase lies between the respective maxima of viscous and elastic moduli. AGPs adsorption proceeds, the number of molecules and interactions increase and a structure emerges showing almost purely elastic features. As discussed in Chapter III, the decrease of elasticity observed in phase 3 was

mainly assigned to heterogeneous interfacial distribution of stresses and limitations of the used Young-Laplace method [28]–[31].

In addition, when plotted over the oil-water interfacial tension γ_{ow}, the maximum elastic moduli (E'_{max}, Table V.2) overlaps with the linear fit obtained with a large range of pure aroma compounds and A. *senegal* dispersion in Chapter III (y = 1.33x, Fig. V.4).

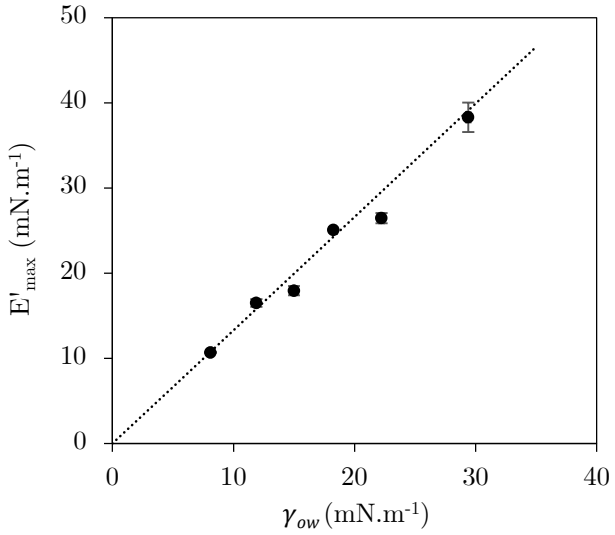

Fig. V.4. Dependency of the dilatational elastic modulus E' on the oil-water interfacial tension γ_{ow}. The oil phase was composed by d-limonene:1-octanol mixtures at ratios (x_1): 0, 0.6, 0.86, 0.95, 0.98 and 1. The black dotted line represents the fit obtained in Chapter III with pure oils and 5 wt% A. *senegal* dispersion (y = 1.33x).

This further confirms the presence of two components into the oil phase does not influence the AGPs 3-phase adsorption process and only changes the stiffness of A. *senegal*-based interfaces through changes of interface hydrophobicity (Fig. V.I). This may be seen when comparing the rheological profiles obtained with d-limonene:1-octanol mixture at ratio 0.6 with the pure aroma compound linalool (Fig. V.5). The comparison can be made as the oil-gum-water interfacial tensions of oil mixture at $x_1 = 0.6$ and pure linalool are similar, respectively at 12.0 $mN.m^{-1}$ and 12.2 $mN.m^{-1}$. The overlap of viscoelastic profiles reveals both elastic modulus and interfacial tension progress according to the oil hydrophobicity. Here, it is independent of the number of compounds (1 or 2) constituting the mixture oil phase (Fig. V.5).

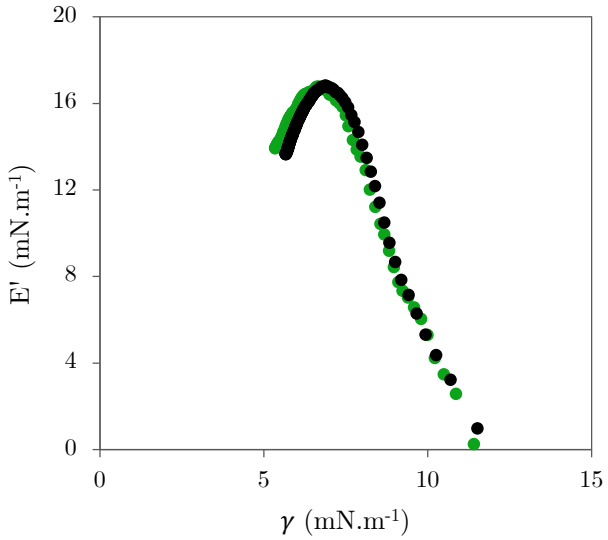

Fig. V.5. Evolution of the dilational elastic modulus E' with the interfacial tension in 5 wt% A. *senegal* dispersion. The oil phases were composed by d-limonene:1-octanol mixture at ratio (x_1) 0.6 (black dots) or pure linalool (green dots).

4. Discussion

The aim of this work was to examine how the presence of multiple components in the oil, and in particular a mixture of two aroma compounds differing in hydrophobicity, leads to changes of the interfacial composition and so, affects the adsorption of Acacia *senegal* gum. As discussed in the introduction, Chapter III outlined the dependence of the gum adsorption on the oil-water interaction energies. Hydrogen bonding between oil and water were found to particularly limit the gum adsorption. Estimations of activation energies of oil-GA-water interphases showed water near highly hydrophobic oils (e.g. myrcene, d-limonene) mainly involved van der Waals interactions while water near weakly hydrophobic oils (e.g. 1-octanol) involved both van der Waals and hydrogen interactions. Energies of interactions were respectively of the order of ~15 and 30-40 kJ.mol^{-1}. This is why the choice was made to study the mixture of 1-octanol, enabling H-bonding with water, and d-limonene, only connecting with water molecules through van der Waals interactions.

Therefore, the main hypothesis explaining results in Fig. V.1 is the better alcohol-water thermodynamic affinity, especially the ability of forming H-bonding and attractive surface van der Waals forces. The latter play a central role in all phenomena involving intermolecular forces

and so, in interfacial phenomena [32]. Although they are not as strong, in standard conditions of temperature and pressure, as Coulombic or H-bonding interactions, they are much more numerous and they are universal. The ensemble of van der Waals interactions, at short and large interaction distances across a medium, has been theoretically described by the Dzyaloshinskii-Lifshitz-Pitaevskii (DLP) theory from which simplified but complete equations (*i.e.* integrating retarded effects) were recently obtained by McDowell [33]. The DLP theory is the solution of the full thermal quantum electrodynamic field theory for the forces between two plates across a dielectric continuum. The intensity of van der Waals interactions in a vacuum for pairs of bodies of different geometries can be approximated using the classical macroscopic approach for calculating the Hamaker function $A_H(r)$ where r refers to the distance between bodies [32]. The McDowell equations capture the long sought crossover from non-retarded (London) to retarded (Casimir) interactions, the effect of polarization in condensed media, and the full suppression of retarded interactions at short distance. Details of calculations are described in supplemental information. At the studied nanoscopic scale, the most relevant geometry is to consider an aroma molecule as a sphere, e.g. 1-octanol, interacting with the surrounding bodies considered as a flat surface, e.g. ensemble of water molecules at the drop interface or ensemble of d-limonene molecules inside the drop. Therefore, van der Waals interaction energies between d-limonene and water, 1-octanol and water, and d-limonene and 1-octanol were estimated through [32]

$$w(D') = \frac{-A_H r_{sp}}{6D'} \quad (1)$$

with A_H the Hamaker constant, r_{sp} the radius of the sphere whose volume corresponds to V_{vdw} of the aroma molecule and D' the distance between the sphere and the flat surface.

The distance D' between the sphere and the flat surface is a vacuum, a region of space depleted in electrons, that we imagine varying according to the surrounding interactions and thus must not be constant [34], [35]. However, D' can be approximated, remarking that it is equivalent to the so-called thermal volume used to describe the protein-water volumetric interface by the Scaled Particle Theory [36]. The thickness of the protein-water thermal volume was first estimated around 1 Å [36] but a value around 0.5 Å has been recently advised [36]. The same order of magnitude was discussed within the framework of organic molecules in water [37]. Therefore, an average distance value D' of 0.5 Å was chosen. The above equation estimated interactions energies $w(D')$ of -3.5 kJ.mol^{-1}, -4.0 kJ.mol^{-1} and -4.1 kJ.mol^{-1} between, respectively,

d-limonene and water, 1-octanol and d-limonene, and 1-octanol and water. This is the same order of magnitude as van der Waals interactions found in the literature that are in the 1-5 kJ.mol^{-1} range [32], [38], [39]. But the main point here is the stronger van der Waals interactions between 1-octanol and water as compared to d-limonene and water. This together with hydrogen bond interaction energy (~10–40 kJ.mol^{-1}) between OH bonds of 1-octanol and water hydrogen (Chapter III), contribute to 1-octanol-water thermodynamics. Therefore, it can be hypothesized 1-octanol molecules in mixtures preferentially accumulate at the interface, as compared to d-limonene molecules, due to the more favorable interactions between 1-octanol and water. This leads to the rapid lowering of the interfacial tension of the oil mixture towards that of 1-octanol as observed in Fig. V.1. Given their chemical structure, 1-octanol molecules would probably orient themselves to place the hydroxyl group towards water for facilitating hydrogen bond and van der Waals interactions [39], while reducing the unfavorable contact between the 1-octanol carbon chain and water as illustrated in the following schematic representation (Fig. V.6).

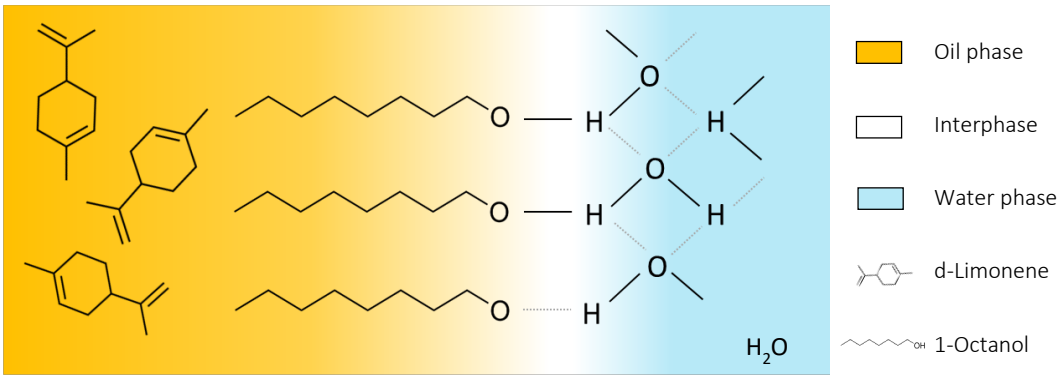

Fig. V.6. Schematic representation of water interface with d-limonene:1-octanol mixtures. Light blue is for the water phase, yellow is for the oil mixture phase and white is for the interphase (the depth of the interphase region and the depth over which interfacial water properties might be different than bulk solution, are not known and therefore, are not to scale).

An analogy can be made with the competitive interfacial adsorption of different types of emulsifiers [18]–[20]. Compounds in mixtures of oil differ in extent of interactions with water. This results in preferential adsorption and/or competitive displacement in order to reduce unfavorable interactions. The oil-water interfacial hydrophobicity is then altered, impacting then the interfacial composition (Chapter III). One can also notice in Fig.V.1, as x_1 decreases

the oil-water interfacial tension reaches a pseudo-plateau close to 1-octanol-water interfacial tension. This suggests the oil droplet surface slowly becomes saturated with 1-octanol molecules. The idea can apply to oil phase of more than two aroma compounds. One can take the example of orange essential oil which composition can vary, depending on harvest time and farming [40]–[42]. The qualitative composition of the used orange essential oil was analyzed by gas chromatography coupled with a mass spectrometer (GC-MS). Only compounds with a proportion greater or equal than 0.1% are reported in Table V.3.

Table V.3. Qualitative composition of orange essential oil analyzed by GC-MS.

Compound	%
d-limonene	93.5
myrcene	2.1
linalool	0.9
decanal	0.5
sabinene	0.4
3-anisaldehyde	0.4
β-phellandrene	0.4
citral	0.3
1-octanol	0.2
octanal	0.2
L-α-terpineol	0.2
3-carene	0.2
anethole	0.2
limonene oxide	0.1

Orange essential oil is essentially composed of highly hydrophobic compounds, *i.e.* d-limonene (93.5%) and myrcene (2.1%), with measured oil-water interfacial tensions of respectively 30.0 $mN.m^{-1}$ and 36.4 $mN.m^{-1}$. Though in small amounts, orange essential oil also contains low hydrophobic molecules such as linalool (0.9%), decanal (0.5%), 1-octanol (0.2%) and octanal (0.2%). On the simple basis of its mass composition, one could intuitively expect the oil-water interfacial tension of orange essential oil to be similar to that of d-limonene. On the contrary, the actual measured interfacial tension is 7.5 $mN.m^{-1}$, not reflecting at all the relative weight of the different compounds but being massively dominated by trace of more polar components. The orange essential oil-water interfacial tension is for instance close to that of weakly hydrophobic compounds such as 1-octanol (8.4 $mN.m^{-1}$), approximatively present at 0.2% (Table V.3) supporting the hypothesis in Fig. V.6. In the aggregate, the number of constituents in the oil phase is not relevant. However, the compound with the greatest water affinity

preferentially accumulates at the interface, influencing the oil surface hydrophobicity. Moreover, even the smallest amount of weakly low hydrophobic compounds is enough to drastically reduce the oil-water interfacial tension and affect the interfacial properties which in turn, might alter the emulsion stability and performance.

5. Conclusions

The present study aimed to examine how a binary mixture of aroma compounds affects the emulsifier adsorption at oil-water interfaces. Interfaces as a function of d-limonene ratio in mixtures with 1-octanol were studied and compared to interfaces of pure d-limonene and 1-octanol. These latter being respectively a highly and a weakly hydrophobic aroma compound. This led to the conclusion the presence of multiple compounds in the dispersed phase impacts the hydrophobicity of the mixture, which in turn influences the interfacial properties. Compounds in the dispersed phase face preferential adsorption and/or competitive displacement. Low hydrophobic compound preferentially accumulates at water interface until saturation, in order to enhance hydrogen and van der Waals interactions with water. Therefore, even the smallest trace of weakly hydrophobic compounds is enough to drastically reduce the oil-water interfacial tension and then, alters the interfacial composition (Chapter III).

6. Acknowledgements

The authors would like to thank ALLAND & ROBERT Company - Natural and organic gums (Port Mort, France) for financial support (Ph.D. C. Faucon).

7. Supplemental Information

7.1. Estimation of the Hamaker constant of oil-water binary systems

The surface free energy between two semi-infinite macroscopic bodies, 1 and 2, separated by a third body, m, of thickness D, may be written in terms of the effective Hamaker function $A_H(D)$ according to [33]:

$$A_H(D) = A_{H\omega=0} + A_{H\omega>0}(D) \quad (2)$$

where $A_{H\omega=0}$ is the "zero frequency contribution" including both the orientation (Keesom) and induction (Debye) interaction energies, and $A_{H\omega>0}$ is the "nonzero frequency contribution" including the dispersion (London) interaction energies.

The first term is independent of the separating distance between bodies 1 and 2 and can be estimated through:

$$A_{H\omega=0} = \frac{3}{4}\left(\frac{\varepsilon_1 - \varepsilon_m}{\varepsilon_1 + \varepsilon_m}\right)\left(\frac{\varepsilon_2 - \varepsilon_m}{\varepsilon_2 + \varepsilon_m}\right)k_B T \quad (3)$$

where ε is the dielectric constant of bodies and medium 1, 2 and m.

The second term is dependent of the separating distance between bodies 1 and 2 and can be estimated through:

$$A_{H\omega>0} = \frac{3\hbar c}{32\sqrt{2}n_{Dm}D}\left(\frac{{n_{D1}}^2 - {n_{Dm}}^2}{{n_{D1}}^2 + {n_{Dm}}^2}\right)\left(\frac{{n_{D2}}^2 - {n_{Dm}}^2}{{n_{D2}}^2 + {n_{Dm}}^2}\right)k_B T \times \left[\left(2 + \frac{3}{2}\nu_T D\right)e^{-\nu_T D} - (2 + \nu_\infty D)e^{-\nu_\infty D}\right] \quad (4)$$

where n_D is the refractive index of bodies and medium 1, 2 and m, $\hbar$ the reduced Planck constant, c the light velocity, and ν_T and ν_∞ constants defined as follow:

$$\nu_T = 2\varepsilon_m^{1/2}\omega_T/c \quad (5)$$

$$\omega_T = \frac{2\pi k_B T}{\hbar} \quad (6)$$

$$\nu_\infty = \frac{\pi}{\sqrt{2}}\frac{n_{Dm}(\overline{n_{D1m}}\,\overline{n_{D2m}})}{\overline{n_{D1m}} + \overline{n_{D2m}}}\frac{\omega_e}{c} \quad (7)$$

$$\overline{n_{lm}} = (n_l^2 + n_m^2)^{1/2} \quad (8)$$

with ω_T the thermal Matsubara frequency, ω_e the resonance frequency and $\overline{n_{Dlm}}$ the root mean square indexes of refraction.

In our systems, bodies 1 and 2 correspond to d-limonene, 1-octanol or water. Medium m is void.

8. Complementary studies

8.1. Oil – water interfacial tension of d-limonene:carvone mixtures

The oil-water interfacial tension was measured for mixtures of carvone (≥98%) and d-limonene (≥97%). The objective was to confirm whether the previously established assumption (Fig. V.6) applies to weaker H-bonding oil mixtures. Therefore, the H-bond donor/acceptor 1-octanol, was replaced by carvone, a H-bond non donor/acceptor ketone, and mixed with the H-bond non donor/non acceptor d-limonene.

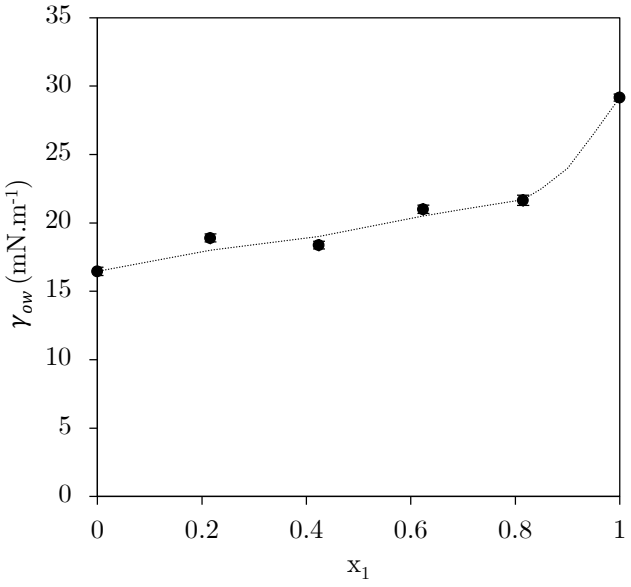

Fig. V.7. Oil-water interfacial tension (γ_{ow}) vs molar fraction of d-limonene (x_1). The oil phase being mixtures of carvone and d-limonene.

The oil-water interfacial tension gap between carvone and d-limonene is lower than the one between 1-octanol and d-limonene, *i.e.* respectively 13.5 and 21.6 mN.m^{-1}. The decrease of the oil-water tension in Fig. V.7 is then less pronounced than in Fig. V.1. However, a sensitivity at high d-limonene fractions is also observed, supporting the hypothesis in Fig. V.6. Thus, oil preferential adsorption is not dependent on the oil types but rules as soon as there is an oil-water interaction energy gap between molecules of the oil binary mixture.

8.2. Oil – water interfacial tension of MCT:1-octanol and MCT:orange essential oil mixtures

The oil-water interfacial tension was measured for mixtures of medium-chain triglyceride (MCT) oil (Miglyol 812 provided by Alland & Robert company) with 1-octanol and with orange essential oil. The objective was to examine the impact of oil phase of more than two compounds and oil phase including a weighting agent as MCT, on the interface with water. MCT is a coconut-oil derivate, composed of saturated triglycerides, and is largely used in food, cosmetic and pharmaceutical industries [43].

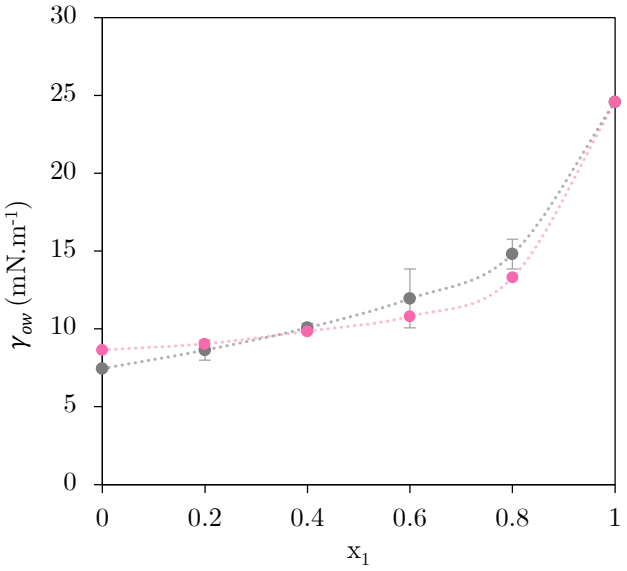

Fig. V.8. Oil-water interfacial tension (γ_{ow}) vs molar fraction of MCT (x_1). The oil phase being mixtures of MCT and orange essential oil (grey dots) or MCT and 1-octanol (pink dots). (The lines are for guiding the eye, the slope between x_1=0.8 and x_1=1 could be more pronounced).

As observed for d-limonene:1-octanol mixtures (Fig. V.1), a sensitivity of the oil-water interfacial tension is observed at high MCT fractions, meaning small amounts of 1-octanol or orange essential oil succeed to largely decrease the oil-water interfacial tension of the mixture. In addition, profiles of MCT:orange essential oil and MCT:1-octanol look similar, supporting interfacial properties of orange oil can be compared to interfacial properties of its weakly hydrophobic compounds such as 1-octanol, even when they are present in small quantities.
Results from Fig. V.8 lead to the observation the hypothesis illustrated in Fig. V.6 stays valid for i) oil phase composed of more than two aroma compounds and for ii) oil phase including weighting agent. Consequently, the hypothesis could be possibly extended to any oil phase consisting of mixtures of aroma compounds, weighting agents, vegetable oils or antioxidants.

8.3. Influence of mixture of two aroma compounds of different hydrophobicity on the formation and aging of Acacia senegal oil-in-water emulsions

The oil hydrophobicity affects the emulsion droplet size distribution of coarse emulsions homogenized with a high shear mixer (Chapter IV). It also influences the fine emulsion aging such as high oil hydrophobicity enhances droplet migration and droplet growth, especially during the first hours of storage (Chapter IV). Then, there is an interest, both in terms of better knowledge of fundamental interfacial phenomena and control of industrial processes, to better apprehend the effect of the presence of varying amounts of OH groups in dispersed oils. The present study aimed to examine how a mixture of two aroma compounds differing in hydrophobicity affects the adsorption of A. *senegal* at oil-water interfaces and emulsion formation and aging.

8.3.1. Emulsification process

The method is reported in details is Chapter IV. Oil-in-water emulsions were formed using a two-step homogenization process. In the first step, coarse emulsions were prepared by adding 5 g of oil blend to 95 g of Acacia *senegal* gum dispersion in order to obtain an emulsion with 20 wt% gum and 5 wt% oil volume fraction. Coarse emulsions were first formed using a rotor/stator homogenizer (Silverson L4RT, Evry, France) equipped with a square hole high shear screen stator at a 7500 rpm speed for 5 min at room temperature (~25°C). Emulsions with smaller oil droplet sizes were then obtained using a microfluidizer with a F12Y diamond interaction chamber (LM20, Microfluidics Corporation, MA, USA) at a pressure of 450 bars for 2 passes.

8.3.2. Measurements of emulsion structure and stability

The droplet size distribution and the volumetric droplet diameter $D_{4,3}$ of emulsions were determined by laser diffraction using a Beckman Coulter LS 13 320 XR (Beckman Coulter, Villepinte, France). Five cycles of measurements were performed 15 minutes after the emulsification step, using an obscuration value of ~10%. The emulsion colloidal stability was monitored using a vertical scan light scattering analyzer type Turbiscan® Tower (Formulaction

Company, France) equipped with a pulsed near infrared light source (λ = 880 nm) and two synchronous transmission (T) and backscattering (BS) detectors. About 15 ml emulsion sample (equivalent to ~4 cm height) were loaded into cylindrical glass tubes 5 minutes after emulsification and scanned throughout its entire height. Backscattered (BS) and transmitted (T) light were recorded every 5 minutes during the first 24h, and then after 2, 3, 7, 14, 21 and 28 days of storage at 25°C. Instability phenomena such as creaming, sedimentation and coalescence of oil droplets were analyzed through the differences in backscattering (BS) and in transmittance (T) profiles between the initial scan and scans over time (ΔBS and ΔT expressed in %). In addition, the Turbiscan stability index (TSI) corresponding to the signal variation at definite positions (h) throughout various height (H) ranges of the sample between the $scan_i$ and the $scan_{i-1}$ was calculated. TSI was determined through Equation (9):

$$TSI = \sum_i \frac{\sum_h |scan_i(h) - scan_{i-1}(h)|}{H} \quad (9)$$

where $scan_i$ is the average backscattering intensity of the i-th scan, $scan_{i-1}$ is the average backscattering intensity of the (i-1)-th scan and H is the scan numbers in the whole measurement. This parameter was calculated over the entire tube height and takes into account the ensemble of destabilization phenomena occurring during storage (creaming, flocculation/coalescence, clarification).

8.3.3. Volumetric droplet diameter of emulsions and aging

The mean diameter $D_{4,3}$ of A. *senegal* stabilized emulsions of d-limonene:1-octanol mixtures at ratios (x_1): 0, 0.6, 0.86, 0.95, 0.98 and 1 were measured and plotted over the initial oil-water interfacial tension (Fig. V.9). Results refer to coarse emulsions obtained upon the first homogenization stage (see Materials & Methods). Droplet size distribution profiles can be found in annex F.

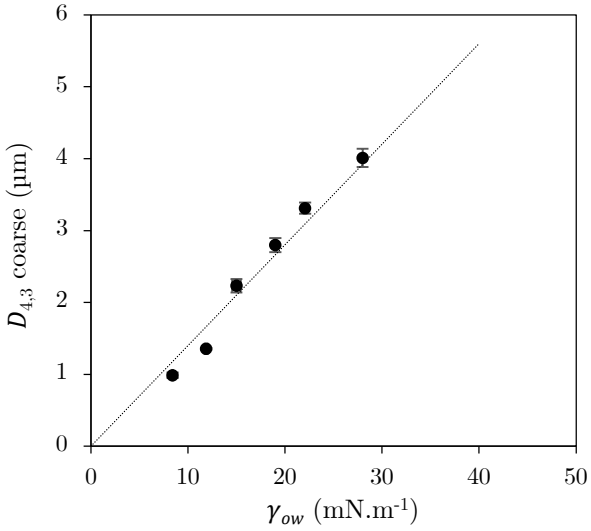

Fig. V.9. Dependency of the volumetric droplet diameter $D_{4,3}$ of the coarse emulsions stabilized by 20 wt% A. *senegal* on the oil-water interfacial tension γ_{ow}. The oil phase was composed by d-limonene:1-octanol mixture at ratio (x_1) 0, 0.6, 0.86, 0.95, 0.98 and 1. The black dotted line represents the fit obtained with pure oils and 20 wt% A. *senegal* dispersion (y = 0.14x) from Chapter IV.

The dependency of $D_{4,3}$ diameter on the oil hydrophobicity is similar than the one obtained with pure aroma emulsions. When applying the same homogenization conditions, the oil hydrophobicity is the only parameter affecting the droplet size of emulsions homogenized using a rotor/stator mixer (Chapter IV). Therefore, the correlation Fig. V.9 could have been expected as d-limonene:1-octanol mixture influence the oil-water interfacial tension (Fig. V.1) and so, the assumed oil interface composition (Fig. V.6). Thus, the dependency of coarse emulsion droplet size on the oil hydrophobicity stays valid for oil phase with two components.

As discussed in Chapter IV, fine emulsions came out whitish upon the second homogenization stage but 1-octanol emulsion tended towards yellow. This is a clear indication of a poorer stability and points to recoalescence phenomena of freshly dispersed droplets during the homogenization process and at the outlet of the microfluidization chamber. The stability of produced emulsions was determined using an optical method that records both backscattered (BS) and transmitted (T) light. The measured BS intensity at t_0 provides a physical signature of the balance between droplet coalescence and fragmentation inside the homogenization chamber. High BS values indicate the presence of a large number of small droplets, then inform about the predominance of droplet fragmentation, while low BS values imply large and

relatively small amounts of droplets, thus the predominance of droplet coalescence. BS results at t_0 of d-limonene:1-octanol emulsions are plotted in Fig. V.10. Changes of backscattered (ΔBS) and transmitted light profiles (ΔT) can be found in annex D.

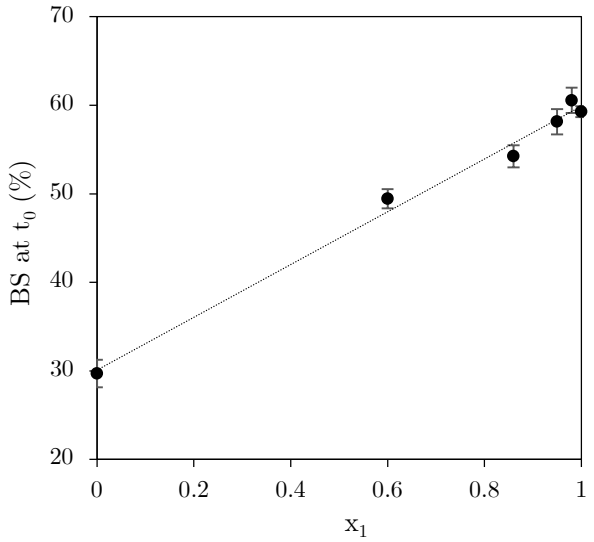

Fig. V.10. Initial BS values of emulsions of d-limonene:1-octanol mixtures stabilized by 20 wt% A. *senegal* over the molar fraction of d-limonene (x_1).

The positively growing linear correlation obtained ($y = 29.8x - 30.1$, $r^2 = 0.99$) indicates that adding a compound with high outlet homogenization stability significantly improves that of a compound with low outlet homogenization stability.

Then, *TSI* signal was analyzed. Normalization using the *TSI* value of day 28 of storage was used to provide a correct comparison (Chapter IV) between the oils (Fig. V.11).

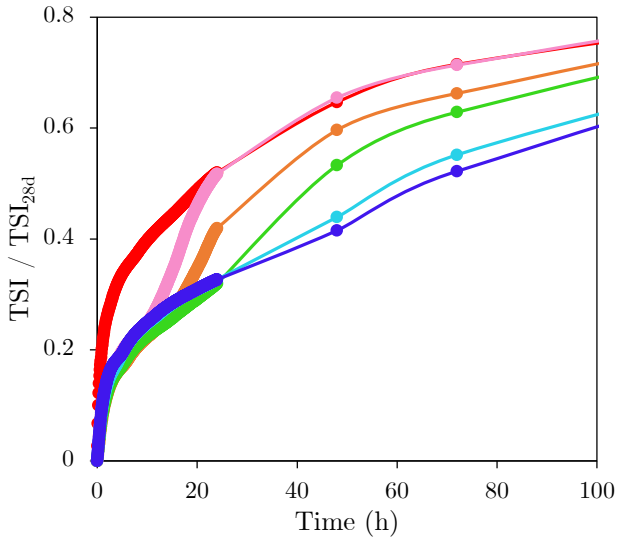

Fig. V.11. Evolution of normalized *TSI* signals at 25°C of d-limonene:1-octanol mixtures emulsions stabilized by 20 wt% A. *senegal*. d-Limonene ratios (x_1) of mixtures are: (●) 0, (●) 0.6, (●) 0.86, (●) 0.95, (●) 0.98 and (●) 1.

1-octanol and d-limonene emulsions are respectively characterized by the highest and lowest normalized *TSI* signals. They are therefore respectively the least and the most stable emulsions of this set of homogenized oils.

As observed in Fig. V.11, the presence of d-limonene into the blend improves the initial emulsion stability. Normalized *TSI* signals of emulsions of mixtures at ratios (x_1) 0.6, 0.86, 0.95 and 0.98 initially overlap the one of pure d-limonene emulsion. Then, increasing the 1-octanol concentration leads to accelerate the *TSI* signal increase. As one could expect, adding a highly hydrophobic compound to a low hydrophobic compound leads to the delay of the emulsion instability. Likewise, adding a low hydrophobic compound to a high hydrophobic compound accelerates the destabilization mechanisms. This is particularly noticeable when examining the time from which emulsions start to cream. To this end, the inflexion point of BS signals, corresponding to the point in which creaming phenomena (increase of BS) exceeds coalescence and/or Ostwald ripening phenomena (decrease of *BS*) was determined. Results are plotted over the molar fraction x_1 in Fig. V.12.

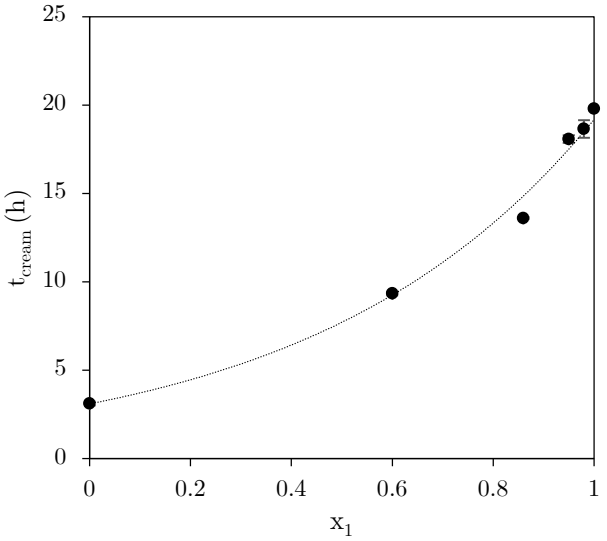

Fig. V.12. Starting creaming time of emulsions (t_{cream}) vs molar fraction of d-limonene (x_1).

Creaming appeared after 3.1 and 19.8h of storage for respectively 1-octanol and d-limonene emulsions. Emulsions with mixtures at ratios (x_1) 0.6, 0.86, 0.95 and 0.98 started to cream after respectively 9.3, 13.6, 18.1 and 18.7h. Then, the creaming index *CI* of fine emulsions was calculated after 28 days according to the following equation [44]:

$$CI(\%) = \frac{H_S}{H_T} \times 100 \quad (10)$$

where H_S is the serum (transparent and turbid) layer from T signal and H_T the total height of emulsion. Results are reported in Table V.4 and were plotted over the oil-water interfacial tension in Fig. V.13.

Table V.4. Creaming index CI of d-limonene:1-octanol mixtures emulsions of ratios (x_1) 0, 0.6, 0.86, 0.95, 0.98 and 1 stabilized by 20 wt% A. *senegal*, after 28 days of storage at 25°C.

x_1	0	0.6	0.86	0.95	0.98	1
CI (%)	41.7 (±2.7)	45.1 (±2.9)	29.0 (±2.8)	23.3 (±2.5)	21.1 (±1.8)	16.5 (±4.8)

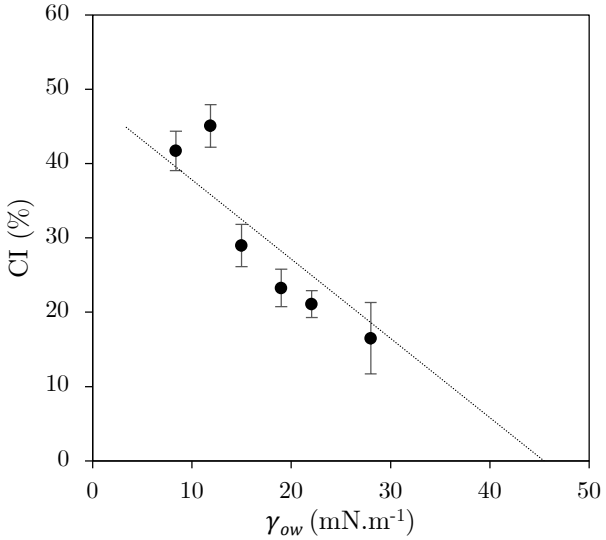

Fig. V.13. Creaming index CI after 28 days of storage at 25°C of emulsions of d-limonene:1-octanol mixtures stabilized by 20 wt% A. *senegal* over the oil-water interfacial tension γ_{ow}. Ratios (x_1) of mixtures are: 0, 0.6, 0.86, 0.95, 0.98 and 1. The black dotted line represents the tendency obtained with pure oils of density of the same order of magnitude (including d-limonene and 1-octanol) and 20 wt% A. *senegal* dispersion from Chapter IV.

The dependency of d-limonene:1-octanol mixtures CI on the oil hydrophobicity is similar than the one obtained with emulsions of pure aroma of density of the same order of magnitude (including d-limonene and 1-octanol).

In the aggregate, adding highly hydrophobic compounds into the dispersed phase may allow to improve outlet homogenization stability and to delay creaming. Similarly, the addition of weakly hydrophobic compounds will have the opposite effect. So far, we cannot conclude on

the impact on the droplet growth as no correlation with the oil hydrophobicity nor with the mixture composition (x_1) has been found. Though, it is believed a synergy might occur between the factors affecting the droplet growth, such as the oil hydrophobicity, viscosity and solubility in water. Therefore, mixing a weighting agent in the oil phase not only reduces the density difference between the aqueous and oil phases, but also influence the oil hydrophobicity (as well as viscosity and solubility).

9. References

[1] McClements and L. Schramm, "Comparison of multiple scattering theories with experimental measurements in Emulsions," *Adv. Chem. ACS*, pp. 849–853, 1992.

[2] D. J. McCLements, *Food Emulsions Principles, Practices, and Techniques*. 2010.

[3] N. Mollakhalili Meybodi, M. A. Mohammadifar, and A. R. Naseri, "Effective factors on the stability of oil-in-water emulsion based beverage: A review," *J. Food Qual. Hazards Control*, vol. 1, no. 3, pp. 67–71, 2014.

[4] R. Chanamai and D. J. McClements, "Impact of weighting agents and sucrose on gravitational separation of beverage emulsions," *J. Agric. Food Chem.*, vol. 48, no. 11, pp. 5561–5565, 2000, doi: 10.1021/jf0002903.

[5] A. R. Taherian, P. Fustier, M. Britten, and H. S. Ramaswamy, "Rheology and stability of beverage emulsions in the presence and absence of weighting agents: A review," *Food Biophys.*, vol. 3, no. 3, pp. 279–286, 2008, doi: 10.1007/s11483-008-9093-4.

[6] M. Atgié, O. Masbernat, and K. Roger, "Emulsions Stabilized by Gum Arabic: Composition and Packing within Interfacial Films," *Langmuir*, vol. 35, no. 4, pp. 962–972, 2019, doi: 10.1021/acs.langmuir.8b02715.

[7] R. Chanamai and D. J. McClements, "Comparison of gum arabic, modified starch, and whey protein isolate as emulsifiers: Influence of pH, CaCl2 and temperature," *J. Food Sci.*, vol. 67, no. 1, pp. 120–125, 2002, doi: 10.1111/j.1365-2621.2002.tb11370.x.

[8] V. Paramita, T. Furuta, and H. Yoshii, "High-Oil-Load Encapsulation of Medium-Chain Triglycerides and d-Limonene Mixture in Modified Starch by Spray Drying," *J. Food Sci.*, vol. 77, no. 2, pp. 38–44, 2012, doi: 10.1111/j.1750-3841.2011.02534.x.

[9] J. Zhang, T. L. Peppard, and G. A. Reineccius, "Preparation and characterization of nanoemulsions stabilized by food biopolymers using microfluidization," *Flavour Fragr. J.*, vol. 30, no. 4, pp. 288–294, 2015, doi: 10.1002/ffj.3244.

[10] E. Dickinson, V. B. Galazka, and D. M. W. Anderson, "Emulsifying behaviour of gum arabic. Part 1: Effect of the nature of the oil phase on the emulsion droplet-size distribution," *Carbohydr. Polym.*, vol. 14, no. 4, pp. 373–383, 1991, doi: 10.1016/0144-8617(91)90003-U.

[11] S. J. Reiner, G. A. Reineccius, and T. L. Peppard, "A comparison of the stability of beverage cloud emulsions formulated with different gum acacia- and starch-based emulsifiers," *J. Food Sci.*, vol. 75, no. 5, 2010, doi: 10.1111/j.1750-3841.2010.01625.x.

[12] R. M. A. Mansour and E. A. Hassan, "Effect of gum concentration and gum protein concentration on emulsifying properties of some Acacia gums," *Int. J. basic Appl. Chem. Sci.*, vol. 6, no. 2, pp. 23–35, 2016.

[13] C. Aphibanthammakit, "Propriétés interfaciales et émulsifiantes de gommes d'Acacia senegal, Acacia seyal et de leurs fractions," 2018.

[14] P. Erni *et al.*, "Interfacial rheology of surface-active biopolymers: Acacia senegal gum versus hydrophobically modified starch," *Biomacromolecules*, vol. 8, no. 11, pp. 3458–3466, 2007, doi: 10.1021/bm700578z.

[15] E. Dickinson, B. S. Murray, G. Stainsby, and D. M. W. Anderson, "Surface activity and emulsifying behaviour of some Acacia gums," *Top. Catal.*, vol. 2, no. 6, pp. 477–490, 1988, doi: 10.1016/S0268-005X(88)80047-X.

[16] M. Elmanan, S. Al-Assaf, G. O. Phillips, and P. A. Williams, "Studies on Acacia exudate gums: Part VI. Interfacial rheology of Acacia senegal and Acacia seyal," *Food Hydrocoll.*, vol. 22, no. 4, pp. 682–689, 2008, doi: 10.1016/j.foodhyd.2007.02.008.

[17] F. Ravera, K. Dziza, E. Santini, L. Cristofolini, and L. Liggieri, "Emulsification and emulsion stability: The role of the interfacial properties," *Adv. Colloid Interface Sci.*, vol. 288, p. 102344, 2021, doi: 10.1016/j.cis.2020.102344.

[18] L. A. Pugnaloni, E. Dickinson, R. Ettelaie, A. R. Mackie, and P. J. Wilde, "Competitive adsorption of proteins and low-molecular-weight surfactants: Computer simulation and microscopic imaging," *Adv. Colloid Interface Sci.*, vol. 107, no. 1, pp. 27–49, 2004, doi: 10.1016/j.cis.2003.08.003.

[19] E. Dickinson, "Mixed biopolymers at interfaces: Competitive adsorption and multilayer structures," *Food Hydrocoll.*, vol. 25, no. 8, pp. 1966–1983, 2011, doi: 10.1016/j.foodhyd.2010.12.001.

[20] V. Mahendran, J. Sangeetha, and J. Philip, "Probing of competitive displacement adsorption of casein at oil-in-water interface using equilibrium force distance measurements," *J. Phys. Chem. B*, vol. 119, no. 22, pp. 6828–6835, 2015, doi: 10.1021/acs.jpcb.5b02612.

[21] C. Zhao *et al.*, "Encapsulation of lycopene within oil-in-water nanoemulsions using lactoferrin: Impact of carrier oils on physicochemical stability and bioaccessibility," *Int. J. Biol. Macromol.*, vol. 153, pp. 912–920, 2020, doi: 10.1016/j.ijbiomac.2020.03.063.

[22] J. Bergfreund, P. Bertsch, and P. Fischer, "Effect of the hydrophobic phase on interfacial phenomena of surfactants, proteins, and particles at fluid interfaces," *Curr. Opin. Colloid Interface Sci.*, vol. 56, p. 101509, 2021, doi: 10.1016/j.cocis.2021.101509.

[23] FAO, "Gum arabic," 1999. https://www.fao.org/3/W6355E/w6355e0g.htm (accessed Jul. 12, 2022).

[24] L. Lopez-Torrez, M. Nigen, P. Williams, T. Doco, and C. Sanchez, "Acacia senegal vs. Acacia seyal gums - Part 1: Composition andstructure of hyperbranched plant exudates," *Food Hydrocoll.*, vol. 51, no. April, pp. 41–53, 2015, doi: 10.1016/j.foodhyd.2015.04.019.

[25] V. Mejia Tamayo *et al.*, "Flexibility and hydration of amphiphilic hyperbranched arabinogalactan-protein from plant exudate: A volumetric perspective," *Colloids and Interfaces*, vol. 2, no. 1, 2018, doi: 10.3390/colloids2010011.

[26] M. H. Cohen and G. S. Grest, "Liquid-glass transition, a free-volume approach," *Phys. Rev. B*, vol. 20, no. 3, pp. 1077–1098, 1979, doi: 10.1103/PhysRevB.20.1077.

[27] C. Faucon, P. Chalier, and C. Sanchez, "On the relationship between volume fluctuations in liquids and the Gibbs free energy of cavity formation," *J. Mol. Liq.*, vol. 364, p. 119845, 2022, doi: 10.1016/j.molliq.2022.119845.

[28] R. Stanimirova, K. Marinova, S. Tcholakova, N. D. Denkov, S. Stoyanov, and E. Pelan, "Surface rheology of saponin adsorption layers," *Langmuir*, vol. 27, no. 20, pp. 12486–12498, 2011, doi: 10.1021/la202860u.

[29] A. Yeung and L. Zhang, "Shear effects in interfacial rheology and their implications on oscillating pendant drop experiments," *Langmuir*, vol. 22, no. 2, pp. 693–701, 2006, doi: 10.1021/la051795w.

[30] M. Nagel, T. A. Tervoort, and J. Vermant, "From drop-shape analysis to stress-fitting elastometry," *Adv. Colloid Interface Sci.*, vol. 247, no. May, pp. 33–51, 2017, doi: 10.1016/j.cis.2017.07.008.

[31] J. D. Berry, M. J. Neeson, R. R. Dagastine, D. Y. C. Chan, and R. F. Tabor, "Measurement of surface and interfacial tension using pendant drop tensiometry," *J. Colloid Interface Sci.*, vol. 454, pp. 226–237, 2015, doi: 10.1016/j.jcis.2015.05.012.

[32] J. N. Israelachvili, *Intermolecular and Surface Forces*. 2011.

[33] L. G. Macdowell, "Surface van der Waals forces in a nutshell," *J. Chem. Phys.*, vol. 150, no. February, 2019, doi: 10.1063/1.5089019.

[34] M. Kanduč, A. Schlaich, E. Schneck, and R. R. Netz, "Water-Mediated Interactions between Hydrophilic and Hydrophobic Surfaces," *Langmuir*, vol. 32, no. 35, pp. 8767–8782, 2016, doi: 10.1021/acs.langmuir.6b01727.

[35] J. Monroe *et al.*, "Water Structure and Properties at Hydrophilic and Hydrophobic Surfaces," *Annu. Rev. Chem. Biomol. Eng.*, vol. 11, pp. 523–557, 2020, doi: 10.1146/annurev-chembioeng-120919-114657.

[36] T. V. Chalikian and R. B. Macgregor, "On empirical decomposition of volumetric data," *Biophys. Chem.*, vol. 246, no. December 2018, pp. 8–15, 2019, doi: 10.1016/j.bpc.2018.12.005.

[37] J. T. Edward and P. G. Farrell, "Relation between van der Waals and Partial Molal Volumes of Organic Molecules in Water," *Can. J. Chem.*, vol. 53, no. 19, pp. 2965–2970, 1975, doi: 10.1139/v75-417.

[38] A. R. Van Buuren, S. J. Marrink, and H. J. C. Berendsen, "A molecular dynamics study of the decane/water interface," *J. Phys. Chem.*, vol. 97, no. 36, pp. 9206–9212, 1993, doi: 10.1021/j100138a023.

[39] Z. Liu and A. E. Clark, "An octanol hinge opens the door to water transport," *Chem. Sci.*, vol. 12, no. 6, pp. 2294–2303, 2021, doi: 10.1039/d0sc04782a.

[40] M. Gavahian, Y. H. Chu, and A. Mousavi Khaneghah, "Recent advances in orange oil extraction: an opportunity for the valorisation of orange peel waste a review," *Int. J. Food Sci. Technol.*, vol. 54, no. 4, pp. 925–932, 2019, doi: 10.1111/ijfs.13987.

[41] G. Sekar, S. Sugumar, A. Mukherjee, and N. Chandrasekaran, "Multiple spectroscopic studies of the structural conformational changes of human serum albumin - Essential oil based nanoemulsions conjugates," *J. Lumin.*, vol. 161, pp. 187–197, 2015, doi: 10.1016/j.jlumin.2014.12.058.

[42] J. R. Ayala *et al.*, "Extraction and Characterization of Orange Peel Essential Oil from Mexico and United States of America," *J. Essent. Oil-Bearing Plants*, vol. 20, no. 4, pp. 897–914, 2017, doi: 10.1080/0972060X.2017.1364173.

[43] K. Dziza *et al.*, "Interfacial properties and emulsification of biocompatible liquid-liquid systems," *Coatings*, vol. 10, no. 4, 2020, doi: 10.3390/coatings10040397.

[44] Y. S. Gu, E. A. Decker, and D. J. McClements, "Influence of pH and carrageenan type on properties of β-lactoglobulin stabilized oil-in-water emulsions," *Food Hydrocoll.*, vol. 19, no. 1, pp. 83–91, 2005, doi: 10.1016/j.foodhyd.2004.04.016.

General Conclusion

General Conclusion

Actually, the demand for Acacia gum (GA) is exponentially increasing according to our partner company Alland&Robert, as consumers and environmental concerns lead to the need of developing "all natural" and sometimes only plant-based products. Consequently, many food companies are examining the possibility of replacing synthetic ingredients with natural ones [1]. One challenge then consists in expanding applications based on new knowledge on Acacia gum composition, structure and techno-functional properties. GA can be used in beverage applications, more specifically through the stabilization of flavoring preparation-in-water emulsions [2], [3]. In this context, this Ph.D. project aims to gain knowledge on the mechanisms involved in GA-stabilized emulsions of aroma compounds in order first to better apprehend the origin of surface properties of gums, then possibly to extend the field of application of GA to a wider range of aroma compounds.

The main objective of this Ph.D. thesis was to study the influence of water, and more specifically of the interactions with water OH bonds, on the mechanism of GA interphase formation and emulsion stability. The approach we choose was to vary the oil (aroma compound) hydrophobicity. The two commercial species of Acacia gums, Acacia *senegal* (A. *senegal*) and Acacia *seyal* (A. *seyal*), were used for this purpose. The specific objectives of the study were: (i) to characterize the thermodynamic properties of liquids with the aim of understanding the fundamental differences between water and hydrophobic compounds in terms of volume fluctuations and interaction energy, (ii) to examine the impact of the oil hydrophobicity on the structure mechanisms of the Acacia gum layer formation at the oil-water interface, as well as (iii) on the droplet formation during homogenization and on the stability of emulsion. Last specific objective was (iv) to investigate whether the presence of more than one component in the oil phase affects the oil-gum-water interphases and Acacia *senegal* emulsion stability.

The main composition of both Acacia gums consists in highly glycosylated hydroxyproline-rich arabinogalactan-proteins (AGPs). AGPs macromolecules are hyperbranched complex polysaccharides, essentially made of sugars D-galactose, L-arabinose, L-rhamnose, D-glucuronic acid, and 4-O-methyl-D-glucuronic acid. In addition, AGPs contain about 1-3% of proteins and 3-4% of minerals. Although AGPs are mostly hydrophilic solutes due to their high sugar content [9] and the specific amino acid composition rich in hydrophilic species [4]–[6], they are

apparently sensitive to the hydrophobic effect. The protein/polysaccharide duality gives rise to the amphiphilic properties allowing the adsorption of GA to gas–liquid, liquid–liquid, and solid–liquid interfaces [4]. Thus, the gum can reduce the interfacial tension between the dispersed and the continuous phases and form an interfacial viscoelastic barrier, promoting the formation of an emulsion with more stable droplets [7]–[11].

1. Water is defined by low microscopic volume fluctuations.

Microscopic volume fluctuations are a signature of a liquid structure and liquid intermolecular energy. Soper [12] suggested that a thermodynamic quantity f_V, can be used to describe how large the density fluctuations are likely to be in any given volume of a liquid. Converting the dimensionless parameter f_V in volume, water was found to display the lowest quantity of volume fluctuations at nanoscale (1 nm^3) compared to more than 200 other liquids. For instance, the volume fluctuations quantity of water was 0.13×10^{-2} nm^3 compared to 2.91×10^{-2} nm^3 for the most hydrophobic compound we selected to study GA interfacial and emulsifying properties, *i.e.* n-hexadecane [13]. Then, the scaled particle theory calculations confirmed these density fluctuations are correlated to the Gibbs free energy of cavity formation ΔG_c, another parameter reflecting the extent of liquid intermolecular energy [14], and first responsible for the "solubility" or "insolubility" of more or less hydrophobic solutes. As already pointed out by others [15], [16], enhanced volume fluctuations were found to lessen the work of cavity formation. Therefore, creating a cavity in water requires the highest energy (65×10^{-20} $J.nm^{-3}$) when compared with the other liquids (2.7×10^{-20} $J.nm^{-3}$ for n-hexadecane). The formation of a cavity is part of the theoretical description of process of solvating a solute molecule in a solvent. Accordingly, the solvation process is divided into two hypothetical stages: (a) formation of a cavity of the size of the solute molecule; (b) introduction of the solute molecule into the cavity, switching on solute-solvent attractive interactions [17], [18]. The consequent water Gibbs free energy of cavity creation may then illustrate the complexity of introducing a nonpolar solute in water, that is believed to be linked to the particular small size of water molecule [14], [19], [20].

The interest of studying such thermodynamic parameters is that they have been associated to solute intrinsic molecular properties and solute-solvent interactions, more specifically solute flexibility and hydration [21]. For instance, hydration-dependent volumetric properties of proteins have been related to their hydrophobicity and surface properties [22]–[27]. Thus,

volumetric properties of biopolymers are important determinants of their functionality. Another advantage is that they allow descriptions of thermodynamic macroscopic properties, and in particular interfacial systems structure.

2. Acacia gum adsorption to oil-water interfaces can be described by a 3-phase volumetric mechanism driven by water interactions.

The thermodynamic state of AGPs, or solute in general, can be captured through their impact on the solvent at their interface. Introducing Acacia gum, *i.e.* a solute of significant size (M_w = 7-8 x10^5 g.mol^{-1}, R_h = 15-25 nm) into water, leads to significant perturbation of the hydrogen-bonded network and a severe reduction in the entropy [28]. In addition, AGPs protein content, protein distribution, protein accessibility, and the presence of minerals (ions Ca screen sugar charges), activate the sensitivity of Acacia gum to water-induced hydrophobic effects. Thus, water tends to exclude the solute from the solution in order to minimize the entropic penalty. On the other hand, the oil-water interface gives rise to a 1-6 Å water density depletion zone [29]–[31], (or hydrophobic gap) that shows vapor characteristics [32] and pronounced density fluctuations [16], [30]. Therefore, water-water, oil-water and AGPs-water interactions constitute the driving force of the Acacia gum 3-phases adsorption. The enhanced density fluctuations of macroscopic hydrophobic interfaces along with the hydrophobic effect inside the bulk water, lead AGPs to concentrate at the interface by displacing first an equivalent volume of water (phase 1). Then, AGPs accumulate, interact and constitute a network at the macroscopic scale resulting in the formation of a viscoelastic layer. As the adsorption proceeds the number of molecules and the interactions increase until a threshold is reached and a transition state is observed. The oil-gum-water system moves from a dominant viscous state with dissipation of energy to a prevailing elastic one (phase 2). Thereafter, the most effective structure is achieved at the maximum of elasticity and shows water contents of no more than 30%, which is consistent with hydration rate estimated for AGP protein moiety [6]. However, the system continues to develop. AGPs pack at the interface. Interfacial fluctuations in density result in the loss of the elasticity and the wrinkling of the drop surface (phase 3).

3. The increase of the oil hydrophobicity leads to the increase of the Acacia gum adsorption.

The favoring adsorption of AGPs molecules to highly hydrophobic oils interfaces has been confirmed. The water two-phase structure model of Sun [33], [34] together with the interfacial thermodynamic activity of water a_w^s [35] have proved effective for describing the oil-water

interface configuration and highlighting the role of oil-water interactions. The thermodynamic activity of water is estimated using the equation $\Pi = -RT\,\Gamma_w\,ln\,a_w^s$ [35], [36] where Π is the surface pressure, R the gas constant, T the temperature, and Γ_w the moles of water per unit area of the interfacial phase. Hence, the surface pressure can be described through the thermodynamic properties of water. In addition, the a_w^s and the model of Sun allow to link the strong oil hydrophobicity influence on the Acacia gum adsorption to the interfacial oil-water interactions. The latter were found to have significant consequences on the phase 1 of Acacia gum adsorption and also to affect the rearrangement during phase 2 and phase 3. The nature of oil was also found important. In the absence of strong interactions at the oil-water interface, the coordination number of water is reduced. This leads to the predominance of H:O van der Waals bonds within the first hydrated layers together with the delocalization and densification of H_2O electrons in the more distant layers, resulting in the increase of the interfacial tension. Therefore, interfaces of highly hydrophobic oils are defined by a decrease of the interfacial water hydrogen bond-network strength, resulting in the partial vaporization of water and in enhanced water interfacial volume fluctuations. It then contributes to the decrease of the energy cost of AGPs adsorption. This is particularly noticeable in the GA interfacial rheology. Two master curves were obtained when plotting the normalized elastic modulus E'/E'_{max} over the normalized interfacial tension γ/γ_{ow}. A first one is observed for the most hydrophobic oils, *i.e.* n-hexadecane, myrcene, purified d-limonene, d-limonene 97%, ethyl octanoate, methyl octanoate and carvone. A second master curve is grouping alcohols, *i.e.* the least hydrophobic oils. The difference between both master curves is then dependent on the presence of chemical groups enhancing interactions with water, namely OH groups.

In addition, the oil hydrophobicity also impacts the AGPs rearrangement within the interphase as low oil hydrophobicity induces less packed and ordered layer network with oil molecules incorporation. Thus, a sufficient oil hydrophobicity is required to enhance the efficiency of the gum adsorption. This better efficiency induces in turn high oil surface coverage, high interfacial layer elasticity and ability to reduce the interfacial tension. Similar behavior was found with proteins [37]–[40].

4. Preferential adsorption at the oil-water interface occurs within the multicomponent oil phase in favor of the lowest hydrophobic compound.

Interfaces as a function of d-limonene ratio in mixtures with 1-octanol were studied and compared to interfaces of pure d-limonene and 1-octanol. These latter being respectively a

highly and a weakly hydrophobic aroma compound. This led to the conclusion the presence of multiple compounds in the dispersed phase impacts the hydrophobicity of the mixture, which in turn influences the interfacial properties. Compounds in the dispersed phase face preferential adsorption and/or competitive displacement. Low hydrophobic compound preferentially accumulates at water interface until saturation in order to reduce unfavorable interactions with water. Therefore, even the smallest trace of low hydrophobic compounds is enough to drastically reduce the oil-water interfacial tension and then, alters the interfacial composition. This was confirmed with the studies of oil-water interfaces of orange essential oil and mixtures of d-limonene:carvone, MCT:1-octanol, as well as MCT:orange essential oil.

d-Limonene:1-octanol-water interface was defined such that the hydroxyl group of 1-octanol is oriented towards water. This configuration eases hydrogen bond and van der Waals interactions, while reducing the unfavorable contact between the 1-octanol carbon chain and water.

The AGPs adsorption mechanism is not altered in the presence of a second aroma compound. This was demonstrated through the comparison of rheological profiles obtained with d-limonene:1-octanol mixture at ratio 0.6 and with the pure aroma compound linalool. Both oil phases are defined by an oil-water interfacial tension of ~12.0 $mN.m^{-1}$. Then, the overlap of viscoelastic profiles revealed both elastic modulus and interfacial tension progress according to the oil hydrophobicity.

5. The oil hydrophobicity increases the resistance of fine emulsions to creaming and coalescence during the first hours of storage.

The oil composition is known to influence the thermodynamic stability of emulsions. Comparing oils with densities of the same order of magnitude (n-hexadecane, d-limonene, ethyl octanoate, 1-decanol and 1-octanol) leads to the suggestion the oil hydrophobicity is the driving force of the gravitational separation. The carvone emulsion data point stood out of the correlation and is characterized by the lowest density difference between the dispersed and continuous phases. This underlines the interest in using weighting agents to reduce the density gap and thus, to delay droplet migration phenomena.

Then, the droplet growth due to coalescence, flocculation and/or Ostwald ripening was found to linearly rises with oil hydrophobicity after 1h of storage. This could originate from the strong elasticity of the interfacial barrier formed by the emulsifier [41]–[46]. However, this linear

correlation weakened as storage time increased, before completely vanishing after 28 days of storage. This is assumed to come from the interconnection of the destabilization processes that may influence each other during the emulsion aging and a synergistic effect between the oil properties (*i.e.* hydrophobicity, density, viscosity, solubility).

In addition, the increase of oil hydrophobicity led to the increase of coarse emulsions droplet size when homogenized using a high shear mixer. This came from the used homogenization conditions inducing the oil-water interfacial tension to be the main variable affecting the droplet disruption mechanisms.

The study of the mixture of two aroma compounds of different hydrophobicity demonstrated that the dependency of coarse emulsion droplet size on the oil hydrophobicity remains valid for a two-component oil phase. Adding highly hydrophobic compounds into the dispersed phase also allows to improve the outlet homogenization stability and creaming. Conversely, the addition of low hydrophobic compounds has the opposite effect. We cannot conclude on the impact on the droplet growth as no correlation with the oil hydrophobicity nor with the mixture composition has been found. Though, it is believed a synergy might occur between the factors affecting the droplet growth, similarly to the pure aroma compounds study.

6. Differences between A. *senegal* and A. *seyal*

Acacia gums are known to differ in the biochemical composition and AGPs conformation. The protein content of A. *senegal* and A. *seyal* are respectively 27.0 $mg.g^{-1}$[a] or 22.0 $mg.g^{-1}$[b] and 10.0 $mg.g^{-1}$[c]. Regarding the structure, A. *senegal* gum is characterized by an average molar mass of $\sim 7\times10^5$ $g.mol^{-1}$ and a branching degree of 78% while A. *seyal* gum is defined by an average molar mass of $\sim 8\times10^5$ $g.mol^{-1}$ and a branching degree of 59%.

During this Ph.D., dependencies of oil hydrophobicity on interfacial properties were found with both varieties of gums. The main difference laid in the adsorption kinetic in favor of A. *senegal*. Within the analyzed time windows, the interfacial pressures ($\Pi = \gamma_{ow} - \gamma$) reached by A. *seyal* are lower than those displayed by A. *senegal*. It was also noticeable on GA dilational rheology profiles, phase 2 and 3 were longer for the A. *seyal* gum. However, both gums reached an equivalent maximum of interfacial layer elasticity E'_{max}. This implies that the interfacial

[a] Batches n° OF110676, Chapter III
[b] Batch n° OF152413, Chapters IV and V
[c] Batches n° OF110724, Chapter III and n° OF183377 Chapter IV

structures formed by both gums are characterized by the same driving forces and rearrangement but with a kinetic difference. Results also showed elastic interphases formed by A. *seyal* gum were less hydrated than those formed by A. *senegal* gum (however, differences are subtle and need complementary confirmation). It is then supposed that in order to reach the same maximum of interfacial layer elasticity, the A. *seyal* interphase requires to be more dehydrated than the A. *senegal* one. Thus, the kinetic differences observed in particular during the phase 2 of the adsorption dynamic, could be due to the extra interphase dehydration, the lower protein content and the lower high molar mass protein-rich AGPs accessibility that leads to additional molecular rearrangements. In addition, the supposed but not demonstrated greater affinity of A. *seyal* with water [4]–[6], [47] could result in additional energy required to dehydrate the interphase.

A. *senegal* also provided significant smaller droplets size than A. *seyal* for low hydrophobic oils (e.g. 1-decanol, 1-octanol). For instance, droplet size of and 1-octanol coarse and fine A. *seyal* emulsions were respectively 2.47 and 1.21 µm, while with A. *senegal* droplet size were of about 1.31 and 0.79 µm. The factors accounting for the weaker interfacial properties of A. *seyal* could then lead to the decrease of the AGPs adsorption rate during emulsification. This could be particularly disturbing for low hydrophobic oils which are prone to (re)coalescence. Then, the low apparent viscosity of A. *seyal* dispersion (38 mPa.s for a 20 wt% concentration at 25°C) was assumed to enhance the creaming rate as compared to the emulsions produced with A. *senegal* (51 mPa.s or a 20 wt% concentration at 25°C). For instance, creaming indexes of 16.5 and 41.7% were measured for respectively d-limonene and 1-octanol emulsions stabilized by A. *senegal.* Meanwhile, the same oils stabilized by A. *seyal* displayed creaming indexes of 66.0 and 88.5% respectively.

Perspectives

- The sensitivity to the hydrophobic effect of both Acacia gums can only come from the protein part and the methyl groups of sugars. However, simply looking to specific amino acid composition does not allow to explain the hydrophobic characteristic of Acacia gum as they are marked by a relatively hydrophilic characteristic. For instance, serine and threonine are classified as polar according to Zhu and al. amino acid hydrophobicity scale [48]. In

addition, they do not have the same accessibility. Furthermore, Goodrum et al. [49] interrogated the possible implication of the secondary structure of hyperbranched sugar units in interfacial properties of gums. Thus, the origin of Acacia gum sensitivity to hydrophobic effect is worth of deeper study.

- The already foreseen relationship between the isothermal compressibility of liquids and the work of cavity formation ($\Delta G_c \sim 1/\beta_T$) was corrected in Chapter II into a correlation involving as well the volume of the liquid molecules ($\Delta G_c \sim 1/(V_M\sqrt{\beta}_T)$). At first sight, the equation suggests the contribution of the volume exceeds that of the isothermal compressibility. Thus, it would be worth identifying the importance of the volume on ΔG_c. On the other hand, the volume is known to be related to the polarizability [50], [51]. Therefore, one may also wonder whether volume fluctuations are correlated to electronic fluctuations [52]. If so, we shall be able to connect the Gibbs free energy of cavity formation to electronic properties of liquids.

- The volume perturbation amplitude of the oil-water interface is believed to be linked to the oil-water interfacial tension. However, the correlation could not be attested by calculation. To this end the density of interfacial water must be known. Then it would be possible to determine the interfacial volume fluctuations f_V^* and highlight the connection to γ_{ow}.

- The drop shape analysis method has proved to be unsuitable for studying super elastic structure with a heterogeneous distribution of AGPs, then of stresses. Other techniques such as Langmuir trough and capillary pressure tensiometry may be more appropriated [53] and should be considered for the study of the Acacia gum interfacial properties in the future. Another suggestion would be to process acquisitioned droplet images as Berry and al. work [54]. They discussed the pendant drop tensiometry complications and limitations due to both Bond number (the balance between interfacial tension and gravitational forces) and drop volume. They introduced a new parameter, the Worthington number, to characterize the measurement precision. They developed as well an open-source acquisition and fitting software that includes important discussions of potential sources of error and dynamic effects. Therefore, it would be interesting to test this technique to further study the oil-gum-water structure.

- Looking at the *TSI* (Turbiscan® Scanning Index) signal, the stability of A. *seyal* emulsions was found to exceed the stability of A. *senegal* emulsions for the two low hydrophobic

oils, 1-octanol and 1-decanol, until respectively days 4 and 14 of storage at 25°C. This is believed to be due to the greater affinity with water of A. *seyal* gum compared to A. *senegal* [4]–[6], [47]. However, this greater affinity was not demonstrated yet and need further study for confirmation.

References

[1] D. J. McCLements, *Food Emulsions Principles, Practices, and Techniques*. 2010.

[2] D. Verbeken, S. Dierckx, and K. Dewettinck, "Exudate gums: Occurrence, production, and applications," *Appl. Microbiol. Biotechnol.*, vol. 63, no. 1, pp. 10–21, 2003, doi: 10.1007/s00253-003-1354-z.

[3] C. Sanchez *et al.*, "Acacia gum: History of the future," *Food Hydrocoll.*, vol. 78, pp. 140–160, 2018, doi: 10.1016/j.foodhyd.2017.04.008.

[4] A. Davantès, M. Nigen, C. Sanchez, A. d'Orlando, and D. Renard, "Adsorption of Hyperbranched Arabinogalactan-Proteins from Plant Exudate at the Solid–Liquid Interface," *Colloids and Interfaces*, vol. 3, no. 2, p. 49, 2019, doi: 10.3390/colloids3020049.

[5] A. Davantès, M. Nigen, C. Sanchez, and D. Renard, "Adsorption Behavior of Arabinogalactan-Proteins (AGPs) fromAcacia senegalGum at a Solid-Liquid Interface," *Langmuir*, vol. 37, no. 35, pp. 10547–10559, 2021, doi: 10.1021/acs.langmuir.1c01619.

[6] V. Mejia Tamayo *et al.*, "Flexibility and hydration of amphiphilic hyperbranched arabinogalactan-protein from plant exudate: A volumetric perspective," *Colloids and Interfaces*, vol. 2, no. 1, 2018, doi: 10.3390/colloids2010011.

[7] M. Elmanan, S. Al-Assaf, G. O. Phillips, and P. A. Williams, "Studies on Acacia exudate gums: Part VI. Interfacial rheology of Acacia senegal and Acacia seyal," *Food Hydrocoll.*, vol. 22, no. 4, pp. 682–689, 2008, doi: 10.1016/j.foodhyd.2007.02.008.

[8] E. Dickinson, B. S. Murray, G. Stainsby, and D. M. W. Anderson, "Surface activity and emulsifying behaviour of some Acacia gums," *Top. Catal.*, vol. 2, no. 6, pp. 477–490, 1988, doi: 10.1016/S0268-005X(88)80047-X.

[9] R. Chanamai and D. J. McClements, "Comparison of gum arabic, modified starch, and whey protein isolate as emulsifiers: Influence of pH, CaCl2 and temperature," *J. Food Sci.*, vol. 67, no. 1, pp. 120–125, 2002, doi: 10.1111/j.1365-2621.2002.tb11370.x.

[10] E. Dickinson, V. B. Galazka, and D. M. W. Anderson, "Emulsifying behaviour of gum arabic. Part 1: Effect of the nature of the oil phase on the emulsion droplet-size distribution," *Carbohydr. Polym.*, vol. 14, no. 4, pp. 373–383, 1991, doi: 10.1016/0144-8617(91)90003-U.

[11] H. Mirhosseini, C. P. Tan, N. S. A. Hamid, and S. Yusof, "Effect of Arabic gum, xanthan gum and orange oil contents on ζ-potential, conductivity, stability, size index and pH of orange beverage emulsion," *Colloids Surfaces A Physicochem. Eng. Asp.*, 2008, doi: 10.1016/j.colsurfa.2007.07.007.

[12] A. . Soper, "Is water one liquid or two ?," *J. Chem. Phys.*, vol. 150, no. 234503, 2019, doi: 10.1063/1.5096460.

[13] C. Faucon, P. Chalier, and C. Sanchez, "On the relationship between volume

fluctuations in liquids and the Gibbs free energy of cavity formation," *J. Mol. Liq.*, vol. 364, p. 119845, 2022, doi: 10.1016/j.molliq.2022.119845.

[14] G. Graziano, "Scaled particle theory study of the length scale dependence of cavity thermodynamics in different liquids," *J. Phys. Chem. B*, vol. 110, no. 23, pp. 11421–11426, 2006, doi: 10.1021/jp0571269.

[15] R. Godawat, S. N. Jamadagni, and S. Garde, "Characterizing hydrophobicity of interfaces by using cavity formation, solute binding, and water correlations," *Proc. Natl. Acad. Sci. U. S. A.*, vol. 106, no. 36, pp. 15119–15124, 2009, doi: 10.1073/pnas.0902778106.

[16] S. N. Jamadagni, R. Godawat, and S. Garde, "Hydrophobicity of proteins and interfaces: Insights from density fluctuations," *Annu. Rev. Chem. Biomol. Eng.*, vol. 2, pp. 147–171, 2011, doi: 10.1146/annurev-chembioeng-061010-114156.

[17] G. Graziano, "Contrasting the hydration thermodynamics of methane and methanol," *Phys. Chem. Chem. Phys.*, vol. 21, no. 38, pp. 21418–21430, 2019, doi: 10.1039/c9cp03213d.

[18] R. A. Pierotti, "Aqueous Solutions of Nonpolar Gases," *J. Phys. Chem.*, vol. 69, pp. 281–288, 1965.

[19] B. Lee, "The physical origin of the low solubility of nonpolar solutes in water," *Biopolymers*, vol. 24, no. 5, pp. 813–823, 1985, doi: 10.1002/bip.360240507.

[20] M. Lucas, "Size effect in transfer of nonpolar solutes from gas or solvent to another solvent with a view on hydrophobic behavior," *J. Phys. Chem.*, vol. 80, no. 4, pp. 359–362, 1976, doi: 10.1021/j100545a004.

[21] T. V. Chalikian and R. Filfil, "How large are the volume changes accompanying protein transitions and binding?," *Biophys. Chem.*, vol. 104, no. 2, pp. 489–499, 2003, doi: 10.1016/S0301-4622(03)00037-1.

[22] K. Gekko and H. Noguchi, "Compressibility of globular proteins in water at 25°C," *J. Phys. Chem.*, vol. 83, no. 21, pp. 2706–2714, 1979, doi: 10.1021/j100484a006.

[23] K. Gekko and Y. Hasegawa, "Compressibility-Structure Relationship of Globular Proteins," *Biochemistry*, vol. 25, no. 21, pp. 6563–6571, 1986, doi: 10.1021/bi00369a034.

[24] M. Bánó and J. Marek, "How thick is the layer of thermal volume surrounding the protein?," *Biophys. Chem.*, vol. 120, no. 1, pp. 44–54, 2006, doi: 10.1016/j.bpc.2005.09.024.

[25] T. V. Chalikian, "Volumetric properties of proteins," *Annu. Rev. Biophys. Biomol. Struct.*, vol. 32, no. February 2003, pp. 207–235, 2003, doi: 10.1146/annurev.biophys.32.110601.141709.

[26] T. V. Chalikian, M. Totrov, R. Abagyan, and K. J. Breslauer, "The hydration of globular proteins as derived from volume and compressibility measurements: Cross correlating thermodynamic and structural data," *J. Mol. Biol.*, vol. 260, no. 4, pp. 588–603, 1996, doi: 10.1006/jmbi.1996.0423.

[27] V. P. Voloshin, N. N. Medvedev, N. Smolin, A. Geiger, and R. Winter, "Disentangling volumetric and hydrational properties of proteins," *J. Phys. Chem. A*, vol. 119, no. 5, pp. 1881–1890, 2015, doi: 10.1021/jp510891b.

[28] N. B. Rego and A. J. Patel, "Understanding Hydrophobic Effects: Insights from Water Density Fluctuations," *Annu. Rev. Condens. Matter Phys.*, vol. 13, no. 1, pp. 303–324, 2022, doi: 10.1146/annurev-conmatphys-040220-045516.

[29] V. R. Hande and S. Chakrabarty, "How Far Is 'Bulk Water' from Interfaces? Depends on the Nature of the Surface and What We Measure," *J. Phys. Chem. B*, vol. 126, no. 5, pp. 1125–1135, 2022, doi: 10.1021/acs.jpcb.1c08603.

[30] C. Sendner, D. Horinek, L. Bocquet, and R. R. Netz, "Interfacial water at hydrophobic and hydrophilic surfaces: Slip, viscosity, and diffusion," *Langmuir*, vol. 25, no. 18,

pp. 10768–10781, 2009, doi: 10.1021/la901314b.

[31] U. Kumar Sur, "Behaviour of water at hydrophobic interfaces," *J. Mol. Liq.*, vol. 348, p. 118433, 2022, doi: 10.1016/j.molliq.2021.118433.

[32] M. K. Coe, R. Evans, and N. B. Wilding, "Density Depletion and Enhanced Fluctuations in Water near Hydrophobic Solutes: Identifying the Underlying Physics," *Phys. Rev. Lett.*, vol. 128, no. 4, p. 45501, 2022, doi: 10.1103/physrevlett.128.045501.

[33] Q. Sun, "The physical origin of hydrophobic effects," *Chem. Phys. Lett.*, vol. 672, pp. 21–25, 2017, doi: 10.1016/j.cplett.2017.01.057.

[34] C. Q. Sun, "Supersolidity of undercoordinated and hydrating water," *Phys. Chem. Chem. Phys.*, vol. 20, no. 48, pp. 30104–30119, 2018, doi: 10.1039/c8cp06115g.

[35] C. S. Rao and S. Damodaran, "Is surface pressure a measure of interfacial water activity? Evidence from protein adsorption behavior at interfaces," *Langmuir*, vol. 16, no. 24, pp. 9468–9477, 2000, doi: 10.1021/la0007168.

[36] L. Ter-Minassian-Saraga, "Protein denaturation on adsorption and water activity at interfaces: an analysis and suggestion," *J. Colloid Interface Sci.*, vol. 80, no. 2, pp. 393–401, 1981, doi: 10.1016/0021-9797(81)90198-3.

[37] J. Bergfreund *et al.*, "Globular protein assembly and network formation at fluid interfaces: effect of oil," *Soft Matter*, pp. 1692–1700, 2021, doi: 10.1039/d0sm01870h.

[38] J. Bergfreund, P. Bertsch, and P. Fischer, "Adsorption of proteins to fluid interfaces: Role of the hydrophobic subphase," *J. Colloid Interface Sci.*, vol. 584, pp. 411–417, 2021, doi: 10.1016/j.jcis.2020.09.118.

[39] J. Bergfreund, P. Bertsch, and P. Fischer, "Effect of the hydrophobic phase on interfacial phenomena of surfactants, proteins, and particles at fluid interfaces," *Curr. Opin. Colloid Interface Sci.*, vol. 56, p. 101509, 2021, doi: 10.1016/j.cocis.2021.101509.

[40] W. Zhang, X. Xu, X. Zhao, and G. Zhou, "Insight into the oil polarity impact on interfacial properties of myofibrillar protein," *Food Hydrocoll.*, vol. 128, no. January, p. 107563, 2022, doi: 10.1016/j.foodhyd.2022.107563.

[41] F. Ravera, K. Dziza, E. Santini, L. Cristofolini, and L. Liggieri, "Emulsification and emulsion stability: The role of the interfacial properties," *Adv. Colloid Interface Sci.*, vol. 288, p. 102344, 2021, doi: 10.1016/j.cis.2020.102344.

[42] M. B. J. Meinders and T. Van Vliet, "The role of interfacial rheological properties on Ostwald ripening in emulsions," *Adv. Colloid Interface Sci.*, vol. 108–109, pp. 119–126, 2004, doi: 10.1016/j.cis.2003.10.005.

[43] D. J. Burgess and J. K. Yoon, "Influence of Interfacial Properties of Lipophilic Surfactants on Water-in-Oil Emulsion Stability," *Colloids Surfaces B Biointerfaces*, vol. 4, no. 5, pp. 297–308, 1995, [Online]. Available: http://linkinghub.elsevier.com/retrieve/pii/0927776594011799.

[44] C. Dicharry, D. Arla, A. Sinquin, A. Graciaa, and P. Bouriat, "Stability of water/crude oil emulsions based on interfacial dilatational rheology," *J. Colloid Interface Sci.*, vol. 297, no. 2, pp. 785–791, 2006, doi: 10.1016/j.jcis.2005.10.069.

[45] T. C. Botti, A. Hutin, E. Quintella, and M. S. Carvalho, "Effect of interfacial rheology on drop coalescence in water-oil emulsion," *Soft Matter*, vol. 18, no. 7, pp. 1423–1434, 2022, doi: 10.1039/d1sm01382c.

[46] M. Geng *et al.*, "Effects of different nut oils on the structures and properties of gel-like emulsions induced by ultrasound using soy protein as an emulsifier," *Int. J. Food Sci. Technol.*, vol. 56, no. 4, pp. 1649–1660, 2021, doi: 10.1111/ijfs.14786.

[47] C. Aphibanthammakit, M. Nigen, S. Gaucel, C. Sanchez, and P. Chalier, "Surface properties of Acacia senegal vs

Acacia seyal films and impact on specific functionalities," *Food Hydrocoll.*, vol. 82, pp. 519–533, 2018, doi: 10.1016/j.foodhyd.2018.04.032.

[48] C. Zhu *et al.*, "Characterizing hydrophobicity of amino acid side chains in a protein environment via measuring contact angle of a water nanodroplet on planarpeptide network," *Proc. Natl. Acad. Sci. U. S. A.*, vol. 113, no. 46, pp. 12946–12951, 2016, doi: 10.1073/pnas.1616138113.

[49] L. J. Goodrum, A. Patel, J. F. Leykam, and M. J. Kieliszewski, "Gum arabic glycoprotein contains glycomodules of both extensin and arabinogalactan-glycoproteins," *Phytochemistry*, vol. 54, no. 1, pp. 99–106, 2000, doi: 10.1016/S0031-9422(00)00043-1.

[50] E. Caldeweyher, C. Bauer, and A. S. Tehrani, "An open-source framework for fast-yet-accurate calculation of quantum mechanical features," *Phys. Chem. Chem. Phys.*, vol. 24, no. 17, pp. 10599–10610, 2022, doi: 10.1039/d2cp01165d.

[51] P. Szabó, S. Góger, J. Charry, M. R. Karimpour, D. V. Fedorov, and A. Tkatchenko, "Four-Dimensional Scaling of Dipole Polarizability in Quantum Systems," *Phys. Rev. Lett.*, vol. 128, no. 7, pp. 1–19, 2022, doi: 10.1103/PhysRevLett.128.070602.

[52] E. S. Minina, E. S. Pyanzina, E. V. Novak, and S. S. Kantorovich, "Compressibility of ferrofluids: Towards a better understanding of structural properties," *Eur. Phys. J. E*, vol. 41, no. 5, 2018, doi: 10.1140/epje/i2018-11678-7.

[53] R. Stanimirova, K. Marinova, S. Tcholakova, N. D. Denkov, S. Stoyanov, and E. Pelan, "Surface rheology of saponin adsorption layers," *Langmuir*, vol. 27, no. 20, pp. 12486–12498, 2011, doi: 10.1021/la202860u.

[54] J. D. Berry, M. J. Neeson, R. R. Dagastine, D. Y. C. Chan, and R. F. Tabor, "Measurement of surface and interfacial tension using pendant drop tensiometry," *J. Colloid Interface Sci.*, vol. 454, pp. 226–237, 2015, doi: 10.1016/j.jcis.2015.05.012.

Valorisation des travaux de recherche

Published article

C. Faucon, P. Chalier, C. Sanchez, (2022). On the relationship between volume fluctuations in liquids and the Gibbs free energy of cavity formation. Journal of Molecular Liquids, Volume 364, 119845. https://doi.org/10.1016/j.molliq.2022.119845.

Article waiting for approval

C. Faucon, P. Chalier, C. Sanchez. Natural hyperbranched biopolymer at liquid interfaces differing in oil-water interaction energy.

Articles waiting for submission

C. Faucon, P. Chalier, C. Sanchez. Effect of the oil hydrophobicity on the stability and structure of Acacia *senegal* gum oil-in-water emulsion.

C. Faucon, P. Chalier, C. Sanchez. Effect of a mixture of two oils of different hydrophobicity on the interfacial properties of Acacia *senegal* gum at oil – water interfaces.

Poster in international congress

C. Faucon, P. Chalier, C. Sanchez. *Interfacial adsorption mechanism of Acacia gum: the effect of aroma hydrophobicity*, European Colloid & Interface Society (ECIS), Athens (Greece), September 5-10, 2021.

Oral presentation in national congress

C. Faucon, P. Chalier, C. Sanchez. *Adsorption mechanism of Acacia gum to fluid interfaces: the effect of fluid hydrophobicity, Séminaire du groupe « Protein Interactions assembly », November 25, 2021.*

Annexes

A. Résumé en français

1. Introduction

La gomme d'acacia (GA, E414) est définie comme un exsudat gommeux produit par les arbres d'Acacia *senegal* (A. *senegal*) ou d'Acacia *seyal* (A. *seyal*). Appelée aussi gomme arabique, elle provient d'un mécanisme de protection en réaction à un stress environnemental, telles que des conditions climatiques extrêmes ou une invasion d'insectes et de moisissures [1]. La gomme d'Acacia est principalement récoltée dans les régions arides de la ceinture sub-saharienne, s'étendant du Sénégal à l'Afrique de l'Est, mais également au Pakistan et en Inde [2].

Les exsudats de gomme d'Acacia sont composés de protéines arabinogalactanes (AGPs), faiblement chargées, hyperbranchées avec une forte proportion de sucres neutres (L-arabinose, D-galactose, L-rhamnose) et chargés (acide glucuronique et 4-O-methyl acide glucuronique), mais comporte aussi des protéines (1-3%) et des minéraux. Bien que les AGPs soient principalement des solutés hydrophiles en raison de leur teneur élevée en sucres [9] et de leur composition spécifique en acides aminés riches en espèces hydrophiles [3]–[5], elles sont sensibles à l'effet hydrophobe. La dualité protéine/polysaccharide de la gomme lui confère des propriétés amphiphiles qui permettent son adsorption aux interfaces gaz-liquide, liquide-liquide et solide-liquide [3]. Ainsi, la gomme permet de réduire la tension interfaciale entre la phase dispersée et la phase continue d'une émulsion et de former une barrière viscoélastique interfaciale autour des gouttelettes, favorisant leur formation et leur stabilité [6]–[10].

2. Objectifs de la thèse

Les consommateurs et les préoccupations environnementales conduisent à la nécessité de développer des produits "entièrement naturels" et parfois uniquement à base de plantes. C'est pourquoi selon notre partenaire industriel Alland&Robert, la demande en gomme d'Acacia (GA) ne cesse d'augmenter. Par conséquent, de nombreuses entreprises alimentaires étudient

la possibilité de remplacer les ingrédients synthétiques usuels par des ingrédients naturels [11]. Un défi consiste alors à élargir les applications de la gomme d'Acacia, en améliorant nos connaissances sur sa composition, sa structure et ses propriétés techno-fonctionnelles. Dans l'industrie alimentaire, la gomme d'Acacia peut être utilisée pour la production de boissons, et plus spécifiquement pour la stabilisation des émulsions d'arômes [1], [12]. Dans ce contexte, ces travaux de thèse s'insèrent dans un projet visant à acquérir des connaissances sur les mécanismes impliqués dans les émulsions d'arômes stabilisées par la gomme d'Acacia. Le but est dans un premier temps de mieux appréhender l'origine des propriétés de surface de la gomme, puis éventuellement d'étendre son champ d'application à une plus large gamme de composés d'arôme.

L'objectif principal est d'étudier l'influence de l'eau et plus particulièrement des interactions avec le groupe hydroxyle (OH) de l'eau, sur les mécanismes impliqués dans la formation d'une interphase arôme-gomme-eau, ainsi que sur la stabilité des émulsions. Pour cela, nous avons fait varier l'hydrophobicité du composé d'arôme (n-hexadécane, myrcène, d-limonène, octanoate d'éthyle, octanoate de méthyle, carvone, 1-décanol, 1-octanol) et utilisé les deux espèces commercialisées de la gomme d'Acacia, *i.e.* l'Acacia *senegal* et l'Acacia *seyal*. Les objectifs spécifiques de l'étude sont : (i) de caractériser les propriétés thermodynamiques des liquides dans le but de comprendre les différences fondamentales entre l'eau et les composés hydrophobes en termes de fluctuations de volume et d'énergie d'interaction, (ii) d'examiner l'impact de l'hydrophobicité de l'arôme sur les mécanismes de structure et de formation de l'interphase arôme-gomme-eau, ainsi que (iii) sur l'homogénéisation conduisant à la formation de gouttelettes et sur la stabilité de l'émulsion. Le dernier objectif spécifique est (iv) d'étudier si la présence de plus d'un composé dans la phase dispersée affecte les interphases arôme-gomme-eau et la stabilité des émulsions d'Acacia *senegal*.

L'eau est définie par de faibles fluctuations de volume microscopiques.

Les fluctuations microscopiques de volume sont une signature de la structure d'un liquide et de son énergie intermoléculaire. Soper [13] a suggéré que le paramètre thermodynamique f_V pouvait être utilisé pour décrire l'importance des fluctuations de masse volumique dans un volume donné d'un liquide. En convertissant ce paramètre sans dimension en volume, l'eau s'est révélée être caractérisée par la plus faible quantité de fluctuations de volume à l'échelle nanométrique (1 nm^3) par rapport à plus de 200 autres liquides. Par exemple, la quantité

estimée pour l'eau était de 0.13×10^{-2} nm^3 [14], contre 2.91×10^{-2} nm^3 pour le composé le plus hydrophobe que nous avons sélectionné pour étudier les propriétés interfaciales et émulsifiantes de la gomme (n-hexadécane). Ensuite, les calculs basés sur la théorie « scaled particle » ont confirmé que ces fluctuations de volume étaient corrélées à l'énergie libre de Gibbs de formation de cavités ΔG_c. Il s'agit d'un autre paramètre reflétant l'étendue de l'énergie intermoléculaire d'un liquide [15] et est le premier responsable de la "solubilité" ou de l'"insolubilité" de solutés plus ou moins hydrophobes. Comme déjà discuté dans la littérature [16], [17], nous avons constaté qu'une plus grande quantité de fluctuations de volume permettait de diminuer l'énergie nécessaire pour former une cavité (Fig. 1).

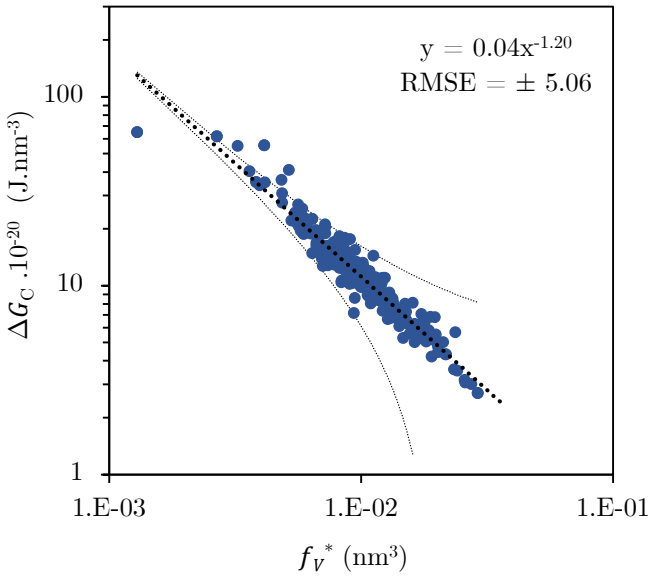

Fig. 1. Graphique log-log de la corrélation entre l'énergie libre de Gibbs (à l'échelle volumétrique) de la formation d'une cavité sphérique de rayon $r_c = 0.12$ nm et les fluctuations de masse volumique en unité de volume (à 25°C).

En conséquence, la création d'une cavité de rayon égale à 0.12 nm dans l'eau nécessite la plus grande énergie ici calculée (65×10^{-20} J.nm^{-3}) par rapport aux autres liquides (2.7×10^{-20} J.nm^{-3} pour le n-hexadécane). Par ailleurs, la formation d'une cavité est prise en compte dans la description théorique du processus de solvatation d'une molécule de soluté dans un solvant. En effet, le processus de solvatation peut être divisé en deux étapes hypothétiques : (a) la formation d'une cavité de la taille de la molécule de soluté ; (b) l'introduction du soluté dans la cavité avec activation des interactions attractives soluté-solvant [18], [19]. Le ΔG_c de l'eau permet alors d'illustrer la complexité de solubiliser un soluté non polaire dans l'eau, supposée être corrélée à la petite taille de la molécule d'eau [15], [20], [21].

L'intérêt d'étudier de tels paramètres thermodynamiques est qu'ils sont liés aux propriétés moléculaires intrinsèques du soluté et aux interactions soluté-solvant, plus particulièrement à la flexibilité et à l'hydratation du soluté [22]. Par exemple, l'hydrophobicité des protéines et leurs propriétés de surface ont été reliées à leurs propriétés volumétriques d'hydratation [23]–[28]. Ainsi, les propriétés volumétriques des biopolymères sont des déterminants importants de leur fonctionnalité. Autre avantage, elles permettent la description de propriétés thermodynamiques macroscopiques et en particulier de la structure des systèmes interfaciaux.

L'adsorption de la gomme d'Acacia aux interfaces arôme-eau peut être décrite par un mécanisme volumétrique en 3 phases guidé par les interactions avec l'eau.

L'état thermodynamique des AGPs, ou plus en général des solutés, peut être appréhendé via leur impact sur le solvant. La solubilisation de la gomme d'Acacia, c'est-à-dire d'un soluté de taille significative (M_w = 7-8×10^5 g.mol^{-1}, R_h = 15-25 nm) dans l'eau, conduit à une perturbation conséquente du réseau de liaisons hydrogènes et à une réduction importante de l'entropie [29]. De plus, la teneur en protéines des AGPs, leur distribution, leur accessibilité, ainsi que la présence de minéraux (Ca), rendent la gomme sensible aux effets hydrophobes induits par l'eau. L'eau tend ainsi à exclure les AGPs de la solution afin de minimiser la pénalité entropique. D'autre part, l'interface arôme-eau génère une zone de 1 à 6 Å déplétée en molécules d'eau (appelée le gap hydrophobe) [30]–[32], qui présente des caractéristiques d'eau sous forme vapeur [33] et des fluctuations de masse volumique prononcées [16], [23]. Par conséquent, les interactions eau-eau, arôme-eau et AGP-eau constituent la force motrice de l'adsorption en trois phases de la gomme d'Acacia (Fig. 2). Les fluctuations de volume plus intenses près des interfaces macroscopiques et hydrophobes ainsi que l'effet hydrophobe présent dans l'eau en solution, conduisent les AGPs à se concentrer à l'interface arôme-eau en déplaçant d'abord un volume équivalent d'eau (phase 1). Ensuite, les AGPs s'accumulent, interagissent et constituent un réseau à l'échelle macroscopique, entraînant la formation d'une couche interfaciale viscoélastique. L'interface 2D peut être alors considérée comme une interphase 3D. Au fur et à mesure de l'adsorption, le nombre de molécules et les interactions augmentent jusqu'à ce qu'un seuil soit atteint et qu'un état de transition soit observé. Le système arôme-gomme-eau passe alors d'un état visqueux prédominant avec dissipation d'énergie à un état élastique (phase 2). Par la suite, la structure la plus efficace est atteinte lorsque l'élasticité est à son maximum et présente des teneurs en eau ne dépassant pas les 30%

(ce qui correspond au taux d'hydratation estimé pour la fraction protéique des AGPs [6]). Cependant, le système continue de se développer. Les AGPs s'agglomèrent dans l'interphase. Les hétérogénéités de distribution des contraintes à la surface entraînent alors une perte d'élasticité et le plissement de la surface de la goutte (phase 3).

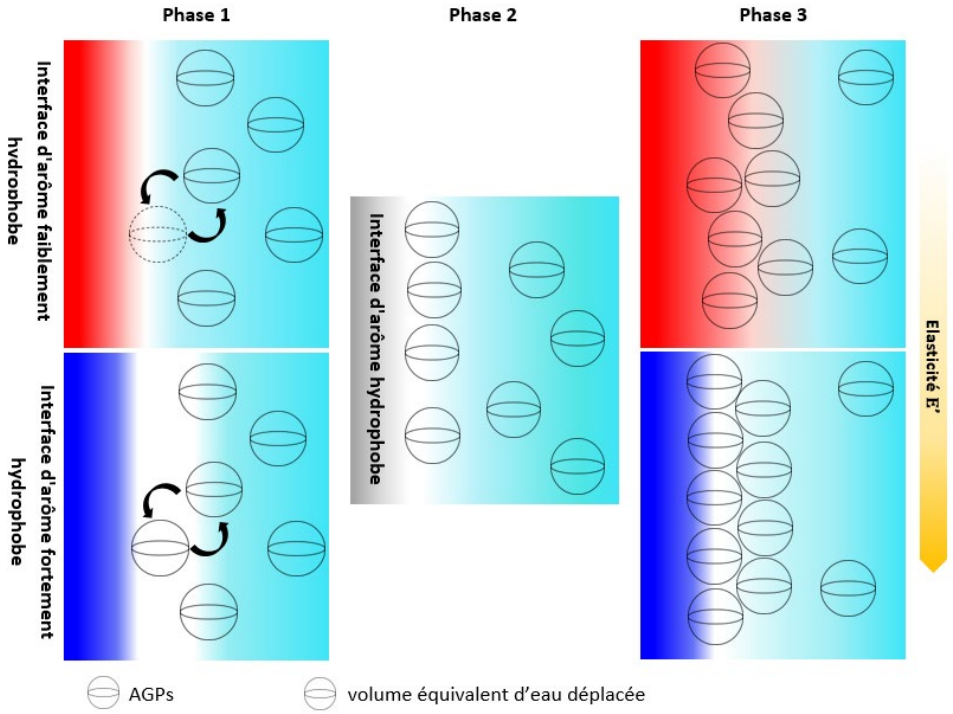

Fig. 2. Représentation schématique de l'adsorption de la gomme d'Acacia aux interfaces arôme-eau. La zone bleu clair représente l'eau en solution ; la zone blanche représente l'eau interfaciale (les épaisseurs de l'interphase et de la région sur laquelle les propriétés de l'eau interfaciale diffèrent de celles de l'eau en solution ne sont pas connues et ne sont donc pas à l'échelle).

L'hydrophobicité de l'arôme contribue à l'adsorption de la gomme d'Acacia.

Les résultats ont confirmé que l'adsorption des molécules d'AGPs était plus favorable aux interfaces d'arômes très hydrophobes. Le modèle de structure en deux phases de l'eau proposé par Sun [34], [35] ainsi que l'activité thermodynamique interfaciale de l'eau a_w^s [36], ont permis la description thermodynamique de l'interphase arôme-gomme-eau et de mettre en évidence le rôle des interactions arôme-eau. L'activité thermodynamique de l'eau est estimée en utilisant l'équation $\Pi = -RT\,\Gamma_w\,ln\,a_w^s$ [36], [37] avec Π la pression de surface, R la constante des gaz, T la température, et Γ_w la quantité molaire d'eau par unité de surface de l'interface. Ainsi, la pression de surface peut être directement décrite par les propriétés thermodynamiques de l'eau. De plus, l'a_w^s et le modèle de Sun permettent de corréler l'influence de l'hydrophobicité du composé d'arôme sur l'adsorption de la gomme avec les interactions arôme-eau. Ces dernières

ont montré un impact significatif sur la phase 1 de l'adsorption de la gomme d'Acacia mais affectent également le réarrangement des AGPs pendant les phases 2 et 3. La nature de l'arôme est également importante puisque l'absence d'interactions fortes entre l'arôme et l'eau dans l'interphase conduit à la diminution du nombre de coordination de l'eau. Les premières couches hydratées de l'interphase sont marquées par une prédominance des liaisons de van der Waals H:O, tandis que les couches plus éloignées subissent une délocalisation et une densification des électrons (ce qui entraîne une augmentation de la tension interfaciale). Les interphases des arômes hautement hydrophobes sont donc définies par une diminution de la force du réseau de liaisons hydrogènes de l'eau, ce qui entraîne la vaporisation partielle de l'eau et donc une augmentation des fluctuations de volume. Ce phénomène contribue alors à la diminution du coût énergétique de l'adsorption des AGPs. Cela est particulièrement visible sur les profils rhéologiques interfaciaux de la gomme. Deux courbes maîtresses ont été obtenues en traçant le module élastique normalisé E'/E'_{max} en fonction de la tension interfaciale normalisée γ/γ_{ow} (Fig. 3). Une première courbe est observée pour les composés les plus hydrophobes, à savoir le n-hexadécane, le myrcène, le d-limonène purifié, le d-limonène pur à 97%, l'octanoate d'éthyle, l'octanoate de méthyle et la carvone. Une deuxième courbe maîtresse regroupe les alcools, c'est-à-dire les arômes les moins hydrophobes. La différence entre les deux groupes dépend alors de la présence de groupements chimiques renforçant les interactions avec l'eau, à savoir les groupements hydroxyles OH.

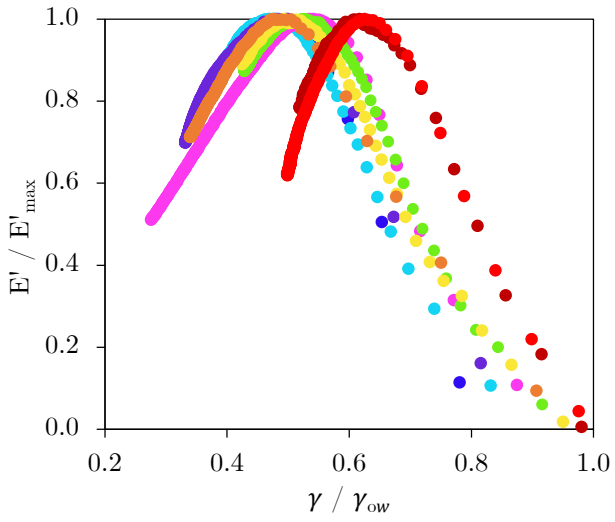

Fig. 3. Module élastique de dilatation E' normalisé par E'_{max} représenté par rapport à la tension interfaciale arôme - GA - eau normalisée par γ_{ow} pour une concentration de 5 %m en A. *senegal* à 25°C. (●) n-Hexadécane, (●) Myrcène, (●) d-Limonène purifié, (●) d-Limonène 97%, (●) Octanoate d'éthyle, (●) Octanoate de méthyle, (●) Carvone, (●) 1-Décanol, (●) 1-Octanol.

De plus, l'hydrophobicité de l'arôme affecte également le réarrangement des AGPs dans l'interphase. Un composé de faible hydrophobicité induit un réseau de couches d'AGPs moins compact et moins ordonné. L'interface gomme-arôme est aussi moins délimitée. Ainsi,

l'efficacité de l'adsorption de la gomme augmente avec l'hydrophobicité du composé d'arôme. Tout comme les protéines [38]–[41], l'hydrophobicité de l'arôme permet alors d'améliorer la concentration en gomme à l'interphase de l'arôme, l'élasticité de la couche interfaciale et la réduction de la tension (Fig. 4).

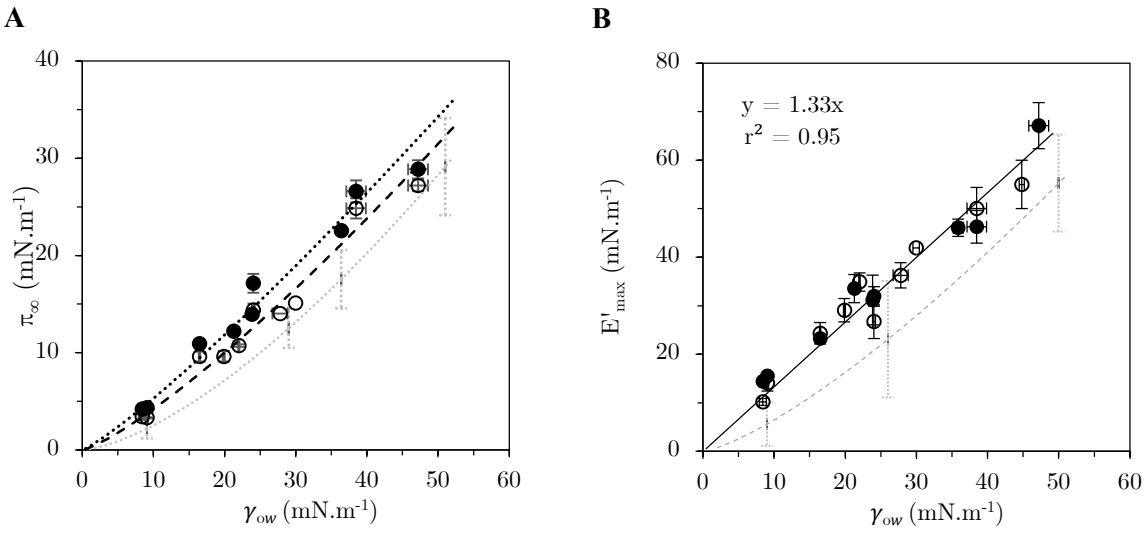

Fig. 4. (A) Corrélation entre la pression interfaciale arôme-gomme-eau Π_∞ et la tension interfaciale arôme-eau γ_{ow}. Les courbes noires en pointillés et tirets représentent respectivement les ajustements pour la gomme A. *senegal* concentrée à 5 %m (●) ($y = 0.36x^{1.16}$) et pour la gomme A. *seyal* concentrée à 5 %m (○) ($y = 0.24x^{1.25}$) ; la courbe grise en pointillés provient des travaux de Bergfreund et al. Elle représente l'ajustement pour 10 mg.L^{-1} de protéines ($y = 0.08x^{1.5}$) [39]. **(B)** Corrélation entre le module élastique maximal E'$_{max}$ et la tension interfaciale arôme-eau γ_{ow}. La courbe noire représente l'ajustement pour les deux gommes A. *senegal* (●) *et A. seyal* (○) concentrées à 5 %m ($y = 1.33x$) ; la courbe grise en pointillés provient des travaux de Bergfreund et al. et représente l'ajustement pour 10 mg.L^{-1} de protéines [38].

Etude des phases dispersées constituées de mélanges de composés : le composé le moins hydrophobe s'accumule préférentiellement à l'interface avec l'eau.

Les interfaces arôme-eau constituées d'un mélange d-limonène:1-octanol ont été étudiées et comparées aux interfaces arôme-eau constituées de d-limonène et 1-octanol purs. Ces deux arômes diffèrent de par leur hydrophobicité, le d-limonène est caractérisé par une grande hydrophobicité contrairement au 1-octanol. L'étude a permis de mettre en évidence que la présence de plusieurs composés dans la phase dispersée impactait l'hydrophobicité du mélange, qui à son tour influençait les propriétés interfaciales de la gomme. Les composés faiblement hydrophobes s'accumulent préférentiellement à l'interface de l'eau afin de réduire les interactions défavorables avec l'eau. Par conséquent, même la plus petite trace de composés

faiblement hydrophobes est suffisante pour réduire considérablement la tension interfaciale arôme-eau, et ainsi modifier la structure arôme-gomme-eau. Ceci a également été confirmé par l'étude des interfaces arôme-eau de l'huile essentielle d'orange ainsi que des mélanges d-limonène:carvone, MCT (Medium-chain triglycerides):1-octanol et MCT:huile essentielle d'orange.

L'interface d-limonène:1-octanol-eau peut être définie comme décrit dans la Fig. 5. Les molécules de 1-octanol sont orientées de telle sorte que le groupe hydroxyle fait face aux molécules d'eau. Cette configuration permet de faciliter les interactions hydrogènes et de van der Waals, tout en réduisant le contact défavorable entre la chaîne carbonée du 1-octanol et l'eau.

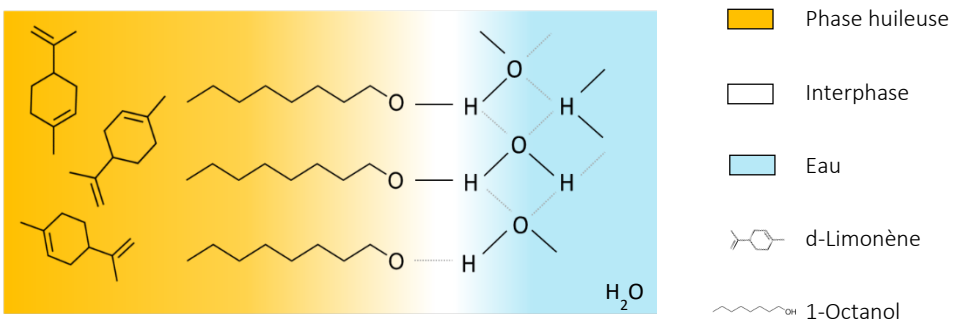

Fig. 5. Représentation schématique de l'interface d-limonène:1-octanol-eau. La couleur bleu clair représente la phase aqueuse, la couleur jaune représente la phase huileuse et la couleur blanche l'interphase (les épaisseurs de l'interphase et de la région sur laquelle les propriétés de l'eau interfaciale diffèrent de celles de l'eau en solution ne sont pas connues et ne sont donc pas à l'échelle).

Le mécanisme d'adsorption des AGPs reste inchangé en présence d'un second composé d'arôme. Ceci peut être démontré en comparant les profils rhéologiques obtenus pour le mélange d-limonène:1-octanol au ratio 0.6 avec le linalool, un composé d'arôme pur. Les deux phases huileuses sont définies par une tension interfaciale huile-eau de ~12.0 $mN.m^{-1}$. La superposition des profils viscoélastiques permet de mettre en évidence que le module élastique et la tension interfaciale dépendent seulement de l'hydrophobicité de l'huile et non du nombre de composés d'arôme (1 ou 2) (Fig. 6).

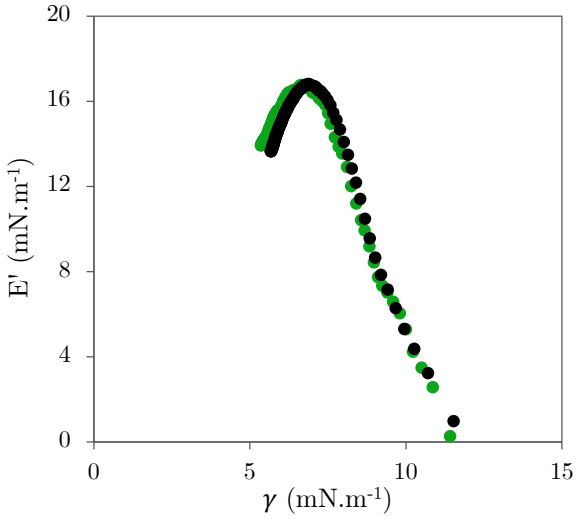

Fig. 6. Évolution du module élastique E' avec la tension interfaciale pour une solution de gomme A. *senegal* concentrée à 5 %m. Les phases huileuses sont composées d'un mélange d-limonène:1-octanol au ratio 0.6 (●) ou de linalool pur (●).

L'hydrophobicité de l'arôme contribue à diminuer le crémage et la coalescence des gouttelettes des émulsions fines d'Acacia *senegal*.

La composition de la phase dispersée influence la stabilité thermodynamique des émulsions. La comparaison des taux de crémage obtenus pour les composés ayant des masses volumiques comparables (n-hexadécane, d-limonène, octanoate d'éthyle, 1-décanol et 1-octanol) conduit à l'hypothèse que l'hydrophobicité du composé est la force motrice de la séparation gravitationnelle. Seul le crémage de l'émulsion de carvone ne s'aligne pas avec les autres points (Fig. 7). Ce résultat pouvait être attendu puisque l'émulsion de carvone est caractérisée par la plus faible différence de masse volumique entre la phase dispersée et la phase continue. Ceci souligne l'intérêt d'utiliser des agents « alourdisseurs » afin de réduire l'écart de masse volumique et ainsi, retarder les phénomènes de migration des gouttelettes.

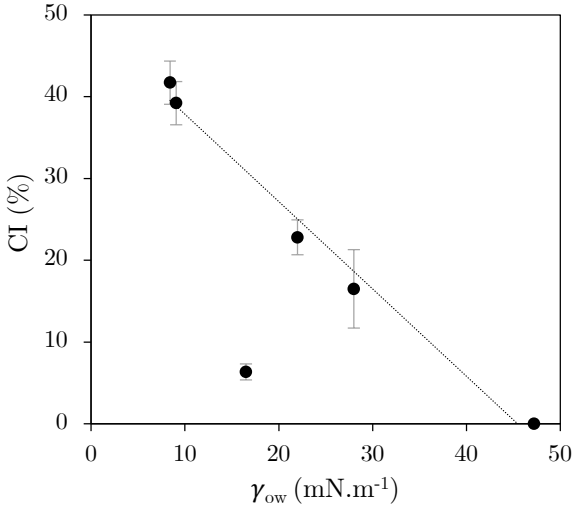

Fig 7. Indice de crémage CI après 28 jours de stockage à 25°C d'émulsions de 5 %m de 1-octanol, 1-décanol, carvone, octanoate d'éthyle, d-limonène et n-hexadécane stabilisées par 20 %m de gomme A. *senegal* en fonction de la tension interfaciale arôme-eau γ_{ow}.

L'étude a également mis en évidence une relation linéaire entre l'hydrophobicité de l'arôme et l'augmentation de la taille des gouttelettes due à la coalescence, à la floculation et/ou au mûrissement d'Ostwald après 1h de stockage. Cependant, cette corrélation linéaire s'affaiblit au fur et à mesure que le temps de stockage augmente, avant de disparaître complètement après 28 jours de stockage. Une des hypothèses expliquant cette perte de corrélation est l'interdépendance des processus de déstabilisation qui s'influencent mutuellement.

Une autre relation est observée entre l'hydrophobicité de l'arôme et la taille des gouttelettes des pré-émulsions homogénéisées à l'aide d'un mélangeur à haut cisaillement. Ce résultat pouvait également être attendu puisque sous les conditions de procédé utilisées, la tension interfaciale est la principale variable affectant les mécanismes de fragmentation des gouttelettes. Il a également été démontré que cette corrélation restait valable pour un mélange de deux composés d'arôme d'hydrophobicité différente.

Différences entre A. *senegal* et A. *seyal*

Les gommes diffèrent de par leur composition biochimique et par la conformation des AGPs. Les teneurs en protéines des gommes A. *senegal* et A. *seyal* sont respectivement de 27.0 $mg.g^{-1}$[a] ou 22.0 $mg.g^{-1}$[b] et 10.0 $mg.g^{-1}$[c]. En ce qui concerne la structure, la gomme A. *senegal* est caractérisée par une masse molaire moyenne de $\sim 7\times10^5$ $g.mol^{-1}$ et un taux de ramification de 78% tandis que la gomme A. *seyal* est définie par une masse molaire moyenne de $\sim 8\times10^5$ $g.mol^{-1}$ et un taux de ramification de 59%.

Au cours de ces travaux de thèse, les propriétés interfaciales des deux gommes se sont montrées impactées par l'hydrophobicité de l'arôme. La principale différence réside dans la cinétique d'adsorption (A. *senegal* étant la plus rapide). Dans les fenêtres de temps étudiées, les pressions interfaciales ($\Pi = \gamma_{ow} - \gamma$) obtenues avec A. *seyal* sont plus faibles que celles obtenues avec A. *senegal*. Il est également possible d'observer la différence de cinétique sur les profils rhéologiques, les phases 2 et 3 s'étendent sur des temps plus longs pour l'A. *seyal*. Cependant, les deux gommes ont atteint un maximum équivalent d'élasticité E'_{max}. Cela implique que les structures interfaciales formées par les deux gommes sont caractérisées par les mêmes forces motrices et les mêmes réarrangements. Les résultats ont également montré que les structures

[a] Batches n° OF110676, Chapitre III
[b] Batch n° OF152413, Chapitres IV et V
[c] Batches n° OF110724, Chapitre III et n° OF183377 Chapitre IV

élastiques formées par la gomme A. *seyal* étaient moins hydratées que celles formées par la gomme A. *senegal* (cependant les différences sont subtiles et nécessitent une confirmation complémentaire). Nous pouvons alors supposer que pour atteindre la même élasticité de structure, l'interphase A. *seyal* doit être davantage déshydratée que l'interphase A. *senegal*. Ainsi, les différences de cinétiques observées en particulier pendant la phase 2 de la dynamique d'adsorption, pourraient être causées à la fois par la déshydratation supplémentaire de l'interphase, à la plus faible teneur en protéines et à leur plus faible accessibilité. De plus, la plus grande affinité (supposée mais non démontrée) de la gomme A. *seyal* avec l'eau [3]–[5], [42] pourrait nécessiter une énergie supplémentaire pour déshydrater l'interphase.

Les émulsions d'arômes faiblement hydrophobes (e.g. 1-décanol, 1-octanol) stabilisées par la gomme A. *senegal* sont caractérisées par une taille de gouttelettes significativement plus petite que celles stabilisées par A. *seyal*. Par exemple, la taille moyenne des gouttelettes des pré-émulsions et des émulsions fines de 1-octanol stabilisées par A. *seyal* était respectivement de 2.47 et 1.21 µm. Sous les mêmes conditions, la gomme A. *senegal* a permis d'obtenir des tailles moyennes de 1.31 et 0.79 µm. Les mêmes facteurs à l'origine des plus faibles propriétés interfaciales de la gomme A. *seyal* pourraient limiter l'adsorption des AGPs pendant l'émulsification. Ceci pourrait être particulièrement marqué pour les arômes faiblement hydrophobes et enclins à la (re)coalescence. De plus, la faible viscosité apparente de la solution d'A. *seyal* (38 mPa.s pour une concentration de 20 %m à 25°C) pourrait expliquer le crémage plus important comparé aux émulsions produites avec la gomme A. *senegal* (51 mPa.s pour une concentration de 20 %m à 25°C). Par exemple, des indices de crémage de 16.5 et 41.7% ont été mesurés pour les émulsions de d-limonène et de 1-octanol stabilisées par A. *senegal*. En revanche, les mêmes arômes stabilisés par A. *seyal* ont présenté des indices de crémage de 66.0 et 88.5% respectivement (Tableau 1).

Tableau 1. Diamètres volumétriques des gouttelettes $D_{4,3}$ et indice de crémage CI des émulsions de 1-octanol et de d-limonène stabilisées par 20 %m d'A. *senegal* ou d'A. *seyal* après 28 jours de stockage à 25°C.

Classe chimique	Nom	A. *senegal* $D_{4,3}$ (µm)	A. *seyal* $D_{4,3}$ (µm)	A. *senegal* CI (%)	A. *seyal* CI (%)
Terpène	d-Limonène	0.54	0.50	16.5 (±4.8)	66.0 (±1.0)
Alcool	1-Octanol	0.79	1.21	41.7 (±2.7)	88.5 (±1.2)

Pour conclure, cette thèse a permis de mettre en évidence le rôle de l'eau et plus particulièrement des interactions hydrogènes et de van der Waals du groupe hydroxyle (OH) de l'eau, sur les mécanismes impliqués dans la formation d'une interphase arôme-gomme-eau. Elles sont à l'origine de l'adsorption de la gomme aux interfaces liquides-liquides et régissent la structure et l'élasticité interfaciale de la gomme, qui à son tour impacte la stabilité des émulsions.

Références

[1] C. Sanchez *et al.*, "Acacia gum: History of the future," *Food Hydrocoll.*, vol. 78, pp. 140–160, 2018, doi: 10.1016/j.foodhyd.2017.04.008.

[2] C. O. Cecil, "Gum arabic," *Saudi Aramco World*, vol. 56(2), pp. 36–39, 2005.

[3] A. Davantès, M. Nigen, C. Sanchez, A. d'Orlando, and D. Renard, "Adsorption of Hyperbranched Arabinogalactan-Proteins from Plant Exudate at the Solid–Liquid Interface," *Colloids and Interfaces*, vol. 3, no. 2, p. 49, 2019, doi: 10.3390/colloids3020049.

[4] A. Davantès, M. Nigen, C. Sanchez, and D. Renard, "Adsorption Behavior of Arabinogalactan-Proteins (AGPs) fromAcacia senegalGum at a Solid-Liquid Interface," *Langmuir*, vol. 37, no. 35, pp. 10547–10559, 2021, doi: 10.1021/acs.langmuir.1c01619.

[5] V. Mejia Tamayo *et al.*, "Flexibility and hydration of amphiphilic hyperbranched arabinogalactan-protein from plant exudate: A volumetric perspective," *Colloids and Interfaces*, vol. 2, no. 1, 2018, doi: 10.3390/colloids2010011.

[6] M. Elmanan, S. Al-Assaf, G. O. Phillips, and P. A. Williams, "Studies on Acacia exudate gums: Part VI. Interfacial rheology of Acacia senegal and Acacia seyal," *Food Hydrocoll.*, vol. 22, no. 4, pp. 682–689, 2008, doi: 10.1016/j.foodhyd.2007.02.008.

[7] E. Dickinson, B. S. Murray, G. Stainsby, and D. M. W. Anderson, "Surface activity and emulsifying behaviour of some Acacia gums," *Top. Catal.*, vol. 2, no. 6, pp. 477–490, 1988, doi: 10.1016/S0268-005X(88)80047-X.

[8] R. Chanamai and D. J. McClements, "Comparison of gum arabic, modified starch, and whey protein isolate as emulsifiers: Influence of pH, CaCl2 and temperature," *J. Food Sci.*, vol. 67, no. 1, pp. 120–125, 2002, doi: 10.1111/j.1365-2621.2002.tb11370.x.

[9] E. Dickinson, V. B. Galazka, and D. M. W. Anderson, "Emulsifying behaviour of gum arabic. Part 1: Effect of the nature of the oil phase on the emulsion droplet-size distribution," *Carbohydr. Polym.*, vol. 14, no. 4, pp. 373–383, 1991, doi: 10.1016/0144-8617(91)90003-U.

[10] H. Mirhosseini, C. P. Tan, N. S. A. Hamid, and S. Yusof, "Effect of Arabic gum, xanthan gum and orange oil contents on ζ-potential, conductivity, stability, size index and pH of orange beverage emulsion," *Colloids Surfaces A Physicochem. Eng. Asp.*, 2008, doi: 10.1016/j.colsurfa.2007.07.007.

[11] D. J. McCLements, *Food Emulsions Principles, Practices, and Techniques*. 2010.

[12] D. Verbeken, S. Dierckx, and K. Dewettinck, "Exudate gums: Occurrence, production, and applications," *Appl.*

Microbiol. Biotechnol., vol. 63, no. 1, pp. 10–21, 2003, doi: 10.1007/s00253-003-1354-z.

[13] A. . Soper, "Is water one liquid or two ?," *J. Chem. Phys.*, vol. 150, no. 234503, 2019, doi: 10.1063/1.5096460.

[14] C. Faucon, P. Chalier, and C. Sanchez, "On the relationship between volume fluctuations in liquids and the Gibbs free energy of cavity formation," *J. Mol. Liq.*, vol. 364, p. 119845, 2022, doi: 10.1016/j.molliq.2022.119845.

[15] G. Graziano, "Scaled particle theory study of the length scale dependence of cavity thermodynamics in different liquids," *J. Phys. Chem. B*, vol. 110, no. 23, pp. 11421–11426, 2006, doi: 10.1021/jp0571269.

[16] R. Godawat, S. N. Jamadagni, and S. Garde, "Characterizing hydrophobicity of interfaces by using cavity formation, solute binding, and water correlations," *Proc. Natl. Acad. Sci. U. S. A.*, vol. 106, no. 36, pp. 15119–15124, 2009, doi: 10.1073/pnas.0902778106.

[17] S. N. Jamadagni, R. Godawat, and S. Garde, "Hydrophobicity of proteins and interfaces: Insights from density fluctuations," *Annu. Rev. Chem. Biomol. Eng.*, vol. 2, pp. 147–171, 2011, doi: 10.1146/annurev-chembioeng-061010-114156.

[18] G. Graziano, "Contrasting the hydration thermodynamics of methane and methanol," *Phys. Chem. Chem. Phys.*, vol. 21, no. 38, pp. 21418–21430, 2019, doi: 10.1039/c9cp03213d.

[19] R. A. Pierotti, "Aqueous Solutions of Nonpolar Gases," *J. Phys. Chem.*, vol. 69, pp. 281–288, 1965.

[20] B. Lee, "The physical origin of the low solubility of nonpolar solutes in water," *Biopolymers*, vol. 24, no. 5, pp. 813–823, 1985, doi: 10.1002/bip.360240507.

[21] M. Lucas, "Size effect in transfer of nonpolar solutes from gas or solvent to another solvent with a view on hydrophobic behavior," *J. Phys. Chem.*, vol. 80, no. 4, pp. 359–362, 1976, doi: 10.1021/j100545a004.

[22] T. V. Chalikian and R. Filfil, "How large are the volume changes accompanying protein transitions and binding?," *Biophys. Chem.*, vol. 104, no. 2, pp. 489–499, 2003, doi: 10.1016/S0301-4622(03)00037-1.

[23] K. Gekko and H. Noguchi, "Compressibility of globular proteins in water at 25°C," *J. Phys. Chem.*, vol. 83, no. 21, pp. 2706–2714, 1979, doi: 10.1021/j100484a006.

[24] K. Gekko and Y. Hasegawa, "Compressibility-Structure Relationship of Globular Proteins," *Biochemistry*, vol. 25, no. 21, pp. 6563–6571, 1986, doi: 10.1021/bi00369a034.

[25] M. Bánó and J. Marek, "How thick is the layer of thermal volume surrounding the protein?," *Biophys. Chem.*, vol. 120, no. 1, pp. 44–54, 2006, doi: 10.1016/j.bpc.2005.09.024.

[26] T. V. Chalikian, "Volumetric properties of proteins," *Annu. Rev. Biophys. Biomol. Struct.*, vol. 32, no. February 2003, pp. 207–235, 2003, doi: 10.1146/annurev.biophys.32.110601.141709.

[27] T. V. Chalikian, M. Totrov, R. Abagyan, and K. J. Breslauer, "The hydration of globular proteins as derived from volume and compressibility measurements: Cross correlating thermodynamic and structural data," *J. Mol. Biol.*, vol. 260, no. 4, pp. 588–603, 1996, doi: 10.1006/jmbi.1996.0423.

[28] V. P. Voloshin, N. N. Medvedev, N. Smolin, A. Geiger, and R. Winter, "Disentangling volumetric and hydrational properties of proteins," *J. Phys. Chem. A*, vol. 119, no. 5, pp. 1881–1890, 2015, doi: 10.1021/jp510891b.

[29] N. B. Rego and A. J. Patel, "Understanding Hydrophobic Effects: Insights from Water Density Fluctuations," *Annu. Rev. Condens. Matter Phys.*, vol. 13, no. 1, pp. 303–324, 2022, doi: 10.1146/annurev-conmatphys-040220-045516.

[30] U. Kumar Sur, "Behaviour of water at hydrophobic interfaces," *J. Mol. Liq.*, vol.

348, p. 118433, 2022, doi: 10.1016/j.molliq.2021.118433.

[31] V. R. Hande and S. Chakrabarty, "How Far Is 'Bulk Water' from Interfaces? Depends on the Nature of the Surface and What We Measure," *J. Phys. Chem. B*, vol. 126, no. 5, pp. 1125–1135, 2022, doi: 10.1021/acs.jpcb.1c08603.

[32] C. Sendner, D. Horinek, L. Bocquet, and R. R. Netz, "Interfacial water at hydrophobic and hydrophilic surfaces: Slip, viscosity, and diffusion," *Langmuir*, vol. 25, no. 18, pp. 10768–10781, 2009, doi: 10.1021/la901314b.

[33] M. K. Coe, R. Evans, and N. B. Wilding, "Density Depletion and Enhanced Fluctuations in Water near Hydrophobic Solutes: Identifying the Underlying Physics," *Phys. Rev. Lett.*, vol. 128, no. 4, p. 45501, 2022, doi: 10.1103/physrevlett.128.045501.

[34] C. Q. Sun, "Supersolidity of undercoordinated and hydrating water," *Phys. Chem. Chem. Phys.*, vol. 20, no. 48, pp. 30104–30119, 2018, doi: 10.1039/c8cp06115g.

[35] Q. Sun, "The physical origin of hydrophobic effects," *Chem. Phys. Lett.*, vol. 672, pp. 21–25, 2017, doi: 10.1016/j.cplett.2017.01.057.

[36] C. S. Rao and S. Damodaran, "Is surface pressure a measure of interfacial water activity? Evidence from protein adsorption behavior at interfaces," *Langmuir*, vol. 16, no. 24, pp. 9468–9477, 2000, doi: 10.1021/la0007168.

[37] L. Ter-Minassian-Saraga, "Protein denaturation on adsorption and water activity at interfaces: an analysis and suggestion," *J. Colloid Interface Sci.*, vol. 80, no. 2, pp. 393–401, 1981, doi: 10.1016/0021-9797(81)90198-3.

[38] J. Bergfreund *et al.*, "Globular protein assembly and network formation at fluid interfaces: effect of oil," *Soft Matter*, pp. 1692–1700, 2021, doi: 10.1039/d0sm01870h.

[39] J. Bergfreund, P. Bertsch, and P. Fischer, "Adsorption of proteins to fluid interfaces: Role of the hydrophobic subphase," *J. Colloid Interface Sci.*, vol. 584, pp. 411–417, 2021, doi: 10.1016/j.jcis.2020.09.118.

[40] J. Bergfreund, P. Bertsch, and P. Fischer, "Effect of the hydrophobic phase on interfacial phenomena of surfactants, proteins, and particles at fluid interfaces," *Curr. Opin. Colloid Interface Sci.*, vol. 56, p. 101509, 2021, doi: 10.1016/j.cocis.2021.101509.

[41] W. Zhang, X. Xu, X. Zhao, and G. Zhou, "Insight into the oil polarity impact on interfacial properties of myofibrillar protein," *Food Hydrocoll.*, vol. 128, no. January, p. 107563, 2022, doi: 10.1016/j.foodhyd.2022.107563.

[42] C. Aphibanthammakit, M. Nigen, S. Gaucel, C. Sanchez, and P. Chalier, "Surface properties of Acacia senegal vs Acacia seyal films and impact on specific functionalities," *Food Hydrocoll.*, vol. 82, pp. 519–533, 2018, doi: 10.1016/j.foodhyd.2018.04.032.

B. Rheological profiles of water-gum-aroma interphases

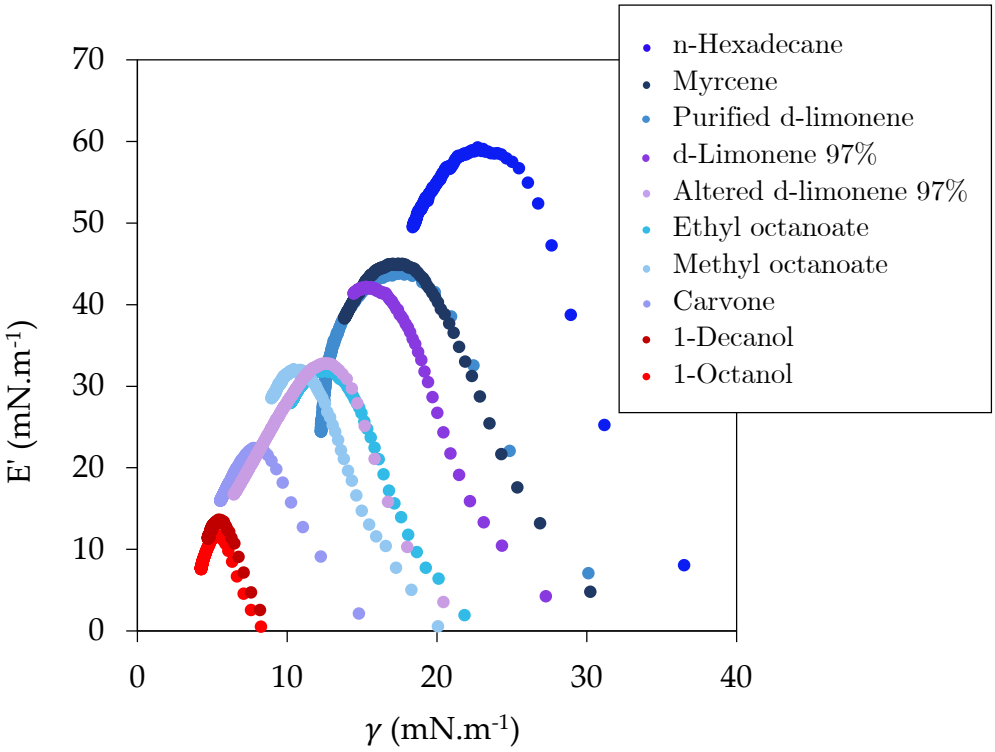

Fig. 1. Evolution of the dilational elastic modulus E' with the interfacial tension in 5 wt% A. *senegal* dispersion.

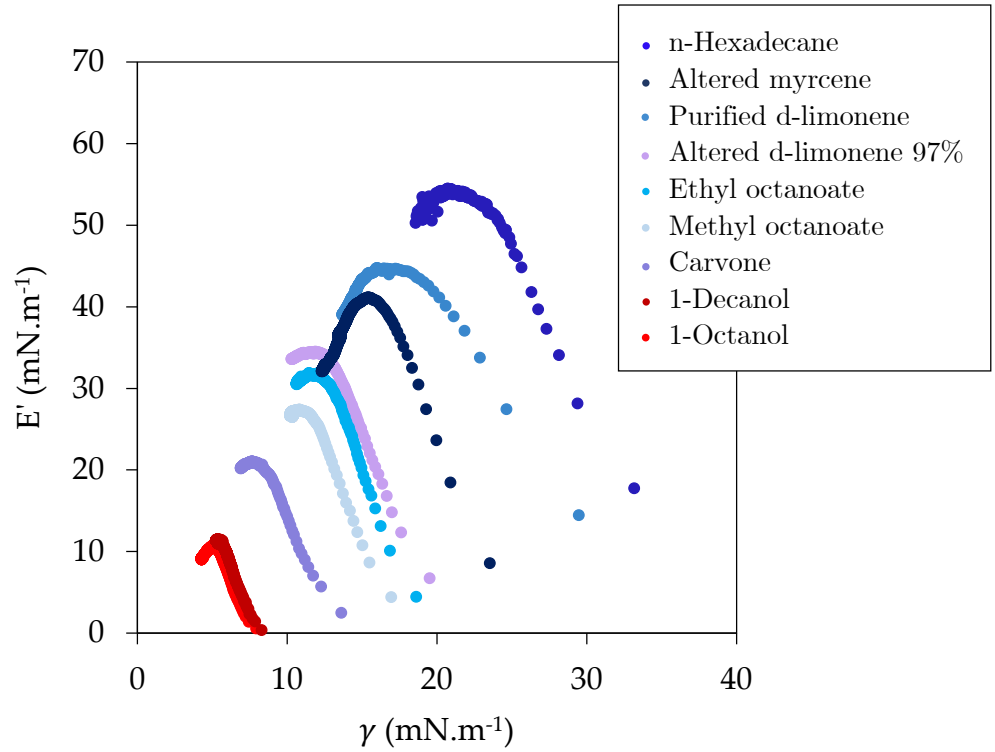

Fig. 2. Evolution of the dilational elastic modulus E' with the interfacial tension in 5 wt% A. *seyal* dispersion.

C. Rheological profiles of water-gum-aroma mixture interphases

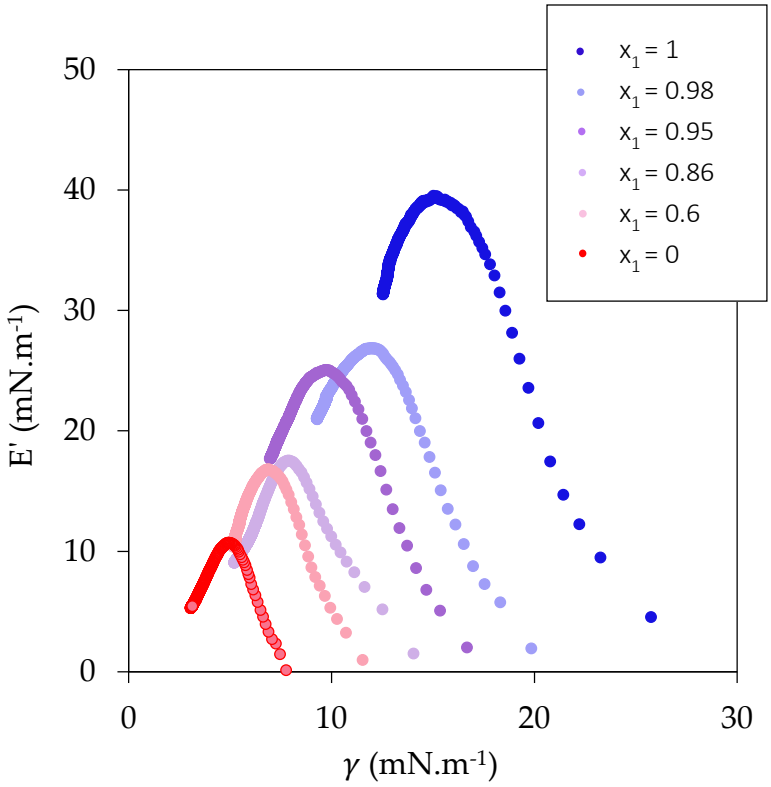

Fig. 1. Evolution of the dilational elastic modulus E' with the interfacial tension in 5 wt% A. *senegal* dispersion. Oil droplet was *d-limonene (x_1):1-octanol (x_2)* mixture.

D. Turbiscan profiles of emulsions stabilized by A. *senegal*

1. Backscattered light

Changes of light backscattering (ΔBS) profiles during 28 days of storage at 25°C of all emulsions containing 5 wt% oil and stabilized by 20 wt% A. *senegal.* Blue curve represents the earliest time point and red curve the latest time point.

1.1. n-Hexadecane

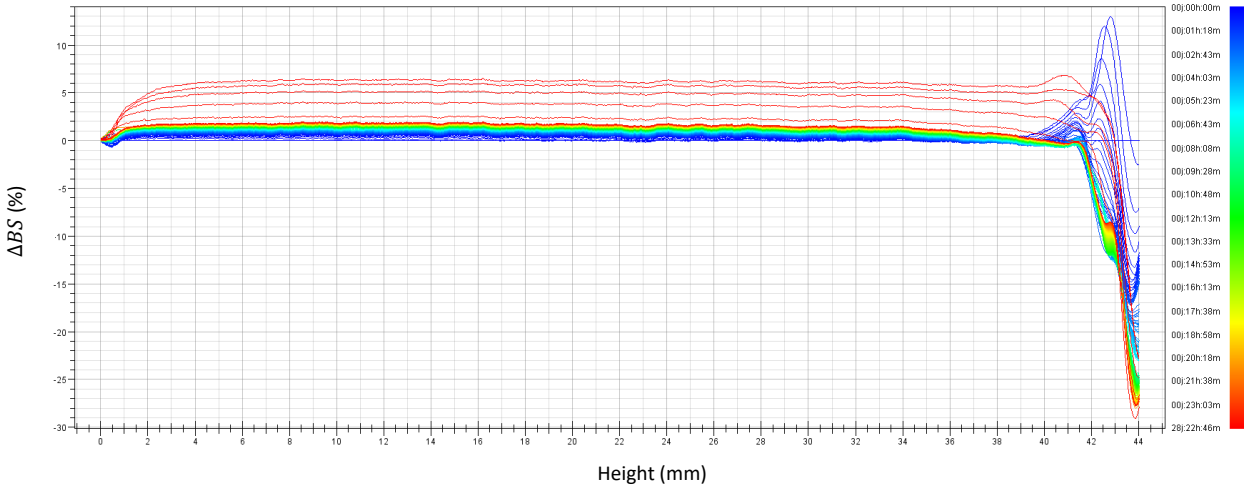

1.2. D-limonene

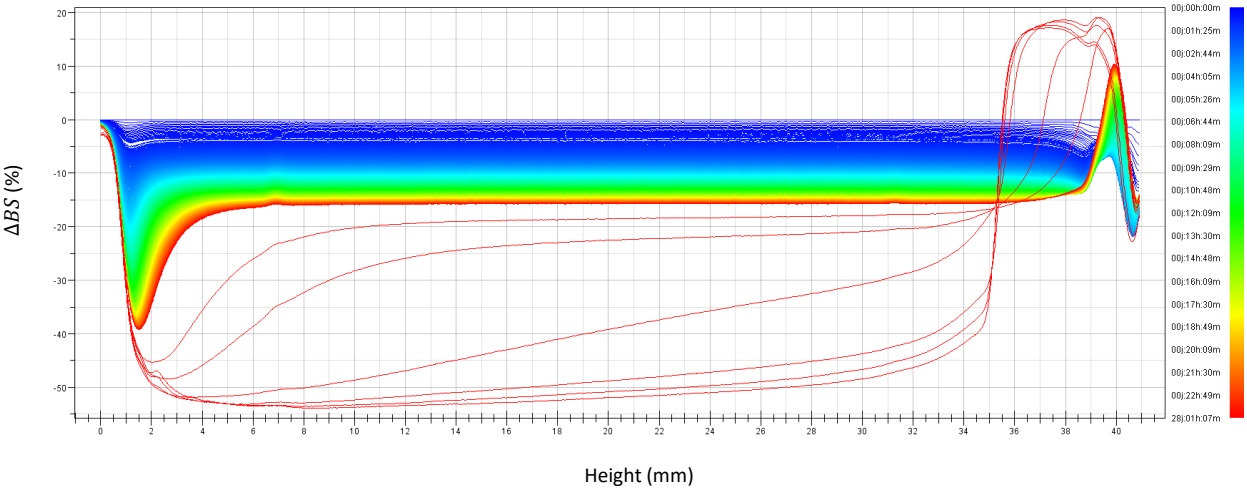

1.3. Ethyl octanoate

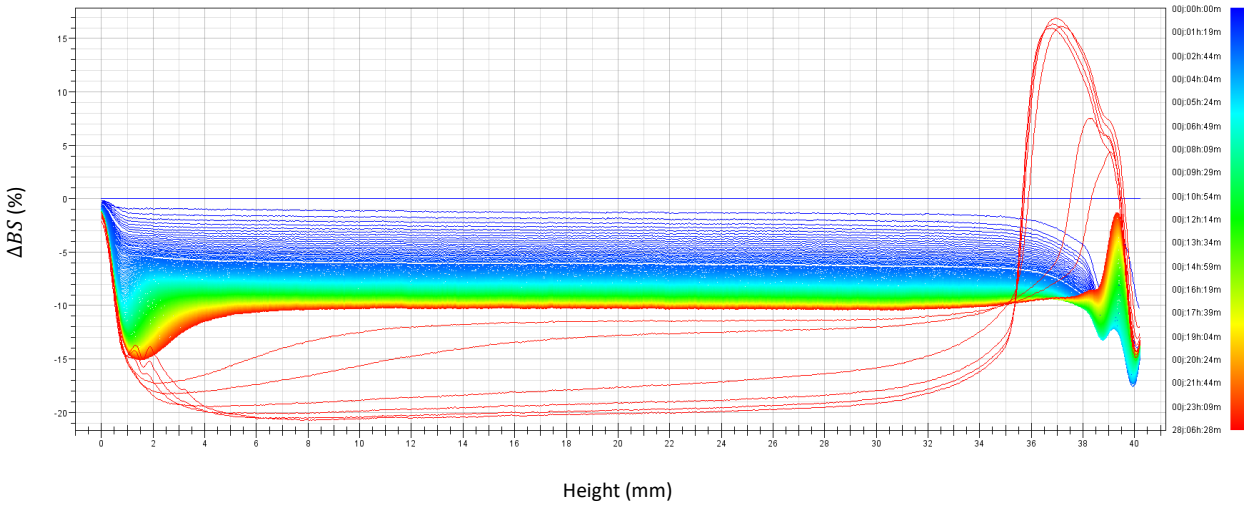

1.4. Carvone

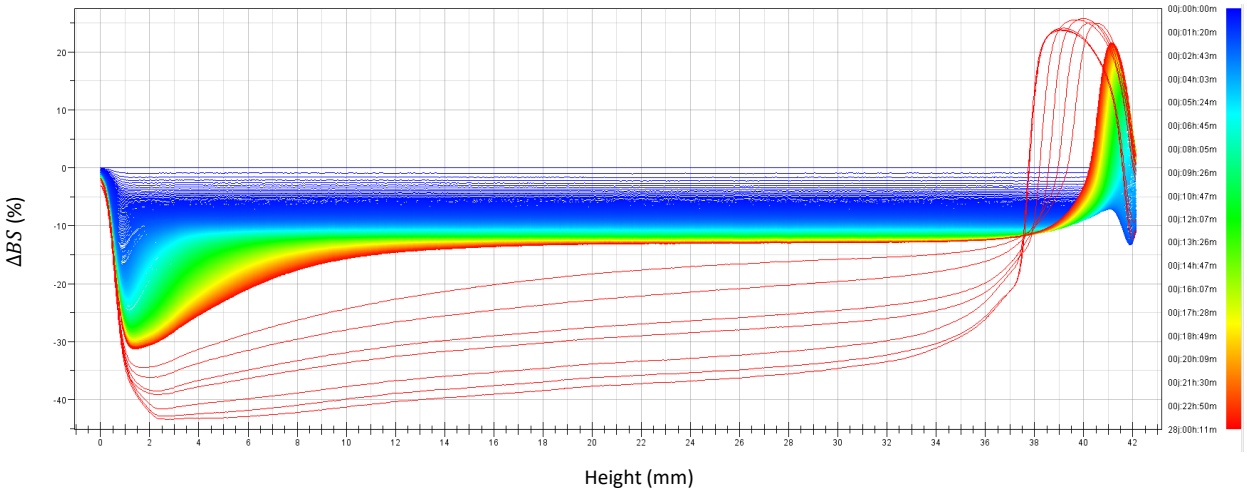

1.5. 1-decanol

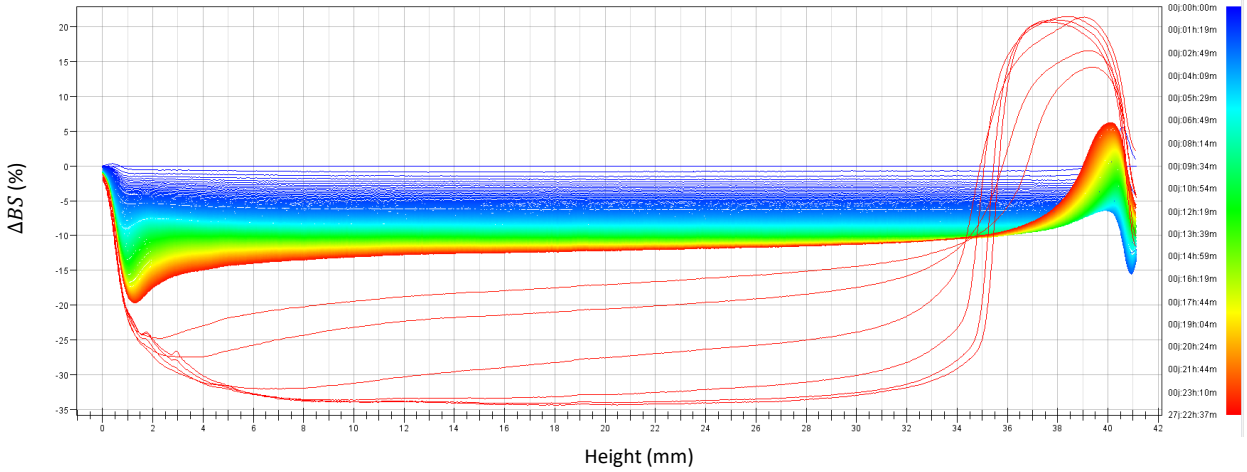

1.6. 1-octanol

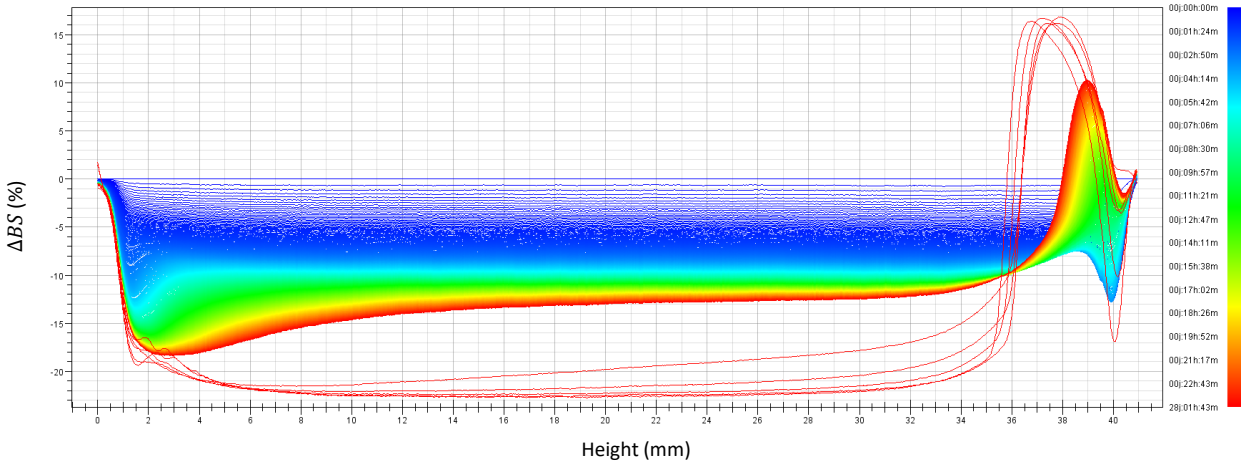

1.7. D-limonene (x_1):1-octanol (x_2), ratio $x_1 = 0.6$

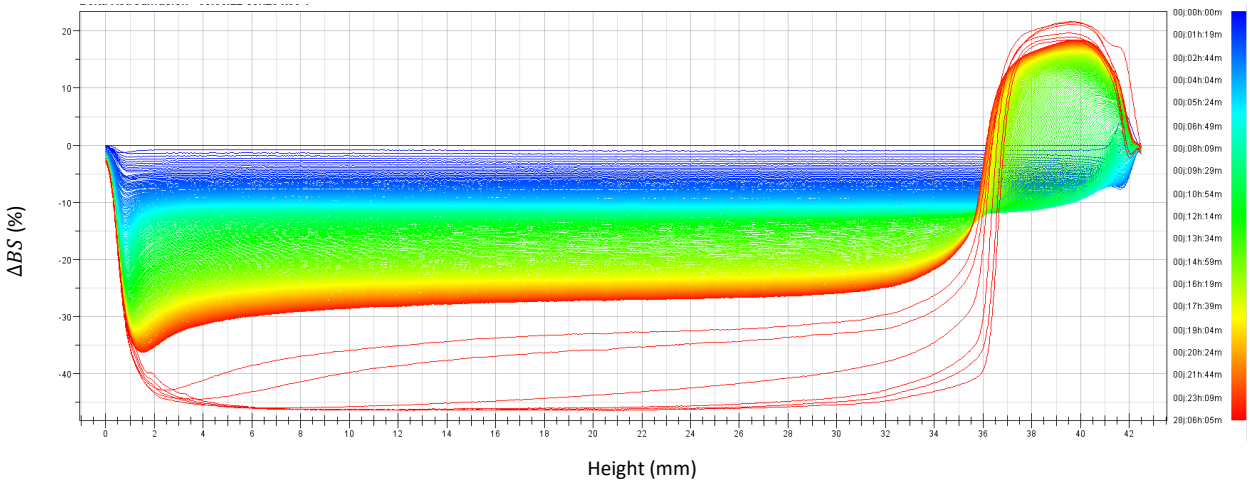

1.8. D-limonene (x_1):1-octanol (x_2), ratio $x_1 = 0.86$

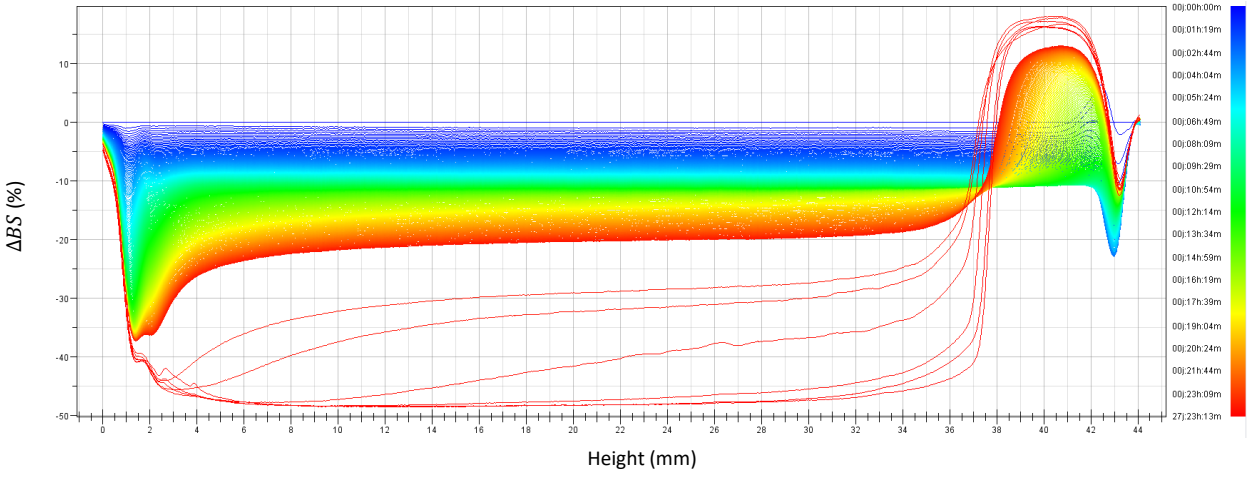

1.9. D-limonene (x_1):1-octanol (x_2), ratio $x_1 = 0.95$

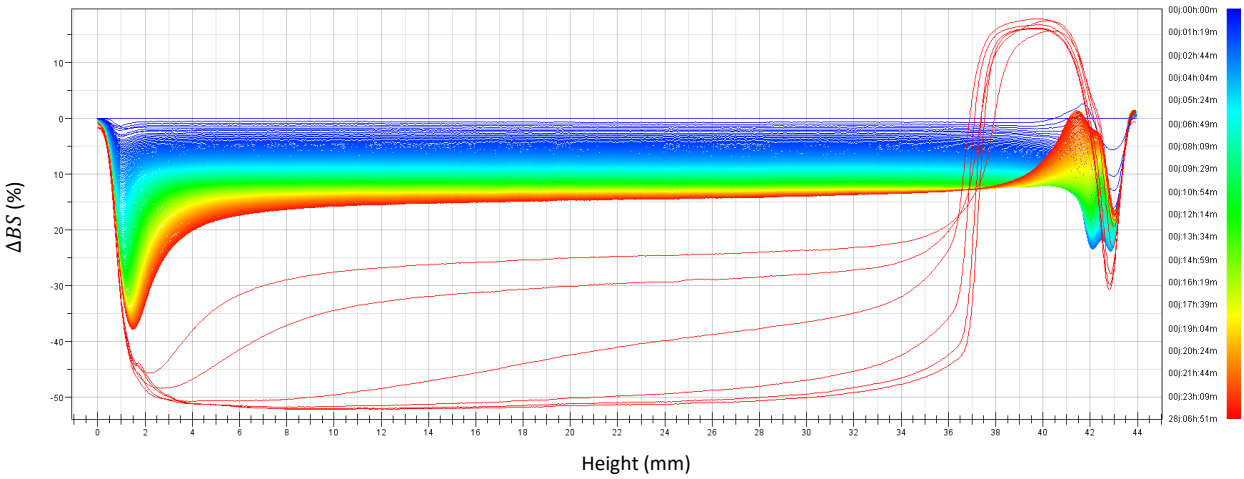

1.9. D-limonene (x_1):1-octanol (x_2), ratio $x_1 = 0.98$

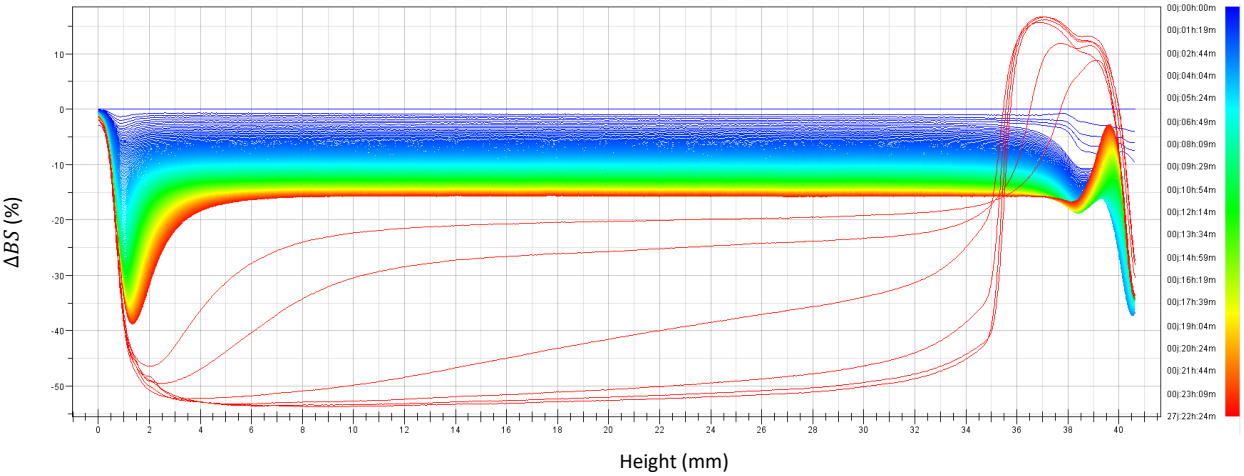

2. Transmitted light

Changes of transmitted light (ΔT) profiles during 28 days of storage at 25°C of all emulsions containing 5 wt% oil and stabilized by 20 wt% A. *senegal*. Blue curve represents the earliest time point and red curve the latest time point.

1.1. n-Hexadecane

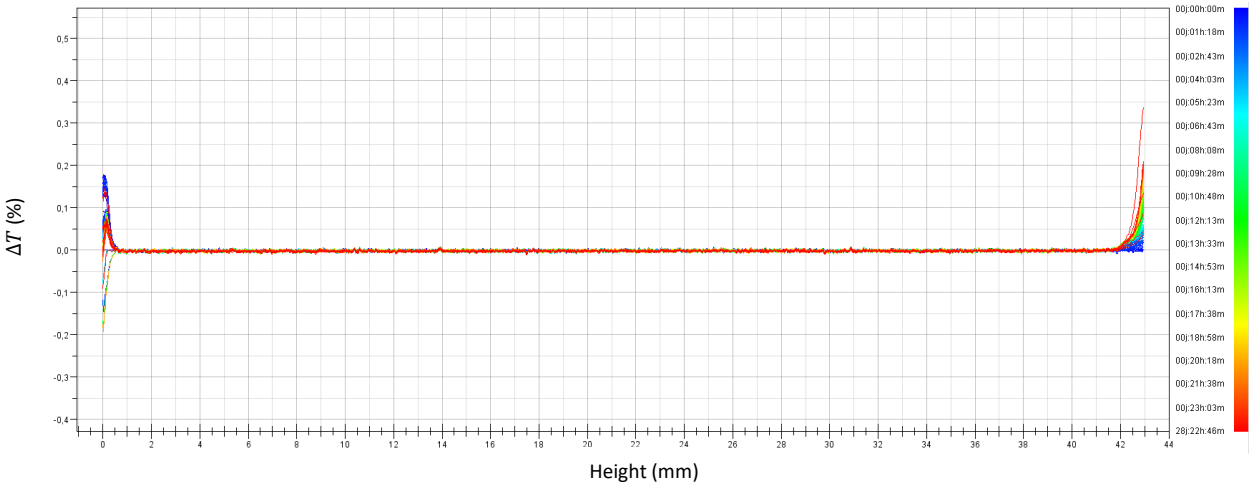

1.2. D-limonene

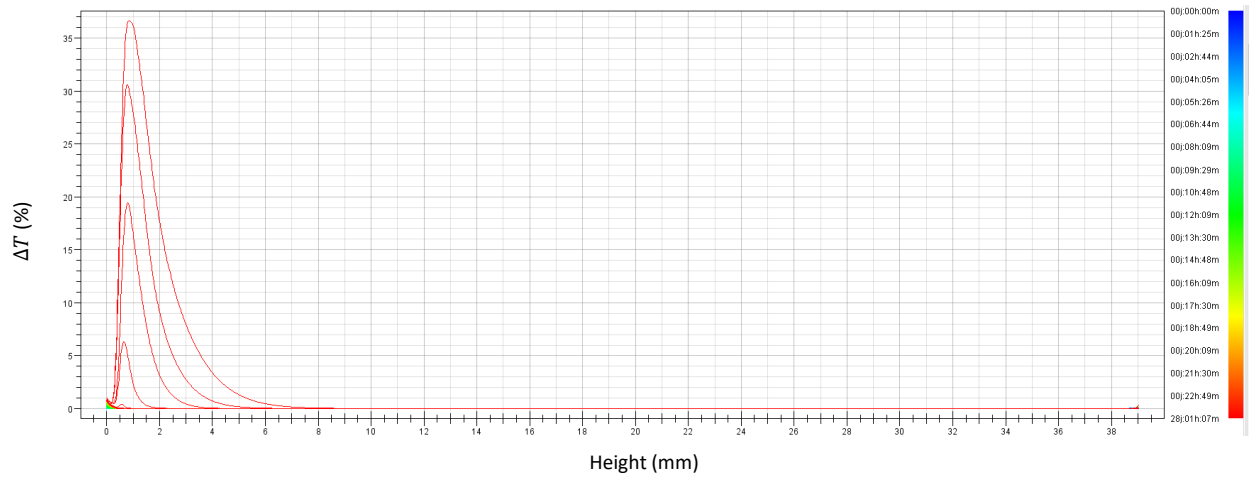

1.3. Ethyl octanoate

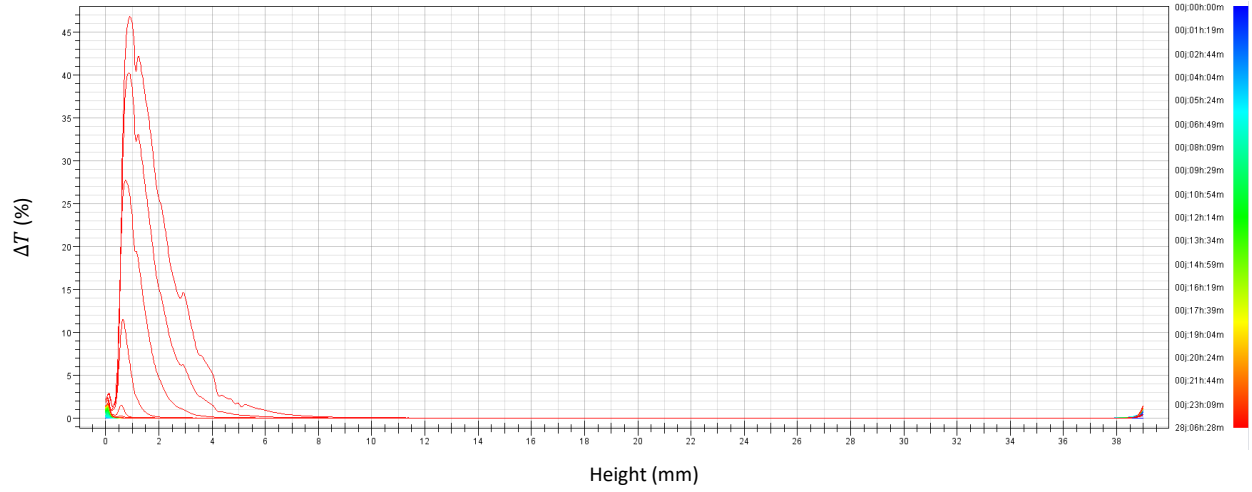

1.4. Carvone

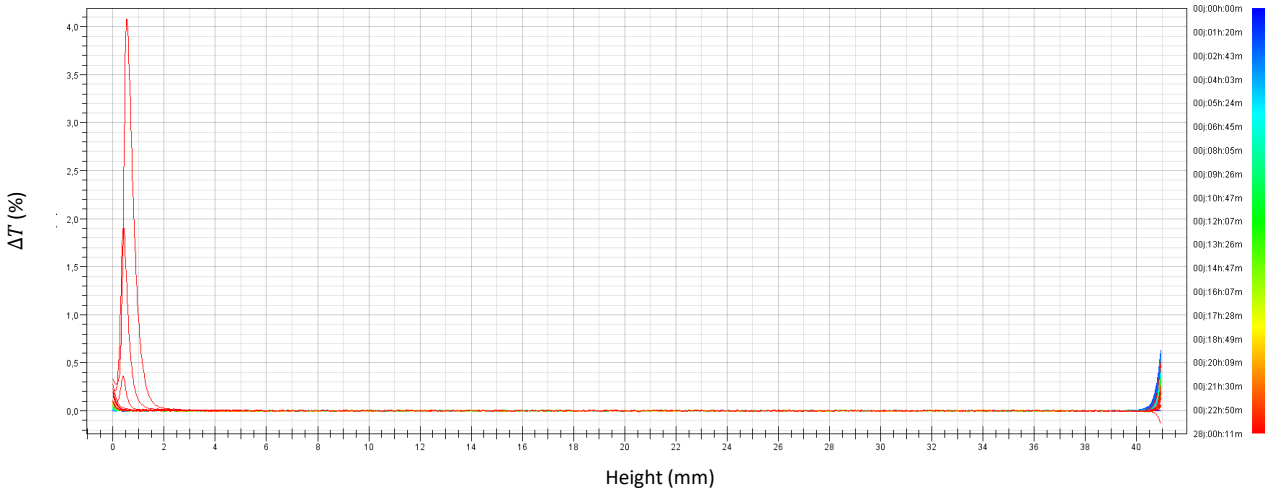

1.5. 1-decanol

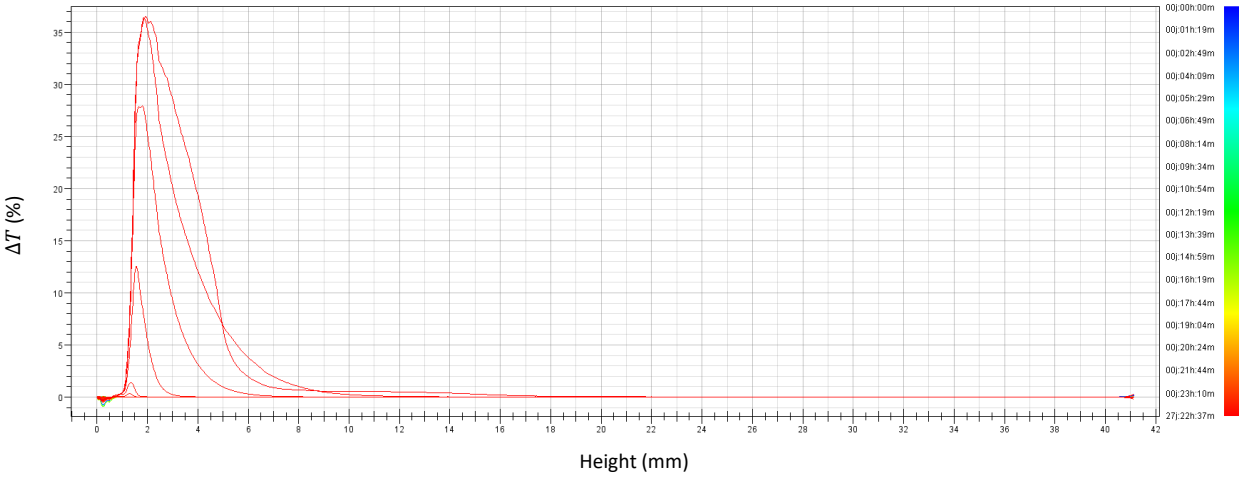

1.6. 1-octanol

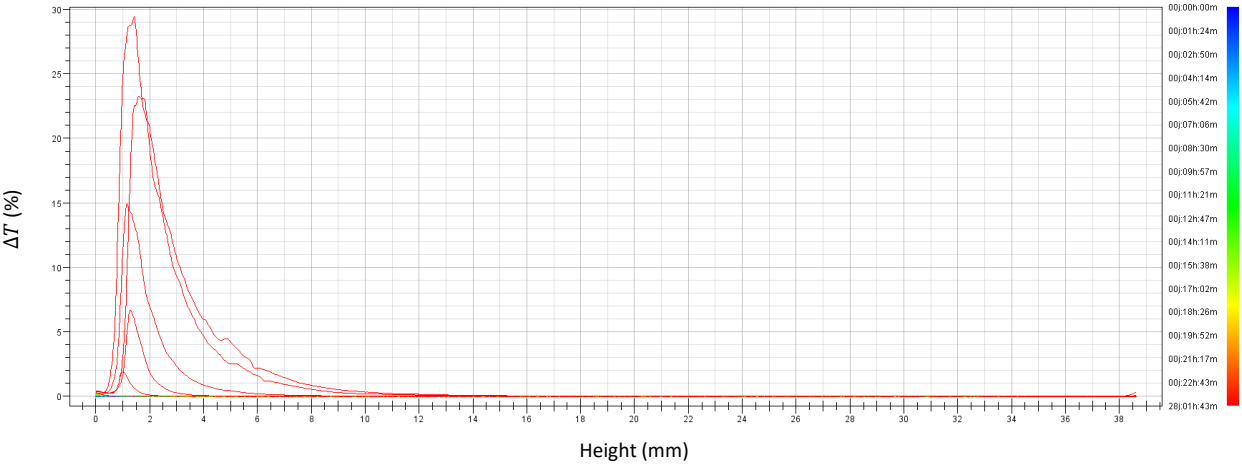

1.7. D-limonene (x_1):1-octanol (x_2), ratio $x_1 = 0.6$

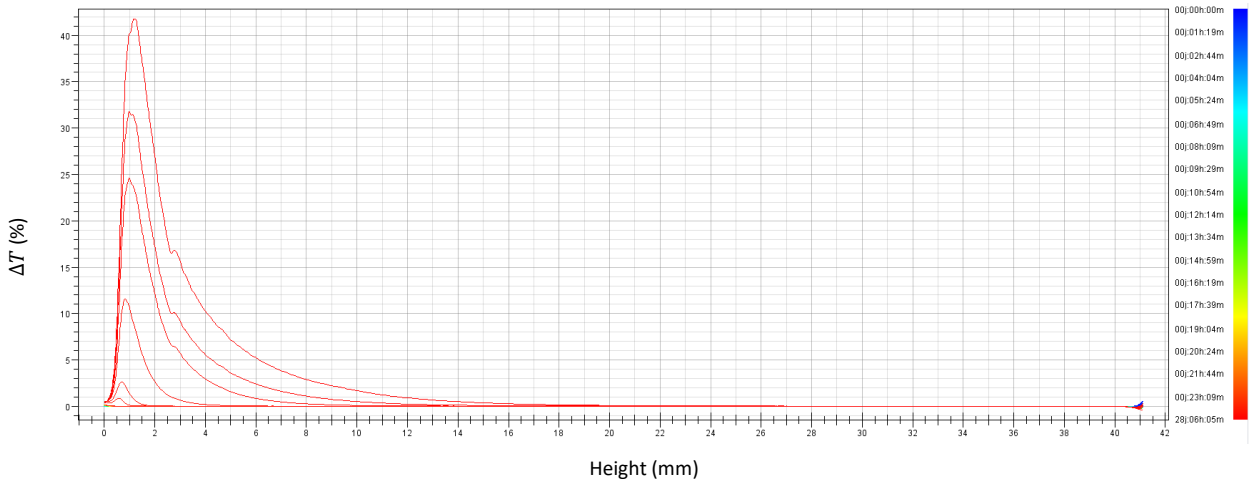

1.8. D-limonene (x_1):1-octanol (x_2), ratio $x_1 = 0.86$

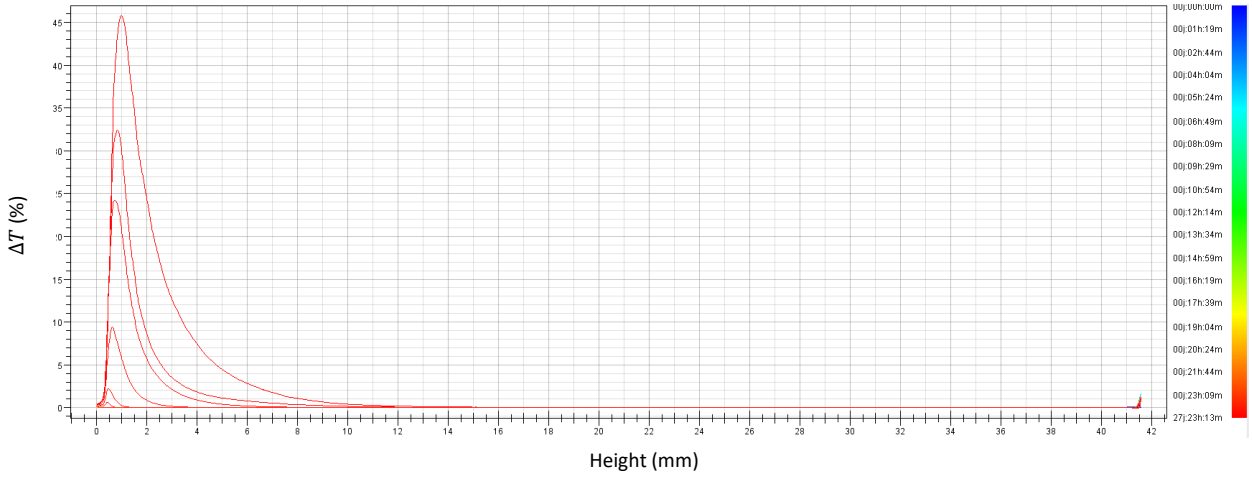

1.9. D-limonene (x_1):1-octanol (x_2), ratio $x_1 = 0.95$

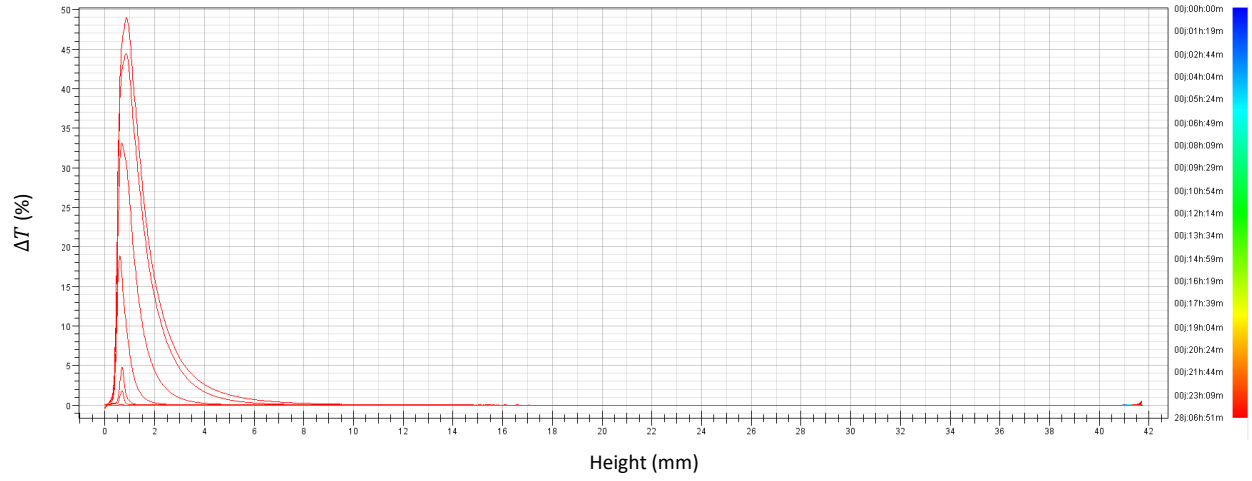

1.9. D-limonene (x_1):1-octanol (x_2), ratio $x_1 = 0.98$

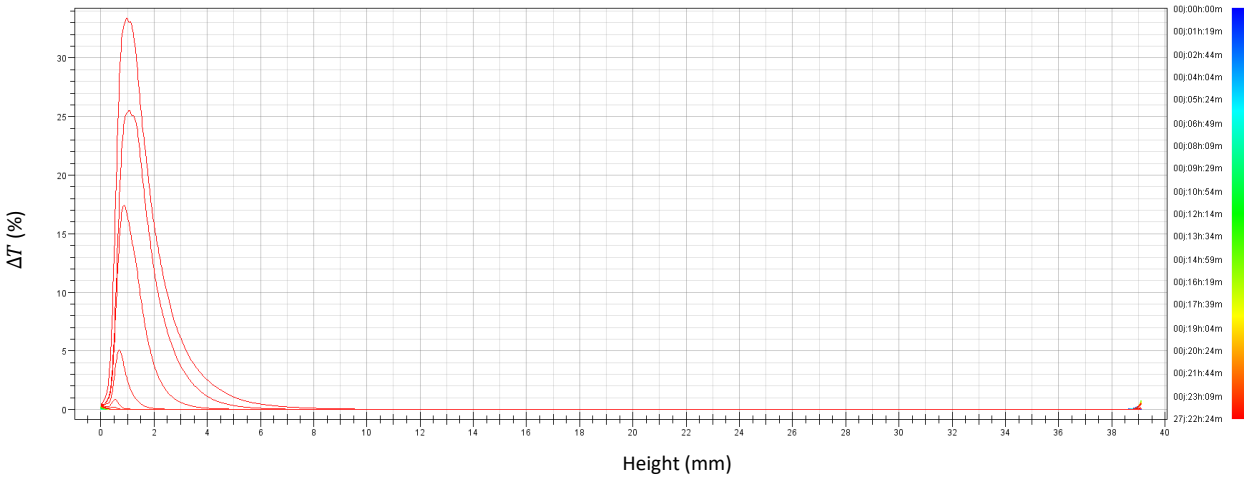

E. Turbiscan profiles of emulsions stabilized by A. *seyal*

1. Backscattered light

Changes of light backscattering (ΔBS) profiles during 28 days of storage at 25°C of all emulsions containing 5 wt% oil and stabilized by 20 wt% A. *seyal*. Blue curve represents the earliest time point and red curve the latest time point.

1.1. D-limonene

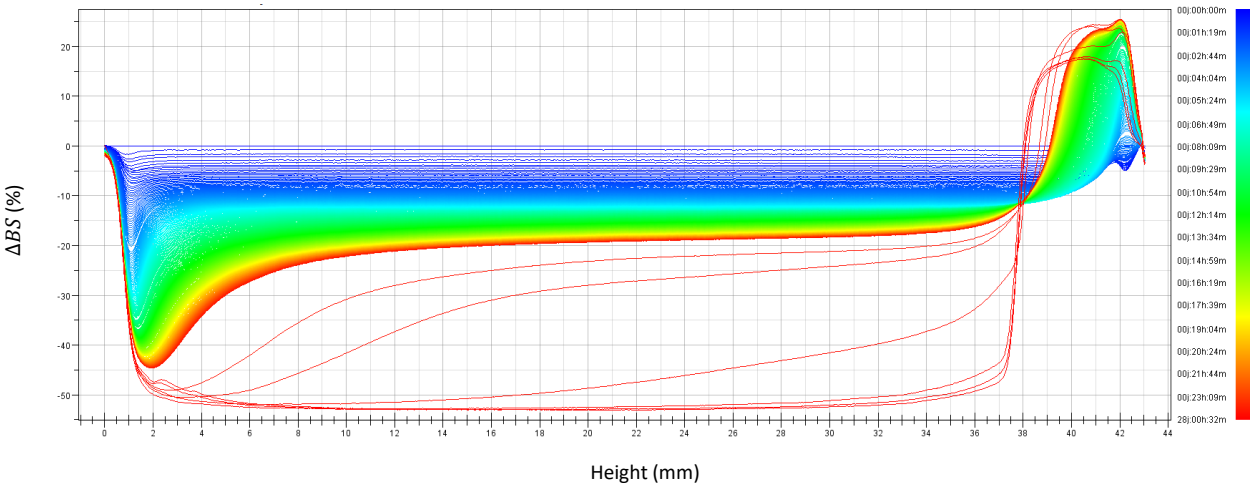

1.2. Carvone

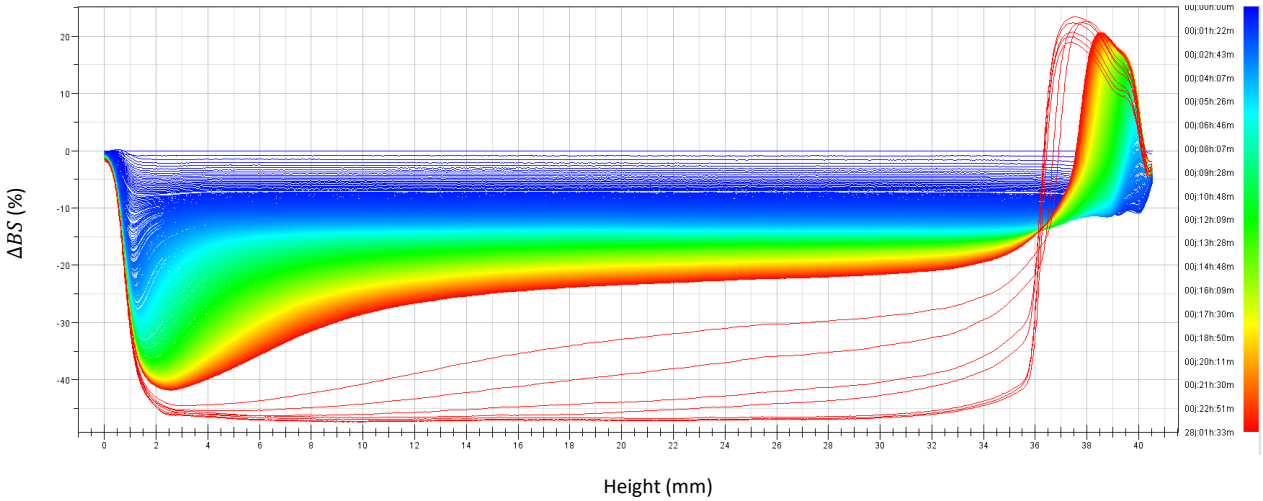

1.3. 1-decanol

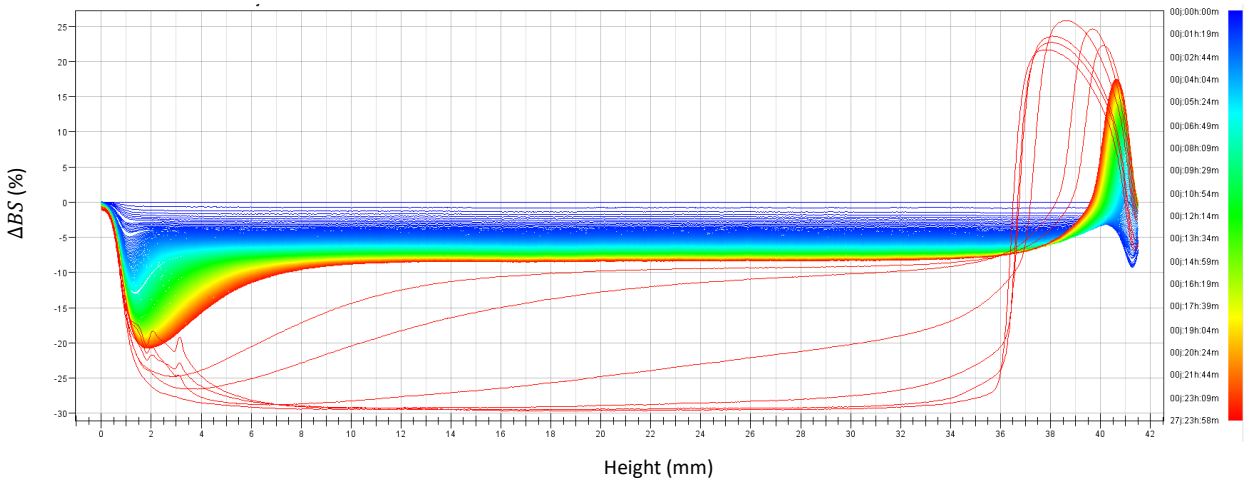

1.4. 1-octanol

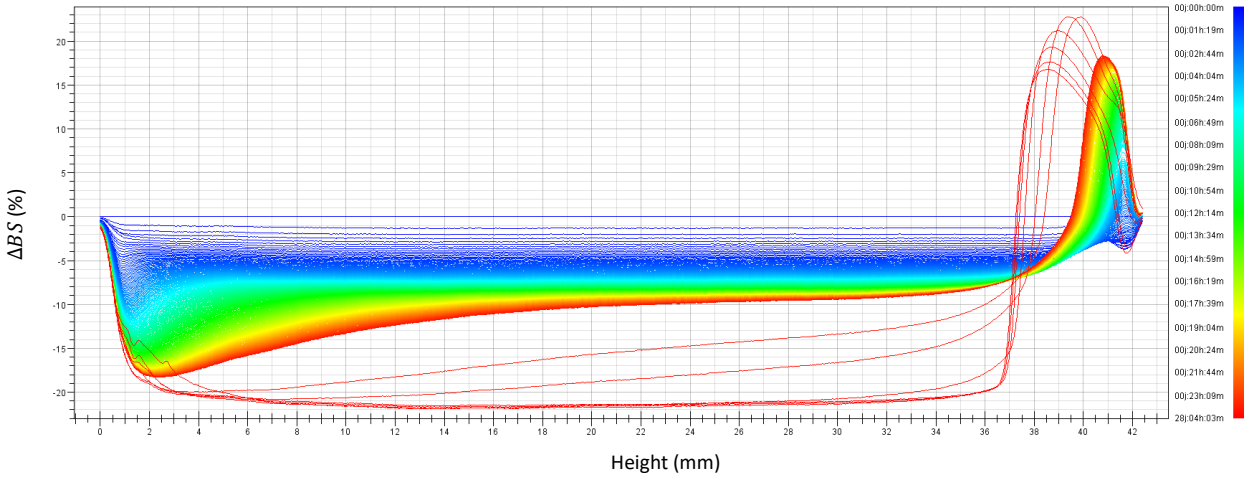

2. Transmitted light

Changes of transmitted light (ΔT) profiles during 28 days of storage at 25°C of all emulsions containing 5 wt% oil and stabilized by 20 wt% A. *senegal*. Blue curve represents the earliest time point and red curve the latest time point.

1.1. D-limonene

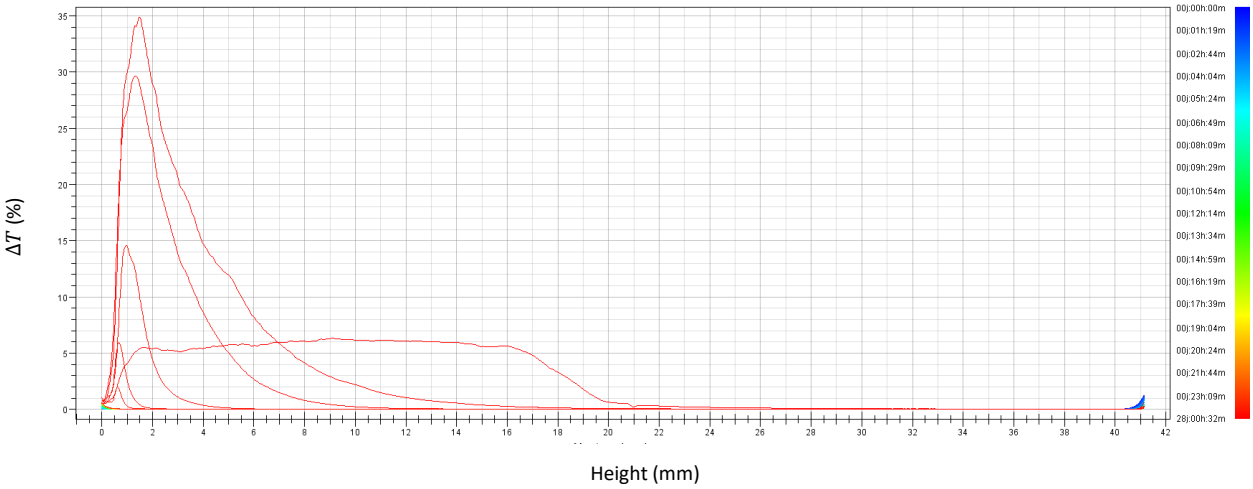

1.2. Carvone

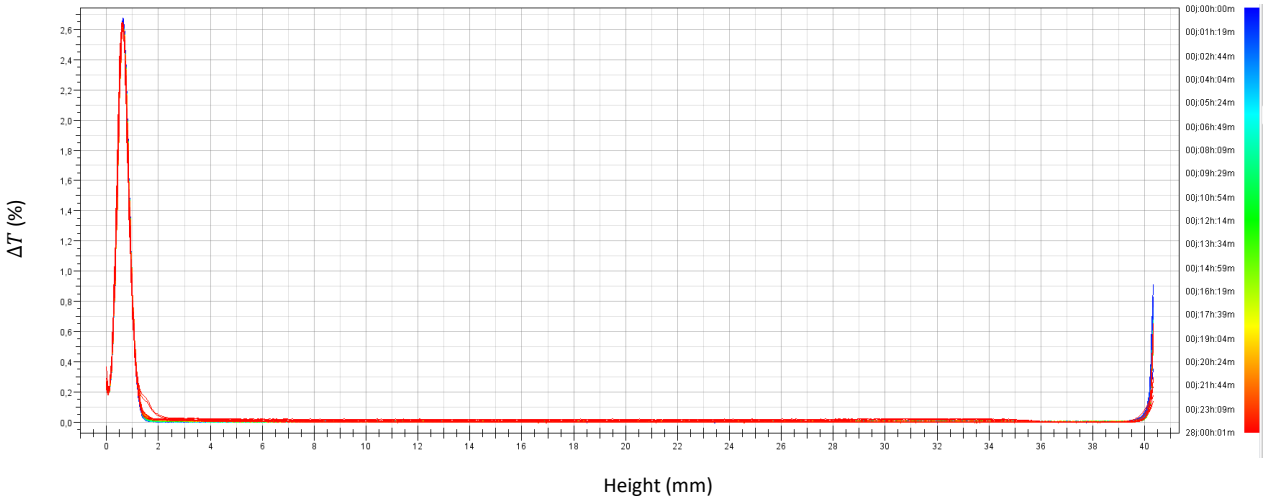

1.3. 1-decanol

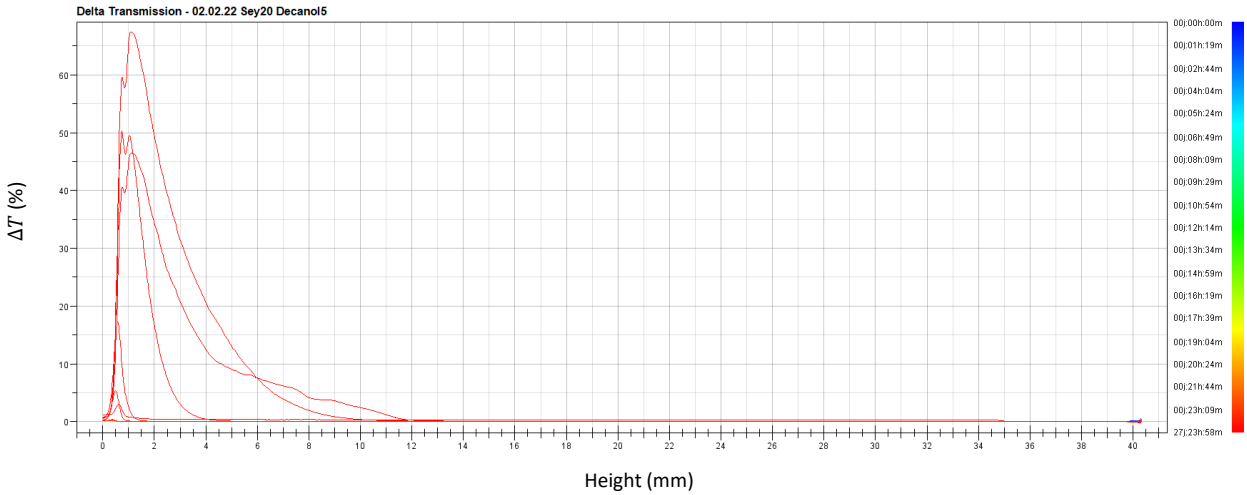

1.4. 1-octanol

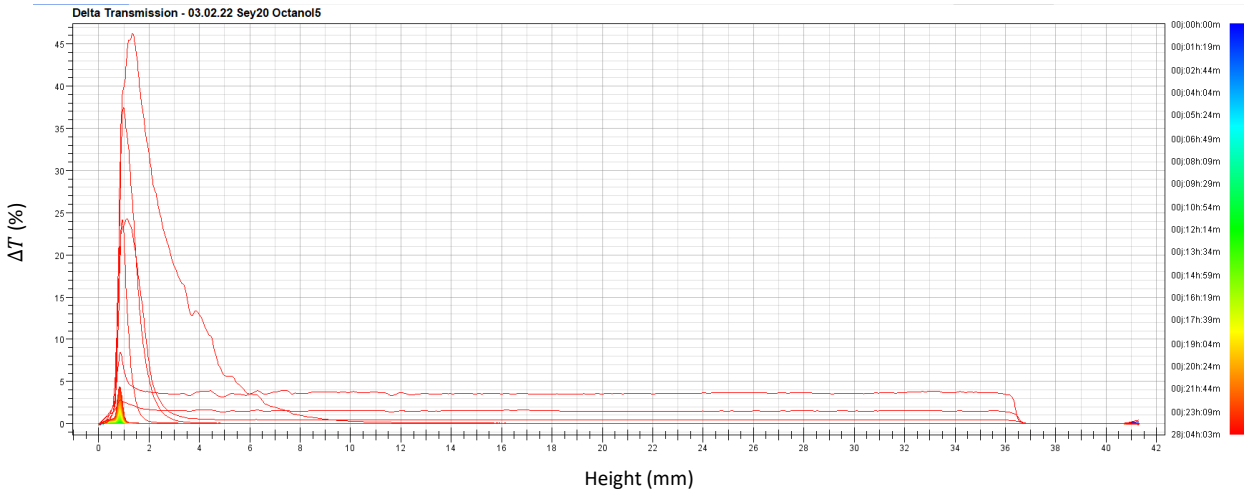
Delta Transmission - 03.02.22 Sey20 Octanol5
ΔT (%)
Height (mm)
00j:00h:00m
00j:01h:19m
00j:02h:44m
00j:04h:04m
00j:05h:24m
00j:06h:49m
00j:08h:09m
00j:09h:29m
00j:10h:54m
00j:12h:14m
00j:13h:34m
00j:14h:59m
00j:16h:19m
00j:17h:39m
00j:19h:04m
00j:20h:24m
00j:21h:44m
00j:23h:09m
28j:04h:03m

F. Droplet size distribution of aroma mixture emulsions

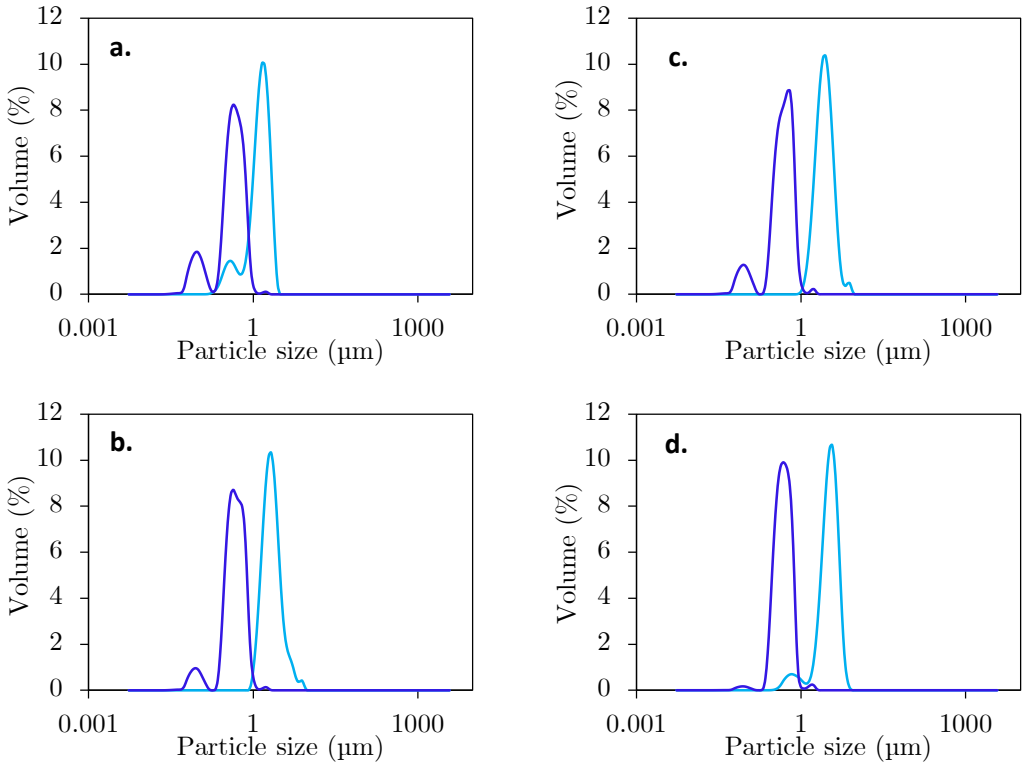

Fig. 1. Droplet size distribution of 20 wt% A. *senegal* stabilized oil-in-water emulsion. Light blue is for coarse emulsions signals and dark blue for fine emulsion signals. Oil load was *d-limonene (x_1):1-octanol (x_2)* mixture and was set at 5 wt%. **(a)** ratio x1 = 0.6, **(b)** ratio x1 = 0.86, **(c)** ratio x1 = 0.95, **(d)** ratio x1 = 0.98.

Stabilization of Aroma Emulsions by Acacia gum-water system: Characterization and Physicochemical Understanding of water-gum-aroma Interactions

Acacia gum (E414) is a dried gummy exudate from Acacia *senegal* and Acacia *seyal* trees. It is mainly composed of weakly charged, hyperbranched arabinogalactan-proteins (AGPs) and contains about 90% of polysaccharides and from 1-3% of proteins and 3-4% of minerals. The protein/polysaccharide duality is the origin of the amphiphilic character of the gum. Thus, Acacia gums are used as a stabilizer and emulsifier for non-food and food applications, in particular with essential oils (mixtures of aroma compounds) in beverages industry. However, the relation between these properties and the nature of the oil received little attention. The objective of this work is to study the mechanisms involved in aroma emulsions stabilized by Acacia gum. A better understanding of the origin of the gum interfacial and emulsifying properties is intended, in order to possibly extend the gum field of application to a wider range of aroma compounds. To this end, the focus is made on the influence of water, and more specifically of aroma-water interactions, on the gum formation mechanism at the oil-water interface and on emulsion stability. The main results showed aroma-water interactions are the driving force of the gum adsorption. Furthermore, the gum adsorbs preferentially at highly hydrophobic interfaces, inducing high oil surface coverage, high interfacial layer elasticity and ability to reduce the interfacial tension. A volumetric adsorption mechanism is proposed based on enhanced volume fluctuations near highly hydrophobic interfaces, favoring the formation of a dehydrated aroma-gum-water interfacial structure. This mechanism is unchanged for a binary mixture of aroma compounds differing in hydrophobicity. Furthermore, the lower hydrophobic compounds constituting the oil phase are shown to preferential accumulate at the oil-water interface. Concerning the emulsifying properties, a relationship, depending on the droplet dispersion mechanisms, between the aroma hydrophobicity and the emulsion droplet size is demonstrated. Finally, the aroma hydrophobicity is shown to influence the aging of the emulsion from the first hour of storage.

Keywords: Acacia gum, Interfacial properties, Emulsifying properties, Aroma, Hydrophobicity, Volume fluctuations.

Stabilisation d'émulsions d'arômes par la gomme d'Acacia : caractérisation et compréhension physico-chimique des interactions eau-gomme-arôme

La gomme d'Acacia (E414) est un exsudat gommeux produit par les arbres d'Acacia *senegal* et Acacia *seyal*. Elle est principalement composée de protéines arabinogalactanes (AGPs), faiblement chargées, hyperbranchées, avec une forte proportion de sucres (90%) et d'environ 1-3% de protéines et 3-4% de minéraux. Cette dualité protéine/sucre est à l'origine du caractère amphiphile de la gomme. Elle est alors utilisée comme stabilisant et émulsifiant pour des applications non-alimentaires et alimentaires, notamment avec les huiles essentielles (mélanges de composés d'arôme) dans l'industrie des boissons. Cependant, les connaissances liant ces propriétés et la nature de l'huile peuvent être améliorées. L'objectif de ce travail est d'étudier les mécanismes impliqués dans les émulsions d'arômes stabilisées par la gomme d'Acacia. Le but est de mieux appréhender l'origine des propriétés interfaciales et émulsifiantes de la gomme, pour éventuellement étendre son champ d'application à une plus large gamme de composés d'arôme. Pour cela, l'accent a été porté sur l'influence de l'eau, et plus particulièrement des interactions entre les arômes et l'eau, sur le mécanisme de formation de la gomme à l'interface huile-eau et la stabilité de l'émulsion. Les principaux résultats ont montré que les interactions arôme-eau constituent la force motrice de l'adsorption de la gomme. De plus, la gomme s'adsorbe préférentiellement aux interfaces très hydrophobes, entraînant une concentration de surface élevée, une meilleure élasticité de la couche interfaciale et une meilleure capacité à réduire la tension. Un mécanisme volumétrique d'absorption est proposé sur la base de fluctuations de volumes plus accrues dans les interfaces très hydrophobes, réduisant le coup énergétique pour former une interphase arôme-gomme-eau déshydratée. Ce mécanisme reste inchangé pour un mélange binaire de composés d'arôme d'hydrophobicité différente. Par ailleurs, il est démontré que les composés les moins hydrophobes de la phase huileuse s'accumulent préférentiellement à l'interface huile-eau. Concernant, les propriétés émulsifiantes, une relation entre l'hydrophobicité de l'arôme et la taille des gouttes de l'émulsion, dépendante des mécanismes de fragmentation, est mise en évidence. De même, il est démontré que l'hydrophobicité influence le vieillissement de l'émulsion, et ce dès la première heure de stockage.

Mots clés : Gomme d'Acacia, Propriétés interfaciales, Propriétés émulsifiantes, Arôme, Hydrophobicité, Fluctuations de volume.